University of Latvia

Faculty of Chemistry

Doctoral thesis

Solvent mediated phase transformations of active pharmaceutical compounds tegafur and theophylline

Raitis Bobrovs

Supervisor

Prof. Dr. chem. Andris Actiņš

Scientific advisor

Dr. chem. Linda Seton

Riga, 2015

This work has been supported by the European Social Fund within the project «Support for Doctoral Studies at University of Latvia».

The doctoral thesis was carried out at the Chair of Physical Chemistry, Department of Chemistry, University of Latvia and Drug Delivery and Materials Science Research Group, School of Pharmacy and Biomolecular Sciences, Faculty of Science, Liverpool John Moores University from 2011 to 2015.

Form of the thesis: dissertation in Chemistry, Physical Chemistry.

Supervisor: Prof.. Dr. Chem., Andris Actiņš

Scientific advisor: Dr. Chem., Linda Seton

Reviewers:

1) Prof., Dr. Chem., Svetlana Čornaja, Riga Technical University;
2) Dr. Chem., Ronalds Zemribo, Latvian Institute of Organic Synthesis;
3) Prof., Dr. Chem., Arturs Vīksna, University of Latvia.

The thesis will be defended at the public session of the Doctoral Committee of Chemistry, University of Latvia on the 26th of June, 2015, at the University of Latvia, Department of Chemistry, Kr. Valdemāra street 48, lecture room 21.

The thesis is available at the Library of the University of Latvia, Multidisciplinary library of computer sciences, law sciences and theology, Raiņa Blvd. 19.

Abstract

Here we have improved a semi-quantitative method (Petkune *et al.*, J. Pharm. Pharmacol., 2011, 63, 9, 1136) for low-level thermodynamically stable polymorph impurity determination in the metastable polymorph. Optimization of sample preparation methodology and conditions allowed to lower the detection limit down to 0.0005% of thermodynamically stable tegafur β polymorph in the metastable α polymorph. Solvent effect on sample preparation have been investigated and the nature of solvent and surface interaction have been characterized using data from solvent desorption studies. Solvent mediated phase transformations (SMPTs) from tegafur α form to β form and theophylline Form II and Form IV have been studied and characterized. It was determined that SMPT rate depend linearly on the supersaturation level, i.e. difference between equilibrium solubility of two polymorphs in the respective solvent. It was revealed that theophylline self-associates in solvents which are good H-bond donors and the presence of these aggregates hinder the nucleation and phase transformation.

Polymorphism, Tegafur, Theophylline, Quantitative powder X-ray diffraction analysis, Solvent mediated phase transformation.

Acknowledgements

I would like to thank my advisor, prof. Dr. chem. Andris Actiņš, for the opportunity to conduct research under his supervision, and for his advice, guidance and encouragement throughout this work. I would also like to express my deepest gratitude to Linda Seton for the opportunity to conduct research in her research group, and her assistance during my stay in Liverpool John Moores University. I thank all of my colleagues and group members, past and present, that were available for discussions and helped with my research.

At last, I would like to acknowledge the funding provided by European Social Fund within the project "Support for Doctoral Studies at University of Latvia" and "Erasmus mobility programme".

Contents

Introduction

Manufacturing of the active pharmaceutical ingredients (API) requires the highest quality standards, due its impact on the life and health of humans. Therefore, a lot of resources are devoted to ensure the required quality of the drugs and improve the manufacturing process.

The majority of small-molecule APIs are typically delivered in the solid dosage form. These pharmaceutical solids are often produced as molecular crystals because of their high physical and chemical stability and ease of processing. A crystalline drug may exist in more than one solid form. Such phenomenon is termed polymorphism, and it is defined as the ability of a substance to exist in more than one crystalline structure resulting from different arrangements and/or conformations of molecules in the crystal lattice [1]. A crystalline drug may exist also as a molecular adduct (drug and a guest component) – solvates, salts and co-crystals. Polymorphic forms are chemically identical, however they exhibit differences in properties of pharmaceutical interest, such as solubility, dissolution rate, bioavailability, tableting, etc. [2]. Therefore, one of the tasks for the pharmaceutical industry is to find and select the solid forms with the optimal characteristics for the intended use. Polymorphism is of great interest also in pigment and explosive manufacturing. Despite the extensive research in the field of polymorphism, there are a lot of unanswered questions concerning the polymorph prediction, polymorph stability landscape, formation causes and mechanisms.

It is a common requirement in the pharmaceutical industry that a manufactured compound must be in one, strictly defined crystalline phase, therefore, crystalline phase screening is one of the first steps during the drug development. During this step the possibility to form different crystalline forms and their relative stability is evaluated. To ensure the stability of the commercial product, the thermodynamically stable polymorph in ambient conditions is normally chosen for manufacturing. However, due to enhanced dissolution or bioavailability profiles, a metastable form might be chosen for manufacturing. To ensure that polymorphs do not transform over time, the polymorphic stability must be evaluated with respect to ambient, storage, and packaging conditions. [3–5]

Crystallization of APIs is governed by a combination of thermodynamic and kinetic factors [3–6], and it often follows Ostwald's rule of stages [7], which postulates that crystallization in a

polymorphic system progresses from supersaturated state to equilibrium state in stages. Thus, according to Ostwald's rule of stages, the metastable form should crystallize first and then the system should move through each possible polymorphic structure before the thermodynamically stable polymorph crystallizes. In the majority of cases the thermodynamically stable polymorph in given conditions is isolated, however, the solvent used for crystallization can affect the crystallization outcome and it might promote the crystallization of a specific metastable polymorph. The metastable polymorph will attempt to transform to the stable form if possible, and therefore it is important to study polymorphic transformation 'reactions' to determine the factors influencing the outcome of a polymorphic crystallization. One type of polymorphic transformation 'reaction' drawing attention is solvent mediated polymorphic transformation (SMPT) [4,8–10]. This is a process, where the metastable polymorph interacts with a bulk solvent phase, and gradually transforms to the more stable polymorph by a process of dissolution and crystallization. SMPTs might be useful for pharmaceutical industry to produce the thermodynamically stable polymorph if crystallization from a solvent gives a metastable polymorph. On the other hand, if a metastable polymorph is desired, knowledge of possible SMPTs of the respective system is important, because there might be situations when metastable polymorph crystallizes, and through unwanted SMPT subsequently transforms to the thermodynamically stable polymorph.

The **aim** of this research was to investigate the solvent mediated phase transformations (SMPT) in polymorphic systems, and evaluate the potential of SMPT applicability in low-level polymorphic impurity quantification.

Following **tasks** were set to address this issue:

1. improve our previously proposed (Petkune *et al.*, J. Pharm. Pharmacol., 2011, 63, 9, 1136) method for low-level (less than 1%) thermodynamically stable polymorph impurity quantification in a mixture with metastable polymorphic form and evaluate the sample preparation conditions effect on the phase quantification;
2. evaluate the solvent effect on the mechanochemical and classical SMPT of the metastable α tegafur to the thermodynamically stable β tegafur;
3. examine the nature of solvent vapour and tegafur surface interaction;

4. apply the knowledge acquired from tegafur α to β SMPT, to determine why thermodynamically stable theophylline Form IV can be obtained only by solvent mediated transformation in specific solvents, and to find out whether solution prenucleation aggregates affect the crystallization result in the case of theophylline.

Scientific novelty

1. Parameters affecting semi-quantitative method of low-level (down to 0.0005%) thermodynamically stable polymorph impurity determination in the metastable polymorph have been evaluated.
2. It has been shown that phase transition dynamics of α tegafur to β tegafur are in good agreement in all SMPTs studied here: solvent drop milling (mechanochemical SMPT), classical SMPT, and in samples, that were exposed to 95% solvent relative vapour pressure ("solvent vapour mediated phase transformation").
3. Solvent desorption from two tegafur polymorphs have been characterized.
4. The SMPTs from α tegafur to β tegafur and from theophylline Form II to Form IV have been examined in detail. The kinetics, phase nucleation and growth aspects of these phase transformations have been described.
5. It has been determined that SMPT rate depend linearly on the supersaturation level, i.e. difference between equilibrium solubilities of thermodynamically stable and metastable polymorph in the respective solvent.
6. The correlation between theophylline prenucleation aggregates in the solution and SMPT rate and outcome have been established.

Practical significance

1. The method, allowing to quantify down to 0.0005% of the thermodynamically stable form in bulk metastable form sample, have been proposed. This method has been successfully applied in the industrial manufacturing.
2. The contribution of several parameters in solvent drop milling have been characterized.
3. The parameters of theophylline Form IV preparation throughout SMPT have been established.

Results published

Articles

1. Determination of micro amounts of β tegafur in the α and β polymorph mixture by powder X-ray diffractometric analysis, *Sanita Petkune, Raitis Bobrovs, Andris Actiņš*, Journal of Pharmacy and Pharmacology, 2011, 63 (**9**), 1136-1140.
2. Optimization of sample preparation conditions for detecting trace amounts of β tegafur in α and β tegafur mixture, *Raitis Bobrovs, Andris Actiņš*, Journal of Pharmaceutical Sciences, 2012, 101 (**12**), 4608–4614.
3. Organic solvent vapour effects on phase transition of α and β tegafur upon grinding with solvent additives. *Raitis Bobrovs, Olga Saveļjeva, Agnese Kapace, Zane Plauka, Andris Actiņš*, International Journal of Pharmaceutics, 2013, 443 (**1**), 193-198.
4. Organic solvent desorption from two tegafur polymorphs. *Raitis Bobrovs, Andris Actiņš*. International Journal of Pharmaceutics, 2013, 457 (**1**), 110-117.
5. Solvent mediated phase transformation between two tegafur polymorphs in various solvents. *Raitis Bobrovs, Linda Seton, Andris Actiņš,* CrystEngComm, 2014, 16 (**46**), 10581-10591.
6. The Reluctant Polymorph. Self-association effect on nucleation and solvent mediated phase transformation of theophylline. *R. Bobrovs, L.Seton, N. Dempster,* CrystEngComm, 2015, DOI: 10.1039/C4CE02484B.

Conferences

1. Determination of micro amounts of β tegafur in the α and β polymorph mixture by powder X ray diffractometric analysis, *Sanita Petkune, Raitis Bobrovs, Andris Actiņš*, 3rd International Conference on Drug Discovery and Therapy, 7-10.02.2011, Dubai, UAE.
2. Detecting trace amounts of thermodynamically stable polymorph in mixture of polymorphs. *Raitis Bobrovs, Andris Actiņš*, PPXRD11, 15-18.05.2012. Fort Myers, USA.
3. Ūdens un to tvaiku ietekme uz FACV fāžu pāreju mikro un makro daudzumu līmenī. *Raitis Bobrovs, Andris Actiņš*, University of Latvia 's 70th Conference,17.02.2012, Riga, Latvia.
4. Organisko šķīdinātāju tvaiku ietekme uz ftorafūra α un β formu fāžu pāreju. *Raitis Bobrovs, Olga Saveļjeva, Agnese Kapace, Zane Plauka, Andris Actiņš*, University of Latvia 's 71th Conference, 22.02.2013, Riga, Latvia.

5. Organic solvent vapor effects on phase transition of α and β tegafur upon grinding with solvent additives. *Raitis Bobrovs, Olga Saveļjeva, Agnese Kapace, Zane Plauka, Andris Actiņš*. 7th Crystal Forms@Bologna, 9-11.06.2013, Bologna, Italia.
6. Experimental study on interaction between two tegafur polymorphs and organic solvents. *Raitis Bobrovs, Andris Actiņš*, 3rd World Conference on Physico Chemical Methods in Drug Discovery and Development, 22-26.09.2013, Dubrovnik, Croatia.
7. The solvent effect on the crystal morphology of two tegafur polymorphs. *Raitis Bobrovs, Līga Mitriķe, Andris Actiņš,* 23th Congress and General Assembly of the International Union of Crystallography. 5-12.08.2014, Montréal, Québec, Canada.
8. The Reluctant Polymorph. *Linda Seton, Raitis Bobrovs*, BACG2014: Annual Conference of the British Association for Crystal Growth, 13-15.06.2014, Leeds, UK.
9. The Reluctant Polymorph: The Effect of Self-Association on the Nucleation and phase transformation of Theophylline. *Linda Seton, Raitis Bobrovs*, Nucleation – A Transition State to the Directed Assembly of Materials, 30.03-1.04.2015, Leeds, UK.

1. Literature review

1.1. Polymorphism

Polymorphism is a well-known phenomenon, which is defined as ability of a compound to crystallize into more than one crystalline form that differs with molecule packing arrangements and/or conformations within the crystal lattice. The different resulting structures are called forms, polymorphs, phases or modifications [1,11]. About two-thirds of organic compounds and about 80% of active pharmaceutical ingredients under certain conditions can exist in more than one polymorphic form [3,5]. Differences in molecule conformation and/or packing in polymorphs results in different physical and physicochemical properties – thermodynamic stability, solubility, dissolution rate, melting and sublimation temperatures, etc. [1,3–6,11–15]. Polymorphism in elements, such as diamond and graphite forms of carbon, is usually termed allotropy [3].

Polymorphism can be divided in two groups – packing and conformation polymorphism [16,17]. Rigid molecules, without the capability of changing conformation, can give alternative crystal structures only by different molecule relative orientation or packing. This is called packing polymorphism. Conformational polymorphs, in addition to packing differences, can have significant differences between the conformations of the molecules in the polymorphs [18,19]. Molecule arrangement and conformation in crystalline solid depend on intramolecular and intermolecular interaction, like hydrogen bonging, van der Waals interactions, π-π interactions and some other weaker forces [20–26].

Term crystalline forms is wider than polymorphism and includes also non-crystalline (amorphous) forms of the same compound and solid phases where parent molecule forms a crystalline molecular adduct with another molecular species – solvates and co-crystals [3,5,11] (see Figure 1.1.). Amorphous forms differ from crystalline forms by the degree of order in solid phase. While crystalline forms have long range order, amorphous forms can have only short range periodicity and molecule arrangement is disordered [27–29]. Solvates are defined as a molecular adducts where solvent molecules are included in to the crystalline structure besides host molecules. There is no strict distinction between co-crystals and solvates, but the main difference here is that co-crystal forming host molecule is solid in normal conditions [30–36].

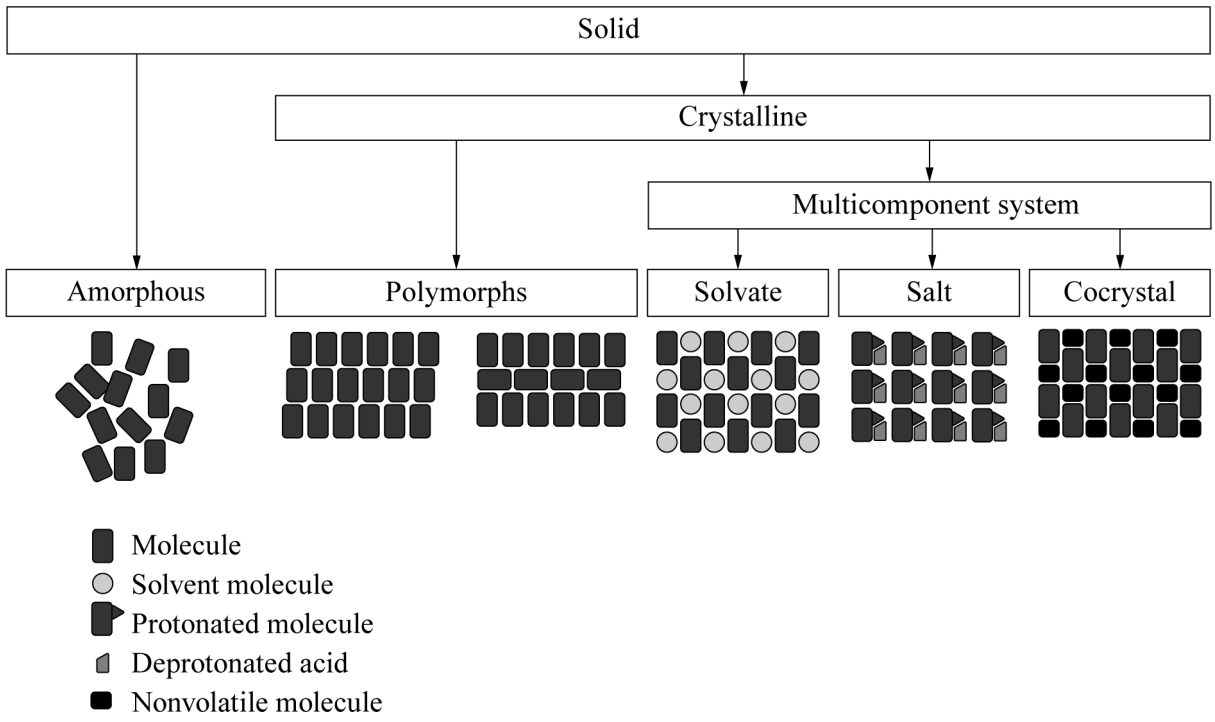

Figure 1.1. Classification of solid materials (adapted from [14])

1.1.1. Thermodynamics of polymorphs

Each solid phase has certain relative stability which is defined by the free energy difference - ΔG [1,3,5]. Only one crystalline phase is thermodynamically stable at a given conditions (with the exception of transition points), and all the rest phases are thermodynamically unstable. Term metastable phase is used to describe solid phase which can exist outside its thermodynamic stability region, and phase transition to thermodynamically stable polymorph do no occur or it is very slow. The relative stability is described with Equation 1.1:

$$\Delta G = \Delta H - T\Delta S \qquad 1.1,$$

where enthalpy difference, ΔH, is the lattice energy difference between two solid phases resulting from different intermolecular interactions in each polymorph; and entropy difference, ΔS, arise from different lattice vibrations and structural disorder in the polymorphs. Schematic polymorphic system free energy, entropy and enthalpy changes depending on temperature are shown in Figure 1.2.A. Over the temperature range in which polymorph can exist, the enthalpy of the crystal increases with the rising temperature due to molar volume increase and intermolecular interaction weakening. The entropy, initially zero at 0 K for ideal crystal, increases due to the increasing population of higher energy levels of lattice vibrations. These thermodynamic parameters are different among the various polymorphs at a given temperature

(see Figure 1.2.B). Since polymorph free energy dependence on temperature differ from one polymorph to another, at some temperature respective polymorph free energy curves cross and two polymorphs have equal free energy – they are in equilibrium. This temperature is referred as a phase equilibrium temperature. Under the equilibrium temperature polymorphic form I is thermodynamically stable ($G_{form\ II} > G_{form\ I}$), whereas above this point polymorphic form II has the lower free energy and is therefore more stable ($G_{form\ II} < G_{form\ I}$). At a given condition only one polymorphic form can be thermodynamically stable, and all other polymorphs must be thermodynamically unstable. Thermodynamics of polymorphic system shows the relative stabilities of polymorphs, but does not indicate anything about phase transition rate.

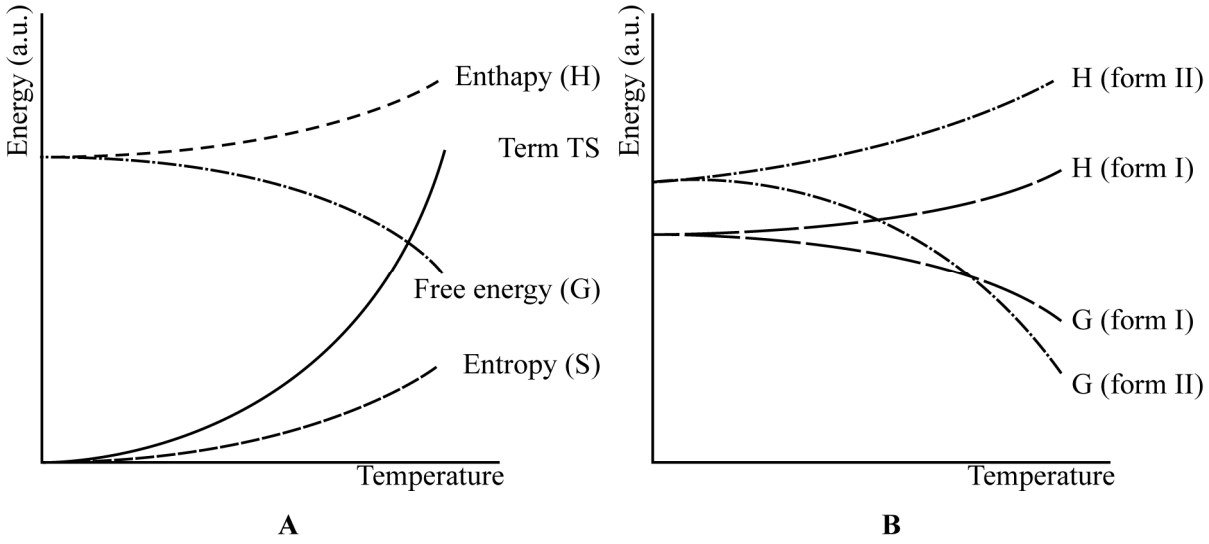

Figure 1.2. A) Variation in enthalpy, free energy, entropy and term TS with temperature for a crystalline phase; B) variation in enthalpy (H) and free energy (G) with temperature for two polymorphic forms (adapted from [3]).

1.1.2. Enantiotropy and monotropy

As mentioned above, there is an equilibrium point at which two polymorphs have equal thermodynamical stability. If this equilibrium point is below the melting point of both polymorphs, i.e. each of the polymorphs has a temperature range in which it is stable with respect to the other polymorph, the two forms are said to be enantiotropically related. Variations in free energy with temperature in enantiotropically related system are given in Figure 1.3.A. Form I is thermodynamically stable below equilibrium temperature, whereas form II is thermodynamically stable in the temperature region from equilibrium temperature up to

melting temperature. If one polymorph is thermodynamically stable with respect to the other polymorph in all temperature region below their melting points, the two forms are said to be monotropically related. Other polymorph in this case is thermodynamically unstable in all temperature-pressure region. Figure 1.3.B illustrates free energy variations in monotropically related polymorphs, where form I has the lowest free energy in all temperature region below melting temperature. In monotropically related system polymorph equilibrium temperature is above melting temperature.

Isolation of specific polymorphic form requires control over the isolation conditions. The isolation of polymorph from enantiotropic system is relatively easy, because it is possible to identify and use the conditions at which one polymorph or the other is thermodynamically stable and will crystallize. The isolation of the thermodynamically stable polymorph in a monotropic system can usually be achieved without great difficulty. Isolation of the unstable form, however, requires conditions where desired polymorph is characterized as being most metastable.

The polymorphic systems studied in this work – α and β tegafur; and theophylline Form II and Form IV – are enantiotropically related.

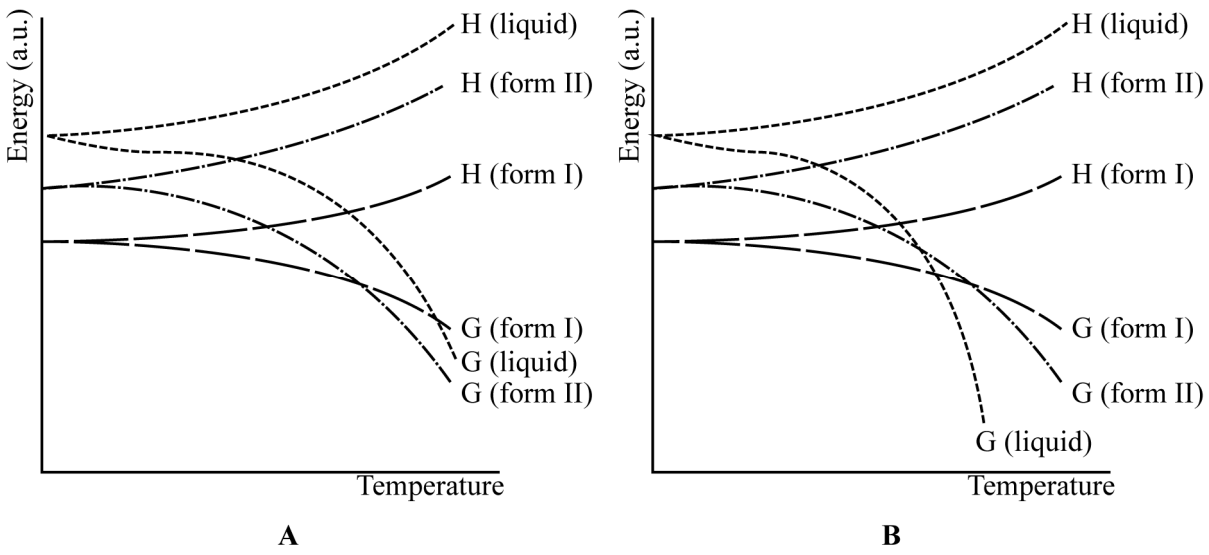

Figure 1.3. Variations in enthalpy (H) and free energy (G) with temperature in: A) enantiotropically related polymorphs; and B) monotropically related polymorphs (adapted from [3]).

1.2. Crystallization

Crystallization is the most common method of chemical compound isolation from solution, and it is governed by a combination of thermodynamic and kinetic factors. It is also the most popular method for polymorph isolation, where different polymorphs are obtained by varying crystallization methods and conditions. Crystallization method typically used in pharmaceutical industry is crystallization from solution (single solvent or solvent mixture), using different experimental conditions, such as temperature, initial supersaturation, rate of desupersaturation, and rate of agitation. Other methods occasionally used in polymorphic crystallizations are crystallization from melt, sublimation, suspendation, etc. [37–41]

Crystallization from solution is a multi-step process, which includes nucleation, crystal growth and Ostwald's ripening [40–44]. Nucleation and crystal growth are the steps which determine the polymorph that will crystallize (discussed further in Section 1.2.1), whereas Ostwald's ripening is a process when crystals tended to achieve minimum total surface energy by reducing crystal surface area [37]. This is achieved by dissolution of smallest particles (because of higher surface energy) and subsequent dissolved material crystallization on the surface of largest particles. Eventually, such crystal agitation should lead to monosized spherical particles.

Crystallization of polymorphs often follows Ostwald's rule of stages [7], which postulates that crystallization in a polymorphic system progresses from supersaturated state to equilibrium state in stages. Thus, according to Ostwald's rule of stages, the metastable form should crystallize first and then the system should move through each possible polymorphic structure before the thermodynamically stable polymorph crystallizes. In the majority of cases the thermodynamically stable polymorph in given conditions is isolated, however, solvent used for crystallization can affect the crystallization outcome and it might promote the crystallization of a specific metastable polymorph.

1.2.1. Nucleation and crystal growth

Crystallization from solution requires supersaturation to initiate crystal formation and continue crystal growth. Supersaturation is defined as the ratio of the actual solute concentration to the solubility of solute, and it is one of the most important factors affecting

crystallization, because it provides the driving force to overcome nucleation activation energy and provides molecule transport to nucleation site [43,45–49]. A supersaturated solution is thermodynamically unstable and eventually undergoes phase separation process where solute molecules self-associates into clusters and can act as centres of crystallization. These molecular clusters increase their size by molecule addition and eventually results in nuclei and further in crystallites. Classical nucleation theory assumes that the viability of pre-nucleation molecular clusters with mean radius r depends on attainment of the critical cluster size (with mean radius r_c). Critical cluster or critical nuclei is the smallest molecular aggregate capable of independent existence in the supersaturated solution. Critical nuclei are too small to be observed directly, and therefore their structure is not known, but Mullin have proposed [37] that the structure of a critical nucleus could be anything from a diffuse molecule agglomerates to a perfect miniature crystal. Term cluster is used to describe thermodynamically unstable molecular aggregates with radius (r) lower than critical radius (r_c), whereas term nuclei represents thermodynamically stable molecular aggregates with $r>r_c$.

Nucleation in the solution can be either homogenous, where nuclei are forming spontaneously in the bulk solution, or heterogeneous, where crystal nucleation is induced by the surfaces, interfaces, or by foreign particles. Homogeneous nucleation virtually does not occur, because nucleation activation energy in the bulk is higher than activation energy at the surface. Therefore, nuclei form heterogeneously at the nucleation sites where activation energy is lower – on the surfaces and interfaces. One special case in nuclei formation is seeding, where crystals of the solute are already present or are deliberately added to the solution. Added parent crystals catalyse the nucleation in the supersaturated solution and therefore nucleation can proceed at lower supersaturation levels than required for homogeneous nucleation. [39,41,48,50,51]

Reduction in free energy is the thermodynamic driving force for both heterogeneous and homogeneous nucleation [52–55]. The total free energy of molecule cluster (ΔG_{Total}) is the sum of a cluster volume free energy (ΔG_{Volume}) that favours molecule aggregation and a cluster surface free energy ($\Delta G_{Surface}$) that favours the dissolution of molecular cluster:

$$\Delta G_{Total} = \Delta G_{Surface} + \Delta G_{Volume} = 4\pi r^2 \gamma + \left(\frac{-4\pi^3 kT \ln \sigma}{3\nu} \right) \qquad 1.2,$$

$$G_c = \left(\frac{16\pi v^2}{3(kT\ln\sigma)^2}\right) \quad 1.3,$$

where r is the mean radius of the cluster, k is Boltzmann's constant, T is absolute temperature, γ is the interfacial free energy between the nucleus and the supersaturated solution, σ is the supersaturation ratio, v is the molecular volume, and ΔG_c^* is the free energy barrier to nucleation. Nucleation free energy barrier, ΔG_c^*, can be used to calculate nucleation rate:

$$J = Ae^{\left(\frac{-\Delta G_c^*}{kT}\right)} = Ae^{\left(\frac{-16\gamma^3 v^2}{3k^3T^3(\ln\sigma)^2}\right)} \quad 1.4,$$

where A is the pre-exponential factor. Interfacial free energy between the nucleus and the supersaturated solution, γ, can be calculated by Mersmann equation:

$$\gamma = 0.414kT\left(c^S N_A\right)^{2/3}\ln\left(\frac{c^S}{c^*}\right) \quad 1.5,$$

where c^s is the molar density of the polymorph, $c^\star$ is the solute concentration, and N_A is Avogadro's number.

The ratio of cluster volume and surface free energy terms in Equation 1.2 define weather cluster will grow into nuclei and larger crystals or dissolve back in the solution phase. During the initial cluster formation, when $r < r_c$, cluster surface free energy, $\Delta G_{Surface}$, is larger than cluster volume free energy, ΔG_{Volume}, and cluster is thermodynamically unstable – it has a tendency to dissolve. Cluster growth is promoted by supersaturation which provides the necessary driving force to overcome the disruptive surface free energy $\Delta G_{Surface}$. Eventually, the cluster size increases and critical nuclei size is reached (r=r_c) at which the surface and volume terms are equal and total free energy of the cluster are maximal (see Figure 1.4.A). This energy corresponds to nucleation activation energy and molecular aggregate at this point is termed critical nuclei or critical cluster. After this stage, when $r > r_c$, cluster becomes viable and can be considered as nucleus that eventually grows into a crystal. If cluster does not reach r_c it dissolves and does not yield a crystal. [5,16]

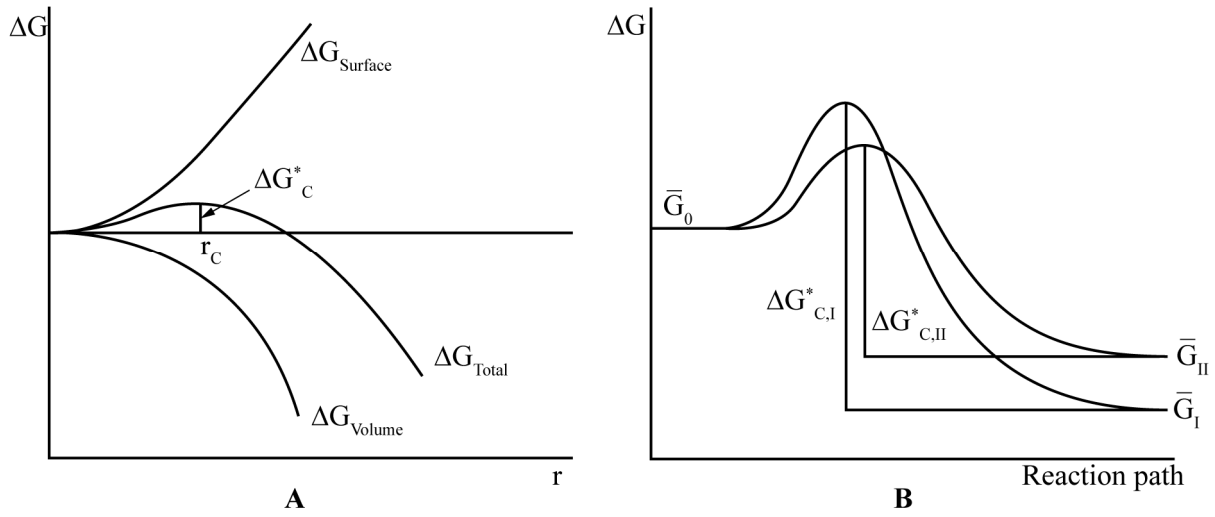

Figure 1.4. A) Cluster free energy change during molecular aggregation depending on cluster/nuclei radius; B) Free energy change during polymorph I and II nucleation (adapted from [5]).

In a solution of polymorphic system (consisting of two polymorphs – thermodynamically stable form I and thermodynamically unstable form II) molecular clusters of both polymorphs are competing for solute molecules during nucleation [56], and concentration of respective nuclei in solution is determined by their free energy. The polymorph with lower free energy barrier will crystallize first, thermodynamically unstable form II in this case, because $\Delta G^*_{c,II} < \Delta G^*_{c,I}$ (see Figure 1.4.B). Thermodynamically unstable form II grows first because cluster formation free energy is lower for this polymorph, however, thermodynamically stable polymorph crystallize because formation of this polymorph is energetically favourable. The nature of polymorph that eventually crystallizes is determined by the relative nucleation and crystal growth rates in respective polymorphic system, however, in most cases nucleation is the key step that determines polymorph that crystallizes. Schematic crystallization process of two competitive polymorphs is given in Figure 1.5.

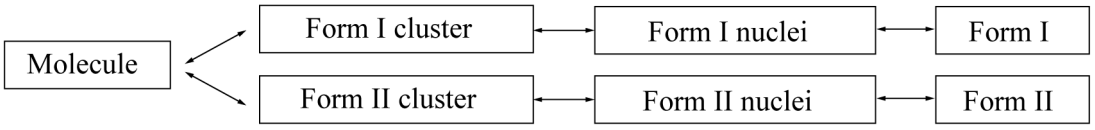

Figure 1.5. Schematic representation of two competitive polymorph crystallization (adapted from [5]).

1.3. Spectroscopic self-association studies

The information about the prenucleation aggregates are essential to understand the process of crystal nucleation and enlighten us on selective polymorph crystallization from specific solvents. Furthermore, Hunter *et al.* [57–59] and Davey *et al.* [60,61] have showed that there is a direct correlation between supramolecular aggregates structure in solution and the solid state structure. However, the main obstacle for prenucleation aggregate studies are the fact that there are only few methods suitable for such task. The techniques successfully used to study crystal emergence in diluted solutions, supersaturated solutions and melts are small angle and wide angle X-ray scattering, Raman spectroscopy, mass spectrometry and solution NMR [62–67]. Here we used ^{1}H NMR spectroscopy to investigate solution aggregation processes, therefore this approach will be discussed in detail.

NMR spectroscopy is mainly used as a method for organic compound identification and characterization; however NMR methods have been demonstrated to be useful for the study of molecular aggregation and self-association in solution. The first attempts to use NMR spectrometry to examine self-association were more than half century ago [68–70]. Becker et al. and Huggins at al. studied the hydrogen bonding in alcohols and phenols. ^{1}H chemical shifts of alcohol and phenol hydroxyl group protons were measured over a wide concentration range and variation of ^{1}H chemical shifts with concentration was consistent with expectations for a system consisting of monomers, dimers, and higher polymers.

It is possible to use solution NMR measurements to study molecular association because ^{1}H chemical shifts are sensitive to changes in the local environment. Hydrogen bonding between solute molecules and associate formation affects ^{1}H local environment and a result of this interaction is a chemical shift displacement in the NMR spectrum.

It is generally recognized that dimer and other associate formation and their concentration are affected by solution concentration – the more concentrated the solution, the more dimers and other associates are present. In order to obtain information about self-association in the solution, the dependence of ^{1}H chemical shifts on concentration is analysed. Self-association studies of adenosine 5'-triphosphate (ATP) [71]; caffeine [72]; adriamycin and daunomycin [73]; chloroquine [74]; actinomycin D [75]; proflavine, Acridine Orange, ethidium bromide, actinomycin D [76]; flavin mononucleotide [77]; acridine homodimer and its complex with

ethidium bromide [78] and vanillin [79] are a few examples of such an approach. This effect also has been used to determine self-association constants, enthalpy and entropy of dimerization [72,73,78,80].

Most of the previous studies show a decrease in the ^{1}H chemical shifts with concentration increase, suggesting that the analysed compounds are involved in self-association processes. The reason why ^{1}H chemical shifts are displaced to the lower field for self-associated compounds can be explained by the hydrogen bond forming proton deshielding. Upon association the hydroxyl group O–H bond (or any other association involved bond) weakens and the bond length increases [81–84]. This produces a decrease in the O–H stretching frequency and a large deshielding of the O–H proton, resulting in a ^{1}H chemical shift displacement to lower field [85]. Hence, the larger the fraction of associated molecules in the solution, the more ^{1}H chemical shifts of hydrogen involved in the association will shift to the lower fields. There is no clear consistency in the chemical shift displacement upon self-association in previously mentioned studies and it varies from compound to compound. For example: Lam and Kotowycz [71] indicated that the ^{1}H chemical shift displacement with concentration changes had a sigmoidal nature for three proton chemical shifts; Abraham and Mobli [84] and Bogdan *et al.* [79] have reported almost linear ^{1}H chemical shift displacement upon concentration change; however, in most cases, exponential ^{1}H chemical shift displacement upon self-association has been observed.

In recent years, ^{1}H NMR chemical shift displacement measurements have been used to provide information on the structure of prenucleation aggregates in the solution [86]. It is possible because the dimer formation and aggregation in solution are the first stages of crystallisation and therefore the structure of the supramolecular aggregate, which is formed in solution, influences the solid state structure obtained on crystallization [58]. Hunter *et al.* [59,87] showed that the predictions from concentration-dependent changes in ^{1}H NMR chemical shifts agreed with the structures of dimers found in the corresponding X-ray crystal structures (see Figure 1.6.). The same approach has been successfully used to study ligand binding [57,88] and cocrystallization [60].

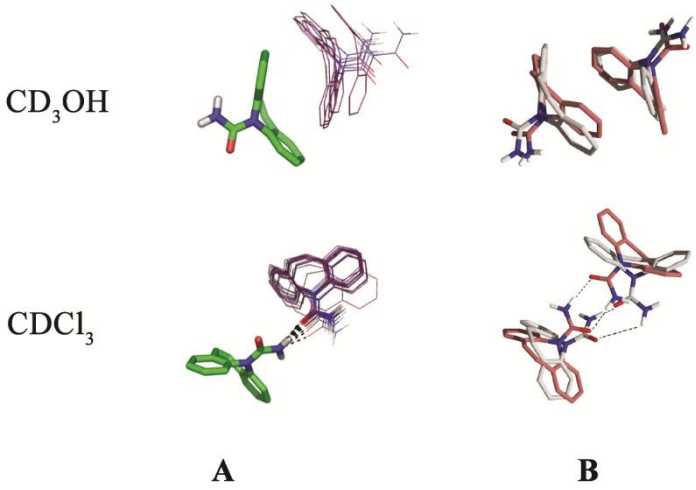

Figure 1.6. A) Carbamazepine dimer structures in CD3OH and CDCl3 calculated using SHIFTY [86]**. One molecule of the dimer is overlaid in a fixed position (green) and the positions of the second molecule in different structures generated by SHIFTY are shown in violet. B) Comparison of dimer motifs found in the X-ray crystal structure of carbamazepine form III (grey molecule) with dimer motifs in the solution calculated by SHIFTY (red molecule) (adapted from** [59]**).**

Other magnetically active nuclei (^{13}C, ^{15}N and others) involved in hydrogen bonding or aromatic stacking also show displacement in chemical shifts upon concentration changes. ^{13}C NMR spectroscopy has been used to study hydrogen-bonded complexes of pyrimidines and purines [89]; self-association of retinoic acid [90]; aromatic stacking interactions of supramolecular zipper complexes [91] and to study fundamental aspects of the crystallization of glycine [92]. Lam and Kotowycz [71] have used ^{31}P NMR spectroscopy to study adenosine 5'-triphosphate (ATP) self-association.

There are several limitations for self-association studies using NMR method. ^{1}H NMR shifts only for nonexchangeable hydrogens can be measured. If the proton, involved in the self-association, easily and completely exchanges with solvent deuterium atoms, no chemical shifts of this proton can be measured, as the deuterium atom replacing the proton is not magnetically active. However, if the solution concentrations are high and complete deuteration does not occur, then ^{1}H NMR shift of exchangeable proton can be observed and measured. Hughes *et al.* [92] have mentioned that the resultant level of deuteration for the exchangeable hydrogens in the glycine and D_2O system ranged from 91.2% for the 3.6 M solution to 99.9% for the 0.05 M solution. It was also observed that the level of deuteration was found to have no significant effect on the NMR spectrum. Another limitation is that the NMR method has a limited sensitivity at

the low concentrations often necessary for initial self-association studies. This problem cannot be solved, therefore other complementary methods, like UV spectrometry are used for self-association studies.

It has been reported [93] that compound hydrogen bound association have an effect on the UV absorption spectrum and it is possible to use this effect to study molecular association as well as self-association [94–96]. The self-association studies by UV spectroscopy use the same approach that NMR studies – UV spectra are measured over the concentration range. The method is based on the detection of deviation from the Beer-Lambert law with concentration changes [94–100]. The variation of apparent molar absorption coefficient as a function of concentration can be used to calculate the self-association constants, with the assumption that the detected hyperchromic and hypochromic effects result exclusively from the self-association of the studied compounds [96].

1.4. Solid state reactions and polymorphic transformations

The most stable phase in given conditions is defined by polymorphic system thermodynamics, whereas phase transformations rate from one phase to another is affected by kinetic assumptions. Kinetics and thermodynamics of chemical reactions were developed for homogeneous systems, where all of the components involved in the reactions are in liquid or gaseous state and molecules are evenly distributed in a reaction volume. The homogeneous reactions usually occur between freely moving, identical reactant molecules with random collisional encounters that are usually unaffected by product formation.

Solid-state reactions studied here, however, are heterogeneous, and homogeneous reaction principles cannot be applied directly. Rate laws describing heterogeneous solid-state reactions are more complex than those in homogenous phases, and therefore universal kinetic model that could describe most of the solid-state reactions properly is still not developed [101]. Technically, polymorphic phase transformations are not solid-state reactions, because no chemical bonds are braked or formed, however, solid-state models are used to describe these transformations as well, because crystal structure and hydrogen bonding network change during polymorphic transformation [102,103]. Kinetic assumptions described in this section applies to both – chemical solid-state reaction and polymorphic transformations.

1.4.1. General aspects of solid-state reactions

Reaction rate in classical homogeneous kinetics is expressed as concentration change throughout reaction. For first order reaction

$$A \rightarrow B \qquad 1.6$$

reaction rate (v) is defined as

$$v = \frac{d[B]}{dt} = -\frac{d[A]}{dt} = k[A] \qquad 1.7,$$

where k is first-order reaction constant. If the rate constant k follows Arrhenius behaviour, we can write that

$$k = Ae^{-E_a/RT} \qquad 1.8,$$

where A is the pre-exponential factor, E_a is the activation energy, and T is the temperature (K). Equation 1.8 describes reaction which has one transition state, however, this is not necessarily the case for reactions in solids and polymorphic transformations, because there is no bond breaking or formation like in homogeneous reaction. The activation energy for reactions in solid-state cannot be interpreted in terms of bond breaking and bond making, therefore activation energy for reactions in solid-state are related to the solid phase nucleation, diffusion or advance of the product phase, or some other process that may be of a physical nature. Because of this, solid-state kinetic reactions and polymorphic transformations are mechanistically classified according to reaction limiting step as: nucleation, geometrical contraction, diffusion, and reaction order models (see section 1.4.2). [101]

Term concentration, generally used in homogeneous reactions, is not applicable (it does not have any physical meaning) in heterogeneous reactions, because reactions take place on the phase contact zone and crystal defects. Therefore reaction rate in solid-state reactions are expressed by the fraction of the sample reacted, α, which show what part of starting material have transformed to reaction product. The degree of conversion, α, changes from 0 to 1. The rate of the reaction may be expressed as $d\alpha/dt$, and the reaction has gone to completion when $\alpha=1$. Very often weight fraction of starting material or reaction product, w, is also used to describe conversion rate. Thickness of the product layer, weight of product, or moles of product can be used as well. Solid-state reaction progress throughout phase transformation (kinetic curve) usually is plotted in coordinates α-*time* (Figure 1.7.). [101,103]

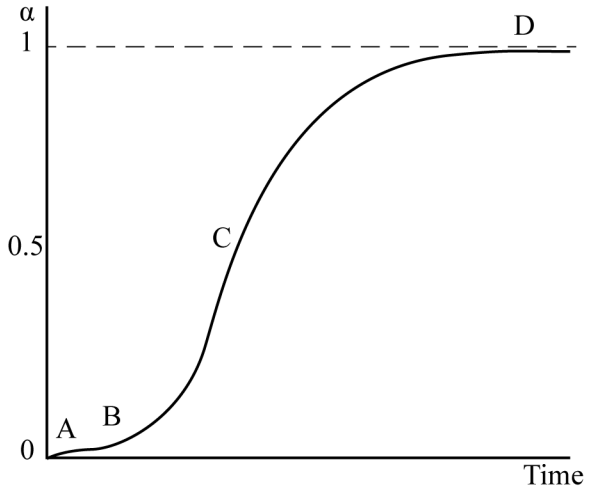

Figure 1.7. Schematic kinetic curve of solid-state reaction (adapted from [5]).

The region A in the kinetic curve represents small mass loss, associated with the removal of adsorbed gases from the sample. This step is not always observed. Following region B represents an induction period where reaction/phase transformation rate is beginning to accelerate. Induction time is associated with critical nuclei size reaching time and/or sample heat up. Region C represents part of kinetic curve where solid-state reaction/phase transformation is progressing at the maximum rate. For most reactions in homogenous phase the initial reaction rate is also the maximum rate, because reactant concentration in highest at the beginning of reaction, however, heterogeneous solid-state reactions reaches maximal rate eventually. This is because solid-state reactions starts in few energetically favoured points – nucleation sites, they spreads over the time, thereafter accelerating the reaction. The final part of kinetic curve is region D where reaction is starting to slow down as the reaction approaches completion.

1.4.2. Solid-state kinetic models

Solid-state kinetic models are theoretical, mathematical descriptions of experimental data and usually are expressed as rate equations. Many solid-state kinetics models have been developed based on certain mechanistic assumptions, while other models are more empirical and may have little mechanistic meaning. Models currently used in solid-state kinetic studies are classified according to their rate limiting mechanistic features, such as nucleation, geometrical contraction, diffusion, and reaction order. [104]

Nucleation models. The limiting step in this case is nucleation of resultant phase into the starting material. Nucleation occur in nucleation sites, where reaction activation energy is

minimized, but when nuclei of resultant phase have formed, phase transformation continues to grow with constant speed (weight fraction of resultant phase increases proportionally to surface area).

Geometrical Contraction models. In this case it is assumed that nucleation occurs rapidly on the surface of the crystal. The rate of transition is controlled by the resulting reaction interface progress toward the centre of the crystal. This means that, transformation rate depends on crystal shape.

Diffusion models. In contrast to homogeneous reactions, where reactant molecules are usually readily available to one another, solid-state reactions often occur between crystal lattices where molecules that must permeate into lattices are restricted and may depend on lattice defects. If reaction rate is controlled by the movement of the reactants to or products from the reaction interface, solid-state transformation is called to be diffusion controlled.

Order-Based models. These models are the simplest models as they are similar to those used in homogeneous kinetics. Here reaction order is proportional to resultant phase concentration raised to a particular power which is the reaction order. Order-based models are derived from the equation

$$\frac{d\alpha}{dt} = k(1-\alpha)^n \qquad 1.9,$$

where $d\alpha/dt$ is the rate of reaction, k is the rate constant, and n is the reaction order.

The kinetic models commonly used to describe phase transformations and reactions are summarized in Appendix 1.

1.4.3. Classical monomolecular reaction kinetics

No induction time has been observed in polymorphic transformation studied, between α and β tegafur [105], and its phase transformation kinetic behaviour coincide with classical kinetic model. Therefore, let's take a look at classical monomolecular reaction kinetics as well.

If reaction follows first order, reaction rate can be expressed through reactant weight fraction change over the time $d\alpha/dt$. If the amount of reactant is represented by its weight (m), then rate law is

$$-\frac{dm}{dt} = km \qquad 1.10.$$

Integrated rate law is

$$\ln\frac{m_0}{m} = kt \qquad 1.11,$$

where m_0 represents the weight of reactant at the beginning of reaction. Conversion degree or fraction reacted (α) is calculated as

$$\frac{m_0 - m}{m_0} = 1 - \frac{m}{m_0} = \alpha \qquad 1.12.$$

We see that $\frac{m}{m_0} = 1 - \alpha$; and substituting this in Equation 1.11 we obtain

$$-\ln(1-\alpha) = kt + C \qquad 1.13,$$

where C is constant, corresponding to initial weight fraction of compound studied in initial sample [106]. In addition to solid-sate kinetic models, this equation in slightly modified form will be used to describe the solid phase transformations between α and β tegafur.

1.5. Mechanochemistry

Term mechanochemistry refers to chemical reactions and solid-state processes that are initiated by mechanochemical treatment or uses mechanically activated reagents [107,108]. Mechanical activation in a ball mill is the most commonly used technique in mechanochemistry, due to methods simplicity, relatively low costs, and because of technologist interest, since it is one of the most popular shredding methods. Mechanochemical processing in ball mill is a combination of two processes – crystal shredding (increase of the surface area) and crystal deformation. Since these processes cannot be separated, studies in this field are encumbered and crystal shredding and deformation are explored jointly [109–112].

The energy in milling system have been categorized into the *energy applied* and the *energy required*. The energy applied is the energy that is provided by the milling equipment to reduce the particle size, whereas energy required is the amount of energy necessary to overcome the particle strengths during particle fragmentation. During the milling process, energy applied far exceeds the energy required, and the excess energy is usually utilized in the processes that are not related to particle size reduction, like, elastic or plastic particle deformation; elastic energy dispersion in the milling equipment; friction, noise, heat and vibration in the milling equipment [108,112–116].

The energy required to reduce particle size vary considerably, as the strength of the material is known to vary with particle size. The largest particles tend to be weaker as compared to their

smaller counterparts, therefore, it is not surprising that sample mechanical properties may vary from particle to particle even for the same size range of a material. This means that there may be situations when under the same applied energy, some particles may undergo size reduction while others don't [112]. A gradual decrease in the size of particles subjected to the mechanical treatment results in a transition from milling to plastic deformation. This means that besides particle size reduction, sample, subjected to mechanochemical treatment, is also mechanochemically activated by formation of crystal defects, plastic and linear deformations, dislocations, ion and atom vacancies, and interstitial ions. Therefore, mechanical treatment can be used to activate the surface of a powder by energy accumulation in the form of defects or other structural modifications of a solid, which makes it possible to minimize the activation energy or improve steric conditions for its subsequent chemical transformations. The accumulated energy is referred as a stress field created in the system. In the single-phase system the relaxation of stress field can proceed by several pathways which are accompanied by various secondary processes, such as heat liberation, formation of new phases or interfaces, crystal defect accumulation, amorphisation or chemical transformations. The factors affecting the formation and relaxation of a stress field are summarized in Figure 1.8. [107,113]

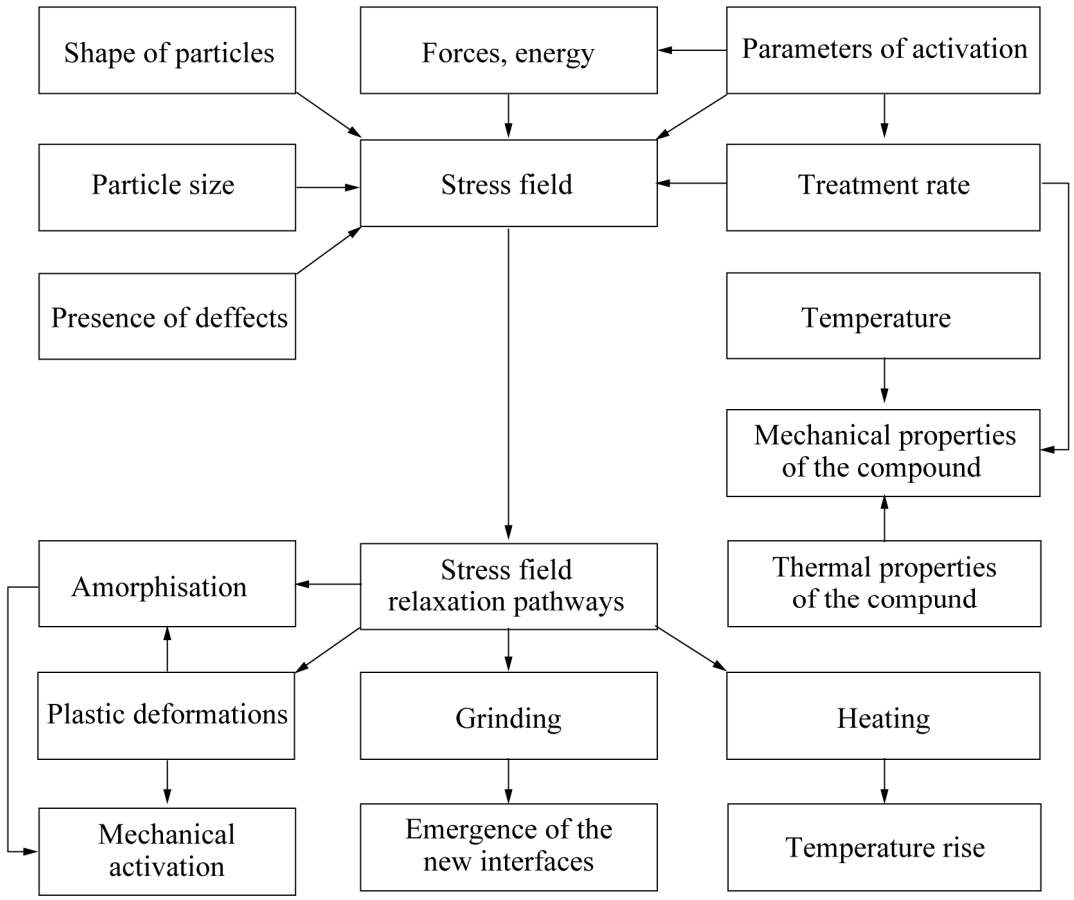

Figure 1.8. Schematic representation of the factors affecting the formation and relaxation of a stress field (adapted from [107]**).**

1.5.1. Milling of pharmaceutical powders

In the pharmaceutical industry, mechanical particle size reduction is a very important operation which affects product handling and performance, such as flow, drug stability, solubility and dissolution rate [109,110,113,117–122]. Other, maybe even more important consequence of the mechanochemical treating, is crystal phase of polymorphic transformation. First crystalline phase changes upon milling was observed by Florence *et al.* [123] in digoxin, and Lee and Hersey [124] in methisazone about half century ago. Nowadays, mechanochemically induced phase transformations are widespread in fundamental research and industry [109,110,118,125–127]. Müller and Polke [128] have reported that human body absorbs amorphous materials much more rapidly than crystalline substances, therefore solubility and biological activity of poorly soluble pharmaceutical drugs are very often improved by drug amorphisation. Lately, besides polymorphic transformation and amorphisation studies,

a lot of studies in this area are devoted to pharmaceutical cocrystal formation upon milling [129–140].

To initiate phase transformation or amorphisation it is necessary to overcome the phase transformation energy barrier, which, as discussed previously, is necessary to change the molecule arrangement and packing in the crystal lattice. The amount of energy induced in the system usually adjust by changing the mechanochemical treatment (milling) time and frequency [113,141].

It is worth noting that mechanochemically induced polymorphic transformations always occur from metastable from to more stable form [142] (amorphous form is not a polymorphic form; see Section 1.1). Changes in the crystalline state occur due to mechanically induced hydrogen bonding and other intra- and intermolecular interaction changes. However, it is common that hydrogen bonding network does not change during the mechanical treatment, but only weakens. Such bond weakening leads to highly energetic intermediate state – amorphous state, which, depending on the system energetic landscape, might be metastable [143]. Very little research has been directed at understanding the mechanism of organic cocrystal formation by solid-state milling, mostly, due to lack of methods suitable for such studies. However, Etter *et al.* [144] stated that in solid-state milling "at least one of the components should have some volatility at the temperature of the milling experiments, and the product dimers should have a stronger intermolecular hydrogen bond than any of the hydrogen bonds in the structures of the two starting materials". The comment regarding volatility, are supported by the findings of Rastogi *et al.* [145,146], that showed that the yield of a solid-state cocrystallization may be improved by heating the starting materials before the milling.

1.6. Solvent-surface interaction

One of the most popular solvents used in the pharmaceutical industry is water, therefore most of the studies in the field are looking at water-solid interactions. Water-solid system will be reviewed here, but generally the same rules apply to other solvent systems.

Water may be introduced into a solid as a result of processing, such as spray-drying, freeze-drying, aqueous film coating, crystallization, wet granulation, or by exposure to water vapour environment at a certain relative humidity [147]. Water molecules can interact with the solid

compounds through hydrogen bonding, van der Waals forces, and, if the solid is ionic, through cation-water and anion-water interactions [148–151]. Water can interact with crystalline solids by sorption at the solid surface, in-corporation into the lattice (hydrate formation), deliquescence and capillary condensation (schematically represented in Figure 1.9.). Water adsorbs on surfaces in the form of individual molecules, clusters, monolayers and multimolecular layers that eventually condense as water. Deliquescence and capillary condensation, where the amount of associated water is much larger than in the rest of the interactions, may result in a water-soluble compound dissolution in the condensed water. Water can dissolve in the solid due to system disorder, as it can act as a plasticizer, penetrate the material, thereby facilitating greater solid compound molecule mobility and crystallization of the amorphous material. [147]

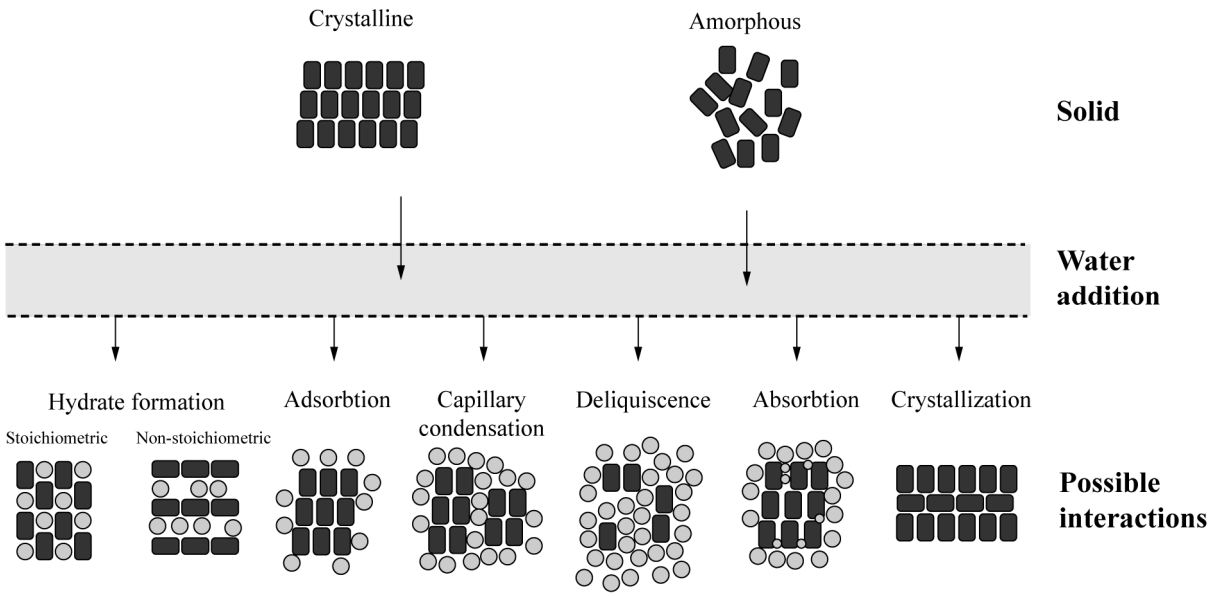

Figure 1.9. Schematic representation of possible water–solid interactions (adapted from [5]**).**

1.6.1. Solvent sorption/desorption

The physicochemical process where components of one phase are accumulated on two phase boundary is called adsorbtion [152]. The adsorption process is sometimes accompanied by absorption, i.e. the process where adsorbent molecules penetrates into the bulk of the solid phase [153]. The term sorption is used to include both – adsorption and absorption processes [154]. Solvent molecules on the solid sample surface adsorb mostly in a monolayer, where solvent molecules are interacting with sample surface through hydrogen bonding [155].

However, in the elevated vapour pressures more than one layer of solvent molecules may adsorb – up to 4-5 molecular layers below the deliquescence point [156,157]. Water sorption on the surface is reversible process, where minor temperature increase or relative vapour pressure decrease promotes water desorption from the sample surface. The amount of water sorbed depend on the nature of the compound and, most of all, on its crystallinity. Samples with high crystallinity can sorb relatively small amounts of vapour due their relatively small surface area, whereas amorphous samples can sorb much larger amount of vapour due to large surface area and lack of the long range order [158–160]. This effect is sometimes used to characterize sample crystallinity [149,161,162].

Experimental sorption isotherms – the curves obtained by plotting the weight change of a sample versus the relative humidity or water vapour pressure, usually show distinct characteristics for every vapour-solid system. The majority of physical adsorption isotherms can be classified into five classes (see Figure 1.10.) [5]. The type I isotherms are typical for chemisorption, where sorption is limited to a few monolayers of absorbate, and at high pressures isotherm plateaus as the pores are filled with absorbate. Type II isotherm is characteristic for physical adsorption on nonporous or microporous adsorbent (inflection indicates the first monolayer formation). In the sorption process, described by type III isotherm, additional adsorption at higher vapour pressures occurs as the adsorbate preferentially interacts with the monolayer than with the adsorbent surface (i.e., heat of adsorption < heat of liquification). Type IV isotherm is typical for porous surfaces (infection indicates monolayer formation), whereas small adsorbate-adsorbant interaction and capillary condensation in porous surfaces is observed in sorption processes described by type V isotherm [5]. Sorption isotherms IV and V given in Figure 1.10. show hysteresis, which is defined as mismatch between sorption and desorption paths. The lower part of hysteresis is observed during vapour pressure increase, whereas upper part (dashed line) is observed when vapour pressure is decreased [163,164]. The presence of the hysteresis depend on the sample nature, but experiments of Kiselev[87] and Carman [165] have showed that sample processing in high pressure induced hysteresis for samples that here described with type II sorption isotherms. These changes were explained by the fact that in increased pressure particles are packed more closely, therefore enabling capillary condensation, which is considered as one of the causes why hysteresis is

observed. Some other causes of hysteresis are: a) sample surface area change during sorption, therefore, the amount of vapour sorbet at given partial pressure changes; b) kinetic factors – equilibrium is not achieved during sorption and/or desorption; c) physicochemical transformation takes place during sorption/desorption [166].

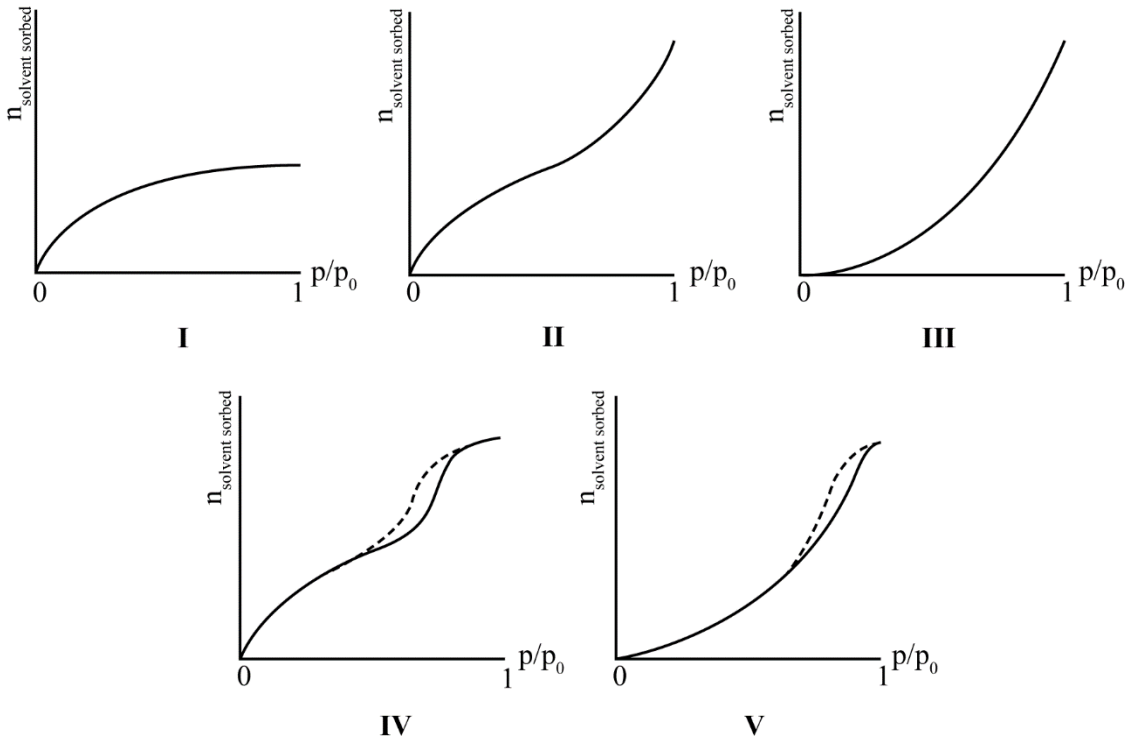

Figure 1.10. Types of sorption/desorption isotherms (adapted from [5]).

Gravimetric vapour sorption methods have been widely used to study the interaction of solvent with the pharmaceutical materials [148,167]. The most popular method of vapour sorption isotherm construction is DVS (Dynamic vapour sorption). The DVS measures the sample mass change over the time at various vapour pressure conditions. The sample mass increase here is associated with vapour sorption, while a decrease is due to vapour desorption. The vapour pressure around the sample is controlled by mixing saturated and dry carrier gas streams, and it is almost exclusively used to study water systems [168,169]. Vapour sorption techniques are widely used to investigate solvate formation, particularly hydrates [148,149]. In the same way vapour sorption/desorption techniques can be used to study amorphous material relaxation to their more stable crystalline state. The amorphous materials typically have a greater water vapour sorption capacity than the crystalline material, due to increased void space, free energy, and/or surface area, but when the material undergoes an amorphous to crystalline

transition, the water sorption capacity drastically decreases [169]. The result of this process is an overall sample mass loss as excess water is desorbed during the crystallization.

Early description of vapour molecule adsorption on a solid surface at a fixed temperature was proposed by Langmuir [170]. The equation was stated as:

$$\theta = \frac{\alpha\left(\frac{p}{p_0}\right)}{1+\alpha\left(\frac{p}{p_0}\right)} \qquad 1.14,$$

where θ is the fractional coverage of the surface; $\left(\frac{p}{p_0}\right)$ is relative vapour pressure; and α is a constant. Brunauer, Emmett and Teller [171–173] extended the Langmuir single layer adsorption equation to describe multilayer adsorption. Their model described situation where adsorbed molecules in one layer can act as adsorption sites for the molecules in the next layer. The proposed equation for the BET model was:

$$W = \frac{W_m C_B\left(\frac{p}{p_0}\right)}{\left(1-\left(\frac{p}{p_0}\right)\right)\left(1-\left(\frac{p}{p_0}\right)+C_B\left(\frac{p}{p_0}\right)\right)} \qquad 1.15,$$

where W – the weight of water adsorbed per unit weight of dry solid at the relative pressure $\left(\frac{p}{p_0}\right)$; W_m – the weight of water adsorbed corresponding to monolayer coverage; and parameter C_B is related to the difference between heat of adsorption on the first layer and heat of water condensation. [154]

1.6.2. Solvent additive effect on the solid-state polymorphic transformations

It is known that several organic and inorganic reactions, as well as cocrystallization and polymorphic transformations are more selective and effective in the solid phase, however in most of the cases they take place much slower than in solution. In order to combine the best features of both reactions types, the approach, where solvent additive is added to the solid-solid reaction medium, have been introduced [138,174]. These researches showed that solid-state milling kinetics may be considerably enhanced by the addition of a few drops of solvent. In addition, this approach can provide a successful means of controlling the polymorphic or cocrystallization outcome [135,175]. This process is called “solvent drop grinding” or “liquid-assisted grinding” [108]. Solvent drop milling have become popular due to its “green” nature –

it avoids excessive use of crystallisation solvent, and the yield in these reactions is nearly 100% [135,137].

The solid-state transformation from ranitidine hydrochloride form 1 to form 2 was confirmed to occur via an amorphous phase [117]. Phase transformation was initiated by form 1 crystal disruption, producing form 2 nuclei. Continued milling produces heat and impact energy that propagates the crystallization. Phase transformation via solvent drop milling occur similar, with the difference that phase transformation occur through solution not amorphous phase. Solvent added dissolves small amount of solid phase and then consequently crystallizes in more stable phase. It is possible that both intermediate steps – amorphisation and dissolution – are involved in solvent drop milling [102,107,108,135,138,175]. Trask *et al.* [175] have showed that succinic acid β form does not transform to α form upon neat milling (milling without solvent additive) and milling with several drops of a polar solvents (water, acetonitrile and methanol), whereas milling with several drops of a less polar solvent (toluene, n-hexane and heptane) induced the formation of α succinic acid. Similar results were observed when caffeine and glutaric acid were ground together. Neat milling and milling with non-polar solvent additives (n-hexane, cyclohexane, and heptane) gave cocrystal form I, whereas milling with polar solvents (chloroform, dichloromethane, acetonitrile, and water) gave cocrystal form II [135]. These experiments show that solvent drop milling outcome is affected by solvent used just like in the crystallization from a solution. This confirm the previously stated assertion that solvent drop milling is actually a small scale crystallization from solution, where necessary energy is supplied by milling. Schematic representation of process occurring during solvent drop milling is given in Figure 1.11. Initially solvent adsorbs/absorbs on the surface of starting material (Form 1). Starting material Form I dissolve in to the solvent, and eventually, in given conditions more stable polymorph 2 nucleates in saturated solution layer. The growth of the newly formed Form 2 proceeds by Form 1 dissolution in the adsorbed solvent layer, and subsequent crystallization on the form 2 seed crystal.

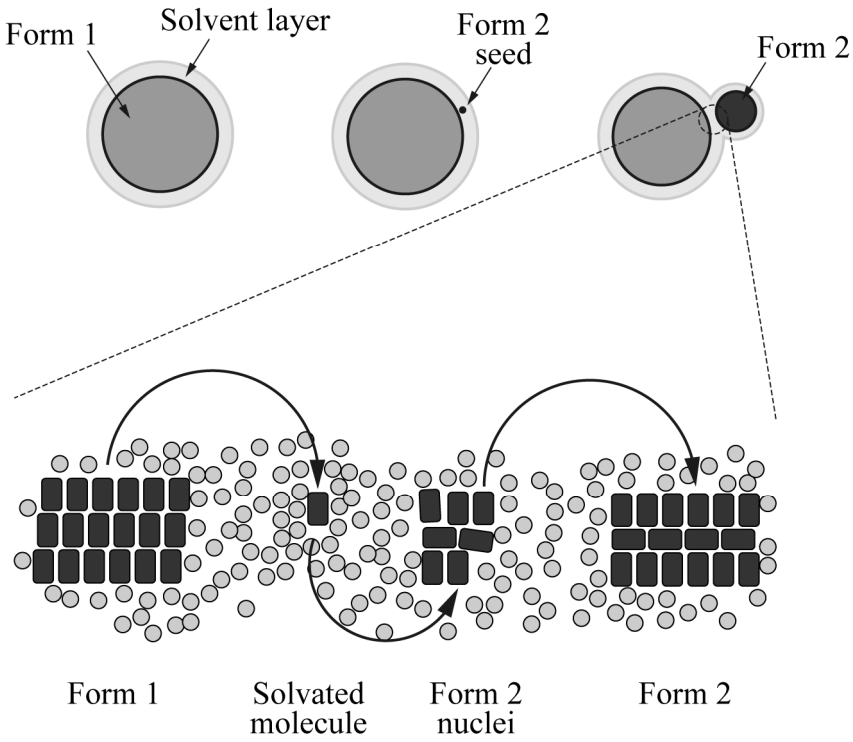

Figure 1.11. Schematic representation of phase transformation during solvent drop milling.

1.7. Solvent mediated phase transformations (SMPT)

Solution or solvent mediated polymorphic transformation (SMPT) is a phase transition process which takes place through the solution phase where solvent molecules are in contact with both crystalline phases and allow the metastable phase molecules to rearrange to form the stable phase. SMPT is interpreted as a three-step process – dissolution of the metastable phase, nucleation of the stable phase, and growth of the stable phase [45,47]. Schematic representation of this process is identical to that given in Figure 1.11., with the difference that during the SMPT solid particles are in the bulk solvent.

The driving force in this process is the difference between the solubilities and dissolution rates of both polymorphs, which consequently determines the supersaturation level during the crystallization of the thermodynamically stable form. Figure 1.12.A shows solubility profile of the dimorphic, monotropic system with the metastable form having the higher solubility. The solution with a concentration c_i at a temperature T_i is supersaturated with respect to both polymorphs at the given temperature and therefore will crystallize. For systems which obey Ostwald's rule of stages (see Section 1.2) the nucleation and growth of the metastable Form 1 will occur first, but it is expected that even in such cases nuclei of the thermodynamically stable

Form 2 will appear and promote the growth of Form 2 and dissolution of Form 1. The nucleation and crystal growth process will cause the supersaturated solution concentration fall. If only Form 1 nucleates, the solubility drop will be limited by the Form 1 solubility c_1, whereas, if polymorph 2 also nucleates, the concentration may fall below the Form 1 solubility to approach the Form 2 solubility, c_2. When the solution concentration drops below the Form 1 solubility c_1, dissolution of metastable Form 1 starts to take place and solution concentration subsequently rises towards the solubility of Form 1. This dissolution-crystallization process is the SMPT. It is considered that the higher the initial supersaturation $\sigma_i = \frac{c_i - c_2}{c_2}$, the more likely the nucleation of Form 2 will be. [176]

Schematic concentration and supersaturation profiles of both polymorphs during SMPT versus time are given in Figure 1.12.B. The plateau region in this plot corresponds to the SMPT step during which the growth and dissolution processes are balanced (it is called steady-state [45]). If crystal growth of Form 2 is rate determining step, the plateau concentration lies close to the solubility of the metastable Form 1, whereas if the rate determining step is the dissolution of Form 1 the plateau concentration lies close to the solubility of Form 2. In the latter case the phase transformation occur from the lower supersaturation and hence it often leads to slower transformation kinetics than in the growth controlled situation [47,176]. The overall SMPT driving force is controlled by the free energy difference between both polymorphs and is not affected by the choice of solvent, however, if the growth of the stable phase is the rate controlling step, solvent may influence the SMPT rate through its impact on the surface integration processes [177]. The phase transformation time together with the magnitude of the plateau concentration defines the kinetics and rate-determining step in the phase transformation process. [176]

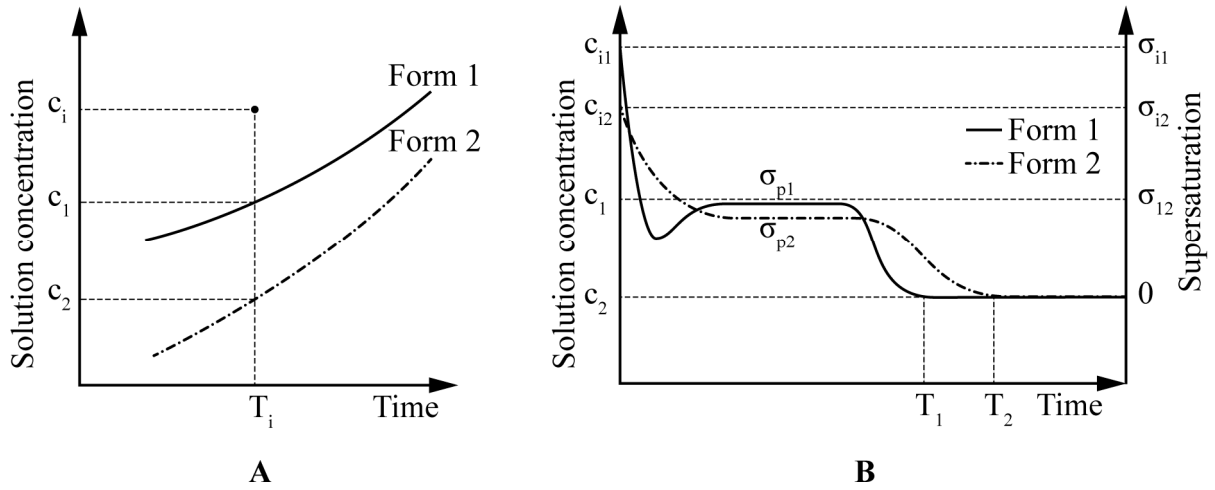

Figure 1.12. Thermodynamic and kinetic features of SMPT. A) Solubility curves of monotropically related forms 1 and 2; B) Schematic representation of the concentration and supersaturation profiles throughout SMPT from form 1 to form 2 (adapted from [176]**).**

The solution concentration profile throughout SMPT in conjunction with composition of the solid phase gives the information about the limiting step in the respective SMPT. There are four principal scenarios possible for SMPTs (see Figure 1.13.). They are described in detail elsewhere [178]. Here we note only the key points. In scenario A, the solution concentration drops immediately after any noticeable amount of the stable phase has been produced. This means that the consumption of supersaturation by crystal growth is fast compared to the overall metastable phase dissolution rate. This is denoted as a "dissolution controlled polymorphic transformation" [45]. In scenario B, the solution concentration stays at the solubility of the metastable form throughout phase transformation and the concentration remains at this level until almost no metastable solid form remains in the suspension. In this scenario the rate of supersaturation consumption by stable form crystal growth is clearly lower than the overall rate of dissolution of the metastable form. This case is denoted as "growth controlled polymorphic transformation" [45,47,179,180]. Scenario C is classified as a "nucleation-dissolution controlled polymorphic transformation". Here the solution concentration drops quite rapidly as soon as the stable phase starts to form (like in case A), however, the nucleation of the stable form exhibits an induction time. Once the thermodynamically stable polymorph have nucleated, the rate of transformation is essentially limited by the rate of dissolution. In case D, the overall growth rate is clearly slower than the overall dissolution rate. The nucleation of the stable phase

holds considerable induction time and solution concentration does not start to decay until most of the metastable form has transformed to the stable form. This scenario is called as a "nucleation–growth controlled polymorphic transformation" [181,182]. [178]

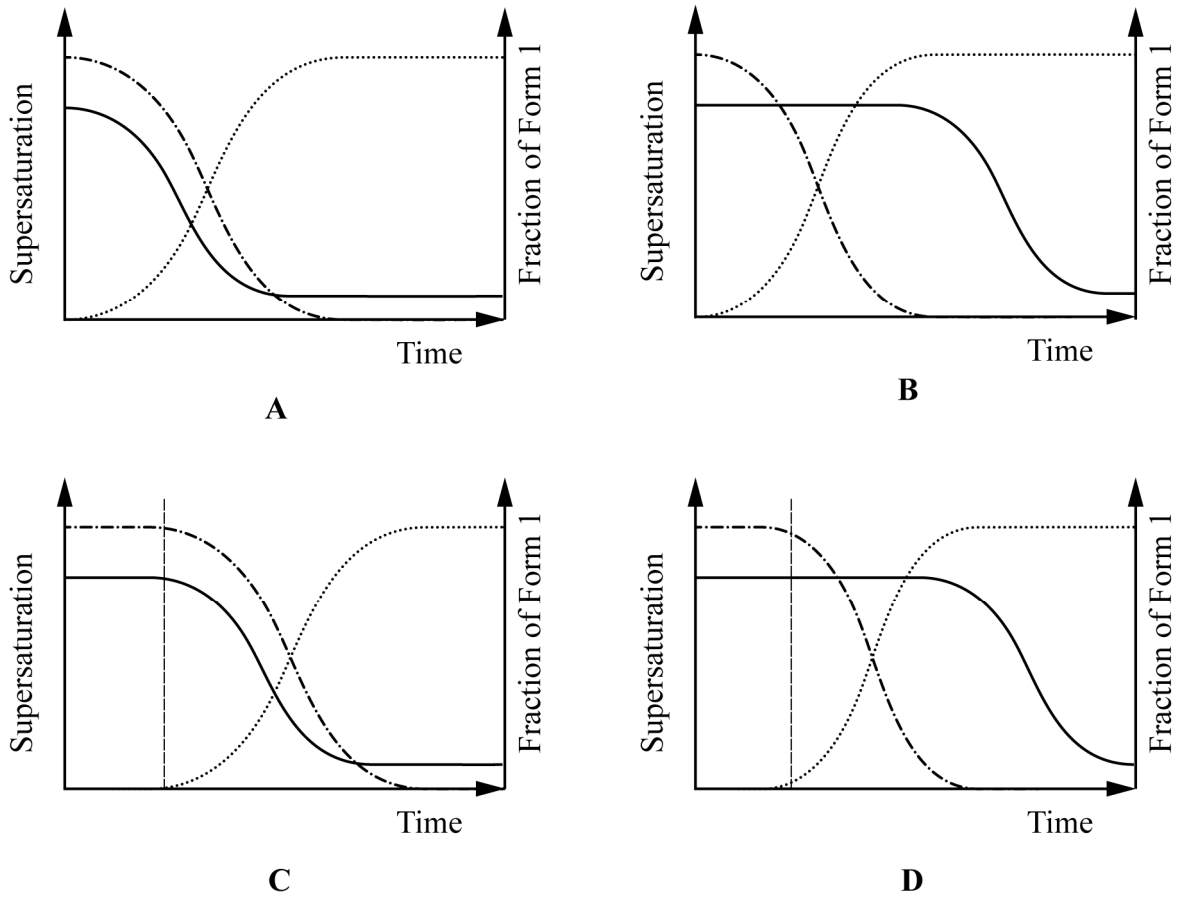

Figure 1.13. Schematic representation of solution concentration/supersaturation profiles and solid state compositions throughout SMPTs. Continues line (–) represents solution concentration profile; dotted line (···) represents the fraction of the thermodynamically stable phase; and dashed line (–·–) represents the fraction of the metastable phase. Vertical line indicates the induction time for nucleation of the stable phase (adapted from [178]**).**

Cases of SMPT have been extensively studied over years [8,178,179,183–192], and the latest studies [179,184,193] demonstrate that during a SMPT the nucleation of the stable polymorph tends to occur on/at the surface of the existing polymorph. The surface of the starting material can act as a nucleation substrate for the thermodynamically stable phase by either decreasing the solution-nucleus interfacial energy, by topographical contribution, by a crystal lattice match [9] or it can be a consequence of a local lattice disorder or amorphous region that have similar molecule arrangement to that of thermodynamically stable polymorph [8].

SMPTs attracts attention also form the pharmaceutical industry, as it is one of the possibilities to prepare the thermodynamically stable polymorph [8,10,194].

1.8. Characterization of polymorphs

There are a wide range of analytical techniques available for polymorphic system characterization, however, crystallographic and thermal methods are the most popular ones and will be looked in more detail. Crystallography provides the most definitive evidence of polymorphism – crystal structures, while other methods are used as a complementary techniques for the characterization of polymorphs. Solid state NMR provides information about magnetic environment of nuclei and molecule mobility, it also gives unique spectra for each polymorph; microscopy methods (hot stage microscopy (HSM), scanning electron microscopy (SEM), atomic force microscopy (AFM)) allows to characterize crystal shape, size, morphology and some processes occurring in crystals; spectroscopic methods (IR and Raman spectroscopy) are sensitive to hydrogen bonding and gives unique spectra for each polymorph. In order to get as full understanding as possible these techniques are always combined. [3,5,12,195,196]

1.8.1. X-ray diffraction (XRD)

Diffraction pattern depend on the atom, molecule or ion arrangement into the crystal, and since different polymorphs have different molecular packing, each polymorph has unique XRD pattern. This makes the XRD the most useful method for distinguishing and identifying polymorphs. [197–199] Single crystal X-ray diffraction (SC XRD) is the ultimate method for polymorph characterization, because it gives direct information on atom's position in the crystal lattice. However, there is one serious obstacle for SC XRD – the preparation of suitable single crystal. Usually it is difficult, sometimes even impossible, to prepare a single crystal of desired quality, especially of a metastable polymorph [3,199]. Since most of the organic compounds are obtained as a micro-crystalline powders, they are analysed with powder X-ray diffraction method (PXRD). Due to simple sample preparation, and the fact that PXRD allows to identify the crystalline phases obtained, determine degree of crystallinity, study phase transformations, quantify phase mixtures, etc., it is appropriate method for the routine characterization of polymorphs and solvates [198,199]. The only disadvantage of PXRD method

is that it does not give enough information to solve crystal structure, however, the development of the PXRD equipment and the increase of the computational power have led to the opportunity to solve crystal structure even from the PXRD data. Though this task is not straight forward, the amount of structures solved from the PXRD data are vastly increasing. [200–209]

Since it is possible to use PXRD method for quantitative phase analysis, PXRD gives the ability to study phase transformations, by monitoring disappearance of the starting material peaks and emergence of product peaks. In order to obtain representative data, a randomly oriented powder sample that will present a substantially random selection of all possible crystal faces, providing information regarding all possible atomic or molecular spacing in the crystal lattice, is required. In order to minimize the errors introduced by the sample preparation and sample inhomogeneity it is recommended to standardize the sample preparation method [210–213]. There are several approaches for quantitative composition calculation from PXRD data, like peak intensity ratio method (can use more than one peak), full profile fitting; and Rietveld method [199]. Rietveld method is the most popular and precise method since it takes in to account the crystallographic structures of the studied compounds. This is also the disadvantage of this method, since not all compounds have determined crystal structures [198,199]. The precision of quantitative PXRD analysis is from several percent with peak intensity ratio method up to 0,1% with Rietveld method [214–219].

1.8.2. Thermal methods

Thermal analysis methods utilise the fact that a thermally induced change in the sample is accompanied by significant heat flow. In *differentially scanning calorimetry (DSC)*, the instrument measures the required heat flow to sustain the temperature of the sample and reference material the same. The resulting thermogram shows a measure of heat flow as a function of temperature. In *differentially thermal analysis (DTA)*, heat loss or gain resulting from physicochemical changes occurring in a sample is recorded as a function of temperature as the substance is heated at a uniform rate. Enthalpic changes observed by DSC and DTA methods are caused by phase transitions. Most of them (fusion, boiling, sublimation, vaporization, solid-solid transition, and solvent loss) generally produce endothermic effect, whereas crystallization produces exothermic effect [220]. The endothermic and exothermic

effect observed allows to estimate polymorph relative stability, gives information about solvent loss and presence of chemical and physical impurities, etc. DTA and DSC gives somehow similar information with the difference that DSC provides thermodynamic data, which can be further used to calculate the heat of fusion, heat of crystallization, etc. Therefore, DSC is the most popular thermal analysis method in pharmaceutical analysis. [1,3–5,16,195,221,222]

Another thermal method, usually combined with the previous ones, is *thermal gravimetric analysis (TGA)*. TGA measures sample weight changes as a function of temperature. This methods is very useful to study processes that are accompanied by weight loss due to temperature changes, like, sublimation, desolvation and decomposition. Furthermore, the mass loss can be used to establish solvate stoichiometry. Due to ability to use TGA method either in thermal or isothermal mode, it is a powerful tool to study the kinetics of various events, such as dehydration. The combination of TGA and DSC or DTA allows to explore the nature of any thermally induced transitions from both qualitative and potentially quantitative perspectives. [3,5,11,220,223]

1.9. Active pharmaceutical compounds

1.9.1. Tegafur

Tegafur, 5-fluoro-1-(tetrahydro-2-furyl)-uracil (see Figure 1.14.A), which was synthetized by Hiller *et al.* [224] as a prodrug of a 5-fluorouracil (Figure 1.14.B), is an antitumor agent widely used in the treatment of various cancers, particularly the gastrointestinal and breast cancer [225–227]. Over many years the α, β, γ, δ and ε polymorphs of tegafur have been reported in the pharmaceutical literature [227–229]. These crystal forms can be prepared as follows: α tegafur can be obtained by crystallization from acetone at ambient conditions; β – by crystallization from methanol at room temperature under reduced pressure; γ – by heating the β tegafur at 130 °C for 1 h, δ – by very slow crystallization from a methanol solution [227], and ε form can be crystallized from the thin layer (3 mm) aqueous solution at 4 °C [228]. No tegafur solvates have been discovered yet. Only α and β modifications are used for therapeutic purposes, therefore our studies focus on these two polymorphs.

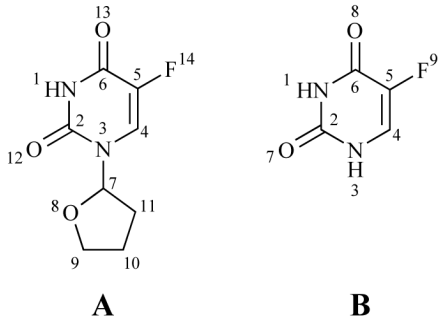

Figure 1.14. A) Tegafur (5-fluoro-1-(tetrahydro-2-furyl)-uracil); B) 5-fluorouracil

The β form is thermodynamically stable polymorph at ambient conditions, whereas α tegafur is stable at elevated temperatures. Several studies have been devoted to determine α and β tegafur equilibrium temperature, and depending on method used, it is from 33 °C to 39 °C [230,231]. The α polymorph is stable up to ~130 °C, where the stability region of γ polymorph starts.

Crystal structures of α and β tegafur have been determined and it is known that α tegafur (Cambridge Structural Database (CSD) reference code BIPDEJ) crystallize in a triclinic P-1 space group with cell parameters *a=8.994(8) Å, b=16.612(9) Å, c=5.981(5) Å, α=86.40(6)°, β=94.06(15)°, γ=80.29(8)°*, four formula units in the unit cell, and the cell volume 886.27 Å^2. β tegafur (CSD reference code BIPDEJ02) crystallize in a monoclinic P2$_1$/n space group with cell parameters *a=11.891(5) Å, b=14.556(2) Å, c=5.062(1) Å, β=99.05(2)°,* four formula units in the unit cell, and the cell volume 865.25 Å^2. The base motif of α and β tegafur crystal structures is a tegafur molecule dimer with a $R_2^2(8)$ motif where tegafur molecules are connected via two N1-H···O12 hydrogen bonds (Figure 1.15.). The dimers are not identical in both polymorphs, because the crystal structure of α tegafur consists of two conformationally different molecules (A and B), whereas β tegafur has one molecule in its asymmetric unit and conformation of this molecule matches the conformation of molecule B in α tegafur [232]. Dimers in α tegafur are formed between conformationally identical molecules, that is, one α tegafur dimer is formed by two A molecules, and the second by two B molecules. Tegafur dimers in the α polymorph are cross-linked by weak C4-H···O8 and C11-H···O13 hydrogen bonds, whereas in β tegafur dimers are stabilized by weak C4-H···O12 and C10-H···F14 hydrogen bonds. It is worth noting that tegafur dimers in α form forms between the same enantiomers (there are two enantiomerically

and conformationally different dimers), whereas in β tegafur dimers forms between two enantiomerically different molecules [232].

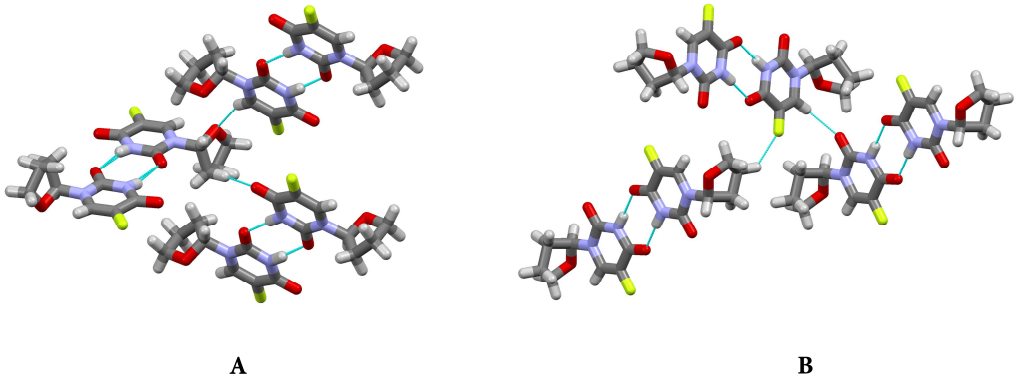

Figure 1.15. Crystal packing of (A) α tegafur and (B) β tegafur. Hydrogen atoms are omitted for clarity.

These two polymorphs have distinctly different crystal morphologies – α polymorph has a needle like crystals, whereas β polymorph has prismatic crystals (see Figure 1.16.). α tegafur crystal growth along the *a* axis is promoted by the relatively easy tegafur dimer access to the growing surface and the possibility to form multiple weak hydrogen bonds between F14, O13, O8 and C4-H, C11-H. Hydrogen bonds in β tegafur are distributed more evenly and they are stronger than in α tegafur. The same groups are involved in hydrogen bonding for β tegafur, with the difference that instead of C11-H hydrogen, C10-H forms hydrogen bond with fluorine atom. Hydrogen bonding in β tegafur enables cross-linked *zigzag chains* in the *b* direction, however no preferred crystal growth orientation is observed for β tegafur.

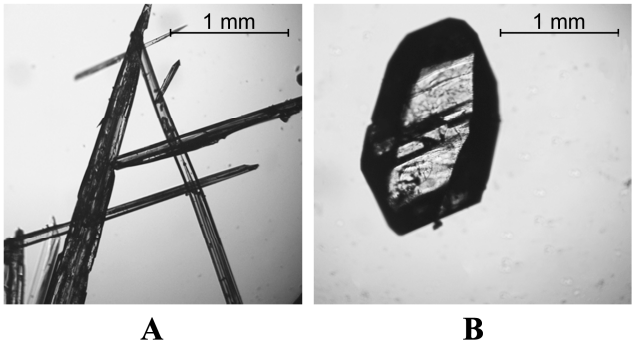

Figure 1.16. Photomicrographs of α and β tegafur crystals.

1.9.2. Theophylline

Theophylline, a methyl xanthine derivative (3, 7 dihydro-1, 3-dimethyl-1H-purine-2,6-dione) (Figure 1.17.), is an oral bronchodilator with anti-inflammatory action that has been used for over 70 years to treat pulmonary conditions such as asthma and Chronic Obstructive Pulmonary Disease [233]. Theophylline can exist in various polymorphic forms (I, II, III and IV) [116,234–241], monohydrate [242–244], dimethyl sulfoxide solvate [245], and as a cocrystals. Most of the complexes formed between theophylline and acids (e.g. oxalic acid, malonic acid, gentisic acid, sulfathiazole, acetaminophen, etc.) as well as bases (e.g. urea, benzylamine, phenobarbital, etc.) have been summarized by Childs *et al.* [246].

Theophylline is one of the pharmaceutically active compounds that have been manufactured and used in a metastable crystalline phase (clearly, because of the lack of comprehensive knowledge on polymorphic landscape of this compound) [235,237]. Theophylline Form II is highly stable metastable polymorph crystallized from majority of solvents at the room temperature and therefore was historically considered as thermodynamically stable polymorph, until Form IV were presented [237] and proved to be more stable. The fact, that thermodynamically stable theophylline polymorph was discovered only lately, most likely, is because it does not crystallise directly from any solution, and is obtained only by slow solvent mediated transformation (SMPT) from Form II in contact with specific solvents [237]. Theophylline Form I has been reported as stable polymorph at higher temperatures, whereas Form III is highly metastable and it has been obtained only during the dehydration of monohydrate [236,243]. Theophylline monohydrate (referred as Form M) is a monoclinic channel type hydrate which has been shown to lose water, either in low humidity or at temperatures above 353 K, to produce Form II [164,247]. Here we focus exactly on the phase transformation between form II and IV.

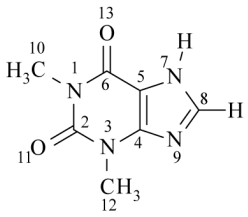

Figure 1.17. Structure of theophylline (3,7 dihydro-1,3-dimethyl-1H-purine-2,6-dione).

The crystal structures of theophylline form II, IV and monohydrate are given in Figure 1.18.

Theophylline Form II (CSD reference code BAPLOT) crystallize in orthorhombic $Pna2_1$ space group with cell parameters *a=24.3301(14) Å, b=3.7707(2) Å, c=8.4850(5) Å*, four formula units in the unit cell, and the cell volume 778.427 Å^2. In the crystal structure of theophylline Form II the best hydrogen bond donor (N7-H) bonds to the hydrogen bond acceptor which would be expected to be the strongest (N9) [234,248] forming hydrogen bond N7-H···N9. This observation is consistent with Etter's rules [249] that the best hydrogen bond donor tends to interact with the best hydrogen bond acceptor. The crystal structure of Form II also has two weak bifurcated C8-H···O13 hydrogen bonds. Mentioned hydrogen bonds form second-level $\boldsymbol{R}_2^2(8)$ motif. The resulting crystal structure of Form II consists of theophylline molecules that are linked in chains where the planar molecules are stacked along (010). This catemer arrangement promotes crystal growth along the molecular chains leading to an elongated crystal morphology.

Theophylline Form IV (CSD reference code BAPLOT03) crystallize in monoclinic $P2_1/n$ space group with cell parameters *a=7.70550(10) Å, b=13.0010(2) Å, c=15.7794(3) Å, β=103.2240(10)°*, eight formula units in the unit cell, and the cell volume 1538.85 Å^2. Unlike other theophylline anhydrous polymorphs, Form IV has two molecules in its asymmetric unit [116]. These molecules form a dimer with a $\boldsymbol{R}_2^2(10)$ motif and are connected via (N7-H···O13) hydrogen bonds. The dimer is discrete and only links to other dimers by weak interactions: C8-H···N9, C8-H···O11, and by π–π stacking, forming two-dimensional network parallel to the (001). Dimer, observed in the Form IV, is similar to the motif observed in the monohydrate and in a number of theophylline cocrystals [246,248]. Presence of such dimer motif in the thermodynamically stable Form IV and theophylline monohydrate, that is considered to be the most stable structure in aqueous environment, may account for the thermodynamic stability of this structural motif compared to the chain motif of Form II.

Theophylline monohydrate M (CSD reference code THEOPH01) crystallize in monoclinic $P2_1/n$ space group with cell parameters *a=4.468(2) Å, b=15.355(5) Å, c=13.121(5) Å, β=97.792(7)°*, four formula units in the unit cell, and the cell volume 891.87 Å^2. In a theophylline monohydrate two centrosymmetrically related theophylline molecules form a dimer through two hydrogen bonds (N7-H···O13) [244]. Theophylline dimers are connected by

water molecules through hydrogen bonds, forming parallel, crosslinked chains, leading to two-dimensional hydrogen bonded layers, parallel to (10-1) plane. Water molecules are situated in the tunnels along the *a* axis, where they are forming hydrogen bonds to theophylline molecule N9 atom.

In theophylline dimethyl sulfoxide solvate one theophylline molecule is hydrogen bonded to one dimethyl sulfoxide molecule through an N7-H···O=S hydrogen bond [245]. The packing consists of molecular chains lying parallel to the (010), stacked by π–π interaction between pyrimidine and imidazole rings, and weak hydrogen bonds between dimethyl sulfoxide methyl groups and theophylline carbonyl group (C_{DMSO}-H···O13).

The crystal structure of the highly-metastable Form III has not been determined due to its metastability.

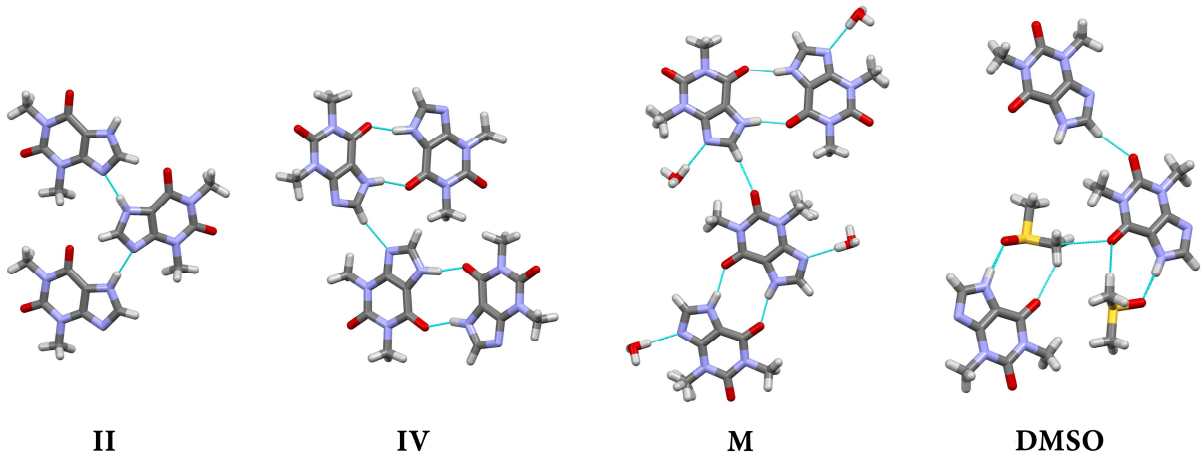

Figure 1.18. Crystal packing motifs in theophylline Form II, Form IV, theophylline monohydrate and DMSO solvate.

2. Experimental

2.1. Materials

Commercial samples of α and β tegafur (>99%) were supplied by JSC Grindeks (Latvia). Samples of α and β tegafur were confirmed to be polymorphicly pure. The entire batches of α and β tegafur used in experiments were ground separately for 3 min to ensure required sample homogeneity and avoid preferred crystal orientation effects. Anhydrous theophylline was purchased from commercial sources and was certified >99% pure. Theophylline was confirmed to be Form II and was used as received. Organic solvents of analytical grade were purchased from commercial sources and used without further purification (for solvent characterization see Appendix 2). Deionized water (electrical conductivity <0.1 μS) was prepared by Adrona, Crystal 5 (Latvia).

2.1.1. Preparation of theophylline crystalline forms

Theophylline Form IV. Theophylline Form IV was prepared as described elsewhere [237]. An excess amount of anhydrous theophylline (~1.0 g) was added to 25 mL of methanol and stirred at 600 rpm for 14 days at 23±1 °C (this and further experiments were performed in air-conditioned laboratory, because temperature deviations during the day hindered Form IV nucleation). Solid phase was filtered through Buchner funnel under reduced pressure. The polymorphic form of dry residue was confirmed using PXRD.

Theophylline Form I. Anhydrous theophylline Form II (~1.0 g), ground in mortar with pestle for 3 min, was transferred to Petri dish, covered by glass slide and heated at 268±1 °C for 2 h. Sample was cooled to room temperature and polymorphic form was confirmed using PXRD.

Amorphous theophylline. The excess amount of anhydrous theophylline (~5.0 g) was added to 250 mL of water and was left to stir overnight. Solid phase was filtered off and a clear solution was spray dried using a Buchi mini spray dryer B-290 (Buchi Labortechnik AG, Switzerland). A top spray method was used with the inlet temperature set at 120 °C, the outlet at 70 °C and the pressure at 6 bar. Crystallinity of the material obtained was examined using PXRD.

Theophylline monohydrate. The excess amount (~3.0 g) of anhydrous theophylline was dissolved in ~100 mL of warm water (~70 °C) and was left to stir overnight. The precipitated solid phase was filtered, air dried and crystalline phase obtained was confirmed using PXRD.

2.2. Characterization methods

2.2.1. Powder X-ray diffraction

PXRD samples of tegafur were recorded with a Bruker D8 Advance and Bruker D8 Discover powder X-ray diffractometers (Bruker AXS, Germany), equipped with a PSD *LYNXEYE* detectors. The measurements were performed with Cu K_α radiation (1.54180 Å) at room temperature. The following conditions were used: step-scan mode with a step size of 0.02°; scan speed: 0.2 s/0.02°; 2θ range: 3.0°–30.0°; voltage: 40 kV; current: 40 mA; divergence slit: 0.6 mm; anti-scattering slit: 8 mm. The powder samples were packed into glass holders and pressed by a glass slide to ensure coplanarity of the powder surface with the surface of the holder.

Theophylline samples were analysed with a Rigaku Miniflex (Rigaku, Japan) powder X-ray diffractometer. Diffraction patterns within the 2θ range of 5° to 40° were recorded at room temperature using Cu Kα radiation at 1.54180 Å, with the following measurement conditions: tube voltage 30 kV, tube current 15 mA, step-scan mode with 2θ step size 0.02°, and the counting time 2 s/step. Diffractometer slits were set as follows: divergence slit – variable; scattering slit – 4.2°, receiving slit – 0.3 mm. Powder samples were packed into aluminium sample holders with and pressed by a glass slide to ensure co-planarity of the powder surface with the surface of the holder.

Qualitative phase analysis. Reference powder patterns were calculated with Mercury 3.3 [250] software from CSD crystal structure data.

Quantitative phase analysis. The quantitative phase analyses were performed using fundamental parameter based Rietveld software BGMN (version 1.8.6b) [251] with Profex (version 3.1.1) interface. Crystal structure data previously mentioned were used for quantitative Rietveld analysis.

2.2.2. FTIR spectroscopy

FTIR spectra were recorded using a Perkin-Elmer Spectrum BX (PerkinElmer Inc., USA) spectrometer fitted with a PIKE Technologies MIRacle sampling accessory. MIRacle liquids plate was used when spectra of solutions were recorded. The samples were scanned at a resolution of 4 cm^{-1} between 4000 cm^{-1} and 600 cm^{-1}. Each spectrum consisted of 16 co-added scans if not otherwise stated.

2.2.3. Scanning electron microscopy (SEM)

SEM imaging was performed using Inspect S SEM (FEI, Holland) or Hitachi S4800 SEM (Hitachi, Japan) system. Samples were initially gold coated using a K550X sputter coater (EMITECH, UK) and subsequently scanned using an acceleration voltage of 5.0 kV or 2.9 kV at a working distance of approximately 10 mm.

2.2.4. Determination of the surface area

Surface area was determined by a modified chromatograph "Hrom 3", detecting the amount of argon involved in a monolayer adsorption–desorption process.

2.2.5. Crystallographic face indexing

Crystallographic face indexing was undertaken using single crystal X- ray diffractometer Nonius Kappa CCD diffractometer (Bruker AXS, Germany) with Mo K_α radiation (0.71073 Å) at 60 kV and 30 mA. Data were collected at room temperature. Face indexing was performed using *Collect* software [252].

2.2.6. Calculation of crystal morphology

Predictions of crystal morphology from structure data were done based on Bravais, Friedel, Donnay and Harker (BFDH) theory using Mercury 3.3 [250] software. Crystal structures necessary for calculations were retrieved from the Cambridge Structural Database.

2.3. Sample preparation

2.3.1. Sample preparation for PXRD method calibration

PXRD calibration was performed using mixtures of 5.0%; 10.0%; 20.0%; 50.0%; 80.0%; 90.0% and 95.0% β tegafur in α tegafur (~0.3 g total sample weight). The mixtures were weighed using

an analytical balance (*BOECO*, Germany, d=±0.1 mg) were used and samples were homogenized by shaking (10 Hz) for 5 min in a *Retsch MM 300* ball mill (Retsch GmbH, Germany) without milling balls in the sample vial. The powder samples were packed into glass holders and pressed by a glass slide to ensure coplanarity of the powder surface with the surface of the holder. Quantitative PXDR analysis were performed as described in section 2.2.1.

2.3.2. Determination of micro amounts of β tegafur in the α and β polymorph mixture by powder X ray diffractometric analysis

2.3.2.1. Determination of optimal sample preparation conditions

The mixture of tegafur α and β forms containing 1.5% weight fraction of β form was prepared and separated into six samples with mass 0.50 grams of each sample. The analytical weights were used. Weighted samples were milled with a ball mill in 50 mL vials at the shaking frequency of 15 Hz at 20±2 °C for 3.0, 5.0 and 7.0 minutes with addition a single drop (~0.07 mL) or two drops (~0.15 mL) of water for each milling time. Water was added to the sample before milling.

PXRD patterns of prepared samples were recorded as described in section 2.2.1.

2.3.2.2. Sample preparation

Pure α and β polymorphs of tegafur were milled separately for 2.0 minutes in the mortar to ensure homogeneity of the sample. The milled β form was weighted in various ratios (1.0%; 0.50%; 0.25%; 0.10%; 0.050%; 0.010% and 0.0050%, ω/ω) with α form. Total mass of the mixture was 0.75 g. Prepared samples were homogenised by shaking for 5.0 minutes in a ball mill without milling balls in the sample vial at the shaking frequency of 15 Hz at 20±2 °C.

The 0.50 g of homogenised sample was weighted for milling, but the rest of the mixture was used for the next sample preparation. A drop of water (~0.07 mL) was added to the sample before milling. The prepared sample was milled for 5.0 minutes with a ball mill in 50 mL vials with the shaking frequency of 15 Hz at 20±2 °C.

PXRD patterns of prepared samples were recorded as described in section 2.2.1.

2.3.3. Optimization of sample preparation conditions for detecting trace amounts of β tegafur in α and β tegafur mixture

2.3.3.1. Determination of optimum milling frequency.

Mixtures of 2.0%; 1.0%; 0.50%; 0.10%; 0.050%, 0.010%; 0.0050%; 0.0010%; 0.00050% and 0.00010% β tegafur in α tegafur (3.0 g each) were prepared from a 2.0% stock mixture that was diluted to the required concentrations. Samples during preparation were homogenized with a ball mill in 50 mL vials for 5 min at 20±2 °C with 15 Hz shaking frequency. The 0.50 g samples of homogenized mixtures were each treated with 0.07 mL water and ground in the ball mill at 7, 10 and 15 Hz shaking frequencies for 5 minutes.

PXRD patterns of prepared samples were recorded as described in section 2.2.1.

2.3.3.2. Determination of the optimum added water volume.

A mixture of tegafur α and β forms containing 1.0% weight fraction of β form was weighed and homogenized in the ball mill for 5 min at 20±2 °C, with 15 Hz shaking frequency. The 0.50 g samples of homogenized mixture were ground in the ball mill with variable water additive amounts for 5 minutes at 20±2 °C, with 10 Hz shaking frequency. The added water volume was from 0.02 mL to 0.20 mL, with 0.01 mL step size. Micropipette (CAPP, Denmark, d=±2%) was used for solvent addition. When the amount of water additive exceeded 0.06 mL, a thick paste formed, and it became necessary to dry the samples for 30 minutes after milling.

PXRD patterns of prepared samples were recorded as described in section 2.2.1.

2.3.3.3. Sample preparation for recrystallization studies.

A sample (0.50 g) of tegafur α and β form mixture, containing 1.0 % weight fraction of β form, was ground in the ball mill for 5 min at 20±2 °C with 15 Hz shaking frequency, with 0.20 mL water added just before milling. The obtained thick paste was pressed into glass sample holder right after milling, and PXRD pattern was recorded immediately. Consecutive PXRD patterns were recorded every 5 min, until no further phase transition was observed (~1 h).

2.3.4. Organic solvent effects on phase transition of α and β tegafur upon milling with solvent additives

2.3.4.1. Determination of solvent effect on phase conversion degree during milling

A sample (10 g) of tegafur α and β form mixture, containing 0.5% weight fraction of β form, was prepared from a 5.0% stock mixture that was diluted to the required concentration. Samples during preparation were homogenized in a ball mill for 5 min at 20±2 °C with 15 Hz shaking frequency.

The 0.20 g samples of prepared 0.5 % mixture were each treated with 0.025 mL of solvent and ground in the ball mill at 10 Hz shaking frequency for 5 minutes. The solvents used in this experiment were methanol, ethanol, *n*-propanol, *n*-butanol, *n*-pentanol, *n*-heptanol, isopropanol, benzyl alcohol, ethyl acetate, *n*-propyl acetate, *n*-butyl acetate, 1,1-dichloroethane, chloroform, acetone, tetrahydrofuran, acetonitrile and toluene. Prepared samples were dried in opened milling vessel for 30 min at 20±2 °C after the milling. Dried samples were packed into glass holders and PXRD patterns were record.

2.3.4.2. Determination of α tegafur solubility in the solvents used

Approximately 0.2 g of α tegafur was added to ~12 mL of solvent in weighing bottle, and the prepared mixture was held at 30±1 °C for 48 h in a sealed weighing bottle and stirred occasionally to obtain a saturated tegafur solution. The clear, saturated mixture (4.0 mL, without any precipitate) was transferred to a tared weighing bottle with a pipet that was also held at 30±1 °C. The weighing bottle with the saturated solution was left to evaporate at 30±1 °C, and then the weighing bottle with the dry residue was weighed on analytical balance. PXRD pattern was recorded for the dry residue. Solubility of α tegafur was determined in all the previously mentioned solvents.

2.3.4.3. Determination of solvent vapour effect on phase transition

Two samples (4 g each) of α and β tegafur mixture with weight ratio 1:1 were prepared. Samples were homogenized during the preparation in a ball mill for 5 min at 20±2 °C with 15 Hz shaking frequency. The prepared homogeneous samples were packed into glass holders and PXRD patterns for initial mixtures and pure α and β forms of tegafur were recorded. The

samples were placed in desiccators with 95% relative solvent vapour pressure at 30±0.5 °C, and depending on the transition rate, PXRD data were recorded at fixed moments.

Obtaining 95% relative solvent vapour pressure. To obtain a relative solvent vapour pressure of 95%, methanol, ethanol, *n*-propanol, 2-propanol, *n*-butanol, *n*-pentanol, *n*-heptanol and benzyl alcohol solution in glycerol were prepared, and acetone, acetonitrile, ethyl acetate, *n*-propyl acetate, *n*-butyl acetate, chloroform, tetrahydrofuran, 1,2-dichloroethane and toluene solution in dimethyl sulfoxide were prepared according to the Raoult's law

$$X = \frac{p_0 - p}{p_0} = \frac{n}{n_0 + n} \qquad 2.1,$$

where X is the solvent's mole fraction in solution; p_o is the vapour pressure of pure solvent; p is the solvent's partial vapour pressure over a solution; n represents the investigated solvent molar amount in the solution; n_o is the moles of glycerol or dimethyl sulfoxide in the solution.

Temperature control. Desiccators with the prepared solvent solutions were placed in an air thermostat (Universal Oven UFB-500, Memmert GmbH, Germany) at 30±0.5 °C 24 hours prior to sample insertion.

2.3.4.4. Solvent sorption studies

Solvent sorption experiments were performed in weighing dishes at 30 °C by using pure α and β tegafur. The 0.20 g samples of pure α and β tegafur were weighed in separate weighing dishes with accuracy ±0.1 mg and placed in desiccators with 95% partial pressure of the relevant solvents (see section 2.3.4.3). Depending on the sorption rate, samples were weighed at fixed moments.

2.3.4.5. Solvent desorption studies

Desorption experiments were performed using completely solvent-saturated samples from the sorption experiment (described in section 2.3.4.4). The 30±2 mg of solvent-saturated samples were quickly placed (in less than 20 seconds) in aluminium sample pan, and desorption experiments were performed using a *TG/DTA6300 EXSTAR6000* (SII Nanotechnologies, Japan) instrument with open aluminium sample pans having internal diameter of 5 mm and height of 2.5 mm, under dry nitrogen atmosphere with flow rate of 250 mL/min in isothermal conditions at 30 °C. It was observed that desorption rate was highly dependent on mass of the

sample, therefore samples with equal mass were used. For fast weighting of the equal amount of sample the sample holder each time was filled up to the edge. The following technique allowed to prepare the samples with mass 30±2 mg and to reduce the time of weighing. If sample weight after this procedure were out of the range, procedure was repeated with fresh solvent-saturated sample. During the experiment mass of the sample was recorded every 0.5 seconds.

2.3.5. Organic solvent desorption from two tegafur polymorphs

2.3.5.1. Sample preparation and fractionation

A sample (~6 g) of α tegafur was ground in a mortar for 3 min and then gradually sieved through sieves with mesh sizes of 150, 75 and 40 μm. Three fractions of α tegafur (~2 g each) were obtained with the following particle sizes: 150 – 75 μm; 75 – 40 μm; and less than 40 μm. The same procedure was repeated for β tegafur.

2.3.5.2. Solvent desorption studies

Samples (~50 mg) of each fraction were placed into separate 2 mL vials and positioned in the prethermostated desiccators with 95% relative solvent vapour pressure at 30±0.5 °C (see section 2.3.4.3) for at least 72 h to obtain completely solvent-saturated samples. Solvent desorption was studied as described in section 2.3.4.5.

2.3.6. Solvent mediated phase transformation between two tegafur polymorphs in several solvents

2.3.6.1. The kinetics of solvent mediated polymorphic transformations

Acetone, ethanol, *i*-propanol, toluene, and water solutions (~100 mL) saturated with respect to α tegafur were prepared by stirring excess α tegafur for ~3 h at 22±1 °C. The excess tegafur was filtered off and the clear solution was used for SMPT. In order to ensure that the solution was saturated with respect to α tegafur, PXRD patterns of filtrates were recorded. Solution concentration was determined as described in Section 2.3.6.2.

SMPT kinetics experiments were performed at 22.0±0.1 °C in a thermostated (Grant TC120, England, d=±0.1°C;) glass flow-through cell (250 mL) with a magnetic stirrer. 1.0 g of α tegafur (used as received) was added to the saturated solution and the solid phase was monitored every

10 min to 2 h throughout the transformation. The stirring of the slurry was stopped for 20 seconds to allow the suspended solid particles to settle. Solid phase samples (~10 mg) for polymorphic composition determination were collected with a metal spoon from the suspension. The collected solid phase was quickly filtered through a 2 μm filter paper using a glass filter funnel with Buchner flask under reduced pressure. The quantity of β tegafur in the sample was monitored and quantified via *ex-situ* PXRD analysis. The PXRD patterns for dry samples were recorded and analysed as described in Section 2.2.1.

The tegafur concentration in solution was measured every 20 min to 2 h throughout SMPT. Samples for solution concentration measurements were gathered at the same time as solid phase samples for polymorphic composition determination were collected. Approximately 2 mL of saturated solution was filtered through a 0.20 μm syringe filter and then 1.00 mL of clear solution was transferred to a preweighed vial with micropipette (±10 μL). The solution was left to evaporate at room temperature, weighed and the tegafur solubility was calculated. Two parallel experiments were performed.

2.3.6.2. Tegafur solubility measurements

An excess amount of the thermodynamically stable β tegafur was added to 15 mL of acetone, cyclohexane, ethanol, *i*-propanol, toluene, and water, and was left to stir overnight at 22±1 °C. The saturated solution was filtered through a 0.20 μm syringe filter and then 10.0 mL of clear solution was transferred to a preweighed vial. Solution was left to evaporate at room temperature, weighed and tegafur solubility was calculated. Solubility of the metastable α tegafur was determined identically, except solutions were stirred for ~3 h at 22±1 °C, in order to prevent phase transformation to the thermodynamically stable β tegafur. PXRD patterns of filtrate were recorded to ensure that the solubility of the desired polymorph was determined. Two parallel experiments were performed.

2.3.7. The Reluctant Polymorph. Self-association effect on nucleation and solvent mediated phase transformation of theophylline

2.3.7.1. Examination of solution mediated phase transformation

An excess amount (2.5 g) of anhydrous theophylline Form II (used as received) was added to 100 mL of methanol. The suspension was stirred at 600 rpm for 14 days at room temperature (23±1 °C) and the following measurements were performed every 7 to 24 h:

(a) *Solution concentration monitoring.* Theophylline concentration in the solution was measured every 1 h to 1 day. The solution (~1 mL) was filtered through a syringe filter of 0.20 μm size, and solution concentration was determined as described in Section 2.3.7.3. Three parallel solution concentration determination experiments were performed.

(b) *Crystallization product from solution.* 2 mL of the solution was filtered through 0.20 μm syringe filter, transferred to a Petri dish and was left to evaporate at room temperature. Crystallized dry residue of three parallel experiments was combined and phase composition was examined using PXRD.

(c) *FTIR spectra of the solution.* ~0.3 mL of the filtered solution was gathered as described above, and the FTIR spectra of solution were recorded immediately after sample gathering.

(d) *Phase composition of the solid phase.* The stirring of the slurry was stopped 30 seconds prior to sample gathering, to allow the suspended solid particles to settle. Solid phase sample (10–20 mg) was collected with a metal spoon from the suspension and was quickly filtered through Buhner funnel filter under reduced pressure. The solid phase was examined using PXRD, FTIR and SEM.

SMPT was repeated in triplicate.

SMPT was additionally performed with different starting materials and solvents (given in Table 1). Single runs were performed for these experiments. The phase composition of the solid phase was monitored every 1 to 7 days, except experiments where Form II and Form IV mixture was used; the phase composition in these experiments was monitored every 10 min to 1 h. The solvent and theophylline ratio in all SMPT experiments were the same (2.5 g of theophylline

and 100 mL of solvent), except SMPT in formic acid, where 15.0 g of theophylline were added to 25 mL of formic acid due to high theophylline solubility in formic acid.

SMPT in methanol-D4 was performed for H^1 NMR studies. An excess amount (0.5 g) of commercial theophylline Form II was added to 4.0 mL of methanol-D. The suspension was stirred at 600 rpm for 10 days at room temperature (23±1 °C). PXRD patterns of solid phase and solution H^1 NMR spectra (see Section 2.3.7.4) were recorded each day. Stirring was stopped 1 min prior to sample collection, and: (a) clear solution (~1 mL) was transferred to NMR tube; (b) solid phase (10–20 mg) was collected with a metal spoon and quickly filtered through Buhner funnel filter under reduced pressure. PXRD and H^1 NMR measurements were performed immediately after sample collection. Solution from NMR experiment was returned back to the reaction vial immediately after recording the NMR spectrum.

Table 1. Starting materials and solvents used in SMPT

Starting material	**Solvent**
Commercial Form II	Methanol
Form II, ground in mortar with pestle for 3 min	Methanol
Lyophilized Form II*	Methanol
Commercial Form II	Methanol saturated to theophylline Form IV
Commercial Form II/Form IV* mixture (w_{II}/w_{IV}; 90/10)	Methanol saturated to theophylline Form II
Commercial Form II/Form IV* mixture (w_{II}/w_{IV}; 90/10)	Methanol saturated to theophylline Form IV
Commercial Form II	Methanol/water mixture (V_{MeOH}/V_{H2O}; 99/1)
Commercial Form II	Methanol/water mixture (V_{MeOH}/V_{H2O}; 95/5)
Commercial Form II	Methanol/water mixture (V_{MeOH}/V_{H2O}; 80/20)
Commercial Form II	Acetone
Commercial Form II	Acetonitrile
Commercial Form II	Chloroform
Commercial Form II	Formic acid
Commercial Form II	Methanol-D4**

* Prepared as described in Section 2.1.1.

** Small scale experiment, V_{total}=4.0 mL

2.3.7.2. Determination of theophylline solubility

Theophylline Form II and Form IV solubility in acetone, acetonitrile, methanol, chloroform and formic acid were determined as follows. An excess amount of theophylline was added to 15 mL of solvent and was left to stir overnight at 23±1 °C. The saturated solution was filtered through a 0.20 μm syringe filter and then 10.0 mL of clear solution was transferred to a preweighed vial. Solution was left to evaporate at room temperature, weighed and theophylline solubility was calculated. The PXRD pattern of the filtrate was recorded to ensure that the solubility of the desired polymorph was determined. Two parallel experiments were performed.

2.3.7.3. UV/Vis spectroscopic solution concentration monitoring

Solution concentration throughout SPMTs in methanol was monitored by measurements of the UV/Vis absorption at 272 nm using a Perkin-Elmer Lambda 25 UV/Vis spectrophotometer (PerkinElmer Inc., USA). Calibration was performed in the concentration region between 0.2 mM and 0.01 mM (R^2=0.99990). For solution concentration determination 20 μL aliquot of filtered reaction medium was diluted with 40 mL of methanol.

2.3.7.4. NMR spectroscopic self-association studies

^{1}H NMR spectra were recorded as a function of theophylline concentration in the solution. Experiments were performed in methanol-D4, chloroform-D, acetone-D6, dimethyl sulfoxide-D6, deuterium oxide, acetonitrile-D3 and formic acid-D2 Concentration region from nearly saturated solutions (1.0 M in formic acid-D2; 0.050 M in methanol-D4; 0.015 M in acetone-D6; 0.10 M in dimethyl sulfoxide-D6, deuterium oxide, chloroform-D and acetonitrile-D3) to 1 μM solutions was covered. Ground anhydrous theophylline Form II was used to prepare the most concentrated solution in each solvent and the rest of the solutions were prepared by subsequent dilution. Additional samples, where an excess amount of ground theophylline was added to deuterated solvents, were prepared to simulate suspensions similar to that examined in SMPT. The mass of theophylline added was 120% of the mass necessary to prepare saturated solution in the respective solvent. An analytical balance (±0.1 mg) and micropipettes (±1 μL) were used for solution preparation. NMR spectra of prepared solutions were recorded right after solution preparation, and repeated after 1 and 2 weeks. NMR tubes of prepared solutions were closed with lids and sealed with parafilm. Samples were stored at 20.0±0.5 °C between measurements.

^{1}H NMR spectra were recorded on a Bruker Avance DRX 400 MHz spectrometer (Bruker BioSpin, Germany) using residual solvent as an internal standard. NMR spectra were recorded at 26.8±0.5 °C (300.0±0.5 K).

Theophylline ^{1}H chemical shifts were allocated by ^{1}H-^{13}C HSQC according to literature assignments [238]. ^{1}H-^{13}C HSQC experiments were carried out using the standard Bruker program hsqcetgpsi2 [253,254].

2.3.7.5. In-situ monitoring of crystallization process.

Two drops (~0.07 mL) of saturated theophylline methanol, acetone, acetonitrile, chloroform, water and formic acid solutions from solubility determination experiments (section 2.3.7.2) were placed on a FTIR spectrometer liquids plate and spectra of the solution were continuously recorded during solvent evaporation/theophylline crystallization. Each FTIR spectra showed the average of 16 co-added scans, recorded in 75 s. For acetone solution 4 co-added scans (recorded in 17 s) were averaged. Spectra were recorded until three continuous spectra were identical and no peaks of solvents were visible. The experiment with each solvent was repeated in triplicate.

3. Results and discussion

3.1. Quantitative PXRD phase analysis

Advantages like uniqueness of X-ray powder pattern of compounds, non-destructive nature and simplicity make PXRD the most preferred and extensively used technique for quantification of polymorphic mixtures [255,256] therefore PXRD were chosen as the most appropriate method for phase quantification in this study. The homogenous composition of the analysed mixtures and equivalent extinction effects for two polymorphs ensure that the diffraction peak intensity of each phase depends linearly on the phase weight fractions in the sample [199].

PXRD method calibration was performed as described in section 2.3.1, and method calibration curve of α and β tegafur mixture is given in Figure 3.1. It is evident that the correlation was not completely linear and the calculated content of β tegafur in the samples was up to 2% higher than was actually weighed. We believe that this was because of the preferred orientation of α tegafur, different degree of crystallinity for both polymorphs and possible microabsorption. Nevertheless, experimental data can be described with linear equation $y=(1.02\pm0.01)x$, with R^2 value of 0.9990. The method used was found to be linear in the range 0 – 100% with limit of detection (LOD) and limit of quantification (LOQ) calculated [215] to be 3.0 and 9.2%, respectively. The method was found to be precise with relative standard deviation (RSD) of 2.0%. Statistical probability (p) used was $p<0.05$. Relatively high LOD, LOQ and RSD values are because of the fast scan speed (0.2 °/min) used in the experiments. In order to maintain consistency, scan speed used for calibration was the same as further used in SMPT quantitative analysis. Scan speed of 0.2 °/min was chosen because of the ability to provide fast PXRD measurements necessary for kinetic SMPT studies.

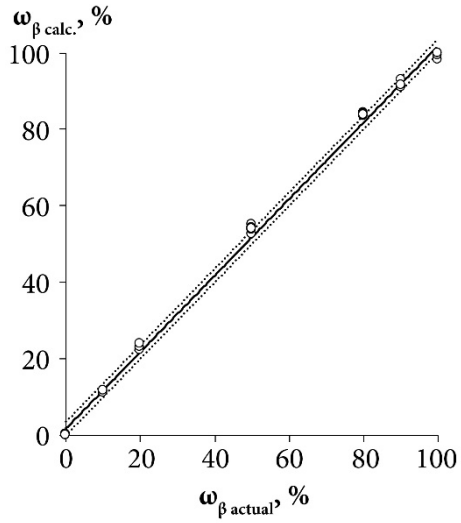

Figure 3.1. The dependence of calculated β tegafur weight fraction ($\omega_{\beta\ calc.}$) upon the actual β tegafur content in the sample ($\omega_{\beta\ actual}$). Statistical probability $p<0.05$.

3.2. Determination of micro amounts of β tegafur in the α and β polymorph mixture by powder X-ray diffractometric analysis.

Results described in this subsection have been previously partially described in PhD thesis of Sanita Skladova "Method improvement of the investigation of phase equilibrium and phase transition kinetics with the goal of throughout polymorph screening of the variety of active pharmaceutical ingredients".

The purpose of this study was to develop a suitable analytical method for determining micro amounts of the thermodynamically stable polymorphic form (<1%) in the mixture of thermodynamically stable β tegafur and metastable α tegafur. The method used here employed controlled polymorphic transformation from metastable α tegafur to the thermodynamically stable β tegafur. Thus, the content of thermodynamically stable polymorph in the sample was increased by solvent drop milling to the amount that can be determined with the quantitative PXRD analysis, and then, the amount of the thermodynamically stable polymorph in the initial sample was calculated from calibration data. Schematic representation of experiment design is shown in Figure 3.2. Analysed samples were milled for fixed time with the certain milling frequency at 20 °C, and the phase transition was stimulated by adding some water to samples before milling [135,175]. The calibration line was constructed using the least-square method.

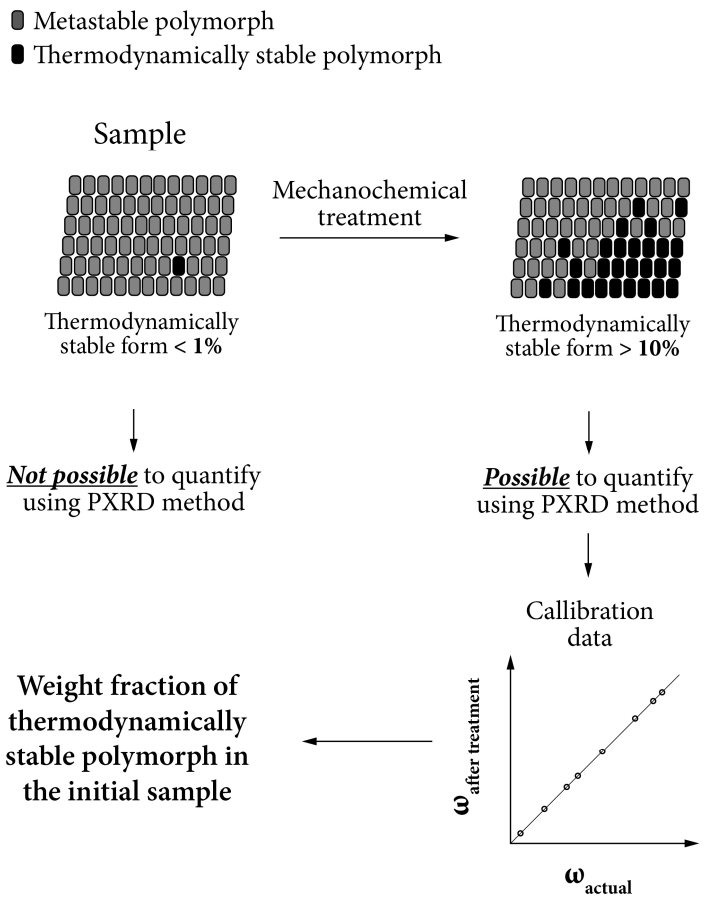

Figure 3.2. Schematic representation of experiment design.

To develop the micro amount quantification method of the thermodynamically stable form in the metastable form, six experiments were carried out to establish the acceptable method for optimal milling conditions. The samples containing 1.5% weight fraction of β tegafur were milled for 3.0, 5.0 and 7.0 minutes after adding a drop (~0.07 mL) or two drops (~0.15 mL) of water. The aim of these experiments were to investigate sample preparation conditions in which α modification after milling does not completely transit to β form, but the sample consist of comparatively high content of α tegafur. The samples that were milled for 5.0 and 7.0 minutes had practically the same composition, but in the samples that were milled for 3.0 minutes β form content was noticeably lower as it can be seen in Figure 3.3.A. To promote the phase transformation of β tegafur to α form, some water – one drop (~ 0.07 mL) or two drops (~0.15 mL), was added to the sample before milling. In all experiments the content of β tegafur in the samples was significantly higher if a single drop of water was added to the sample before milling (see Figure 3.3.B).

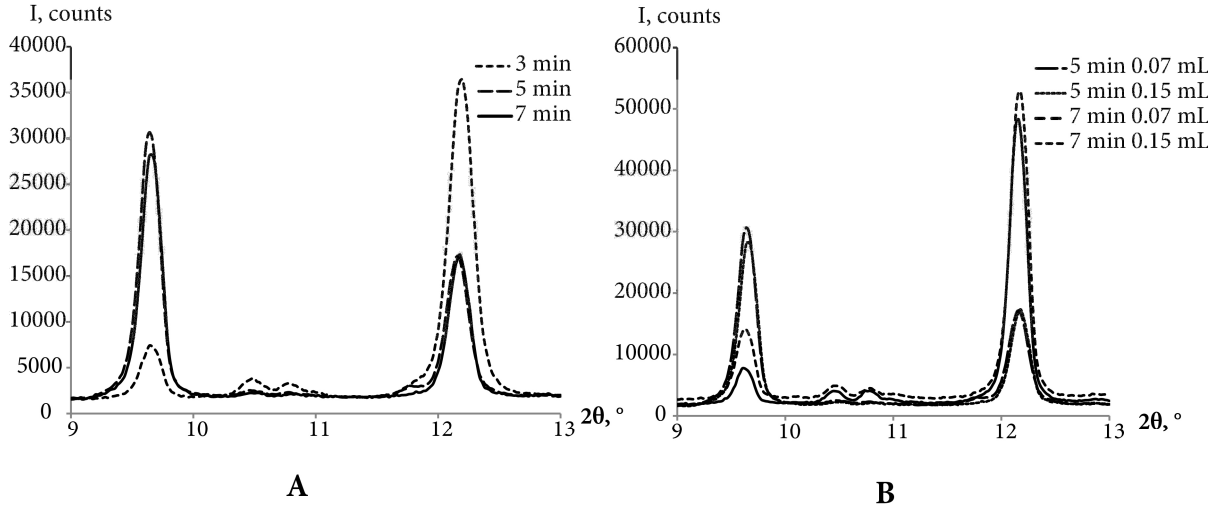

Figure 3.3. A) Powder X-ray diffraction patterns of the tegafur α and β form mixture containing 1.5% weight fraction of β tegafur after milling for 3.0; 5.0 and 7.0 minutes; and B) powder X-ray diffraction patterns of the tegafur α and β form mixture containing 1.5% weight fraction of β tegafur after milling for 5.0 and 7.0 minutes if the phase transition was induced adding a single drop (~0.07 mL) or two drops (~0.15 mL) of water.

Any solvent that does not form solvates or hydrates with analysed polymorphic forms could be used to quicken the phase transformation. For the method development as the optimal sample preparation conditions were chosen the milling for 5.0 minutes and adding a single drop of water.

Powder X-ray diffraction patterns of calibration samples after milling for 5.0 minutes inducing the phase transformation with adding a drop of water to the sample are shown in Figure 3.4.A, whereas the dependence of tegafur β form weight fraction after milling upon the initial β form content in the sample is shown in Figure 3.4.B.

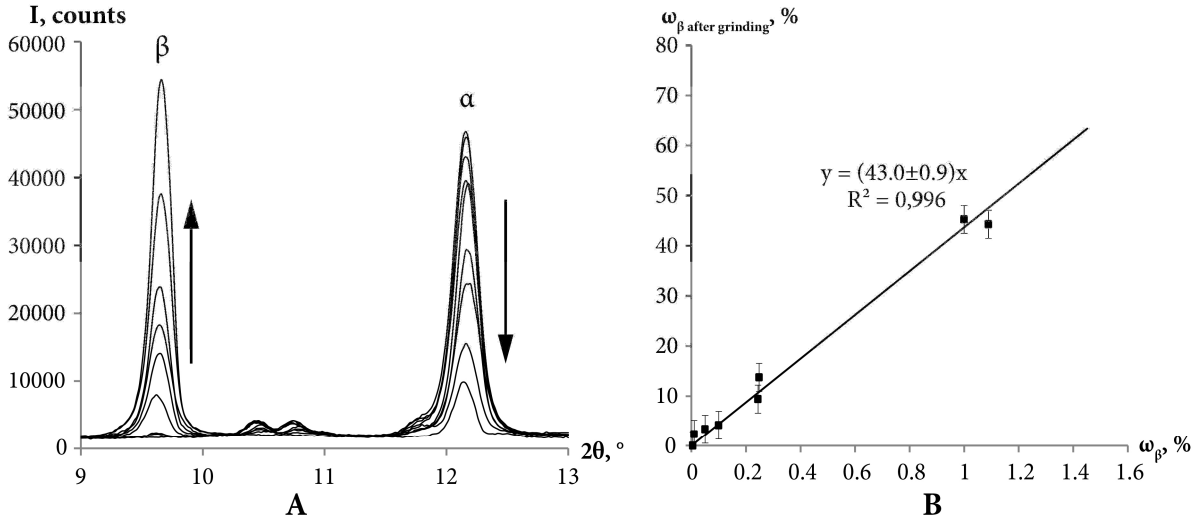

Figure 3.4. A) Powder X-ray diffraction patterns of calibration samples after milling for 5.0 min inducing the phase transformation with adding a single drop of water to the sample; and B) the dependence of tegafur β form weight fraction after milling upon the initial β form content in the sample.

The calibration factor is equivalent to a linear slope of the linear regression equation. The regression line was described by relationship $y=ax$, taking into account the intersection with the origin. If the calibration factor would be calculated from the equation $y=ax+b$ in this case the approximated line intersect y-axis at non-zero value and that means positive phase content at zero peak intensity ($I_{peak}\neq 0$, when $\omega=0$), which is physically impossible. The optimal linear slope was calculated using *MS Excel* [257] function *Linest*. The equation of calibration curve was $y=(43.0\pm0.9)x$, the correlation coefficient $R^2=0.996$ and the regression residual mean square error or the standard deviation S_n, which characterizes the dispersion between the measured (y_i) and theoretically calculated value (Y_i), was 1.5%.

3.2.1. Conclusions

The results of this study demonstrate that the quantification of low levels (<1%) of unwanted polymorphs in pharmaceuticals can be made using the semi-quantitative, but sensitive X-ray diffractometric method. Employed method is based on controlled thermodynamically stable polymorph increase by solvent drop milling to the amount that can be determined with the quantitative PXRD analysis, and then, the amount of the thermodynamically stable polymorph in the initial sample is calculated from calibration data. The content of tegafur β form after milling is proportional to the initial β form mass fraction in the sample.

3.3. Optimization of sample preparation conditions for detecting trace amounts of β tegafur in α and β tegafur mixture

As shown in Section 3.1, it is possible to determine trace amounts (less than 0.01%) of the thermodynamically stable form in mixtures of thermodynamically stable and metastable forms. In this section we estimate sample preparation condition impact on proposed quantification method.

It is worth noting, that our first experiments in this direction indicated that phase transition did not occur when pure α and β tegafur were ground separately without a solvent, therefore the initial sample preparation by milling of pure α and β tegafur did not promote phase transition and could not affect the results of quantitative analysis.

3.3.1. Optimum milling frequency determination.

Tegafur α and β form mixtures with β form weight fraction from 2.0% to 0.0001% were ground at three different milling frequencies: 7 Hz, 10 Hz and 15 Hz to establish an acceptable milling frequency. The recorded PXRD patterns (down to ω_β=0.50%) and calibration curves for all three milling frequencies are shown in the Figure 3.5. In the higher range of initial β tegafur weight fraction (up to ~20%) all of the calibration curves had an exponential nature, but in the lower range of β form mass fraction (<2.0%) the calibration curves of samples ground at 7 Hz and 10 Hz frequencies could be considered as linear. At the same time, the conversion degree curve for samples ground at a 15 Hz frequency maintained an exponential nature also in the lower range. Conversion degree dependence on the initial β tegafur weight fraction most likely exhibits an exponential nature, because the degree of phase transition is more affected by the surface area of β tegafur, thus also the phase boundary area, and less by the initial weight fraction of β tegafur. The weight fraction of β tegafur in the sample is not linearly proportional to phase boundary area, and therefore the weight fraction after milling does not depend linearly on the initial weight fraction of β tegafur.

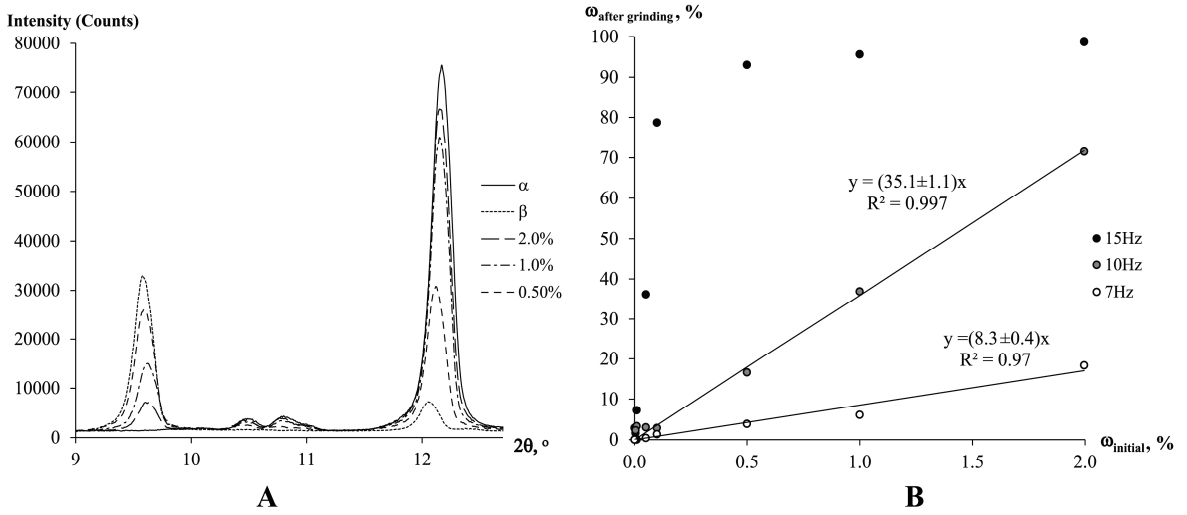

Figure 3.5. A) Powder X-ray diffraction patterns of pure α and β tegafur and calibration samples after milling with 10 Hz frequency for 5 min in 20 °C; B) conversion degree depending from initial β form weight fraction and milling frequency.

The calibration factor for samples ground at 7 Hz and 10 Hz frequencies was equivalent to the linear slope of the linear regression equation. The liner regression was described as previously (see section 3.1). Calibration equation for those samples ground with 7 Hz frequency was $y=(8.3\pm0.4)x$ with correlation coefficient $R^2=0.97$ and standard deviation $S_n=1.1$%, but for samples ground with 10 Hz frequency the calibration equation was $y=(35.1\pm1.1)x$ with the correlation coefficient $R^2=0.997$ and standard deviation $S_n=1.4$%.

Experimental points for samples ground with 15 Hz frequency could be described with the exponential equation

$$\omega_{\beta,teor} = \omega_{\beta,\infty}(\omega_{\beta,\infty} - \omega_{\beta,0})e^{-k\omega_{\beta,initial}} \qquad 3.1,$$

where $\omega_{\beta,teor}$ was the theoretically calculated weight fraction of β tegafur after milling; $\omega_{\beta,\infty}$ was the final weight fraction of β tegafur when the phase transition had ceased; $\omega_{\beta,0}$ was the weight fraction of β tegafur after milling when $\omega_{\beta,initial} = 0$; k was the phase transition rate constant and $\omega_{\beta,initial}$ was the weight fraction of β tegafur before milling. The *MS Excel* [257] optimization add-on *Solver*, based on the least squares method, was used to optimize equation 3.1 constants. The equation

$$\omega_\beta = 96.6(1 - e^{-12.4\omega_{\beta,initial}}) \qquad 3.2,$$

was thus obtained. Experimental point dependence on the initial weight fraction of β tegafur ($\omega_{\beta,initial}$) was empirical in this case, and the exponential nature of experimental curve may be

considered as coincidence. The polymorphic phase transition rate depends on the mass transition rate from one phase to another [258], therefore it may be considered that the main factor influencing overall phase transition rate is related to the surface properties of both phases.

If the weight fraction of β tegafur in the sample ground at 15 Hz frequency does not exceed 0.10%, then it is possible to use a linear regression equation $y=(770.0\pm0.1)x$ with the correlation coefficient $R^2=0.995$ and standard deviation $S_n=2.2\%$.

In the initial β tegafur weight fraction region from 2.0% to ~0.05% the best correlation was achieved, when the samples were ground with 10 Hz frequency, but if lower thermodynamically stable form contamination in metastable form must be determined, then the milling frequency of 15 Hz is preferred.

3.3.2. Optimum water additive amount determination.

Tegafur α and β form mixture with the β form weight fraction of 1.0% was ground with various amounts of added water. The conversion degree was determined, depending on the volume of added water, and is shown in the Figure 3.6. The sum of two empirical equations (Langmuir and Cauchy–Lorentz equations; equation 3.3) was chosen to describe the experimental data, because there are no equations in literature that would fit these experimental data:

$$\omega = \frac{dkV}{1+kV} + f\frac{1}{\pi}\left(\frac{b}{(V-a)^2+b^2}\right) \qquad 3.3,$$

where ω is the weight fraction of β tegafur in the samples after milling, V is the volume of added water (mL), f is the contribution factor, a is the volume of added water at which the highest conversion degree was observed, b is the distribution width ratio, and d and k are empirical constants.

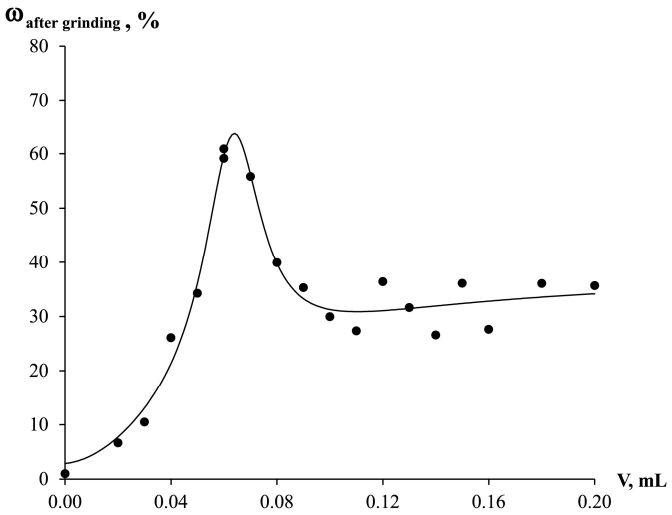

Figure 3.6. Conversion degree of ground (10 Hz, 5 min at 20 °C) 1.0% β tegafur sample, depending on the added water volume.

Cauchy–Lorentz equation term or another statistical "bell shaped" function was introduced into the equation 3.3 to describe the milling efficiency depending on the volume of added water. A "bell shaped" statistical distribution term was selected, because surface area determination experiments demonstrated (see section 0) that the milling efficiency, and thus also the surface, is dependent on the added water volume, matching a statistical "bell shaped" distribution. Thus, if no water sorption on the surface of tegafur occurs, the conversion degree depends only on the milling efficiency, while that depends on the amount of water added. Langmuir equation term was introduced into the equation 3.3 to describe a phase transition occurring in the adsorbed water layer on the surface of tegafur, and it is not related to the phase transition promoted by milling.

It was observed that samples with additive volume of less than 0.06 mL were free flowing powders after milling, but, when the water additive volume was greater than 0.06 mL, the samples formed thick paste and stuck to the milling vessel walls. Water can be considered as a lubricant in this process and increasing the volume of water additive above 0.06 mL decreased the conversion degree, while at water volumes below 0.06 mL the conversion degree of α tegafur to β tegafur increased.

3.3.3. Phase transition during sample drying.

The metastable α tegafur transforms to the thermodynamically stable β form during a process involving tegafur dissolution in water, and subsequent thermodynamically stable form

crystallization due to water additive evaporation. The kinetic curve of this process is shown in the Figure 3.7. The highest conversion degree was observed for samples prepared with 0.06 mL of water (see section 3.3.2), yet this experiment was performed with 0.20 mL of water, to extend the water evaporation time and to enable acquisition of more experimental data. Experiments with smaller amounts of water exhibited the same trend, but results were less obvious. The kinetic curve can be described with a kinetic equation $\omega_\beta = 35.8 - 20.7e^{-0.063t}$ (equation constants were optimized with *MS Excel* [257] optimization add-on *Solver*). Not only an increase of β tegafur peak was observed during this process, but there was also a minimal increase of α form diffraction peaks indicating increasing crystallinity of α form, or an increasing preferred orientation due to the fracture of crystals along certain cleavage planes. As can be seen in Figure 3.7., the conversion degree to β tegafur was highly dependent on sample drying time; thus for a precise trace amount quantification all samples should be dried for the same duration (at least 1 h).

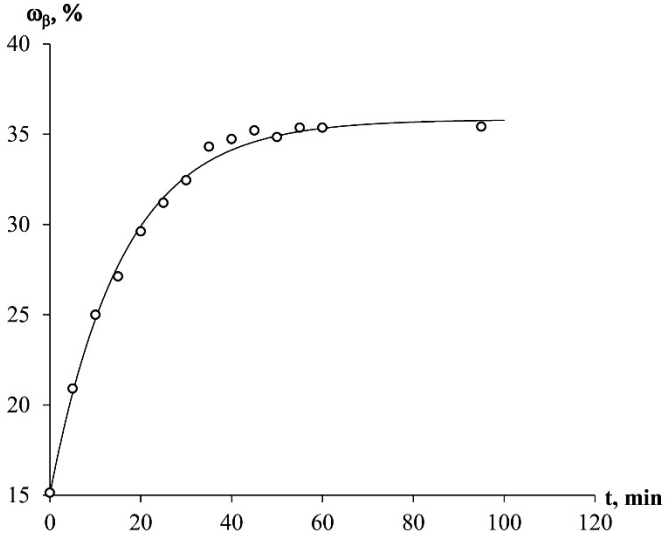

Figure 3.7. β tegafur weight fraction changes during recrystallization process of 1.0% β tegafur sample after milling with 10 Hz frequency for 5 min at 20 °C with 0.20 mL water additive.

3.3.4. Surface area determination.

Surface areas of unground samples, as well as samples ground without water, and with 0.06 mL and 0.12 mL of water were determined for estimating the impact of water on milling efficiency. The determined surface areas are shown in the Table 2. The surface area of unground 1.0% β tegafur in mixture with α tegafur was 13.4 m^2/g, but the surface area of sample ground

with 0.12 mL water was 13.9 m^2/g, which indicated that water volume above 0.06 mL did not improve milling efficiency, as discussed in section 3.3.2. The surface area of the sample ground without water was significantly higher than for the sample ground with a 0.12 mL water additive. These differences can be related to different sample dispersion in the milling vessels; dry sample after milling was homogenously distributed in the milling vessel, whereas the wet sample after milling was located on the mill walls. The maximum surface area, hence the maximum milling efficiency, was achieved when phase transition during milling was stimulated with a 0.06 mL water additive.

Table 2. Surface areas of unground, dry ground and with 0.06 mL and 0.12 mL water additive ground (5 min, 10 Hz, 20 °C) samples.

Sample	Surface area, m^2/g
unground	13.4
ground without additive	16.9
ground with 0.06 mL water additive	18.3
ground with 0.12 mL water additive	13.9

3.3.5. Conclusions

Sample preparation condition optimization allowed us to quantify down to 0.0005% of the thermodynamically stable β tegafur in α tegafur. The amount of the thermodynamically stable form after sample processing was proportional to its initial weight fraction.

In β tegafur weight fraction range from 2.0% to ~0.05% the best correlation was achieved when samples were ground for 5 minutes at 20 °C with 10 Hz frequency. At lower weight fraction of β tegafur the milling frequency of 15 Hz was preferred. The optimum results were achieved when 0.06 mL of water was added to 0.50 g of tegafur. A sum of Langmuir and Cauchy–Lorentz equations could be used to describe the change in conversion degree depending on the added water volume. The indirectly determined surface areas and the dependence of conversion degree on water additive volume demonstrated that increasing the added the water volume above 0.06 mL did not improve milling effectiveness. Conversion degree from α tegafur to β tegafur was highly dependent on sample drying time.

This method is generally applicable when the sample has phases with similar particle properties, and the peak intensity is not particularly dependent on preferred orientation and perhaps line broadening effects.

3.4. Organic solvent effects on phase transition of α and β tegafur upon milling with solvent additives

In all previously described experiments phase transformation was stimulated using water additive, however it is expected that used solvent will affect the efficiency and outcome of solvent drop milling just like in any other crystallization. Here we will investigate the effect of solvent additive on phase transition of α and β tegafur.

3.4.1. Solvent effect on the degree of phase conversion during milling

Initially conversion degrees for samples containing 0.5% of β tegafur in α and β tegafur mixture were determined, and a complete conversion to β tegafur occurred when *n*-propyl acetate, acetonitrile, ethyl acetate, 1,2-dichloroethane, acetone, tetrahydrofuran, *n*-butanol and methanol were used as additives (see Table 3). To find out, which of these solvents promotes the α tegafur conversion to β tegafur the most, samples containing 0.1% of β tegafur in α and β tegafur mixture were examined. None of the solvents promoted complete conversion to β tegafur in the case of samples containing 0.1% of β tegafur in α and β tegafur mixture with current milling conditions (5 min at 20 °C with 15 Hz shaking frequency). Experiments with pure α tegafur were also performed, to find out if there might be any solvents that promote phase transition without any β tegafur seeds in the sample.

Our quantitative composition calculation method was not suitable for quantifying phases with weight fraction below 3% after the milling, so the results for samples, where β tegafur peak was detected, but was not large enough to quantify, are given as "<3%".

The most complete phase transition to β tegafur, for samples containing 0.1% of β tegafur, occurred when methanol or 1,2-dichloroethane additive was used – the weight fraction for β tegafur increased during milling from 0.1% to 82% and 72%, respectively. The most marked decrease in conversion degree between samples with the initial β tegafur content of 0.5% and 0.1% occurred in those cases, when acetone or *n*-butanol additive was used – complete conversion was detected when samples with the initial β tegafur content of 0.5% were ground, but when 0.1% mixture was ground, only a slight increase of β tegafur content was detected (less than 5%).

Table 3. Conversion degrees of 0.5% and 0.1% β tegafur mixture in α tegafur and pure α tegafur during the milling (5 min at 20 °C with 15 Hz shaking frequency), depending on the used solvent additive, and corresponding phase transition rates from α tegafur to β in the presence of respective solvent vapour.

	$\omega_{\beta,after\ grinding}$, %			
$\omega_{\beta,initial}$, % / **Solvent**	**0.5% β**	**0.1% β**	**α**	**k, days^{-1}**
Methanol [HBD]	100	82	<3	0.073
1,2-Dichloroethane [AP]	100	72	92	0.049
n-Propyl acetate [AP]	100	37	-	-
Tetrahydrofuran [EPD]	100	15	-	1.878
Ethyl acetate [AP]	100	13	13	0.042
Acetonitrile [AP]	100	6	8	0.194
n-Butanol [HBD]	100	3	<3	0.015
Acetone [AP]	100	<3	-	2.167
Benzyl alcohol [AA]	95	52	25	0.033
n-Butyl acetate [AP]	92		-	0.004
Ethanol [HBD]	86		-	0.019
Toluene [AA]	83		6	0.017
n-Pentanol [HBD]	57		-	0.007
n-Propanol [HBD]	57		-	0.058
Chloroform	44		42	0.007
Water	23		-	0.038
2-Propanol [HBD]	31		-	0.007
n-Heptanol [HBD]	30		-	0.007

AP – aprotic polar, AA – aromatic apolar, EPD – electron pair donor, HBD – hydrogen bond donors (for more information see Appendix 3).

As we can see, a 1,2-dichloroethane additive promotes almost complete phase transition in all cases, even when pure α tegafur is used. Similar situation can be observed when chloroform additive is added, only then the conversion proceeds by ~40%. This could be related to a solvent structure that promotes only one polymorphic form regardless of whether the seed crystals are

added to a sample or not. Conversion of pure α tegafur to β tegafur occurs due to solvent structure factors, similar to those in crystallization [259]. Hydrogen bond donor solvents do not promote phase transition of pure α tegafur, but both investigated aromatic aprotic solvents promote phase transition of pure α tegafur, even though they do not ensure a complete phase transition for samples with 0.5% β tegafur additive.

Changes in conversion degrees are not proportional from one solvent to another when the initial weight fraction of β tegafur changes from 0.5% to 0.1%. For example, when acetone additive is added to a sample, conversion degree changes form 100% to less than 3%, but when methanol additive is added, conversion degree changes form 100% to 82%. There is no clear understanding about the causes of these differences, but it could be related to solubility or dissolution rates of tegafur in the investigated solvents, or simply due to structural peculiarities of each solvent.

To ensure that phase transition is not stimulated by the water impurity in solvents, Karl Fischer titration was performed for all used solvents, and it was determined that water amount in the solvents did not correlate with the conversion degree to β tegafur.

3.4.2. Solvent vapour effect on phase transition

It is known that solvent vapours accelerate phase transition [105], however it is not known if the effect on solid phase transition is the same for solvent vapour and liquid solvent additives. For this purpose an atmosphere of solvent vapour with 95% relative pressure was created by using the same solvents as in the previous experiments. Phase transition kinetic curves were recorded by using PXRD (see Figure 3.8.), and transition rates were calculated as described elsewhere [105].

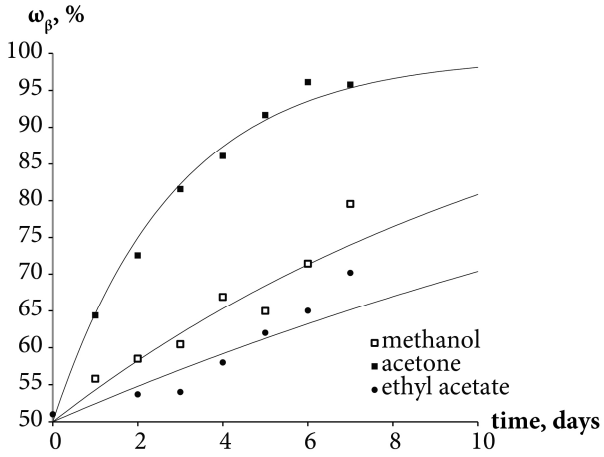

Figure 3.8. β Tegafur weight fraction changes during sample exposure to 95% relative vapour pressure of methanol, acetone and ethyl acetate.

Saturated solvent vapour atmosphere was not used to prevent condensation and sample wetting with a condensed solvent. Mixture with a weight ratio of 1:1 was used because no phase transition was observed for samples with only 0.5% of β tegafur.

Phase transition rates for samples exposed to solvent vapour atmosphere with a 95% relative pressure are given in Table 3. The general tendency matches the observations from α and β tegafur mixture milling experiments – aprotic polar solvents with the smallest molecules are the best promoters of this phase transition. Rough correlation between ground sample conversion degrees and phase transition rates from α tegafur to β in the presence of solvent vapours suggests that solvent role in both types of phase transformations are similar.

In the case of ethyl acetate and *n*-propyl acetate there was a very high conversion degree, despite the low sorption and phase transition rates in samples exposed to these solvents at 95% relative pressure, indicating that the phase transition during the milling procedure is affected not just by solvents in gaseous state, but also in their liquid state.

3.4.3. Conclusions

The results of these studies demonstrate that the conversion degree of metastable α tegafur to the thermodynamically stable β tegafur upon a milling with solvent additive is highly dependent on the solvent used. The most complete phase transition to β tegafur occurs when methanol or 1,2-dichloroethane additive is used, however only *n*-propyl acetate, tetrahydrofuran and water are suitable for developed quantitative analysis method. Phase

transition dynamics of α tegafur to β tegafur is in a good agreement for samples ground in ball mill with solvent additive and samples, that were exposed to 95% solvent relative vapour pressure.

3.5. Organic solvent desorption from two tegafur polymorphs

Here we try to understand the nature of solvent and surface interaction using data from solvent desorption studies. Desorption process of several solvents from both polymorphic forms of tegafur was examined to compare solvent-tegafur surface interaction behaviour. As seen in section 3.5.2 (see Figure 3.10.), solvent desorption experiment indicated that in most cases desorption occurred in two steps. There is no clear understanding on this phenomenon, but it could be a case of classical monolayer and multilayer (with possible capillary condensation) desorption. Solvent molecule desorption from the top solvent multilayers can be associated with the beginning of desorption curve (part I in Figure 3.10.B), where rapid sample mass decrease was detected. The next stage, after the initial rapid loss of solvent, in most cases appeared exponential and involved solvent monolayer desorption (part II in Figure 3.10.B). Following experiments were performed to get some understanding about these processes.

3.5.1. Surface area and relative sample surface coverage

Amount of each solvent necessary to form solvent monolayer was calculated using determined surface area data (see Table 4), adsorbed solvent mass and solvent molecule dimensions [260]. Using mass of solvent, adsorbed during sample storage in 95% relative solvent vapour pressure, and theoretical mass of solvent in monolayer, sample surface coverage for each sample was calculated. These results are given in Figure 3.9.

Table 4. Surface areas of α and β tegafur samples depending on particle size.

Polymorph	Particle size, mm	Surface area, m^2/g
α	<40	12.4
	40-75	12.2
	75-150	5.9
β	<40	14.8
	40-75	12.8
	75-150	9.2

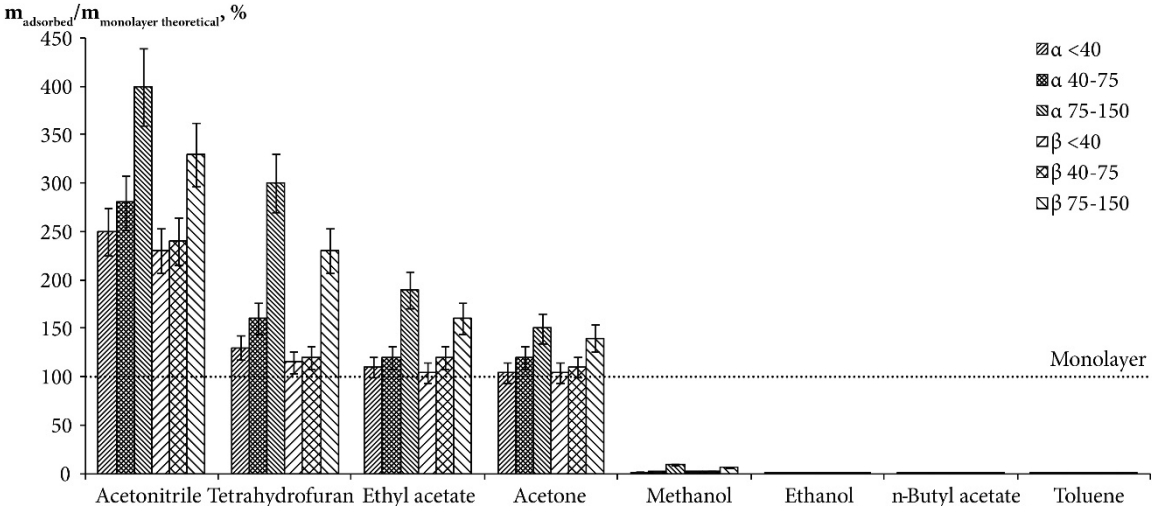

Figure 3.9. Relative sample surface coverage with used solvents in 30 °C, for samples stored in 95% relative solvent vapour pressure ($m_{adsorbed}/m_{theoretical}$).

If we take a look at sample surface areas (Table 4), it can be seen that the surface areas of samples with particle size 40–75 μm and less than 40 μm were almost the same for both polymorphs. SEM examinations shows distinct differences in particle size distribution for both fractions, therefore similar surface areas for both fractions most likely are due to differences in bulk density – fraction with smaller particles forms more dense sample, but fraction with larger particles forms less dense sample. These changes in the sample density affects the effective/accessible surface area of the sample and the greater bulk density for fraction with particle size less than 40 μm causes the apparent reduction of the surface area in the experimental measurement.

From relative sample surface coverage data we see that the amount of acetonitrile, tetrahydrofuran, ethyl acetate and acetone adsorbed on the tegafur surface is enough to form at least solvent monolayer and that the decrease of sample surface area increases the relative sample surface coverage. These calculations shows that amount of acetonitrile adsorbed on the surface is enough to form up to 4 solvent molecular layers in the case of 75–150 μm α tegafur sample, but adsorbed methanol amount is sufficient to cover up to 10% of the sample surface (for samples with particle size 75–150 μm), while adsorbed toluene, ethanol and *n*-butyl acetate covers less than 3% of the sample surface.

The decrease of particle size from 75–150 μm to 40–75 μm increases the relative sample surface coverage by about 20 to 40%, but particle size decrease from 40–75 μm to less than

40 μm increases the relative sample surface coverage by about 5 to 15%. We believe that the observation that less solvent multilayers formed on the smaller particles if compared to the larger particles, is related to previously mentioned differences in the bulk densities. Sample with the smallest particles (less than 40 μm) has higher bulk density then the rest fractions and therefore effective/accessible surface area of this sample is lower than it would be if all the samples had the same density. It is also possible that such results could be due to the effective surface area decrease during the solvent adsorption process because of sample recrystallization and/or solvent sorption on the previous solvent layers; especially for sample with particle size less than 40 μm.

3.5.2. Solvent desorption studies

As can be seen from ethyl acetate, acetone and tetrahydrofuran desorption curves (see Figure 3.10.A), desorption occurs in two steps – at the beginning part of the solvent is desorbed from the surface of tegafur, and afterwards desorption progresses throughout the volume of tegafur particles.

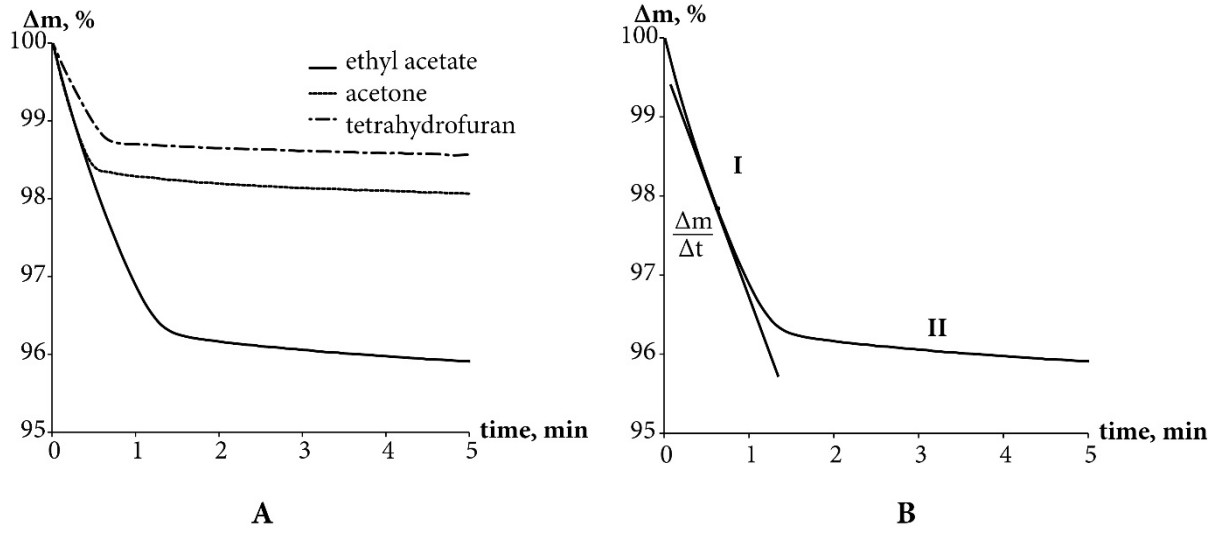

Figure 3.10. A) Ethyl acetate, acetone and tetrahydrofuran desorption curves from α tegafur; and B) example of desorption rate calculation

Solvent desorption from the surface can be associated with the linear part of desorption curve. The next stage, after the initial rapid loss of solvent, appears exponential and involves solvent desorption from the entire volume. Solvent surface desorption rates were compared by using the average desorption rate equation

$$\alpha = \frac{dm}{dt} \qquad 3.4,$$

where α is desorption rate, m is sample mass, and t is time. An obstacle to the determination of desorption rate was the posed by the observation that the beginning of desorption curve cannot be used due to a possible desorption delay. The best way for avoiding this problem could be to calculate desorption rate in the middle of a desorption process, using a middle point calculated from the sample mass before and after desorption, thereby preventing errors stemming from desorption delay and from imprecise end point determination (see Figure 3.10.B). Solvent desorption rates depending on tegafur polymorphic form, particle size and the selected solvent for samples stored at 95% relative solvent vapour pressure are summarized in Figure 3.11. (monolayer desorption in Figure 3.11.A. and multilayer desorption in Figure 3.11.B.). No acetonitrile and tetrahydrofuran monolayer desorption from α and β tegafur were observed.

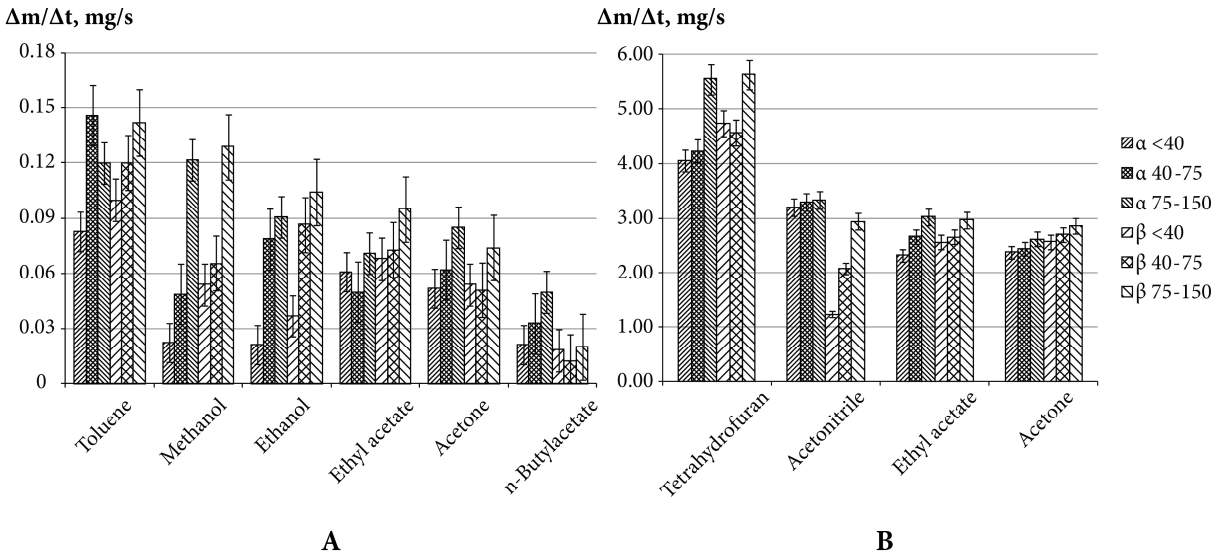

Figure 3.11. Desorption rates of A) acetone, ethyl acetate, n-butyl acetate, ethanol, methanol and toluene monolayers; B) acetone, acetonitrile, ethyl acetate and tetrahydrofuran multilayers; depending on tegafur polymorphic form and particle size.

The general trend was that desorption rates increased with increasing particle size and there was no distinct difference between desorption rates from both polymorphs. Faster desorption from the samples with the larger particles was due to easier solvent removal from the sample surface, which is favoured by large volume between particles where solvent can diffuse more easily if compared to sample with smaller particles. A lack of major changes between both

polymorphs indicated that differences in crystal structure and surface properties had no great importance on the solvent desorption rates, therefore the main factor affecting desorption rate is sample particle size and morphology. Difference in multilayer solvents desorption rates from samples with particle size 40–75 μm and less than 40 μm in most cases was considerably lower than those for multilayer solvent desorption rates from samples with particle size 75 to 150 μm and 40–75 μm just like the surface areas of the analysed samples.

Solvent desorption rates from α and β tegafur samples showed that desorption rates of acetone, acetonitrile, ethyl acetate and tetrahydrofuran from solvent multilayers were approximately 30 times higher than those from solvent monolayers. Further experiments with samples stored in 50% relative solvent vapour pressure confirmed that the higher desorption rates for tetrahydrofuran, acetonitrile, acetone and ethyl acetate most likely were due to multilayer sorption. Thus, at 95% relative solvent vapour pressure the sample surface was covered with tetrahydrofuran, acetonitrile, acetone and ethyl acetate as molecular multilayer, and the desorption rates for molecules situated at the higher layers were much higher than for molecules in direct contact with the surface. However, if samples were stored in the same solvents at 50% relative solvent vapour pressure, then monolayer solvent sorption dominated and only partial surface saturation above the monolayer occurred. This information was also confirmed by sorption results, as the amount of adsorbed solvent at 95% and 50% relative solvent vapour pressure differed 1.5–3 times for tetrahydrofuran, acetonitrile, acetone and ethyl acetate. This suggests that at 95% relative solvent vapour pressure of acetone, acetonitrile, ethyl acetate and tetrahydrofuran, the solvent sorption noticeably exceeded monolayer coverage, but for *n*-butyl acetate, ethanol, methanol and toluene the sorption on the tegafur surface was significantly below monolayer coverage.

Schematically solvent desorption process from the surface and its effect on the desorption kinetics are illustrated in Figure 3.12. Section A shows the solvent desorption process, the solvent molecules in monolayer having a different interaction energy than the rest of the solvent molecules (multilayer molecules), and two separate solvent desorption phases were observed (solvent molecules with higher interaction energy than the rest of the molecules are schematically represented by filled circles). From the solvents used, acetone and ethyl acetate exhibited such a desorption behaviour. Desorption of acetonitrile and tetrahydrofuran differed

from the rest of the solvents by the absence of the monolayer desorption part (see Figure 3.12.B). This means that all of the adsorbed solvent molecules were energetically equal and the ground layer solvent molecule interaction with sample surface was not significantly stronger than interaction between the solvent molecules themselves. Our assumption was that this phenomenon could be related to solvent ability to form hydrogen bonds and other effective intermolecular interactions between solvent and surface, as well as between two solvent molecules. Ethanol, *n*-butyl acetate, methanol, and toluene desorption behaviour is schematically illustrated in Figure 3.12.C. These solvents were desorbed in one step like in the previously described case; with the difference that in this case it was a monolayer desorption.

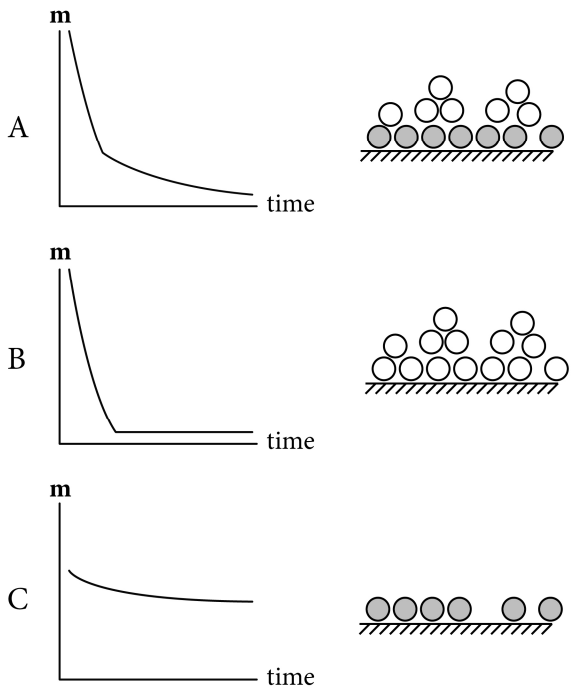

Figure 3.12. Schematic depiction of solvent desorption behaviour and solvent molecule position on the surface.

The effect of the particle size and solvent vapour relative pressure on desorption curve are summarized in Figure 3.13., by illustrating that solvent relative vapour pressure affects only the amount of solvent adsorbed on the surface (Figure 3.13.A), but particle size affects the solvent desorption rate, if the same amount of solvent was adsorbed (Figure 3.13.B).

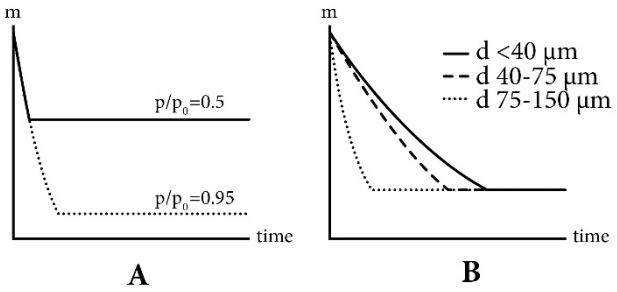

Figure 3.13. Schematic representation of A) solvent relative vapour pressure and B) particle size effect on solvent desorption curve.

3.5.3. Sample morphology changes during sample storage

Tegafur sample morphology studies with scanning electron microscope were performed for the β tegafur fraction with particle size of 40 μm and less. Scanning electron micrographs for sample before and after the experiment (storage at 95% relative acetone vapour pressure for 72 h) are shown in Figure 3.14. An accelerating voltage of 2.0 kV was chosen because of the high sample charging.

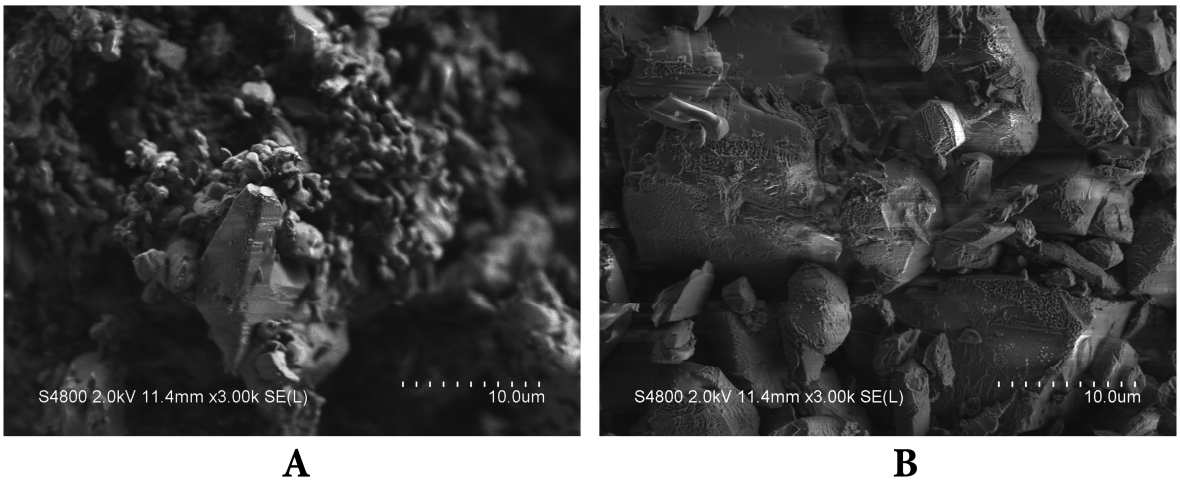

Figure 3.14. Scanning electron micrographs of β tegafur samples with particle size 40 μm and less; A) before and B) after sample storage at 95% relative acetone vapour pressure for 72 h.

Scanning electron micrographs show that the sample before storage in solvent atmosphere consisted of small particle (<2 μm) agglomerates, but after storage there were almost no such particles. This was due to Ostwald's ripening – small particles with large surface, thus high surface energy, tend to reduce their free energy by reducing the ratio of surface to mass, and

this occurs by recrystallization to larger particles. Another difference between samples before and after storage in solvent atmosphere can be seen if we take a look at the edges and faces of the large particles. The edges of β tegafur particles were quite sharp and well defined before storage, but after storage became rounded and hardly visible. Differences could be seen also on the surface of large particles – after the sample storage at 95% relative acetone vapour pressure the surface of the particles became rough and there are signs that tegafur crystallized from the solution (see Figure 3.14.B). This experiment shows that minor changes in sample morphology occur during sample storage, and actually sample with slightly different particle size and morphology are analysed during the experiment.

3.5.4. Conclusions

The results of this study demonstrated that solvent desorption from α and β tegafur did not differ significantly between these two phases, and solvent desorption in all cases occurred faster from samples with the largest particle size. Structure differences and their surface properties are not of great importance on the solvent desorption rates and the main factor affecting desorption rate is sample particle size and sample morphology.

Two different solvent desorption behaviours can be distinguished depending on the solvent and surface interaction energy. If the solvent and surface interaction was stronger than interaction between solvent molecules, than multilayer and monolayer desorption was observed, but, if the adsorbed solvent molecules were of equal energy, then only one desorption phase was observed. Solvent desorption rates of acetone, acetonitrile, ethyl acetate and tetrahydrofuran multilayers from α and β tegafur were approximately 30 times higher than those from solvent monolayers.

Small tegafur particles recrystallized to larger particles during sample exposure to solvent vapour atmosphere, and there were morphological signs of tegafur recrystallization from solution on the surface of the particles.

3.6. Solvent mediated phase transformation between two tegafur polymorphs in several solvents

In order to gain more fundamental insight on solvent stimulated polymorphic transformations – both solvent drop milling and solvent vapour induced phase transformations, classical solvent mediated phase transformation (see section 1.7) from metastable α tegafur to the thermodynamically stable β tegafur in several popular solvents from different solvent classes was studied.

During our first SMPT kinetics experiments we noticed that the sample drying time had an impact on the extent of phase transition – samples, dried at ambient temperature, had increased β tegafur content. This was because the thermodynamically stable β tegafur crystallized from the saturated tegafur solution that was sampled together with the solid phase, i.e., phase transition to β tegafur partially occurred during sample drying, not only during the slurrying. In order to avoid this effect, samples for SMPT kinetic experiments were quickly filtered using a glass filter funnel with Bunsen flask under reduced pressure.

The results of the kinetics experiments performed at room temperature (22±1 °C) represent a series of plots documenting the composition of the solid phase during the SMPT, as detected with the PXRD method. Figure 3.15. shows the composition of the solid phase during the SMPT in acetone, ethanol, *i*-propanol, toluene, and water. These data were used to generate an additional data plot where phase transition kinetics curves were normalized to the state where a complete transition to β tegafur was observed (Figure 3.16.). This means that the time when a complete phase transition was observed was considered as 100%. Using this approach we could compare the reaction rate and reaction path in all the solvents used. This figure clearly demonstrates that the phase transition models were the same in all the solvents, and the only factor that changed was the phase transition rate. An induction time was observed at the beginning of phase transitions in all solvents. We cannot clearly assure whether the observed delay of the phase transition is an induction time or the time that is necessary for β tegafur crystals to grow; however, we believe that this was the limiting step in investigated SMPTs. We see that the induction times in all the solvents were proportionally the same – about 10% of the phase transition time. It is worth noting that the LOD of our quantitative analysis method was

3.0%, therefore the observed induction time might be the time that was necessary to overcome this 3.0% range.

Solution concentration throughout SPMT stayed at the level of α tegafur solubility, and started to decay only when all α tegafur transformed to the stable β tegafur (Figure 3.17.). This means, that the overall rate of consumption of supersaturation by β tegafur crystal growth was lower than the overall rate of α tegafur dissolution. This case is denoted as "nucleation-growth controlled polymorphic transformation" [185].

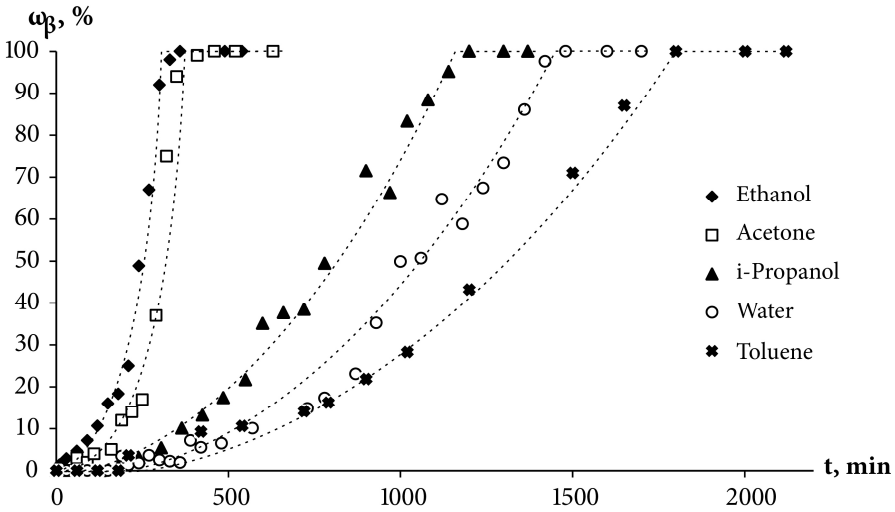

Figure 3.15. The weight fraction of β tegafur during the SMPT from α tegafur to β tegafur in acetone, ethanol, *i*-propanol, toluene, and water at 22 °C. Line added as a guide.

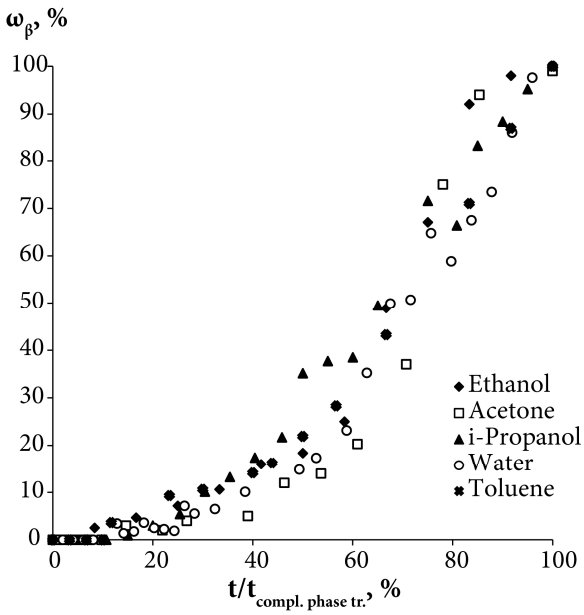

Figure 3.16. The weight fraction of β tegafur during the SMPT in acetone, ethanol, *i*-propanol, toluene, and water at 22 °C, normalized to the state where the transition to β tegafur is complete.

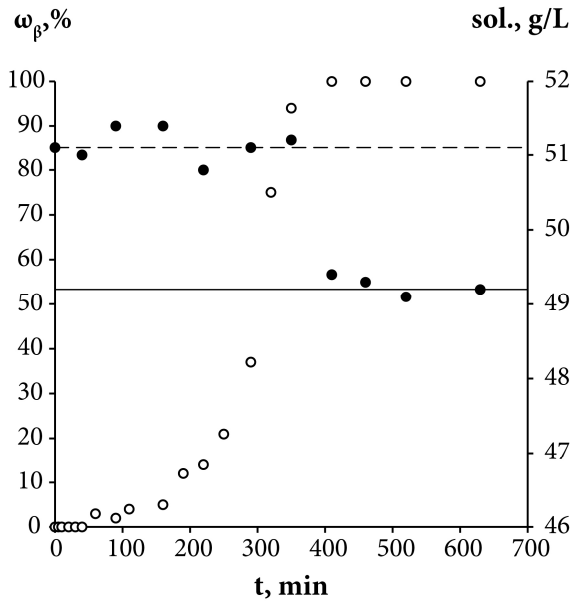

Figure 3.17. Solution concentration (●), and weight fraction of β tegafur in the solid phase (○) during the SMPT from α tegafur to β tegafur in acetone at 22 °C. The dashed line (---) represents the solubility of α tegafur, continuous line (—) represents the solubility of β tegafur.

The induction time was followed by a gradual increase of the thermodynamically stable β tegafur fraction. SEM analysis of the sample, where β tegafur was first detected using PXRD method, revealed that the blocky β tegafur crystal were in contact with the surface of α tegafur needle-like crystal side faces (Figure 3.18.). Although it is possible that α and β tegafur crystals simply agglomerated together during the sample filtration and drying, the fact that it was not possible to separate these crystals without damaging them, indicated that β tegafur, most likely, nucleated epitaxially on the surface of α tegafur. Observed epitaxially driven polymorphic transformations are common in SMPTs [8,9,179,184,191,193,261]. The surface of the α tegafur here acted as a nucleation substrate for the β tegafur by either decreasing the solution-nucleus interfacial energy, by topographical contribution or by a crystal lattice match [9]. The surface nucleation might have also been a consequence of a local lattice disorder or amorphous region that had similarity to crystallizing β tegafur [8].

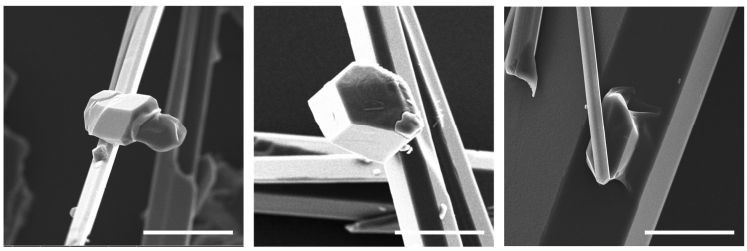

Figure 3.18. SEM images of the solid phase of SMPT in acetone taken at 60 min. Scale bar 40 μm.

In order to estimate the nucleation mechanism and understand which α and β tegafur crystal faces were in contact, crystal face indexing was performed for both polymorphs. Crystals, where β tegafur was in contact with α tegafur (like those in Figure 3.18.), were not suitable for β tegafur crystal face indexing, therefore individual β tegafur crystals were indexed. Crystals for β tegafur face indexing were collected at 300 min, when individual β tegafur crystals suitable for crystal face indexing were in the sample. Appropriate β tegafur crystals were picked out from the phase mixture. Face indexing of α tegafur crystals were performed for sample collected at 60 min.

SEM images showed that β tegafur nucleated on one of the needle-like crystal side faces, while crystallographic face indexing of α tegafur crystal (Figure 3.19.A) indicated that these faces were {001}, {011} and {010}. A visual comparison of epitaxially nucleated β tegafur crystal morphology and indexed crystal morphology (Figure 3.19.B) indicated that crystal face family {100}, {110} or {010} must be in contact with α tegafur surface. Intermolecular distance and molecule alignment analysis along these faces revealed that there was a good agreement at a molecular level between the {110} face of β tegafur and {010} face of α tegafur crystal (Figure 3.20.), while no match was observed along other crystal faces. Possible lattice match between {100}, {110} and {010} face of β tegafur and {001}, {011} and {010} face of α tegafur was examined using EpiCalc 5.0 software [262]. The lattice matching calculations indicated that there was no lattice matching between any of the studied faces (EpiCalc data can be found in Appendix 4).

However, it should be taken into account that crystal surface molecules are not static – they change their position, arrangement and conformation [37,263], and therefore they could arrange into the state, which promoted the growth of β tegafur. This means that the nucleation of the β tegafur might be favoured by the surface molecule rearrangement. The {110} surface of β tegafur and the {010} surface of α tegafur have similar tegafur molecule arrangement at the surface and distances between tegafur dimers are the same for both polymorphs in relevant

directions. Because of this, nucleation of β tegafur on {010} face of α tegafur might be initiated by minor surface tegafur dimer displacement, conformation change, rotation. The strongest hydrogen bond donor and acceptor groups are involved in dimer formation and interactions between dimers are relatively weak. These weak interactions at the growing surface are less efficient at directing the orientation on an incoming dimer synthon and therefore tegafur dimers at the surface are relatively mobile. Figure 3.21. shows, that tegafur dimer arrangement similar to that in β tegafur, could be achieved by minor α tegafur surface molecule rotation. Such local lattice disorder would spread and eventually thermodynamically stable β tegafur would nucleate and continue to grow.

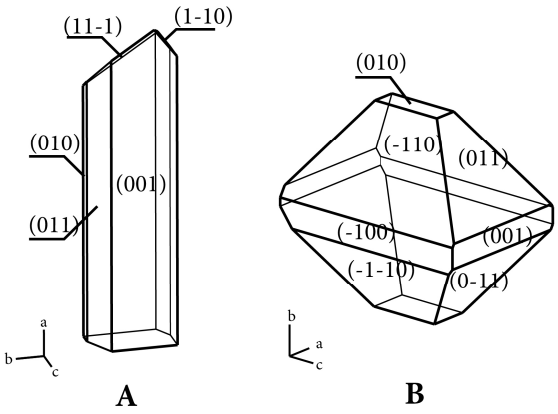

Figure 3.19. Single crystal face indexing of α and β tegafur.

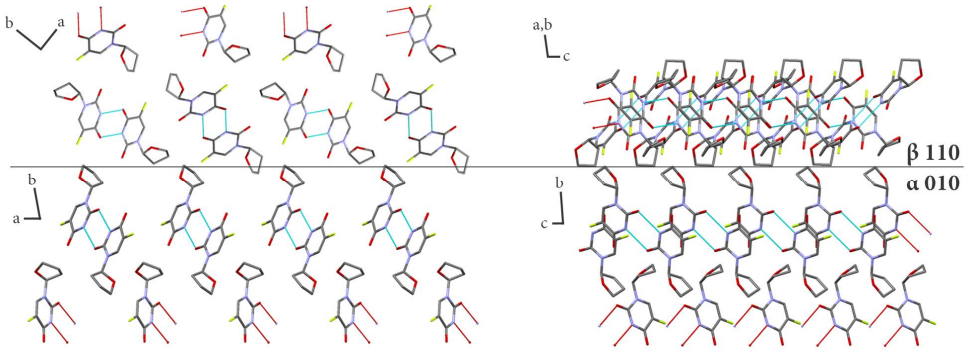

Figure 3.20. Schematic model of β tegafur growing on the α tegafur surface (010). Hydrogen atoms are omitted for clarity.

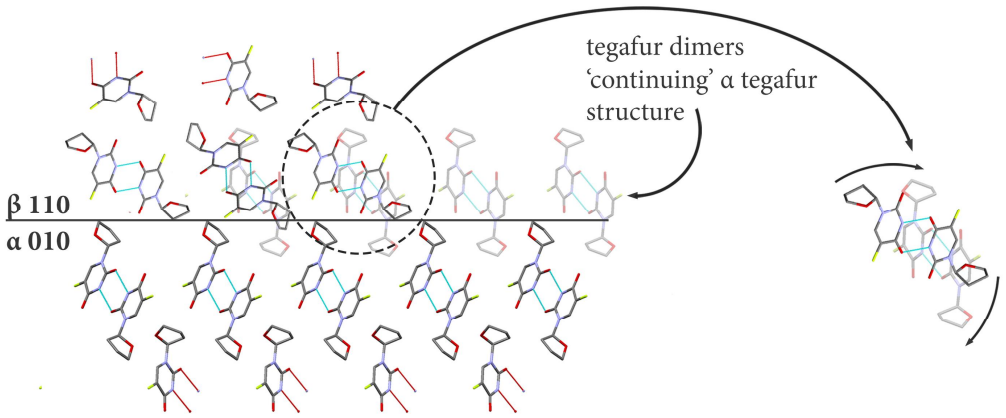

Figure 3.21. Schematic representation of tegafur dimer rearrangement on the α tegafur surface to initiate the growth of β tegafur. Hydrogen atoms are omitted for clarity.

In order to quantitatively compare SMPT rates in different solvents, experimental data were described with appropriate kinetic model. SEM imaging of the studied SMPT revealed that the phase transition took place on the solid phase surface (the phase transition was heterogeneous), therefore attempts were made to describe experimental data points with the most common solid-state kinetic models [104]. Evaluation of observed phase transformation nature and crystal growth morphology indicated that experimental data were in agreement with power solid-sate kinetics models. The best correlation was observed when the experimental data points were fitted to the power model P2:

$$\alpha = (kt)^2 \qquad 3.5,$$

where k is the phase transition rate constant, α is the weight fraction of β tegafur in sample, and t is time. The correlation of the experimental data with the theoretical model and phase transition rate constants in each solvent are given in Table 5. Rate constants were calculated using *MS Excel* [257] optimization add-on *Solver*, based on the least squares method [264,265].

The power law model P2 used here assumes that the nucleation rate follows the power law, while nuclei growth is assumed to be constant [104,266,267]. Nuclei and crystal growth was constant, because it took place through crystallization from saturated α tegafur solution. The limiting step in nuclei growth was the transport of the tegafur molecule to the crystallization zone. Diffusion of tegafur molecules was expected to occur at a constant rate throughout the phase transition, because the studied phase transition occurred in solution, which was saturated with respect to α tegafur (supersaturation was constant during phase transformation). Taking

this into account, nuclei growth rate can be assumed to be constant. This means that the rate-controlling step in the examined SMPT was the nucleation. There are two scenarios for nucleation [267]. The first option is a simultaneous formation of all nuclei; the second option is that nucleation occurs stepwise, with nuclei forming over a period of time. SEM imaging (Figure 3.18.) shows that β tegafur crystals, observed in the sample where β tegafur was first detected, had deviations in the crystal size. This indicates that nucleation in the examined SMPT occurred over a period of time. Besides, it is very unlikely that all the nucleation sites would have approximately the same reaction (phase transition) activation energy minimum, which would be necessary for a simultaneous nucleation. Clearly, nuclei formed first at the nucleation sites with the lowest activation energy, and then nucleation gradually spread to the other nucleation sites in a rising activation energy order. Since nuclei and crystal growth was constant, this nucleation behaviour can be described with a second-order power function.

Table 5. The P2 model rate constants of SMPT and correlation coefficients, depending on the solvent used; the experiment was performed at 22 °C.

Solvent	Rate constant, min^{-1}	Correlation with P2 model, R^2
Acetone	0.028	0.92
Ethanol	0.023	0.96
i-Propanol	0.0090	0.92
Water	0.0065	0.98
Toluene	0.0056	0.98

The fact that the best experimental and theoretical data correlation was observed for the 2 dimensional model indicates that the phase transition rate most likely was proportional to the surface area of the β tegafur crystals formed [267]. With that said, we can conclude that in the examined SMPT β tegafur crystals nucleation corresponds to a second-order power function, their growth rate was constant, and the phase transition rate was proportional to the β tegafur crystal surface area.

Despite the fact that solubility and phase transformation kinetic data suggested that this phase transformation was limited by nucleation, the correlation between SMPT rate constant

and the difference between α and β tegafur solubility in the respective solvent was observed: a faster phase transition was observed for the samples slurried in solvents where the difference in polymorph solubilities was high (Figure 3.22.). This trend in the SMPT from α tegafur to β tegafur was described with equation:

$$k = (0.038 \pm 0.003)\Delta sol. + (0.005 \pm 0.001) \qquad 3.6,$$

where $\Delta sol.$ is difference between α and β tegafur equilibrium solubilities in the respective solvent, and k is the rate constant of the SMPT in the same solvent. The correlation coefficient was $R^2=0.97$. This correlation means that the driving force in the studied SMPT was excess concentration above the equilibrium concentration of β tegafur, i.e. supersaturation with respect to β tegafur.

Supersaturation provided the necessary driving force to overcome the energy barrier to promote β tegafur nuclei and crystal growth [5]. In this case supersaturation coincided with the difference between α and β tegafur equilibrium solubility in the respective solvent, because the solution concentration throughout the phase transformation was fixed at the equilibrium concentration of α tegafur. Such solution concentration profile also means that the driving force was constant throughout the SMPT. Higher tegafur supersaturation in the solution promoted faster phase transformation to the thermodynamically stable β tegafur, because of the increased degree of local organization in the solution necessary for crystallization [37], and faster tegafur molecule transfer to the crystallization zone (molecules were relatively close). Absolute tegafur solubility and the difference between polymorph solubilities depends on the chosen solvent, however, the free energy (ΔG) difference between polymorphs does not depend on the solvent [176]. This means that the overall driving force of phase transformation was not dependent on the chosen solvent, and the SMPT rate depended only on the difference between polymorph solubilities (supersaturation). The only SMPT step that might be affected by solvent choice was β tegafur nucleation [58,61,268,269]. Tegafur molecules were solvated in the solution, similar to the surface of molecular aggregates and crystals. In order to nucleate and continue crystallization, tegafur molecules had to be desolvated, and solvent molecules on the nuclei or crystal surface had to be replaced by incoming tegafur molecules. This process, most likely, was affected by the nature of the solvent and its electron donor/acceptor properties, because strong

solute-solvent interaction would inhibit desolvation and therefore nuclei growth, while weak solute-solvent interaction would not have a significant impact on nuclei growth.

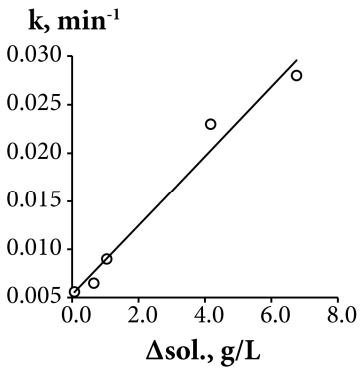

Figure 3.22. Correlation between SMPT rate constant in acetone, ethanol, *i*-propanol, toluene, and water, and difference between α and β tegafur solubility (Δsol.) in respective solvent. Correlation equation *y=(0.038±0.003)x+(0.005±0.001)*; R^2=0.97.

3.6.1. Conclusions

The SMPT from α tegafur to β tegafur in acetone, cyclohexane, ethanol, *i*-propanol, toluene, and water at 22 °C is nucleation-growth controlled and it can be described with the P2 power model. The rate constants for this process were in the range from 0.028 min^{-1} to 0.0056 min^{-1}. In all the employed solvents an induction time (about 10% of the time required for complete phase transition) was observed, indicating that nucleation and/or initial crystal growth was the limiting factor for SMPTs performed in saturated solutions. In the examined SMPT the nucleation of β tegafur crystals corresponded to second-order power function, nuclei and crystal growth rate was constant, and the phase transition rate was proportional to the β tegafur crystal surface area. Surface nucleation was observed in studied SMPT. Crystal habit investigation indicated that β tegafur nucleated on the {010} face of α tegafur, and the {110} face of β tegafur was in contact with α tegafur crystal. The SMPT rate depended linearly on the supersaturation level, i.e. difference between α and β tegafur equilibrium solubility in the respective solvent.

3.7. The Reluctant Polymorph. Self-association effect on nucleation and solvent mediated phase transformation of theophylline

The knowledge acquired during previously described studies were used to study solvent mediated phase transformation of pharmaceutically active compound of academic importance – theophylline. Theophylline is an active compound that has been manufactured and used in a metastable crystalline phase (clearly, because of the lack of comprehensive knowledge of the polymorphic landscape of this compound). The fact that the thermodynamically stable theophylline polymorph was discovered only recently, is because it does not crystallise directly from solution, and is obtained only by slow, solvent mediated transformation (SMPT) from Form II in contact with solvent e.g. methanol, 2-propanol or chloroform [237]. Here we try to understand why the thermodynamically stable theophylline Form IV can be obtained only by solvent mediated transformation in specific solvents, and to investigate the presence of prenucleation aggregates which direct the polymorphic outcome of crystallisation.

Early experiments [270–273] on theophylline self-association provide evidence that theophylline does self-associate in aqueous solution and the proposed aggregate is the theophylline dimer. The theophylline dimer discussed in these studies is present in the thermodynamically stable Form IV, and theophylline monohydrate, Form M, which crystallises from aqueous solutions. Theophylline Form II, the polymorph commonly crystallized from most non-aqueous solutions, does not contain this dimer motif (crystal structures of theophylline polymorphs are discussed in detail in section 1.9.2). Such behaviour raises two questions: why does metastable Form II crystallize from non-aqueous solvents; what prenucleation aggregates are present in non-aqueous solvents? In order to answer these questions, we need to determine (a) does theophylline self-associate in other solvents besides water, and, if it does, what is the nature of the association, and (b) since the nucleation of Form IV is kinetically slow, does solution aggregation change over time?

3.7.1. Characterisation of SMPT from theophylline Form II to Form IV

The SMPT of unprocessed commercial anhydrous theophylline Form II in methanol was investigated. Three parallel experiments were performed, but for the sake of clarity only one

case is taken as an example of the whole set of experiments to describe and discuss in detail the results obtained.

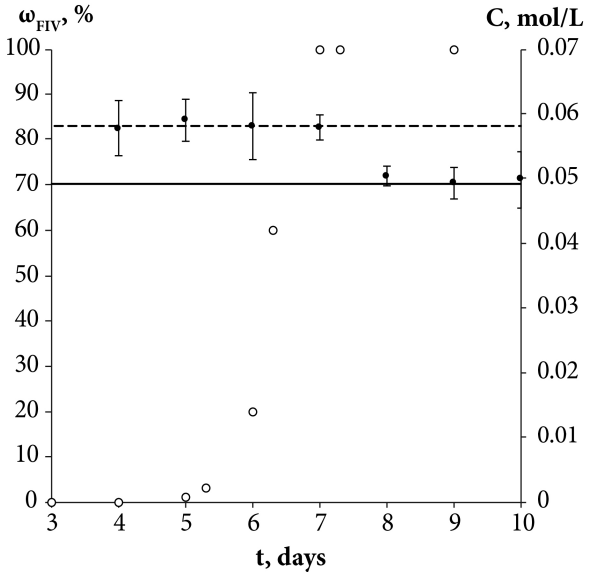

Figure 3.23. Solution concentration (●), and weight fraction of the theophylline Form IV in the solid phase (○) during the solution mediated transformation from theophylline Form II to Form IV in methanol at 23 °C. The dashed line (---) represents the solubility of theophylline Form II, continuous line (—) – solubility of theophylline Form IV.

During the solvent mediated phase transformation qualitative and quantitative analysis of the solid phase were performed using powder X-ray diffractometry (PXRD), Fourier transform infrared spectroscopy (FTIR) and scanning electron microscopy (SEM) methods; while the solution concentration throughout the transformation was monitored using ultraviolet-visible (UV/Vis) spectroscopy. The composition of solid phase determined by PXRD method and solution concentration throughout SMPT is presented in Figure 3.23. Results of all three experiments showed that the phase transformation from theophylline Form II to Form IV showed a considerable induction time which varied from 4 to 6 days while the phase transition itself consistently took ~2 days. Such behaviour, that induction time for parallel experiments had a great variation, while the phase transition time in all cases was approximately the same, suggests that the limiting step for this SMPT is the nucleation of Form IV. The main factors that might affect the nucleation and hence the induction time are discussed further.

The equilibrium saturation of the metastable Form II was reached ~3 h after the theophylline addition to methanol. The concentration of the solution remained the same until phase

transformation was completed. Solution concentration dropped to the equilibrium saturation of the thermodynamically stable Form IV within a few hours of the phase transformation being completed, indicating that, once all of the Form II in the sample had dissolved, Form IV continued to grow until the solution reached the Form IV equilibrium concentration. This shows that the dissolution rate of theophylline Form II was faster than the growth of Form IV and dissolution was not the limiting step in the phase transformation. Such a solution concentration profile and pronounced induction period indicates that the SMPT was a 'nucleation-growth controlled polymorphic transformation' [185]. The fact that phase transformation is also growth limited was confirmed by the time scale of the studied SMPT – most of the SMPTs described in the literature take place within a few hours [9,176,178,179,184,185,187,274–276], but here phase transformation took ~2 days from the moment when Form IV nucleated. This might be due to low supersaturation, which provided the necessary driving force to overcome the energy barrier and promoted Form IV crystallization [5]. In this case, supersaturation is the difference between the solubilities of Form II and Form IV.

The increase of the Form IV content in the sample exhibited an *exponential* nature – the amount of Form IV increased slowly in the initial stage and then accelerated. Such behaviour suggests that the growth of Form IV might be limited by the surface area of Form IV in the sample; hence, the rate of SMPT increased as the crystal size (surface area) in the sample increased. This assumption was consistent with SEM imaging data, shown in Figure 3.24.

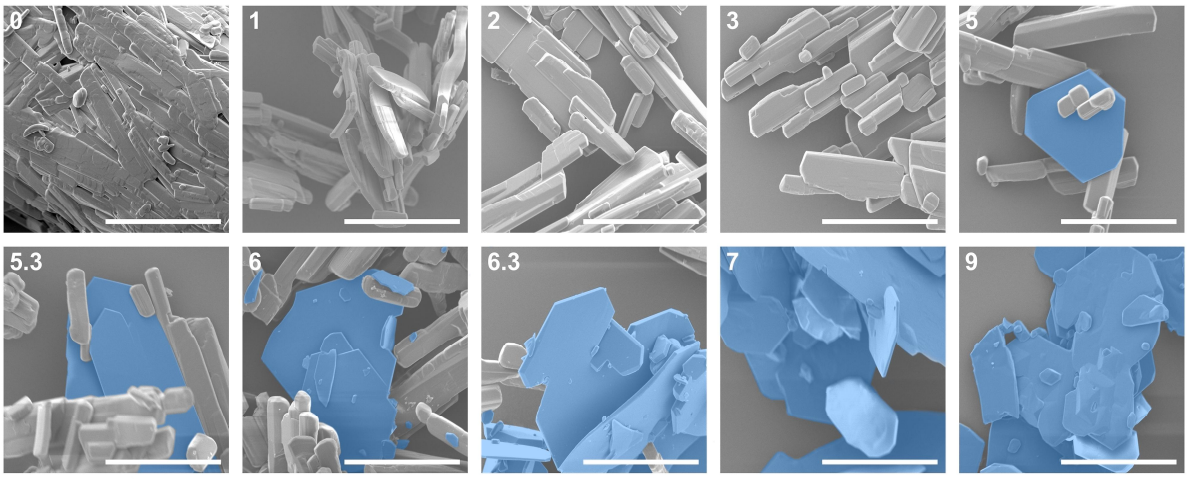

Figure 3.24. SEM images throughout SMPT from theophylline Form II to Form IV in methanol at 23 °C. Inset: time of sample gathering (days), 40 μm scale bar, Form IV indicated with blue colour.

It is known [237] that theophylline Form II exhibits a needle-like morphology, while Form IV crystallizes in hexagonal plate-like crystals. These distinct differences in the crystal shape allowed phase transition monitoring using microscopy methods. SEM imaging of the solid phase throughout SMPT (Figure 3.24.) revealed that during the first days, while no phase transformation was observed, the only apparent change in the solid phase was the agitation and Ostwald's ripening of the theophylline Form II crystals – Form II crystals dissolved mostly from the top of the elongated crystals (along *c* axis) and then recrystallized on the Form II crystal side planes (see Figure 3.24., day 1 and day 3). Theophylline Form IV crystals were first observed after 5 days, and all observed hexagonal Form IV crystals were approximately the same size: ~40 μm in diameter and 1–2 μm thick. A similar size for all observed Form IV crystals suggests that they nucleated simultaneously or in a very short time interval. Recent studies [179,184,191,261] show that surface nucleation dominates in most of SMPTs, however in our case there was no clear evidence of such behaviour. Over time Form IV crystals grew significantly in 2 dimensions, forming large, plate-like crystals. This growth pattern indicates that the growth of the Form IV was governed by the surface of the crystal edges. Eventually, breakage of Form IV crystals was observed (day 6), which would lead to increased surface area of the edge faces, where crystal growth was fastest, thereby accelerating the crystallization rate of Form IV.

Preferred Form IV crystal growth directions were determined by the PXRD method. It is observed that the PXRD pattern of Form IV crystals after the SMPT have two very intensive peaks at 12 and 23° 2θ (Figure 3.25.), suggesting that the sample exhibits preferred orientation. Comparison of the pattern with that simulated from the crystal structure revealed that these intensive diffraction peaks arise from crystal planes (002) and (004) – the multiple planes of the {001} face family. Since plate-like crystals tend to lay down with the dominant faces parallel to the PXRD sample holder, the most intense diffraction should occur from this plane. It can therefore be concluded that the dominant face in the Form IV crystals obtained during SMPT is {001} and crystal growth occurred almost exclusively along this plane. The reason for such crystal growth behaviour is that there are no significant intermolecular interactions in the *c*-direction of theophylline Form IV, whereas crystal growth along {001} plane is favoured by hydrogen bonding and π-π stacking (Figure 3.26.).

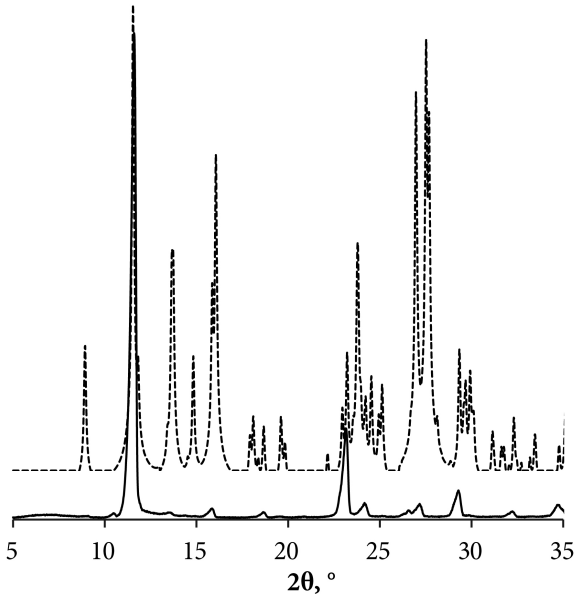

Figure 3.25. PXRD patterns of Form IV obtained by SMPT in methanol (—); and simulated from crystal structure (---).

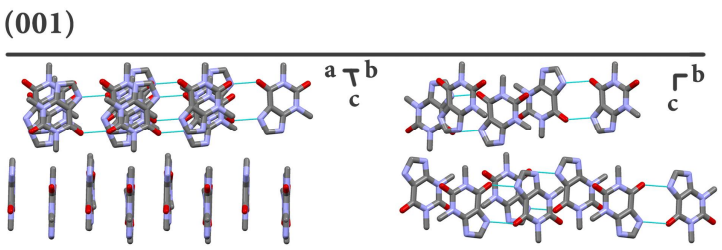

Figure 3.26. Crystal packing in theophylline Form IV along {001} plane. Hydrogens are omitted for clarity.

Based on morphological observation, Form IV crystal growth perpendicular to {001} was observed only when phase transformation was finished – during the SMPT the surfaces of Form IV crystal plane {001} were flat (Figure 3.24., day 8.3), whereas 2 days after the SMPT elevations on the surface of the Form IV were observed because of crystal agitation (Figure 3.24., day 10). The crystal growth rate along {001} was considerably higher than growth rate perpendicular to {001} during phase transformation, likely to be because energy released on solution molecule attachment to growing crystal edge surface was higher [277]. When phase transformation was complete, Ostwald's ripening [37] took place and crystals tended to achieve minimum total surface energy by reducing the crystal surface area. Here, this means that crystals grew perpendicular to the large {001} plane at the expense of plate like crystal edges, which dissolved more easily [37].

Surface nucleation dominates in the majority of SMPTs, therefore experiments with ground and lyophilized theophylline as a starting material were performed to evaluate the effect of the Form II surface on the nucleation and crystallization of Form IV. There were no significant differences in the phase transformation behaviour when ground and unground theophylline was used. PXRD and SEM data showed that when the ground Form II was agitated, Ostwald`s ripening took place, and crystallization of Form IV followed only after 6 days. If theophylline Form IV nucleated on the surface of the Form II, the increase of the Form II surface area in the ground sample should reduce the induction time. However, this was not observed, suggesting that Form IV did not nucleate on the surface of Form II. When lyophilized theophylline, confirmed as a mixture of amorphous theophylline and microcrystalline Form II, was used, no phase transition to Form IV was observed within the studied time (90 days). The lyophilized material agitated in solution and the crystallinity of Form II increased (Figure 3.27.), but no phase transition was detected. It is not clear why crystallinity of the Form II starting material should influence the nucleation of Form IV since this is not a surface nucleation process. Later experiments on water content (see below) indicate that the ability of amorphous material to absorb water might be more important than crystallinity.

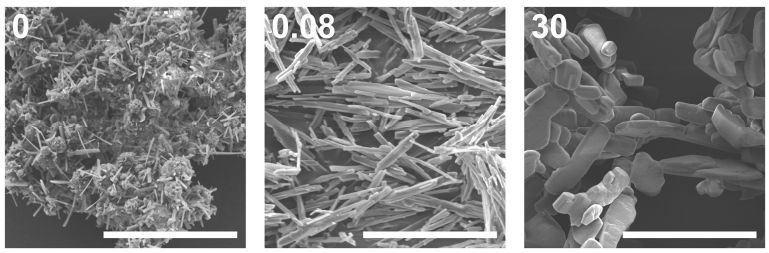

Figure 3.27. SEM images throughout lyophilized theophylline slurrying in methanol at 23 °C. Inset: time of sample gathering (days) and 20 μm scale bar.

In order to ascertain whether theophylline aggregates present in the methanol solution affect the phase transformation, an experiment using methanol solution saturated with respect to Form IV as a solution medium was performed. The SMPT held approximately the same induction and phase transformation time (5 and 2 days, respectively) as experiments in methanol.

Similar experiments with theophylline Form II and Form IV mixture (w_{II}/w_{IV}; 90/10) as a starting material were performed to exclude induction time and observe only phase transformation. No induction times were observed in either case, and phase transformation rates were the same regardless of solution composition (Figure 3.28.). This means the molecular aggregates, if there were any at all, in both saturated solutions were the same and/or they did not play a significant role in the phase transformation. If we compare theophylline Form IV weight fraction change over the time in these experiments and those, performed with commercial Form II as a starting material, we see that phase transformation with theophylline Form II and IV mixture as a starting material occurs three times faster. We believe that this phase transformation rate mismatch is due to differences in the Form IV crystal *active* edge surface areas for the samples. SEM imaging confirmed that Form IV edge surface area in prepared polymorphic mixtures were larger, than in the sample where the same amount of Form IV was generated by SMPT. Since this is the region in which growth of Form IV dominates, larger surface area leads to faster rate of growth, therefore a faster transformation.

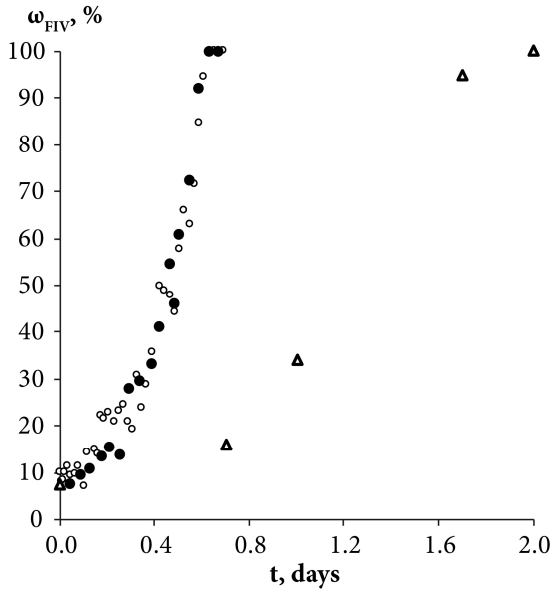

Figure 3.28. Weight fraction of the theophylline Form IV in the SMPT from theophylline Form II/Form IV mixture (w_{II}/w_{IV}; 90/10) to Form IV, in saturated (○) Form IV and (●) Form II methanol solutions at 23 °C. Δ represents the weight fraction of the theophylline Form IV in the solid phase during the SMPT from theophylline Form II in methanol at 23 °C. All kinetic curves are fitted to the time when weight fraction of Form IV in solid phase was 10%.

Seton *et al.* [237] reported that theophylline equilibrium solid phase depends on the water activity in the solution, and that Form IV is preferred when water activity in the solution is below 0.69 (V_{MeOH}/V_{H2O}, 55/45). To investigate the possibility that water activity affects also the phase transformation rate to Form IV, SMPT was observed in solvents samples with different water contents. SMPT from theophylline Form II to Form IV, performed in dried methanol and methanol/water mixtures with volume ratios (V_{MeOH}/V_{H2O}) 99:1, 95:5 and 80:20, clearly showed that increased water in the solution increased the induction time (Figure 3.29.A). Phase transformation rate also increased but with a lesser effect – from 1.5 days in dried methanol to 5 days in methanol/water mixture (V_{MeOH}/V_{H2O}; 95/5).

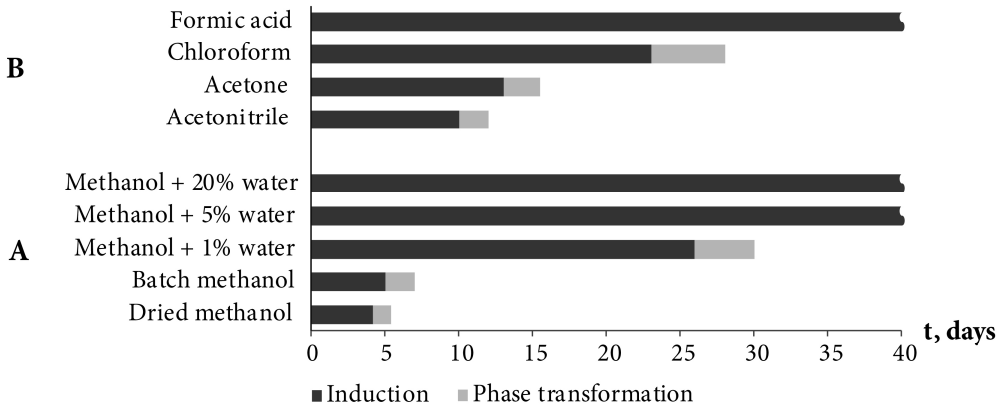

Figure 3.29. Induction and phase transformation times of SMPT from theophylline Form II to Form IV at 23 °C depending on used solvent environment. No phase transformation to Form IV was been observed in formic acid and methanol/water mixtures with 5% and 20% of water within the studied period (40 days).

These results might explain why fluctuation of induction time were observed in the earlier SMPTs. Methanol used in initial experiments was used as received and was taken from different batches, therefore the water content (adsorbed from the air) was not the same in all samples. Karl Fisher titration showed that batch methanol contained ~0.2% of water, whereas methanol dried with anhydrous $NaSO_4$ contained less than 0.1% water. These minor water impurities affected the induction time of the SMPT. This might be the reason why phase transformation with lyophilized theophylline as starting material was hindered. Theophylline lyophilisation resulted in partially amorphous theophylline, which tends to absorb more water from the air than crystalline phases [149], and it is possible that the phase transition in this case was slowed down by adsorbed water.

The induction times and transformation times in a range of solvents were measured and compared (Figure 3.29.B). We see that phase transition times correlated to induction times – the longer the induction time, the slower the phase transformation. This might indicate that nucleation and Form IV growth were limited by the same factors.

It has been shown previously [278] that in the nucleation-growth controlled SMPT between α and β tegafur, the phase transformation rate and induction time linearly depends on supersaturation level, i.e. difference between solubilities of the polymorphs. Here we do not

observe such a correlation. This might be because Form IV nucleation and growth is not affected by supersaturation level, perhaps, because the difference in solubilities is small.

Crystallization always gave Form II, including crystallization from solutions with Form IV equilibrium concentration. Even seeding with Form IV, gave Form II and Form IV mixture.

Induction and phase transition times were longer in solvents (solvent mixtures) which had good proton donor groups. Fastest phase transformation and shortest induction time were observed in dried methanol, followed by stock methanol, acetonitrile and acetone. Longest induction times were observed in proton donor solvents – chloroform and formic acid, and previously discussed methanol/water mixtures. In fact, no Form IV has been detected in formic acid and methanol/water mixtures 95/5 and 80/20 within the studied period of 90 days. An influencing factor might be theophylline molecule and aggregate solvation/desolvation behaviour. Theophylline molecules are solvated in the solution, but in order to nucleate Form IV and continue its growth, theophylline molecules have to be desolvated, and solvent molecules on the nuclei or crystal surface be replaced by incoming theophylline molecules. Taking in to the account that induction time was several days and phase transformation was very slow, we can assume that solute-solvent interaction in studied SMPT was strong compared to solute-solute interaction and thus the desolvation process inhibited Form IV nucleation and growth.

In order to further understand how the solvent environment affects SMPT rate and induction time, NMR spectroscopy was used to investigate for prenucleation aggregates in the solution.

3.7.2. Theophylline self-association studies

To understand solution chemistry and ascertain possible aggregation of theophylline molecules in solution, the influence of theophylline solution concentration on ^{1}H NMR chemical shift displacement was analysed. ^{1}H NMR experiments were carried out in seven solvents (methanol-D4, chloroform-D, acetone-D6, dimethyl sulfoxide-D6, deuterium oxide, acetonitrile-D3 and formic acid-D2). These solvents were chosen because: (a) it is known that in dimethyl sulfoxide and water theophylline crystallizes as solvates and the crystal structures of these solvates are not similar; (b) they have different H-bond donor/acceptor properties:

acetone, acetonitrile and dimethyl sulfoxide are H-bond acceptor; chloroform is H-bond donor; water, methanol and formic acid are both – H-bond donor and acceptor; and (c) from formic acid theophylline crystallizes into Form II with no subsequent transformation observed.

The concentration range covered in this experiment was the same for all solvents – from saturated to 1 μM theophylline solution. The number of scans for NMR spectra acquisition was adjusted depending on solution concentration. Theophylline solutions with lower concentrations were not studied because the NMR spectra acquisition time, necessary to obtain spectra with acceptable signal/noise ratio, would be unreasonably long.

The theophylline used in the experiment had natural $^{1}H/^{2}H$ abundances and therefore the most acidic imidazolium group proton (N7-H) took part in proton exchange with the deuterated solvent deuterium atoms. As a result, the imidazolium group proton was visible in the NMR spectra in solvents where only partial proton exchange took place - chloroform-D, dimethyl sulfoxide-D6 and acetonitrile-D3. Methyl group protons and alkene group proton (C8-H) did not showed any effect on proton exchange.

If there are multiple structures that have different thermodynamic stabilities and perturb the ^{1}H NMR chemical shifts in different ways, the shapes of the dilution curves differ for different signals. While this does not rule out the possibility of multiple structures, the data can be treated as a simple two state equilibrium, and the complexation-induced changes in chemical shift are assumed to relate to a single specific aggregate structure [87]. Since the solubility of the theophylline in all selected solvents except formic acid is low (>0.06 M) multiple aggregate structures are not expected.

No chemical shift displacement upon concentration changes were observed in methanol-D4, acetone-D6, dimethyl sulfoxide-D6 and acetonitrile-D3. This means that no self-association takes place in these solvents, or theophylline undergoes dimerization or other self-association at concentrations lower than those covered in the experiment, i.e. below 1 μM, and other agglomerates do not form in the concentration region studied. It is unlikely that self-association occurs at such low concentrations, and it is probable that solvated theophylline monomers were the main species in the solution.

^{1}H NMR dilution studies in chloroform-D, deuterium oxide and formic acid-D2 showed large concentration-dependent changes in chemical shifts. In the chloroform-D all chemical

shifts were displaced to lower fields as concentration increased (Figure 3.30.A). In deuterium oxide methyl groups ^{1}H chemical shifts were displaced to higher field while the alkene group proton (C8-H) chemical shift was displaced to the lower field (Figure 3.30.B). Imidazolium group proton (N7-H) chemical shift was not observed in the deuterium oxide due to proton exchange. In formic acid-D2 alkene group proton (C8-H) chemical shift was displaced to higher field, whereas imidazolium group proton (N7-H) chemical shift was displaced to lower field (Figure 3.30.C). Minor methyl groups ^{1}H chemical shift displacement to higher and field were observed as concentration increased. The pattern and magnitude of chemical shift changes are completely different in all solvents, indicating that aggregates present in these solutions are different. It is likely the associate existing in the deuterium oxide is the theophylline dimer which is also present in the crystal structure of theophylline monohydrate (Figure 3.31.A). The associates in chloroform-D solution might be the asymmetric dimer corresponding to Etters rule (Figure 3.31.B), π-π stacked dimer or some associate involving solvent molecules. It is also possible, that chemical shift displacement is reflecting the average structure of multiple aggregates. Since theophylline solubility in formic acid is noticeably higher than in other solvents (more than 30 times), it is possible that associates present in formic acid-D2 were oligomers and not dimers. Data shows that theophylline concentration at which self-associates were formed were different in each solvent. In deuterium oxide theophylline formed self-associates at 10^{-4} M solution, in chloroform at 10^{-3} M solution, and in formic acid-D2 at 10^{-2} M solution.

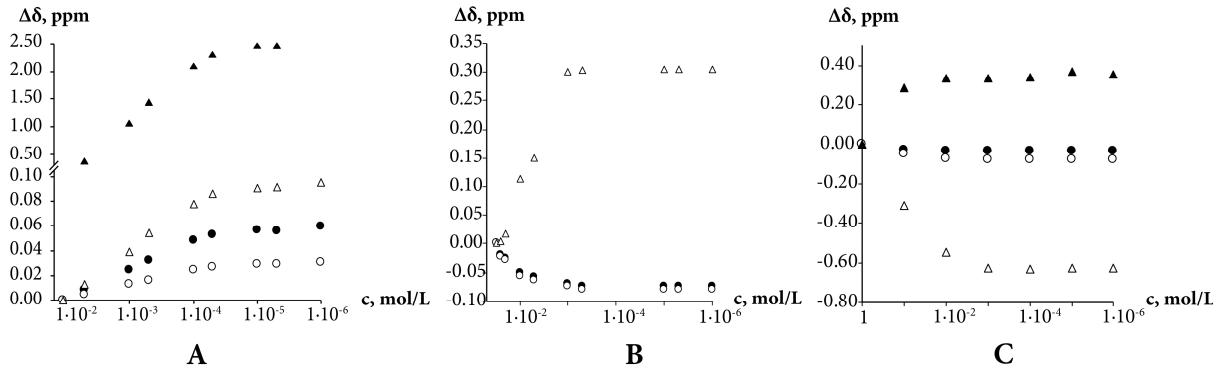

Figure 3.30. Theophylline chemical shift displacement depending on chloroform-D (A); deuterium oxide (B); and formic acid-D2 (C) concentration. Chemical shifts are indicated as: methyl group C10 protons (●); methyl group C12 protons (○); alkene group proton (C8-H) (Δ); and imidazolium group proton (N7-H) (▲).

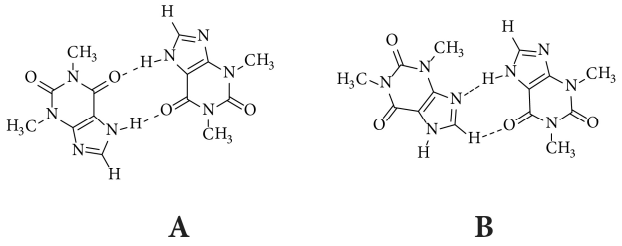

Figure 3.31. Theophylline dimer present in crystal structures of monohydrate, Form IV and most cocrystals (A); and the preferred theophylline dimer according to Etters rules (B).

No change in chemical shift displacement was observed with time (>20 days) in any studied solvents. Small scale SMPT performed in methanol-D4 showed the same – solution composition did not change over time; hence, no aggregates are formed or disarranged during slurrying indicating that this is not the reason for long induction times.

Theophylline dimers/aggregates formed in solvents which are good proton donors [279]. These were the solvents where SMPT exhibited longest induction times and phase transition rates (we should mention that SMPT in water does not occur, because theophylline monohydrate is the most stable crystalline form in aqueous environments). Such correlation implies that the presence of theophylline dimers or aggregates in the solution hinders the nucleation and growth of Form IV. It is likely that the reason why good proton donors inhibit phase transformation and extend induction time is the formation of solvent molecule stabilized theophylline dimers/aggregates. Trask *et al.* [248] have suggested that the theophylline dimer motif is favoured by the presence of a competing strong hydrogen bond donor in the system (in

this case formic acid, chloroform or water in methanol/water mixture). The strongest hydrogen bond donor in theophylline solution forms a hydrogen bond with the system's most basic group – theophylline imidazole group nitrogen (N9). This bond fulfils the 'best-donor–best-acceptor' rule and consequently permits theophylline dimer formation by secondary hydrogen bonding (N7-H···O13). Such solvated theophylline dimer should be the most stable aggregate in the solution, since it uses the system's best donors and acceptors. This explains why increasing water in the methanol sample increased induction time and extended phase transformation time. The increase of water in methanol/water mixture increased the level of hydrated aggregates in the solution, and the more solution theophylline molecules were bound in these dimers, the more formation of Form IV was hindered.

Solvated theophylline aggregates inhibit nucleation and growth of Form IV, either because they are not the correct structure to nucleate Form IV or because these associates need to be desolvated or disarranged in order to crystallize. If the solute solvent bonds are stronger than the weak inter dimer interactions in the solid structure, then the desolvation process is unfavourable and therefore phase transition is slow.

3.7.3. FTIR studies of theophylline crystallization from saturated solutions

It is known [3,5,256,280,281] that FTIR spectra of polymorphs and their solutions are different. Parveen *et al.* [64] have shown that FTIR spectroscopy can be used to show a direct relationship between molecular self-associates in solution and motifs in the subsequently crystallised solid phases. Here we use FTIR spectroscopy to monitor theophylline crystallization from acetone, acetonitrile, chloroform, methanol and water. FTIR spectra of saturated theophylline solution were continuously recorded during solvent evaporation and subsequent – theophylline crystallization. FTIR spectra of both theophylline polymorphs studied in this work are clearly different and therefore suitable for such an experiment (Figure 3.32.). However, due to low theophylline solubility in the selected solvents, only the strongest carbonyl group stretching bands were visible in the initial spectra.

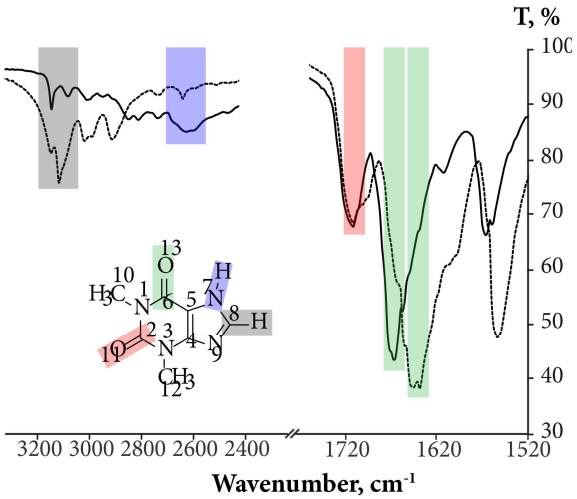

Figure 3.32. FTIR spectra of theophylline Form II (—) and Form IV (---), showing carbonyl group, alkene group hydrogen bond and imidazolium group hydrogen bond stretching band assignment.

It is known [282] that hydrogen bonding lengthens and weakens the C=O bond, therefore the carbonyl group stretching band is observed at a lower frequency; thus the stronger the hydrogen bonding, the lower the stretching frequency. This rule can be clearly seen in the case of theophylline. Carbonyl group C2=O11, which is not involved in the hydrogen bonding in either polymorph (there are only weak interactions with theophylline methyl group hydrogens), have an identical band position in the FTIR spectra (1706 cm^{-1}) and the stretching frequency is higher than that of C6=O13 carbonyl group. In Form IV, the carbonyl group C6=O13 is involved in strong hydrogen bonding with the best hydrogen bond donor (N7-H) and this results in a stretching frequency of 1640 cm^{-1}; while in Form II, the C6=O13 group is involved in two weak bifurcated C8-H···O13 hydrogen bonds, stretching band is observed at 1664 cm^{-1}.

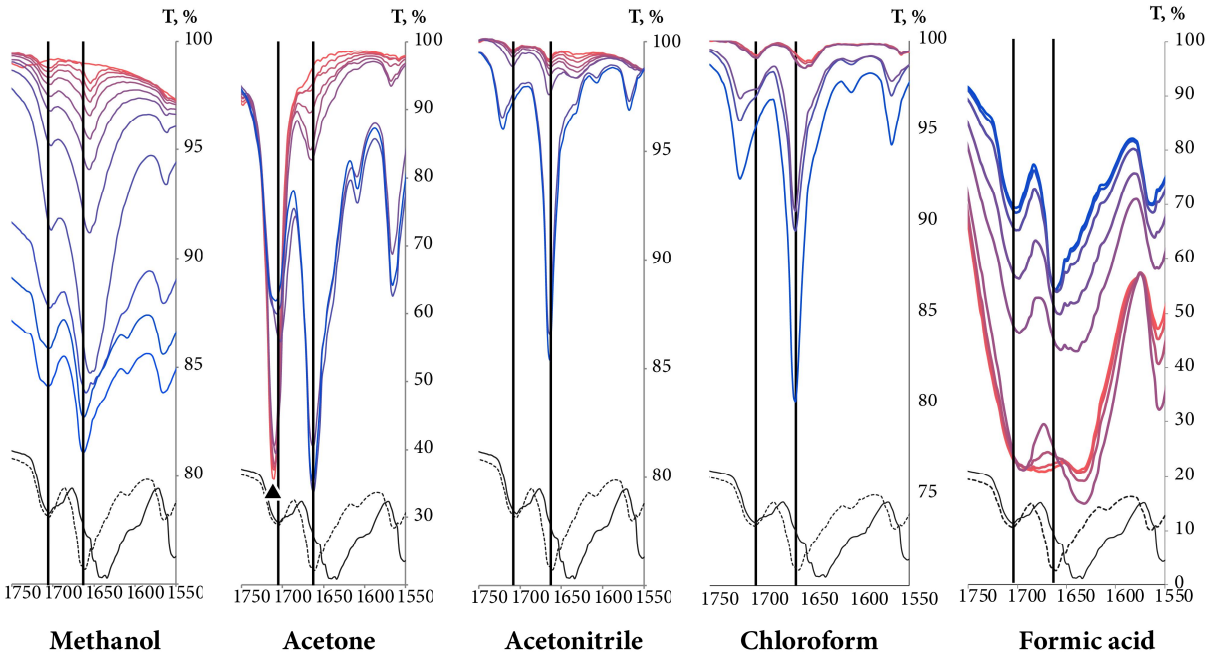

Figure 3.33. FTIR spectra of carbonyl group stretching band region during theophylline crystallization from saturated solutions upon solvent evaporation at room temperature. Colour gradient shows FTIR spectra changes throughout crystallization (red – saturated solution, blue – crystallization product). FTIR spectra of solid theophylline Form II (dashed line) and IV (continuous line) are added for comparison purpose. Acetone carbonyl group stretching band is marked with ▲.

Figure 3.33. illustrates the carbonyl group stretching band position and intensity changes during theophylline crystallization from saturated Form II solutions during solvent evaporation.

The stretching bands of other groups/bonds expected to take part in self-association – alkene group hydrogen bond and imidazolium group hydrogen bond – were not visible in solution FTIR spectra due to low theophylline solubility in the chosen solvents, and they were observed only when all the solvent had evaporated. During the solvent evaporation the intensities of all theophylline bands increased because of increasing theophylline concentration in the solution. An exception to this was the final part of crystallization from saturated methanol solution, where theophylline carbonyl group intensities decreased. For clarity these spectra are shifted by *y* axis. Crystallization from acetone, acetonitrile, chloroform, methanol and formic acid gave theophylline Form II, and water produced theophylline monohydrate. Intensive water OH bending band was overlapping with both theophylline carbonyl group stretching bands,

therefore the crystallization experiment from saturated water solution was not suitable for studies.

The strongest carbonyl group stretching bands in theophylline solution spectra were observed in concentrated solution, whereas weaker spectral bands appeared only when theophylline crystals emerged. In all solvents the most distinct changes in theophylline band positions and intensities were observed at the moment when solid theophylline emerged. This was due to fact that, before the crystallization FTIR spectra represented mostly solvated theophylline and theophylline associates, whereas during the crystallization, spectra were reflecting the average spectra of solvated theophylline, multiple theophylline associates and crystalline theophylline. The ratio of these species changed during the evaporation/crystallization and therefore, the band position of functional groups involved in these processes also changed. Finally, when all solvent have evaporated, FTIR spectra of crystalline theophylline was observed.

The position of C2=O11 carbonyl group stretching band in methanol, acetonitrile and chloroform solutions were the same (1706 cm^{-1}) and it coincided with the position of this group in both polymorphs, therefore we can conclude that this group was not involved in strong hydrogen bonding in the solution (similar to crystalline theophylline) and the nearby environment of this group was similar to that in both polymorphs. The position of this stretching band in acetone solution cannot be determined, as acetone carbonyl group stretching bands overlaps with this carbonyl group stretching band. The position of C2=O11 carbonyl group stretching band does not change during the crystallization from methanol solution, whereas during the crystallization from acetonitrile and chloroform solutions the band shifted to 1720 cm^{-1} indicating a change in bonding. The final position of this group stretching band does not match that in the solid Form II. FTIR spectra did not change within 5 h. Such band shift to higher frequency indicates that hydrogen bonding was weaker in the crystallized material than in solution. Crystallizations from both solvents were repeated in larger scale. PXRD showed that crystallization products were Form II, and FTIR spectra of obtained material coincided with Form II spectra. The reason why C2=O11 carbonyl group stretching band position in FTIR *in-situ* experiment does not match the position of this band in Form II spectra might be related to theophylline crystallization manner from acetonitrile and chloroform. No

distinct theophylline crystals were observed on the FTIR spectrometer liquids plate after solvent evaporation, meaning that theophylline crystalized as a thin film. Such crystallization behaviour might promote *monolayer* product along {100} plane, where this carbonyl group is on the surface and it is not involved in any hydrogen bonding. Consequently, C2=O11 carbonyl group stretching band would be shifted to higher frequency for such crystallization product.

In saturated formic acid solution position of C2=O11 carbonyl group stretching band was 1696 cm^{-1} and during the crystallization it gradually shifted to the position of this carbonyl group in crystalline theophylline. This happened because in the solution this carbonyl group was involved in hydrogen bonding with formic acid proton, whereas during the crystallization this hydrogen bond was disarranged.

Unlike C2=O11 carbonyl group, the position of the C6=O13 carbonyl group stretching bands were not the same in the methanol solution and crystallized material. In the methanol solution the carbonyl group C6=O13 stretching band was observed at 1656 cm^{-1}, i.e. in between the stretching bands of this carbonyl group in solid Form II and Form IV. This suggest that the associates (dimers, aggregates, solvated entities) in the solution were not the same as in the solid phases and that the hydrogen bonding in the solution was stronger than that in the Form II and weaker than that in Form IV. From ^{1}H NMR experiment we know that there was no theophylline self-association in methanol, therefore we can conclude that the association causing band shift must be hydrogen bonding between the carbonyl group and methanol -OH group proton. The changes of the C6=O13 stretching band position were observed at the final part of the crystallization and the band position shifted from 1656 to 1664 cm^{-1}, which is the position of this band in theophylline Form II.

In chloroform, analogous C6=O13 carbonyl group stretching band shift were observed, with the only difference that initially this band had two maxima – at 1656 cm^{-1} and 1648 cm^{-1}. The band at 1656 cm^{-1} corresponds to solvated theophylline species, analogous to those in methanol, whereas the band at 1648 cm^{-1} most likely corresponds to the dimer detected by NMR measurements. A similar situation was observed when theophylline crystallized from formic acid; with the difference that in saturated formic acid solution a wide band in this region was observed. The wider carbonyl group stretching band must be a result of multiple associates. The concentration of saturated formic acid solution was ~100 times higher than the

concentration of saturated chloroform solution, therefore it was expected that associates formed were more complex than dimers and with some diversity. Upon crystallization these agglomerates were disarranged and desolvated, and the final position of C6=O13 carbonyl group stretching band matched the position of Form II.

Minor changes in the position of the C6=O13 carbonyl group stretching band were observed when theophylline crystallized from acetone solution. This suggests that theophylline hydrogen bonding did not change significantly upon crystallization from acetone, at least as regards to this carbonyl group. The position of C6=O13 carbonyl group stretching band remained the same during the crystallization from acetonitrile. Such behaviour points out, that this theophylline carbonyl group does not form hydrogen bonds in acetone and acetonitrile solutions, neither to solvent molecules, nor to other theophylline molecules. It is understandable – acetone and acetonitrile are not proton donor solvents. However it was expected that these solvents would compete with the basic theophylline imidazole group nitrogen (N9) to form a hydrogen bond with the most acidic theophylline proton (N7-H). NMR experiments showed that theophylline molecules in the acetone and acetonitrile solution are monomeric and self-association does not occur in these solvents, meaning that species with solvated (N7-H) group dominated in acetone and acetonitrile.

The same FTIR *in-situ* crystallization experiment was repeated with saturated Form IV solution in methanol and identical results were obtained, suggesting that there are the same associates in the solution regardless of to which polymorph the solution is saturated.

3.7.4. Conclusions

The SMPT from theophylline Form II to Form IV is a very slow nucleation-growth controlled polymorphic transformation. Form IV nucleation is homogenous and slow. Nucleation of and therefore induction of the phase transformation is hindered by solution aggregates. Form IV crystals grow along the {001} direction, forming plate-like crystals. SMPT induction times correlate to phase transition times in studied solvents, indicating that nucleation and Form IV growth is limited by the same factors. Theophylline self-associates in solvents which are good H-bond donors i.e. chloroform, water and formic acid. There are the same molecular aggregates in the solutions saturated with respect to Form II and Form IV. The

theophylline aggregates present in solution do not change over time and therefore the long induction time of Form IV is not dependent on solution processes. NMR and FTIR data suggest that the nature of solution aggregates is solvent dependent, most likely linked to hydrogen bonding character of the solvent.

4. Conclusions

1. Sample preparation conditions and detection limit of previously published (Petkune et al., J. Pharm. Pharmacol., 2011, 63, 9, 1136) semi-quantitative method for low-level thermodynamically stable polymorph impurity determination in the metastable polymorph have been improved. Detection limit was lowered down to 0.0005% of thermodynamically stable tegafur β polymorph in the metastable α polymorph.
2. In β tegafur weight fraction range from 2.0% to approximately 0.05%, the best correlation was achieved when 0.50 g samples were ground for 5 min at 20 °C with 10 Hz frequency. At lower weight fraction of β tegafur, the milling frequency of 15 Hz was preferred. The optimum results were achieved when 0.06 mL of water was added to 0.50 g of tegafur.
3. It has been shown that a sum of Langmuir and Cauchy–Lorentz equations could be used to describe the change in conversion degree depending on the added water volume. The determined surface areas and the dependence of conversion degree on water additive volume demonstrated that increasing the added water volume above 0.06 mL did not improve milling effectiveness.
4. Conversion degree of β tegafur was highly dependent on sample drying time, and the recrystallization process could be described with a kinetic equation $\omega_\beta = 35.8 - 20.7e^{-0.063t}$.
5. Phase transition dynamics of β tegafur to α tegafur is in a good agreement for samples ground in ball mill with solvent additive and samples, that were exposed to 95% solvent relative vapour pressure.
6. Solvent desorption from α and β tegafur do not differ significantly and solvent desorption in all cases occur faster from samples with the largest particle size. Structure differences and their surface properties are not of great importance on the solvent desorption rates and the main factor affecting desorption rate is sample particle size and sample morphology.
7. Two different solvent desorption behaviours can be distinguished depending on the solvent and surface interaction energy. If the solvent and surface interaction was stronger than interaction between solvent molecules, than multilayer and monolayer desorption was

observed, but, if the adsorbed solvent molecules were of equal energy, then only one desorption phase was observed.

8. Solvent desorption rates of acetone, acetonitrile, ethyl acetate and tetrahydrofuran multilayers from α and β tegafur were approximately 30 times higher than those from solvent monolayers.
9. Small tegafur particles recrystallized to larger particles during sample exposure to solvent vapour atmosphere, and there were morphological signs of tegafur recrystallization from solution on the surface of the particles.
10. The SMPT from α tegafur to β tegafur in acetone, cyclohexane, ethanol, *i*-propanol, toluene, and water at 22 °C is nucleation-growth controlled and it can be described with the P2 power model. The rate constants for this process were in the range from 0.028 min^{-1} to 0.0056 min^{-1}. In all the employed solvents an induction time (about 10% of the time required for complete phase transition) was observed, indicating that nucleation and/or initial crystal growth was the limiting factor for SMPTs performed in saturated solutions.
11. Surface nucleation was observed in studied SMPT from β tegafur to α tegafur. Crystal habit investigation indicated that β tegafur nucleated on the {010} face of α tegafur, and the {110} face of β tegafur was in contact with α tegafur crystal.
12. The SMPT rate from β tegafur to α tegafur depended linearly on the supersaturation level, i.e. difference between α and β tegafur equilibrium solubility in the respective solvent. Similar correlation was observed in mechanochemical SMPT.
13. Studied SMPT from theophylline Form II to Form IV is very slow nucleation-growth controlled polymorphic transformation. Form IV nucleation is homogenous and Form IV crystals grow along {001} face, forming plate-like crystals. SMPT induction times correlate to phase transition times in studied solvents, indicating that nucleation and Form IV growth is limited by the same factors.
14. Theophylline solution phase studies revealed that phase transformation to Form IV occur faster in weak hydrogen bond donor or aprotic solvents, where theophylline exists as a monomers. Good hydrogen bond donor solvents – chloroform, water and formic acid – promotes theophylline self-association which hinders phase transformation to Form IV.

5. References

1. Haleblian, J.; McCrone, W. Pharmaceutical applications of polymorphism. *J. Pharm. Sci.* **1969**, 58, 911–929.
2. Borka, L. Review on crystal polymorphism of substances in the European Pharmacopoeia. *Pharm. Acta Helv.* **1991**, 66, 16–22.
3. Brittain, H. G. *Polymorphism in Pharmaceutical Solids*, 2nd Ed.; Informa Healthcare USA, Inc.: New York, NY, 2009, 640.
4. Vippagunta, S. R.; Brittain, H. G.; Grant, D. J. W. Crystalline solids. *Adv. Drug Deliv. Rev.* **2001**, 48, 3–26.
5. Hilfiker, R. *Polymorphism: in the Pharmaceutical Industry*; Wiley-VCH: Weinheim, 2006, 433.
6. Caira, M. R. Crystalline Polymorphism of Organic Compounds. In: *Des. Org. Solids*; Weber, E., Ed.; 1998, pp. 163–208.
7. Ostwald, W. Studies on the formation and transformation of solid compounds: report I. Supersaturation and practicing cooling. *Zeitschrift Für Phys. Chemie* **1897**, 22, 289.
8. Murphy, D.; Rodríguez-Cintrón, F.; Langevin, B.; Kelly, R. C.; Rodríguez-Hornedo, N. Solution-mediated phase transformation of anhydrous to dihydrate carbamazepine and the effect of lattice disorder. *Int. J. Pharm.* **2002**, 246, 121–134.
9. Rodríguez-Hornedo, N.; Lechuga-Ballesteros, D. Phase transition and heterogeneous/epitaxial nucleation of hydrated and anhydrous theophylline crystals. *Int. J. Pharm.* **1992**, 85, 149–162.
10. Rodríguez-Hornedo, N.; Murphy, D. Significance of controlling crystallization mechanisms and kinetics in pharmaceutical systems. *J. Pharm. Sci.* **1999**, 88, 651–660.
11. Haleblian, J. K. Characterization of Habits and Crystalline Modification of Solids and Their Pharmaceutical Applications. *J. Pharm. Sci.* **1975**, 64, 1269–1288.
12. Storey, R. A.; Ymén, I. (Eds.). *Solid State Characterization of Pharmaceuticals*; John Wiley & Sons, Ltd: Chichester, UK, 2011, 506.
13. Bernstein, J. Crystal growth, polymorphism and structure-property relationships in organic crystals. *J. Phys. D. Appl. Phys.* **1993**, 26, B66–B76.
14. Aitipamula, S.; Nangia, A. Polymorphism : Fundamentals and Applications. *Eng. Life Sci.* **2012**, 3, 103–112.
15. Pangarkar, P. A.; Tayade, A. M.; Uttarwar, S. G.; Wanare, R. S. Drug Polymorphism: An Overview. *Int. J. Pharm. Technol.* **2013**, 5, 2374–2402.
16. Rodriguez-Spong, B.; Price, C. P.; Jayasankar, A.; Matzger, A. J.; Rodriguez-Hornedo, N. General principles of pharmaceutical solid polymorphism:: A supramolecular perspective. *Adv. Drug Deliv. Rev.* **2004**, 56, 241–274.
17. Davey, R. J. Pizzas, polymorphs and pills. *Chem. Commun.* **2003**, 1463.
18. Cruz-Cabeza, A. J.; Bernstein, J. Conformational polymorphism. *Chem. Rev.* **2014**, 114, 2170–2191.
19. Nangia, A. Conformational polymorphism in organic crystals. *Acc. Chem. Res.* **2008**, 41, 595–604.
20. Desiraju, G. R. Hydrogen bridges in crystal engineering: interactions without borders. *Acc. Chem. Res.* **2002**, 35, 565–73.

21. Desiraju, G. R. C-H...O and other weak hydrogen bonds. From crystal engineering to virtual screening. *Chem. Commun. (Camb).* **2005**, 2995–3001.
22. Steiner, T. The Hydrogen Bond in the Solid State. *Angew. Chemie Int. Ed.* **2002**, 41, 48–76.
23. Desiraju, G.; Steiner, T. *The Weak Hydrogen Bond: In Structural Chemistry and Biology*; Oxford University Press: New York, NY, 2001, 507.
24. Desiraju, G. R. Chemistry beyond the molecule. *Nature* **2001**, 412, 397–400.
25. Arunan, E.; Desiraju, G. R.; Klein, R. A.; Sadlej, J.; Scheiner, S.; Alkorta, I.; Clary, D. C.; Crabtree, R. H.; Dannenberg, J. J.; Hobza, P.; Kjaergaard, H. G.; Legon, A. C.; Mennucci, B.; Nesbitt, D. J. Defining the hydrogen bond: An account (IUPAC Technical Report). *Pure Appl. Chem.* **2011**, 83, 1619–1636.
26. Kwan, E. E. *Intermolecular Forces and Hydrogen Bonding*; 2011, 727–734.
27. Clawson, J. S.; Kennedy-Gabb, S.; Lee, A. Y.; Copley, R. C. B. One-phase crystal disorder in pharmaceutical solids and its implication for solid-state stability. *J. Pharm. Sci.* **2011**,.
28. Vranić, E. Amorphous pharmaceutical solids. *Bosn. J. Basic Med. Sci.* **2004**, 4, 35–39.
29. Yu, L. Amorphous pharmaceutical solids: preparation, characterization and stabilization. *Adv. Drug Deliv. Rev.* **2001**, 48, 27–42.
30. Brittain, H. G. Polymorphism and solvatomorphism 2010. *J. Pharm. Sci.* **2012**, 101, 464–84.
31. Brittain, H. G. Cocrystal Systems of Pharmaceutical Interest: 2010. *Cryst. Growth Des.* **2012**, 12, 1046–1054.
32. Aitipamula, S.; Banerjee, R.; Bansal, A. K.; Biradha, K.; Cheney, M. L.; Choudhury, A. R.; Desiraju, G. R.; Dikundwar, A. G.; Dubey, R.; Duggirala, N.; Ghogale, P. P.; Ghosh, S.; Goswami, P. K.; Goud, N. R.; Jetti, R. R. K. R.; Karpinski, P.; Kaushik, P.; Kumar, D.; Kumar, V.; Moulton, B.; Mukherjee, A.; Mukherjee, G.; Myerson, A. S.; Puri, V.; Ramanan, A.; Rajamannar, T.; Reddy, C. M.; Rodriguez-Hornedo, N.; Rogers, R. D.; Row, T. N. G.; Sanphui, P.; Shan, N.; Shete, G.; Singh, A.; Sun, C. C.; Swift, J. A.; Thaimattam, R.; Thakur, T. S.; Kumar Thaper, R.; Thomas, S. P.; Tothadi, S.; Vangala, V. R.; Variankaval, N.; Vishweshwar, P.; Weyna, D. R.; Zaworotko, M. J. Polymorphs, Salts, and Cocrystals: What's in a Name? *Cryst. Growth Des.* **2012**, 12, 2147–2152.
33. Babu, N. J.; Nangia, A. Solubility Advantage of Amorphous Drugs and Pharmaceutical Cocrystals. *Cryst. Growth Des.* **2011**, 11, 2662–2679.
34. Schultheiss, N.; Newman, A. Pharmaceutical Cocrystals and Their Physicochemical Properties. *Cryst. Growth Des.* **2009**, 9, 2950–2967.
35. Shan, N.; Zaworotko, M. J. The role of cocrystals in pharmaceutical science. *Drug Discov. Today* **2008**, 13, 440–446.
36. Vishweshwar, P.; McMahon, J. A.; Bis, J. A.; Zaworotko, M. J. Pharmaceutical co-crystals. *J. Pharm. Sci.* **2006**, 95, 499–516.
37. Mullin, J. W. *Crystallization*, 4th Ed.; Butterworth-Heinemann: Oxford, 2001, 600.
38. Schüth, F. Nucleation and crystallization of solids from solution. *Curr. Opin. Solid State Mater. Sci.* **2001**, 5, 389–395.
39. De Yoreo, J. J. Principles of Crystal Nucleation and Growth. *Rev. Mineral. Geochemistry* **2003**, 54, 57–93.

40. Chen, J.; Sarma, B.; Evans, J. M. B.; Myerson, A. S. Pharmaceutical Crystallization. *Cryst. Growth Des.* **2011**, 11, 887–895.
41. De Yoreo, J. Crystal nucleation: more than one pathway. *Nat. Mater.* **2013**, 12, 284–5.
42. Cardew, P. T. The growth shape of crystals. *J. Cryst. Growth* **1985**, 73, 385–391.
43. Boistelle, R.; Astier, J. P. Crystallization mechanisms in solution. *J. Cryst. Growth* **1988**, 90, 14–30.
44. Etter, M. C.; Jahn, D. A.; Donahue, B. S.; Johnson, R. B.; Ojala, C. Growth and characterization of small molecule organic crystals. *J. Cryst. Growth* **1986**, 76, 645–655.
45. Cardew, P. T.; Davey, R. J. The Kinetics of Solvent-Mediated Phase Transformations. *Proc. R. Soc. A Math. Phys. Eng. Sci.* **1985**, 398, 415–428.
46. Davey, R. J. The effect of impurity adsorption on the kinetics of crystal growth from solution. *J. Cryst. Growth* **1976**, 34, 109–119.
47. Davey, R. J.; Cardew, P. T.; McEwan, D.; Sadler, D. E. Rate Controlling Processes in Solvent-Mediated Phase Transformations. *J. Cryst. Growth* **1986**, 79, 648–653.
48. Davey, R. J.; Allen, K.; Blagden, N.; Cross, W. I.; Lieberman, H. F.; Quayle, M. J.; Righini, S.; Seton, L.; Tiddy, G. J. T. Crystal engineering - nucleation, the key step. Based on the presentation given at CrystEngComm Discussion, 29th June 1st July 2002, Bristol, UK. *CrystEngComm* **2002**, 4, 257.
49. Davey, R. J.; Schroeder, S. L. M.; ter Horst, J. H. Nucleation of organic crystals--a molecular perspective. *Angew. Chem. Int. Ed. Engl.* **2013**, 52, 2166–79.
50. Myerson, A. S.; Lo, P. Y. Diffusion and cluster formation in supersaturated solutions. *J. Cryst. Growth* **1990**, 99, 1048–1052.
51. Kashchiev, D.; van Rosmalen, G. M. Review: Nucleation in solutions revisited. *Cryst. Res. Technol.* **2003**, 38, 555–574.
52. Gibbs, J. W. *The collected works of J. Willard Gibbs*; Longmans, Green: 1928.
53. Volmer, M. Kinetik der Phasenbildung. *Steinkopf, Leipzig* **1939**,.
54. Becker, R.; Döring, W. Kinetische behandlung der keimbildung in übersättigten dämpfen. *Ann. Phys.* **1935**, 416, 719–752.
55. Turnbull, D.; Fisher, J. C. Rate of Nucleation in Condensed Systems. *J. Chem. Phys.* **1949**, 17, 71.
56. Etter, M. C. Hydrogen bonds as design elements in organic chemistry. *J. Phys. Chem.* **1991**, 95, 4601–4610.
57. Cioffi, M.; Hunter, C. A.; Packer, M. J.; Pandya, M. J.; Williamson, M. P. Use of quantitative (1)H NMR chemical shift changes for ligand docking into barnase. *J. Biomol. NMR* **2009**, 43, 11–9.
58. Musumeci, D.; Hunter, C. A.; McCabe, J. F. Solvent Effects on Acridine Polymorphism. *Cryst. Growth Des.* **2010**, 10, 1661–1664.
59. Hunter, C. A.; McCabe, J. F.; Spitaleri, A. Solvent effects of the structures of prenucleation aggregates of carbamazepine. *CrystEngComm* **2012**, 14, 7115–7117.
60. Chadwick, K.; Davey, R. J.; Dent, G.; Pritchard, R. G.; Hunter, C. A.; Musumeci, D. Cocrystallization: A Solution Chemistry Perspective and the Case of Benzophenone and Diphenylamine. *Cryst. Growth Des.* **2009**, 9, 1990–1999.
61. Davey, R. J.; Dent, G.; Mughal, R. K.; Parveen, S. Concerning the Relationship between Structural and Growth Synthons in Crystal Nucleation: Solution and Crystal

Chemistry of Carboxylic Acids As Revealed through IR Spectroscopy. *Cryst. Growth Des.* **2006**, 6, 1788–1796.
62. Mei, X.; Wolf, C. Formation of New Polymorphs of Acridine Using Dicarboxylic Acids as Crystallization Templates in Solution. *Cryst. Growth Des.* **2004**, 4, 1099–1103.
63. Kulkarni, S. A.; McGarrity, E. S.; Meekes, H.; ter Horst, J. H. Isonicotinamide self-association: the link between solvent and polymorph nucleation. *Chem. Commun. (Camb).* **2012**, 48, 4983–5.
64. Parveen, S.; Davey, R. J.; Dent, G.; Pritchard, R. G. Linking solution chemistry to crystal nucleation: the case of tetrolic acid. *Chem. Commun.* **2005**, 1531–1533.
65. Davey, R. J.; Blagden, N.; Righini, S.; Alison, H.; Quayle, M. J.; Fuller, S. Crystal Polymorphism as a Probe for Molecular Self-Assembly during Nucleation from Solutions: The Case of 2,6-Dihydroxybenzoic Acid. *Cryst. Growth Des.* **2001**, 1, 59–65.
66. Davey, R. J.; Liu, W.; Quayle, M. J.; Tiddy, G. J. T. In Situ Monitoring of Crystallization Processes Using Synchrotron X-ray Diffraction: The Search for Structural Precursors. *Cryst. Growth Des.* **2002**, 2, 269–272.
67. Quayle, M. J.; Davey, R. J.; McDermott, A. J.; Tiddy, G. J. T.; Clarke, D. T.; Jones, G. R. In situ monitoring of rapid crystallisation processes using synchrotron X-ray diffraction and a stopped-flow cell. *Phys. Chem. Chem. Phys.* **2002**, 4, 416–418.
68. Becker, E. D. NMR Studies of Hydrogen Bonding in Alcohols and Phenol. *J. Chem. Phys.* **1959**, 31, 269.
69. Huggins, C. M.; Pimentel, G. C.; Shoolery, J. N. Proton Magnetic Resonance Studies of the Hydrogen Bonding of Phenol, Substituted Phenols and Acetic Acid. *J. Phys. Chem.* **1956**, 60, 1311–1315.
70. Becker, E. D.; Liddel, U.; Shoolery, J. N. Nuclear magnetic resonance studies of hydrogen bonding in ethanol. *J. Mol. Spectrosc.* **1958**, 2, 1–8.
71. Lam, Y.; Kotowycz, G. Nuclear magnetic resonance studies on the self-association of adenosine 5′-triphosphate in aqueous solutions. *Can. J. Chem.* **1977**, 55, 3620–3630.
72. Horman, I.; Dreux, B. Estimation of Dimerisation Constants from Complexatin-Induced Displacements of1H-NMR Chemical Shifts: Dimerisation of Caffeine. *Helv. Chim. Acta* **1984**, 67, 754–764.
73. McLennan, I. J.; Lenkinski, R. E.; Yanuka, Y. A nuclear magnetic resonance study of the self-association of adriamycin and daunomycin in aqueous solution. *Can. J. Chem.* **1985**, 63, 1233–1238.
74. Marchettini, N.; Valensin, G.; Gaggelli, E. 1H-NMR studies on the self-association of chloroquine in aqueous solution. *Biophys. Chem.* **1990**, 36, 65–70.
75. Veselkov, A. N.; Dymant, L. N.; Baranovskii, S. F.; Bolotin, P. A.; Zav'yalova, O. S.; Veselkov, D. A.; Parkes, H.; Davies, D. 1H NMR study of self-association of actinomycin D in an aqueous solution. *J. Struct. Chem.* **1995**, 36, 69–75.
76. Davies, D. B.; Djimant, L. N.; Veselkov, A. N. 1H NMR investigation of self-association of aromatic drug molecules in aqueous solution. Structural and thermodynamical analysis. *J. Chem. Soc. Faraday Trans.* **1996**, 92, 383.
77. Bastian, M.; Sigel, H. The self-association of flavin mononucleotide (FMN2−) as determined by 1H NMR shift measurements. *Biophys. Chem.* **1997**, 67, 27–34.

78. Evstigneev, M. P.; Evstigneev, V. P.; Davies, D. B. 1H NMR determination of the self-association of an acridine homodimer and its complexation with ethidium bromide in aqueous solution. *J. Mol. Struct.* **2006**, 784, 162–168.
79. Bogdan, M.; Floare, C. G.; Pîrnău, A. 1 H NMR investigation of self-association of vanillin in aqueous solution. *J. Phys. Conf. Ser.* **2009**, 182, 012002.
80. Chen, J. S.; Shirts, R. B. Iterative determination of the NMR monomer shift and dimerization constant in a self-associating system. *J. Phys. Chem.* **1985**, 89, 1643–1646.
81. Becker, E. D. Infrared studies of hydrogen bonding in alcohol-base systems. *Spectrochim. Acta* **1961**, 17, 436–447.
82. Kuhn, L. P.; Bowman, R. E. The hydrogen bond—IV. Intramolecular hydrogen bonding in triols. *Spectrochim. Acta* **1961**, 17, 650–660.
83. Liddel, U.; Becker, E. D. Infra-red spectroscopic studies of hydrogen bonding in methanol, ethanol, and t-butanol. *Spectrochim. Acta* **1957**, 10, 70–84.
84. Abraham, R. J.; Mobli, M. An NMR, IR and theoretical investigation of (1)H chemical shifts and hydrogen bonding in phenols. *Magn. Reson. Chem.* **2007**, 45, 865–77.
85. Hibbert, F.; Emsley, J. Hydrogen bonding and chemical reactivity. *Adv. Phys. Org. Chem.* **1990**, 26, 255–379.
86. Hunter, C. A.; Packer, M. J. Complexation-Induced Changes in1H NMR Chemical Shift for Supramolecular Structure Determination. *Chem. - A Eur. J.* **1999**, 5, 1891–1897.
87. Spitaleri, A.; Hunter, C. A.; McCabe, J. F.; Packer, M. J.; Cockroft, S. L. A 1H NMR study of crystal nucleation in solution. *CrystEngComm* **2004**, 6, 489–493.
88. Cioffi, M.; Hunter, C. A.; Packer, M. J.; Spitaleri, A. Determination of protein-ligand binding modes using complexation-induced changes in (1)h NMR chemical shift. *J. Med. Chem.* **2008**, 51, 2512–7.
89. Gmeiner, W. H.; Poulter, C. D. NMR studies of nucleic acids. Deuterium isotope effects on carbon-13 chemical shifts in hydrogen-bonded complexes of pyrimidines and purines. *J. Am. Chem. Soc.* **1988**, 110, 7640–7647.
90. Waterhous, D. V.; Muccio, D. D. 1H and13C NMR studies on the self-association of retinoic acid. *Magn. Reson. Chem.* **1990**, 28, 223–226.
91. Cockroft, S. L.; Perkins, J.; Zonta, C.; Adams, H.; Spey, S. E.; Low, C. M. R.; Vinter, J. G.; Lawson, K. R.; Urch, C. J.; Hunter, C. A. Substituent effects on aromatic stacking interactions. *Org. Biomol. Chem.* **2007**, 5, 1062–80.
92. Hughes, C. E.; Hamad, S.; Harris, K. D. M.; Catlow, C. R. A.; Griffiths, P. C. A multi-technique approach for probing the evolution of structural properties during crystallization of organic materials from solution. *Faraday Discuss.* **2007**, 136, 71.
93. Dearden, J. C. Investigation of the Self-Association of Phenols and Anilines By Ultraviolet Spectroscopy. *Can. J. Chem.* **1963**, 41, 2683–2691.
94. Singh, S.; Rao, C. N. R. Spectroscopic studies of self-association due to hydrogen bonding. *J. Phys. Chem.* **1967**, 71, 1074–1078.
95. Morcillo, J.; Gallego, E.; Peral, F. A critical study of the application of ultraviolet spectroscopy to the self-association of adenine, adenosine and 5′-AMP in aqueous solution. *J. Mol. Struct.* **1987**, 157, 353–369.

96. Peral, F.; Gallego, E. Self-association of pyrimidine and some of its methyl derivatives in aqueous solution. *J. Mol. Struct.* **1995**, 372, 101–112.
97. Peral, F.; Gallego, E. Self-association of imidazole and its methyl derivatives in aqueous solution. A study by ultraviolet spectroscopy. *J. Mol. Struct.* **1997**, 415, 187–196.
98. Peral, F.; Gallego, E. Self-association of pyridine-2,6-dicarboxylic acid in aqueous solution as determined from ultraviolet hypochromic and hyperchromic effects. *Spectrochim. Acta Part A Mol. Biomol. Spectrosc.* **2000**, 56, 2149–2155.
99. Peral, F.; Gallego, E. A study by ultraviolet spectroscopy on self-association of purine, 6-methylpurine, benzimidazole, and imidazo [1,2-a]pyridine in aqueous solution. *Spectrochim. Acta Part A Mol. Biomol. Spectrosc.* **2000**, 56, 747–759.
100. Peral, F.; Gallego, E. A study by ultraviolet spectroscopy on the self-association of diazines in aqueous solution. *Spectrochim. Acta Part A Mol. Biomol. Spectrosc.* **2003**, 59, 1223–1237.
101. House, J. E. *Principles of chemical kinetics*; Academic Press: 2007.
102. Rhodes, C. T. Drug Development and Industrial Pharmacy. *Drug Dev. Ind. Pharm.* **1995**, 21, 2263–2285.
103. Khawam, A.; Flanagan, D. R. Basics and Applications of Solid-State Kinetics : A Pharmaceutical Perspective. *J. Pharm. Sci.* **2006**, 95, 472–498.
104. Khawam, A.; Flanagan, D. R. Solid-state kinetic models: basics and mathematical fundamentals. *J. Phys. Chem. B* **2006**, 110, 17315–28.
105. Petkune, S.; Bobrovs, R.; Actiņš, A. Organic solvents vapor pressure and relative humidity effects on the phase transition rate of α and β forms of tegafur. *Pharm. Dev. Technol.* **2012**, 17, 625–631.
106. Galwey, A. K.; Brown, M. E. Application of the Arrhenius equation to solid state kinetics: can this be justified? *Thermochim. Acta* **2002**, 386, 91–98.
107. Boldyrev, V. V. Mechanochemistry and mechanical activation of solids. *Russ. Chem. Rev.* **2006**, 75, 177–189.
108. James, S. L.; Adams, C. J.; Bolm, C.; Braga, D.; Collier, P.; Friščić, T.; Grepioni, F.; Harris, K. D. M.; Hyett, G.; Jones, W.; Krebs, A.; Mack, J.; Maini, L.; Orpen, a G.; Parkin, I. P.; Shearouse, W. C.; Steed, J. W.; Waddell, D. C. Mechanochemistry: opportunities for new and cleaner synthesis. *Chem. Soc. Rev.* **2012**, 41, 413–447.
109. Fabbiani, F. P. A.; Pulham, C. R. High-pressure studies of pharmaceutical compounds and energetic materials. *Chem. Soc. Rev.* **2006**, 35, 932–942.
110. Kwan, C. C.; Chen, Y. Q.; Ding, Y. L.; Papadopoulos, D. G.; Bentham, A. C.; Ghadiri, M. Development of a novel approach towards predicting the milling behaviour of pharmaceutical powders. *Eur. J. Pharm. Sci.* **2004**, 23, 327–336.
111. Richardson, J. F.; Harker, J. H.; Backhurst, J. *Coulson and Richardson's Chemical Engineering*; Butterworth-Heinemann: 2002.
112. Kwan, C. C.; Mio, H.; Qichen, Y.; Longding, Y.; Saito, F.; Papadopoulos, D. G.; Craigbentham, a; Ghadiri, M.; Qi Chen, Y.; Long Ding, Y.; Craig Bentham, A. Analysis of the milling rate of pharmaceutical powders using the Distinct Element Method (DEM). *Chem. Eng. Sci.* **2005**, 60, 1441–1448.

113. Coulson, J.; Richardson, J.; Backhurst, J.; Harker, J. Size Reduction of Solids. In: *Coulson Richardson's Chem. Eng. Part. Technol. Sep. Process. Butterworth-Heinemann Ltd, Oxford*; 1996, pp. 55–94.
114. Pauw, O. G. The minimization of overbreakage during repetitive impact breakage of single ore particles. *Powder Technol.* **1988**, 56, 251–257.
115. Pauw, O. G. Optimization of individual events in grinding mills during which breakages occur. *Powder Technol.* **1988**, 55, 247–256.
116. Khamar, D.; Pritchard, R. G.; Bradshaw, I. J.; Hutcheon, G. A.; Seton, L. Polymorphs of anhydrous theophylline: stable form IV consists of dimer pairs and metastable form I consists of hydrogen-bonded chains. *Acta Crystallogr. C.* **2011**, 67, o496–9.
117. Chieng, N.; Zujovic, Z.; Bowmaker, G.; Rades, T.; Saville, D. Effect of milling conditions on the solid-state conversion of ranitidine hydrochloride form 1. *Int. J. Pharm.* **2006**, 327, 36–44.
118. Crowley, K. J.; Zografi, G. Cryogenic grinding of indomethacin polymorphs and solvates: Assessment of amorphous phase formation and amorphous phase physical stability. *J. Pharm. Sci.* **2002**, 91, 492–507.
119. Kotake, N.; Kuboki, M.; Kiya, S.; Kanda, Y. Influence of dry and wet grinding conditions on fineness and shape of particle size distribution of product in a ball mill. *Adv. Powder Technol.* **2011**, 22, 86–92.
120. Lin, S.-Y.; Cheng, W.-T.; Wang, S.-L. Thermodynamic and kinetic characterization of polymorphic transformation of famotidine during grinding. *Int. J. Pharm.* **2006**, 318, 86–91.
121. Német, Z.; Hegedűs, B.; Szántay Jr., C.; Sztatisz, J.; Pokol, G. Pressurization effects on the polymorphic forms of famotidine. *Thermochim. Acta* **2005**, 430, 35–41.
122. Otsuka, M.; Kaneniwa, N. Effect of seed crystals on solid-state transformation of polymorphs of chloramphenicol palmitate during grinding. *J. Pharm. Sci.* **1986**, 75, 506–511.
123. Florence, A. T.; Salole, E. G.; Stenlake, J. B. The effect of particle size reduction on digoxin crystal properties. *J. Pharm. Pharmacol.* **1974**, 26, 479–480.
124. Lee, K. C.; Hersey, J. A. Crystal modification of methisazone by grinding. *J. Pharm. Pharmacol.* **1977**, 29, 249–250.
125. Caira, M. R.; Robbertse, Y.; Bergh, J. J.; Song, M.; De Villiers, M. M. Structural characterization, physicochemical properties, and thermal stability of three crystal forms of nifedipine. *J. Pharm. Sci.* **2003**, 92, 2519–2533.
126. Byrn, S. R.; Pfeiffer, R. R.; Stowell, J. G. *Solid state chemistry of drugs*, 2nd Ed.; SSCI, Inc: West Lafayette, 2001, 999.
127. Altheimer, B. D.; Pagola, S.; Zeller, M.; Mehta, M. A. Mechanochemical Conversions Between Crystalline Polymorphs of a Complex Organic Solid. *Cryst. Growth Des.* **2013**, 13, 3447–3453.
128. Müller, F.; Polke, R. F. From the product and process requirements to the milling facility. *Powder Technol.* **1999**, 105, 2–13.
129. Yamashita, H.; Hirakura, Y.; Yuda, M.; Teramura, T.; Terada, K. Detection of cocrystal formation based on binary phase diagrams using thermal analysis. *Pharm. Res.* **2013**, 30, 70–80.

130. Li, S.; Chen, J.-M.; Lu, T.-B. Synthon polymorphs of 1 : 1 co-crystal of 5-fluorouracil and 4-hydroxybenzoic acid: their relative stability and solvent polarity dependence of grinding outcomes. *CrystEngComm* **2014**, 16, 6450.
131. Aitipamula, S.; Wong, A. B. H.; Chow, P. S.; Tan, R. B. H. Cocrystallization with flufenamic acid: comparison of physicochemical properties of two pharmaceutical cocrystals. *CrystEngComm* **2014**, 16, 5793.
132. Lin, H.-L.; Wu, T.-K.; Lin, S.-Y. Screening and characterization of cocrystal formation of metaxalone with short-chain dicarboxylic acids induced by solvent-assisted grinding approach. *Thermochim. Acta* **2014**, 575, 313–321.
133. Eddleston, M. D.; Arhangelskis, M.; Friščić, T.; Jones, W. Solid state grinding as a tool to aid enantiomeric resolution by cocrystallisation. *Chem. Commun. (Camb).* **2012**, 48, 11340–2.
134. Eddleston, M. D.; Sivachelvam, S.; Jones, W. Screening for polymorphs of cocrystals: a case study. *CrystEngComm* **2013**, 15, 175.
135. Trask, A. V; Motherwell, W. D. S.; Jones, W. Solvent-drop grinding: green polymorph control of cocrystallisation. *Chem. Commun. (Camb).* **2004**, 890–891.
136. Trask, A. V; van de Streek, J.; Motherwell, W. D. S.; Jones, W. Achieving Polymorphic and Stoichiometric Diversity in Cocrystal Formation: Importance of Solid-State Grinding, Powder X-ray Structure Determination, and Seeding. *Cryst. Growth Des.* **2005**, 5, 2233–2241.
137. Trask, A. V; Jones, W. Crystal engineering of organic cocrystals by the solid-state grinding approach. *Org. Solid State React. Top. Curr. Chem.* **2005**, 254, 41–70.
138. Shan, N.; Toda, F.; Jones, W. Mechanochemistry and co-crystal formation: effect of solvent on reaction kinetics. *Chem. Commun.* **2002**, 2372–2373.
139. Etter, M. C.; Frankenbach, G. M. Hydrogen-bond directed cocrystallization as a tool for designing acentric organic solids. *Chem. Mater.* **1989**, 1, 10–12.
140. Pedireddi, V. R.; Jones, W.; Chorlton, A. P.; Docherty, R. Creation of crystalline supramolecular arrays: a comparison of co-crystal formation from solution and by solid-state grinding. *Chem. Commun.* **1996**, 987–988.
141. Boldyreva, E. High-pressure-induced structural changes in molecular crystals preserving the space group symmetry: anisotropic distortion/isosymmetric polymorphism. *Cryst. Eng.* **2003**, 6, 235–254.
142. Lin, I. J.; Nadiv, S. Review of the phase transformation and synthesis of inorganic solids obtained by mechanical treatment (mechanochemical reactions). *Mater. Sci. Eng.* **1979**, 39, 193–209.
143. Dunitz, J. D. Phase changes and chemical reactions in molecular crystals. *Acta Crystallogr. Sect. B Struct. Sci.* **1995**, 51, 619–631.
144. Etter, M. C.; Frankenbach, G. M.; Adsmond, D. A. Using Hydrogen Bonds to Design Acentric Organic Materials for Nonlinear Optical Users. *Mol. Cryst. Liq. Cryst. Inc. Nonlinear Opt.* **1990**, 187, 25–39.
145. Rastogi, R. P.; Bassi, P. S.; Chadha, S. L. Kinetics of reaction between naphtalene and piridic acid in the solid state. *J. Phys. Chem.* **1962**, 66, 2707–2708.
146. Rastogi, R. P.; Bassi, P. S.; Chadha, S. L. Mechanism of the reaction between hydrocarbons and piric acid in the solid state. *J. Phys. Chem.* **1963**, 67, 2569–2573.

147. Zografi, G. States of Water Associated with Solids. *Drug Dev. Ind. Pharm.* **1988**, 14, 1905–1926.
148. Hancock, B. C.; Shamblin, S. L. Water vapour sorption by pharmaceutical sugars. *Pharm. Sci. Technolo. Today* **1998**, 1, 345–351.
149. Hancock, B. C.; Zografi, G. Characteristics and significance of the amorphous state in pharmaceutical systems. *J. Pharm. Sci.* **1997**, 86, 1–12.
150. Zografi, G.; Grandolfi, G. P.; Kontny, M. J.; Mendenhall, D. W. Prediction of moisture transfer in mixtures of solids: transfer via the vapor phase. *Int. J. Pharm.* **1988**, 42, 77–88.
151. Jelinski, L. W.; Dumais, J. J.; Stark, R. E.; Ellis, T. S.; Karasz, F. E. Interaction of epoxy resins with water. A quadrupole echo deuterium NMR study. *Macromolecules* **1983**, 16, 1019–1021.
152. Rouquerol, J.; Rouquerol, F.; Llewellyn, P.; Maurin, G.; Sing, K. S. W. *Adsorption by powders and porous solids: principles, methodology and applications*; Academic press: 2013.
153. Thiel, P. A.; Madey, T. E. The interaction of water with solid surfaces: Fundamental aspects. *Surf. Sci. Rep.* **1987**, 7, 211–385.
154. Chen, D. Hygroscopicity of pharmaceutical crystals., University of Minnesota, 2009.
155. Thiel, P. A.; Madey, T. E.; Sloan, A. P. The interaction of water with solid surfaces:fundamental aspects. *Surf. Sci. Rep.* **1987**, 7, 211–385.
156. Ewing, G. E. Ambient thin film water on insulator surfaces. *Chem. Rev.* **2006**, 106, 1511–26.
157. Rahaman, A.; Grassian, V. H.; Margulis, C. J. Dynamics of Water Adsorption onto a Calcite Surface as a Function of Relative Humidity. *J. Phys. Chem. C* **2008**, 112, 2109–2115.
158. El-Sabaawi, M.; Pei, D. C. T. Moisture Isotherms of Hygroscopic Porous Solids. *Ind. Eng. Chem. Fundam.* **1977**, 16, 321–326.
159. Ahlneck, C.; Zografi, G. The molecular basis of moisture effects on the physical and chemical stability of drugs in the solid state. *Int. J. Pharm.* **1990**, 62, 87–95.
160. Lappalainen, M.; Pitkänen, I.; Harjunen, P. Quantification of low levels of amorphous content in sucrose by hyperDSC. *Int. J. Pharm.* **2006**, 307, 150–155.
161. Munson, E. J. Analytical Techniques in Solid-state Characterization. In: *Theor. Tech. Charact. DRUG Subst. EXCIPIENTS*; 2009, pp. 61–74.
162. Carvajal, M. T.; Staniforth, J. N. Interactions of water with the surfaces of crystal polymorphs. *Int. J. Pharm.* **2006**, 307, 216–24.
163. Sacchetti, M. Determining the relative physical stability of anhydrous and hydrous crystal forms of GW2016. *Int. J. Pharm.* **2004**, 273, 195–202.
164. Ticehurst, M. D.; Storey, R. A.; Watt, C. Application of slurry bridging experiments at controlled water activities to predict the solid-state conversion between anhydrous and hydrated forms using theophylline as a model drug. *Int. J. Pharm.* **2002**, 247, 1–10.
165. Carman, P. C.; Raal, F. A. Diffusion and flow of gases and vapours through micropores. III. Surface diffusion coefficients and activation energies. *Proc. R. Soc. London. Ser. A. Math. Phys. Sci.* **1951**, 209, 38–58.

166. Hollenbeck, R.; Swarbrick, J.; Boylan, J. Moisture in Pharmaceutical Products. *Encycl. Pharm. Technol.* **1994**, 31.
167. Kontny, M. J.; Zografi, G. Sorption of water by solids. *Drugs Pharm. Sci.* **1995**, 70, 387.
168. Giron, D.; Goldbronn, C.; Mutz, M.; Pfeffer, S.; Piechon, P.; Schwab, P. Solid State Characterizations of Pharmaceutical Hydrates. *J. Therm. Anal. Calorim.* **2002**, 68, 453–465.
169. Burnett, D. J.; Naderi, M.; Acharya, M.; Garcia, A. R. Characterizing Disorder in Pharmaceutical Materials by Vapor Sorption Techniques. **n.d.**, 1–18.
170. Langmuir, I. The constitution and fundamental properties of solids and liquids. Part I. Solids. *J. Am. Chem. Soc.* **1916**, 38, 2221–2295.
171. Brunauer, S. Adsorption of Gases and Vapors. In: *Phys. Adsorpt.*; Princeton Univ. Press: 1943, p. 511.
172. Brunauer, S.; Deming, L. S.; Deming, W. E.; Teller, E. On a Theory of the van der Waals Adsorption of Gases. *J. Am. Chem. Soc.* **1940**, 62, 1723–1732.
173. Brunauer, S.; Emmett, P. H.; Teller, E. Adsorption of Gases in Multimolecular Layers. *J. Am. Chem. Soc.* **1938**, 60, 309–319.
174. Yoshizawa, K.; Toyota, S.; Toda, F. A novel transformation of a 1: 1: 1 racemic complex of 2, 2 -dihydroxy-1, 1 -binaphthyl, Me 4 N+ Cl–and MeOH into a conglomerate in the solid state by heating or contact with MeOH vapour. *Chem. Commun.* **2004**, 2004, 1844–1845.
175. Trask, A. V; Shan, N.; Motherwell, W. D. S.; Jones, W.; Feng, S.; Tan, R. B. H.; Carpenter, K. J. Selective polymorph transformation via solvent-drop grinding. *Chem. Commun.* **2005**, 2005, 880–882.
176. Davey, R. J.; Blagden, N.; Righini, S.; Alison, H.; Ferrari, E. S. Nucleation Control in Solution Mediated Polymorphic Phase Transformations: The Case of 2,6-Dihydroxybenzoic Acid. *J. Phys. Chem. B* **2002**, 106, 1954–1959.
177. Weissbuch, I.; Lahay, M. Lock-And-Key Processes at Crystalline Interfaces: Relevance to the Spontaneous Generation of Chirality. In: *Perspect. Supramol. Chem.*; Behr, J.-P., Ed.; John Wiley & Sons, Ltd.: Chichester, UK, 1994, pp. 173–246.
178. Maher, A.; Croker, D. M.; Rasmuson, Å. C.; Hodnett, B. K.; O'Mahony, M. a. Examining Solution and Solid State Composition for the Solution-Mediated Polymorphic Transformation of Carbamazepine and Piracetam. *Cryst. Growth Des.* **2012**, 12, 1925–1932.
179. Schöll, J.; Bonalumi, D.; Vicum, L.; Mazzotti, M.; Müller, M. In Situ Monitoring and Modeling of the Solvent-Mediated Polymorphic Transformation of l -Glutamic Acid. *Cryst. Growth Des.* **2006**, 6, 881–891.
180. Kelly, R. C.; Rodríguez-Hornedo, N. Solvent Effects on the Crystallization and Preferential Nucleation of Carbamazepine Anhydrous Polymorphs: A Molecular Recognition Perspective. *Org. Process Res. Dev.* **2009**, 13, 1291–1300.
181. Maruyama, S.; Ooshimab, H.; Katob, J. Crystal structures and solvent-mediated transformation of Taltireline polymorphs. *Chem. Eng. J.* **1999**, 75, 193–200.
182. Yang, X.; Lu, J.; Wang, X.; Ching, C. B. In situ monitoring of the solution-mediated polymorphic transformation of glycine: characterization of the polymorphs and

observation of the transformation rate using Raman spectroscopy and microscopy. *J. Raman Spectrosc.* **2008**, 39, 1433–1439.
183. Croker, D. M.; Davey, R. J.; Rasmuson, Å. C.; Seaton, C. C. Solution mediated phase transformations between co-crystals. *CrystEngComm* **2013**, 15, 2044.
184. O'Mahony, M. a.; Seaton, C. C.; Croker, D. M.; Veesler, S.; Rasmuson, Å. C.; Hodnett, B. K. Investigation into the Mechanism of Solution-Mediated Transformation from FI to FIII Carbamazepine: The Role of Dissolution and the Interaction between Polymorph Surfaces. *Cryst. Growth Des.* **2013**, 13, 1861–1871.
185. Maher, A.; Croker, D. M.; Rasmuson, Å. C.; Hodnett, B. K. Solution Mediated Polymorphic Transformation: Form II to Form III Piracetam in Ethanol. *Cryst. Growth Des.* **2012**, 12, 6151–6157.
186. Maher, A.; Seaton, C. C.; Hudson, S.; Croker, D. M.; Rasmuson, Å. C.; Hodnett, B. K. Investigation of the Solid-State Polymorphic Transformations of Piracetam. *Cryst. Growth Des.* **2012**, 12, 6223–6233.
187. Lehto, P.; Aaltonen, J.; Tenho, M.; Rantanen, J.; Hirvonen, J.; Tanninen, V. P.; Peltonen, L. Solvent-Mediated Solid Phase Transformations of Carbamazepine : Effects of Simulated Intestinal Fluid and Fasted State Simulated Intestinal Fluid. *J. Pharm. Sci.* **2009**, 98, 985–996.
188. Horst, J. H. Ter; Cains, P. W. Co-Crystal Polymorphs from a Solvent-Mediated Transformation. *Cryst. Growth Des.* **2008**, 8, 2537–2542.
189. Qu, H.; Louhi-Kultanen, M.; Rantanen, J.; Kallas, J. Solvent-Mediated Phase Transformation Kinetics of an Anhydrate/Hydrate System. *Cryst. Growth Des.* **2006**, 6, 2053–2060.
190. Aaltonen, J.; Heinänen, P.; Peltonen, L.; Kortejärvi, H.; Tanninen, V. P.; Christiansen, L.; Hirvonen, J.; Yliruusi, J.; Rantanen, J. In situ measurement of solvent-mediated phase transformations during dissolution testing. *J. Pharm. Sci.* **2006**, 95, 2730–7.
191. Ferrari, E. S.; Davey, R. J. Solution-Mediated Transformation of α to β l -Glutamic Acid: Rate Enhancement Due to Secondary Nucleation. *Cryst. Growth Des.* **2004**, 4, 1061–1068.
192. Maruyama, S.; Ooshima, H. Mechanism of the solvent-mediated transformation of taltirelin polymorphs promoted by methanol. *Chem. Eng. J.* **2001**, 81, 1–7.
193. Cashell, C.; Corcoran, D.; Hodnett, B. K. Effect of Amino Acid Additives on the Crystallization of L -Glutamic Acid. *Cryst. Growth Des.* **2005**, 5, 593–597.
194. Byrn, S.; Pfeiffer, R.; Ganey, M.; Hoiberg, C.; Poochikian, G. Pharmaceutical Solids: A Strategic Approach to Regulatory Considerations. *Pharm. Res.* **1995**, 12, 945–954.
195. Brittain, H. G.; Bogdanowich, S. J.; Bugay, D. E.; DeVincentis, J.; Lewen, G.; Newman, A. W. Physical Characterization of Pharmaceutical Solids. *Pharm. Res.* **1991**, 8, 963–973.
196. Urakami, K. Characterization of pharmaceutical polymorphs by isothermal calorimetry. *Curr. Pharm. Biotechnol.* **2005**, 6, 193–203.
197. Birkholz, M. *Thin Film Analysis by X-Ray Scattering*; Wiley: 2006, 378.
198. Dinnebier, R. E. *Powder diffraction: theory and practice*; Royal Society of Chemistry: 2008.

199. Jenkins, R.; Snyder, R. L. *Introduction to X-ray Powder Diffractometry*; John Wiley & Sons, Inc.: Hoboken, NJ, USA, 1996, 432.
200. Coelho, A. A. Whole-profile structure solution from powder diffraction data using simulated annealing. *J. Appl. Crystallogr.* **2000**, 33, 899–908.
201. David, W. I. F.; Shankland, K.; McCusker, L. B.; Bärlocher, C. *Structure determination from powder diffraction data*; Oxford University Press: 2006.
202. David, W. I. F.; Shankland, K.; Shankland, N. Routine determination of molecular crystal structures from powder diffraction data. *Chem. Commun.* **1998**, 931–932.
203. David, W. I. F.; Shankland, K.; van de Streek, J.; Pidcock, E.; Motherwell, W. D. S.; Cole, J. C. DASH : a program for crystal structure determination from powder diffraction data. *J. Appl. Crystallogr.* **2006**, 39, 910–915.
204. Engel, G. E.; Wilke, S.; König, O.; Harris, K. D. M.; Leusen, F. J. J. PowderSolve – a complete package for crystal structure solution from powder diffraction patterns. *J. Appl. Crystallogr.* **1999**, 32, 1169–1179.
205. Favre-Nicolin, V.; Černý, R. FOX , "free objects for crystallography": a modular approach to ab initio structure determination from powder diffraction. *J. Appl. Crystallogr.* **2002**, 35, 734–743.
206. Harris, K. D. M.; Johnston, R. L.; Kariuki, B. M. The Genetic Algorithm: Foundations and Apllications in Structure Solution from Powder Diffraction Data. *Acta Crystallogr. Sect. A Found. Crystallogr.* **1998**, 54, 632–645.
207. Harris, K. D. M.; Tremayne, M.; Lightfoot, P.; Bruce, P. G. Crystal Structure Determination from Powder Diffraction Data by Monte Carlo Methods. *J. Am. Chem. Soc.* **1994**, 116, 3543–3547.
208. Putz, H.; Schön, J. C.; Jansen, M. Combined method for ab initio structure solution from powder diffraction data. *J. Appl. Crystallogr.* **1999**, 32, 864–870.
209. Shankland, K.; Spillman, M. J.; Kabova, E. a; Edgeley, D. S.; Shankland, N. The principles underlying the use of powder diffraction data in solving pharmaceutical crystal structures. *Acta Crystallogr. Sect. C Cryst. Struct. Commun.* **2013**, 69, 1251–1259.
210. Suryanarayanan, R. Determination of the Relative Amounts of α-carbamazepine and β-carbamazepine in a Mixture by Powder X-Ray Diffractometry. *Powder Diffr.* **2013**, 5, 155–159.
211. Suryanarayanan, R. Determination of the Relative Amounts of Anhydrous Carbamazepine (C15H12N2O) and Carbamazepine Dihydrate (C15H12N2O·2H2O) in a Mixture by Powder X-ray Diffractometry. *Pharm. Res.* **1989**, 6, 1017–1024.
212. Suryanarayanan, R.; Herman, C. S. Quantitative analysis of the active ingredient in a multi-component tablet formulation by powder X-ray diffractometry. *Int. J. Pharm.* **1991**, 77, 287–295.
213. Bugay, D. E.; Newman, a W.; Findlay, W. P. Quantitation of cefepime.2HCl dihydrate in cefepime.2HCl monohydrate by diffuse reflectance IR and powder X-ray diffraction techniques. *J. Pharm. Biomed. Anal.* **1996**, 15, 49–61.
214. Takehira, R.; Momose, Y.; Yamamura, S. Quantitative analysis of crystalline pharmaceuticals in tablets by pattern-fitting procedure using X-ray diffraction pattern. *Int. J. Pharm.* **2010**, 398, 33–38.

215. Campbell Roberts, S. N.; Williams, A. C.; Grimsey, I. M.; Booth, S. W. Quantitative analysis of mannitol polymorphs. X-ray powder diffractometry--exploring preferred orientation effects. *J. Pharm. Biomed. Anal.* **2002**, 28, 1149–1159.
216. Giron, D.; Monnier, S.; Mutz, M.; Piechon, P.; Buser, T.; Stowasser, F.; Schulze, K.; Bellus, M. Comparison of quantitative methods for analysis of polyphasic pharmaceuticals. *J. Therm. Anal. Calorim.* **2007**, 89, 729–743.
217. Suryanarayanan, R.; Herman, C. Quantitative analysis of the active teblet ingedient by x-ray powder diffractometry.pdf. *Pharm. Res.* **1991**, 8, 393–399.
218. Tiwari, M.; Chawla, G.; Bansal, A. K. Quantification of olanzapine polymorphs using powder X-ray diffraction technique. *J. Pharm. Biomed. Anal.* **2007**, 43, 865–72.
219. Yamamura, S.; Momose, Y. Quantitative analysis of crystalline pharmaceuticals in powders and tablets by a pattern-fitting procedure using X-ray powder diffraction data. *Int. J. Pharm.* **2001**, 212, 203–212.
220. Wendlandt, W. W. *Thermal methods of analysis*; Interscience Publishers: 1964, 424.
221. Austin, T. K. Hydration, polymorphism and disorder in organic solids, including materials of pharmaceutical relevance, Cardiff University, 2006.
222. Giron, D. Monitoring of Polymorphism – From Detection to Quantification. *Eng. Life Sci.* **2003**, 3, 103–112.
223. Bourne, S. A.; Coetzee, A.; Ndlovu, M. E. Benztropine mesylate : crystal structure and kinetics of dehydration. *J. Chem. Crystallogr.* **1998**, 28, 885–892.
224. Hiller, S. A.; Zhuk, R. A.; Lidak, M. J.; Zidermane, A. A. Substituted Uracils. **1968**.
225. Karev, N. I.; Blokhina, N. G.; Vozny, E. K.; Pershin, M. P. Experience with ftorafur treatment in breast cancer. *Neoplasma* **1972**, 19, 347.
226. Benvenuto, J. A.; Lu, K.; Ti, L. L. High-pressure liquid chromatographic analysis of ftorafur and its metabolites in biological fluids. *J. Chromatogr. A* **1977**, 134, 219–222.
227. Uchida, T.; Yonemochi, E.; Oguchi, T.; Terada, K.; Yamamoto, K.; Nakai, Y. Polymorphism of tegafur: physico-chemical properties of four polymorphs. *Chem. Pharm. Bull.* **1993**, 41, 1632–1635.
228. Actiņš, A.; Beļakovs, S.; Orola, L.; Veidis, M. V. Molecular and crystal structure of novel form of tegafur. *Latv. J. Chem.* **2006**, 2, 120–124.
229. Needham, F.; Faber, J.; Fawcett, T. G.; Olson, D. H. X-ray powder diffraction analysis of tegafur. *Powder Diffr.* **2006**, 21, 245–247.
230. Bobrovs, R. Ftorafūra polimorfo formu kristalizācija un fāžu pārejas, Latviajs Universitāte, 2009.
231. Asatrjana, K. Ftorafūra polimorfo formu termodinamiskā stabilitāte, Latvijas Univeritāte, 2004.
232. Nakai, Y.; Yamamoto, K.; Terada, K.; Uchida, T.; Yamaguchi, K.; Shimizu, N. The crystal structure of tegafur (β-form): comparison with α-form. *Chem. Pharm. Bull.* **1986**, 34, 1242–1248.
233. Barnes, P. J. Theophylline. *Pharmaceuticals* **2010**, 3, 725–747.
234. Ebisuzaki, Y.; Boyle, P. D.; Smith, J. A. Methylxanthines. I. Anhydrous Theophylline. *Acta Crystallogr. Sect. C Cryst. Struct. Commun.* **1997**, 53, 777–779.
235. Khamar, D.; Bradshaw, I. J.; Hutcheon, G. A.; Seton, L. Solid State Transformations Mediated by a Kinetically Stable Form. *Cryst. Growth Des.* **2012**, 12, 109–118.

236. Matsuo, K.; Matsuoka, M. Solid-State Polymorphic Transition of Theophylline Anhydrate and Humidity Effect. *Cryst. Growth Des.* **2007**, 7, 411–415.
237. Seton, L.; Khamar, D.; Bradshaw, I. J.; Hutcheon, G. A. Solid State Forms of Theophylline: Presenting a New Anhydrous Polymorph. *Cryst. Growth Des.* **2010**, 10, 3879–3886.
238. Smith, E. D. L.; Hammond, R. B.; Jones, M. J.; Roberts, K. J.; Mitchell, J. B. O.; Price, S. L.; Harris, R. K.; Apperley, D. C.; Cherryman, J. C.; Docherty, R. The Determination of the Crystal Structure of Anhydrous Theophylline by X-ray Powder Diffraction with a Systematic Search Algorithm, Lattice Energy Calculations, and 13 C and 15 N Solid-State NMR: A Question of Polymorphism in a Given Unit Cell. *J. Phys. Chem. B* **2001**, 105, 5818–5826.
239. Sutor, D. J. The structures of the pyrimidines and purines. VI. The crystal structure of theophylline. *Acta Crystallogr.* **1958**, 11, 83–87.
240. Szterner, P.; Legendre, B.; Sghaier, M. Thermodynamic properties of polymorphic forms of theophylline. Part I: DSC, TG, X-ray study. *J. Therm. Anal. Calorim.* **2009**, 99, 325–335.
241. Phadnis, N. V; Suryanarayanan, R. Polymorphism in anhydrous theophylline--implications on the dissolution rate of theophylline tablets. *J. Pharm. Sci.* **1997**, 86, 1256–63.
242. Suihko, E.; Ketolainen, J.; Poso, A.; Ahlgren, M.; Gynther, J.; Paronen, P. Dehydration of theophylline monohydrate—a two step process. *Int. J. Pharm.* **1997**, 158, 47–55.
243. Nunes, C.; Mahendrasingam, A.; Suryanarayanan, R. Investigation of the multi-step dehydration reaction of theophylline monohydrate using 2-dimensional powder X-ray diffractometry. *Pharm. Res.* **2006**, 23, 2393–2404.
244. Sun, C.; Zhou, D.; Grant, D. J. W.; Young, V. G. Theophylline monohydrate. *Acta Crystallogr. Sect. E Struct. Reports Online* **2002**, 58, o368–o370.
245. Cardin, C.; Gan, Y.; Lewis, T. Low-temperature determination of theophylline dimethyl sulfoxide solvate. *Acta Crystallogr. Sect. E Struct. Reports Online* **2007**, 63, o3175–o3175.
246. Childs, S. L.; Stahly, G. P.; Park, A. The salt-cocrystal continuum: the influence of crystal structure on ionization state. *Mol. Pharm.* **2007**, 4, 323–38.
247. Zhu, H. Influence of water activity in organic solvent + water mixtures on the nature of the crystallizing drug phase. 1. Theophylline. *Int. J. Pharm.* **1996**, 135, 151–160.
248. Trask, A. V; Motherwell, W. D. S.; Jones, W. Physical stability enhancement of theophylline via cocrystallization. *Int. J. Pharm.* **2006**, 320, 114–123.
249. Etter, M. C. Encoding and decoding hydrogen-bond patterns of organic compounds. *Acc. Chem. Res.* **1990**, 23, 120–126.
250. Macrae, C. F.; Bruno, I. J.; Chisholm, J. A.; Edgington, P. R.; McCabe, P.; Pidcock, E.; Rodriguez-Monge, L.; Taylor, R.; Streek, J. van de; Wood, P. A. Mercury CSD 2.0 - new features for the visualization and investigation of crystal structures. *J. Appl. Cryst.* **2008**, 41, 466–470.
251. Bergmann, J.; Friedel, P.; Kleeberg, R. BGMN—A new fundamental parameters based Rietveld program for laboratory X-ray sources, its use in quantitative analysis and structure investigations. *CPD Newsl.* **1998**, 20, 5–8.

252. Nonius BV; Nonius KappaCCD Collect. **1998**,.
253. Kay, L.; Keifer, P.; Saarinen, T. Pure absorption gradient enhanced heteronuclear single quantum correlation spectroscopy with improved sensitivity. *J. Am. Chem. Soc.* **1992**, 114, 10663–10665.
254. Palmer, A. G.; Cavanagh, J.; Wright, P. E.; Rance, M. Sensitivity improvement in proton-detected two-dimensional heteronuclear correlation NMR spectroscopy. *J. Magn. Reson.* **1991**, 93, 151–170.
255. Yu, L.; Reutzel, S. M.; Stephenson, G. A. Physical characterization of polymorphic drugs: an integrated characterization strategy. *Pharm. Sci. Technolo. Today* **1998**, 1, 118–127.
256. Stephenson, G. A.; Forbes, R. A.; Reutzel-Edens, S. M. Characterization of the solid state: quantitative issues. *Adv. Drug Deliv. Rev.* **2001**, 48, 67–90.
257. Microsoft Corporation. Microsoft Office Excel 2010. **2010**,.
258. Actiņš, A.; Petkune, S. Tegafūra beta un alfa modifikāciju maisījuma rentgendifraktometriskā analīze un sastāva maiņa ilgstošas glabāšanas apstākļos. *Latv. Ķīmijas Žurnāls* **2009**, 1, 43–52.
259. Allesø, M.; van den Berg, F.; Cornett, C.; Jørgensen, F. S.; Halling-Sørensen, B.; de Diego, H. L.; Hovgaard, L.; Aaltonen, J.; Rantanen, J. Solvent diversity in polymorph screening. *J. Pharm. Sci.* **2008**, 97, 2145–59.
260. Kodaka, M. Correlation between Molecular Size and Packing Density of Solvents. *J. Phys. Chem. B* **2004**, 108, 1160–1164.
261. Croker, D.; Hodnett, B. K. Mechanistic Features of Polymorphic Transformations: The Role of Surfaces. *Cryst. Growth Des.* **2010**, 10, 2806–2816.
262. Hillier, A.; Ward, M. Epitaxial interactions between molecular overlayers and ordered substrates. *Phys. Rev. B* **1996**, 54, 14037–14051.
263. Tung, H.-H.; Paul, E. L.; Midler, M.; McCauley, J. A. *Crystallization of Organic Compounds: An Industrial Perspective*; John Wiley & Sons, Inc.: Hoboken, NJ, USA, 2009, 304.
264. Bērziņš, A.; Actiņš, A. Effect of experimental and sample factors on dehydration kinetics of mildronate dihydrate: mechanism of dehydration and determination of kinetic parameters. *J. Pharm. Sci.* **2014**, 103, 1747–55.
265. Berman, M.; Shahn, E.; Weiss, M. F. The Routine Fitting of Kinetic Data to Models. *Biophys. J.* **1962**, 2, 275–287.
266. Allnatt, A. R.; Jacobs, P. W. M. Theory of nucleation in solid state reactions. *Can. J. Chem.* **1968**, 46, 111–116.
267. Harrison, L. G. The Theory of Solid Phase Kinetics. In: *Theory Kinet.*; Compton, R. G., Bamford, C. H., Tipper, C. F. H., Ed.; Elsevier Scientific Publishing Company: 1969, pp. 377–462.
268. Kulkarni, S. A.; McGarrity, E. S.; Meekes, H.; ter Horst, J. H. Isonicotinamide self-association: the link between solvent and polymorph nucleation. *Chem. Commun. (Camb).* **2012**, 48, 4983–5.
269. Davey, R.; Garside, J. *From molecules to crystallizers*; Oxford University Press: 2000, 96.
270. Kirschbaum, J. Self-association of theophylline in aqueous solution. *J. Pharm. Sci.* **1973**, 62, 168–169.

271. Guttman, D.; Higuchi, T. NMR evidence for self-association of theophylline in aqueous solution: A response. *J. Pharm. Sci.* **1971**, 60, 1269–1270.
272. Thakkar, A. L.; Tensmeyer, L. G.; Wilham, W. L. NMR evidence for self-association of theophylline in aqueous solution. *J. Pharm. Sci.* **1971**, 60, 1267–1269.
273. Guttman, D.; Higuchi, T. Reversible association of caffeine and of some caffeine homologs in aqueous solution. *J. Am. Pharm. Assoc.* **1957**, 46, 4–10.
274. Dharmayat, S.; Calderon De Anda, J.; Hammond, R. B.; Lai, X.; Roberts, K. J.; Wang, X. Z. Polymorphic transformation of l-glutamic acid monitored using combined on-line video microscopy and X-ray diffraction. *J. Cryst. Growth* **2006**, 294, 35–40.
275. Tian, F.; Rades, T.; Sandler, N. Visualizing solvent mediated phase transformation behavior of carbamazepine polymorphs by principal component analysis. *AAPS PharmSciTech* **2008**, 9, 390–394.
276. Dharmayat, S.; Hammond, R. B.; Lai, X.; Ma, C.; Purba, E.; Roberts, K. J.; Chen, Z.; Martin, E.; Morris, J.; Bytheway, R. An Examination of the Kinetics of the Solution-Mediated Polymorphic Phase Transformation between α- and β-Forms of l -Glutamic Acid as Determined Using Online Powder X-ray Diffraction †. *Cryst. Growth Des.* **2008**, 8, 2205–2216.
277. Docherty, R.; Clydesdale, G.; Roberts, K. J.; Bennema, P. Application of Bravais-Friedel-Donnay-Harker, attachment energy and Ising models to predicting and understanding the morphology of molecular crystals. *J. Phys. D. Appl. Phys.* **1991**, 24, 89–99.
278. Bobrovs, R.; Seton, L.; Actiņš, A. Solvent-mediated phase transformation between two tegafur polymorphs in several solvents. *CrystEngComm* **2014**, 16, 10581–10591.
279. Snyder, L. R. Classification of the solvent properties of common liquids. *J. Chromatogr. A* **1974**, 92, 223–230.
280. Brittain, H. G. Spectral methods for the characterization of polymorphs and solvates. *J. Pharm. Sci.* **1997**, 86, 405–12.
281. Bugay, D. E. Characterization of the solid-state: spectroscopic techniques. *Adv. Drug Deliv. Rev.* **2001**, 48, 43–65.
282. Coleman, P. B. *Practical sampling techniques for infrared analysis*; CRC Press: London, 1993, 320.
283. Vyazovkin, S. Kinetic concepts of thermally stimulated reactions in solids: A view from a historical perspective. *Int. Rev. Phys. Chem.* **2000**, 19, 45–60.
284. Khawam, A.; Flanagan, D. R. Complementary use of model-free and modelistic methods in the analysis of solid-state kinetics. *J. Phys. Chem. B* **2005**, 109, 10073–80.
285. Khawam, A.; Flanagan, D. R. Role of isoconversional methods in varying activation energies of solid-state kinetics I. isothermal kinetic studies. *Thermochim. Acta* **2005**, 429, 93–102.
286. Khawam, A.; Flanagan, D. R. Role of isoconversional methods in varying activation energies of solid-state kinetics II. Nonisothermal kinetic studies. *Thermochim. Acta* **2005**, 436, 101–112.
287. Gramatica, P.; Navas, N.; Todeschini, R. Classification of organic solvents and modelling of their physico-chemical properties by chemometric methods using different sets of molecular descriptors. *TrAC Trends Anal. Chem.* **1999**, 18, 461–471.

288. Gu, C.-H.; Li, H.; Gandhi, R. B.; Raghavan, K. Grouping solvents by statistical analysis of solvent property parameters: implication to polymorph screening. *Int. J. Pharm.* **2004**, 283, 117–25.

Appendix 1. Solid state kinetic models

Table A.1. Solid-state integral expressions g(α) for the most often used solid-state kinetic models [103,104,283–286].

Model	Differential form $f(\alpha) = (\frac{1}{k})(\frac{d\alpha}{dt})$	Integral form $g(\alpha) = kt$
Nucleation models		
Power law (P2)	$2\alpha^{1/2}$	$\alpha^{1/2}$
Power law (P3)	$3\alpha^{2/3}$	$\alpha^{1/3}$
Power law (P4)	$4\alpha^{3/4}$	$\alpha^{1/4}$
Avrami-Erofeyev (A3/2)		
Avrami-Erofeyev (A2)	$2(1-\alpha)(-\ln(1-\alpha))^{1/2}$	$(-\ln(1-\alpha))^{1/2}$
Avrami-Erofeyev (A3)	$3(1-\alpha)(-\ln(1-\alpha))^{2/3}$	$(-\ln(1-\alpha))^{1/3}$
Avrami-Erofeyev (A4)	$4(1-\alpha)(-\ln(1-\alpha))^{3/4}$	$(-\ln(1-\alpha))^{1/4}$
Prout-Tompkins (B1)	$\alpha(1-\alpha)$	$\ln(\alpha/(1-\alpha)) + c^a$
Geometrical contraction models		
Contracting area (R2)	$2(1-\alpha)^{1/2}$	$(1-(1-\alpha)^{1/2})$
Contracting volume (R3)	$3(1-\alpha)^{2/3}$	$(1-(1-\alpha)^{1/3})$
Diffusion models		
1-D diffusion (D1)	$1/2\alpha$	α^2
2-D diffusion (D2)	$(-\ln(1-\alpha))^{-1}$	$\big((1-\alpha)\ln(1-\alpha)\big) + \alpha$
3-D diffusion – Jander (D3)	$3(1-\alpha)^{2/3}/2(1-(1-\alpha)^{1/3})$	$\big(1-(1-\alpha)^{1/3}\big)^2$
Ginstling-Brounshtein (D4)	$(3/2((1-\alpha)^{-1/3}-1)$	$1-(2\alpha/3)-(1-\alpha)^{2/3}$
Reaction-order models		
First-order (F1)	$(1-\alpha)$	$-\ln(1-\alpha)$
Second-order (F2)	$(1-\alpha)^2$	$(1-\alpha)^{-1}-1$
Third-order (F3)	$(1-\alpha)^3$	$0.5((1-\alpha)^{-2}-1)$

Appendix 2. Characterization of solvents used

Table A.2. Characterization of solvents used.

Solvent	Purity	Manufacturer
Acetone	>99.5%	Penta, Fisher Scientific
Acetonitrile	>99.9%	Fluka, Fisher Scientific
Benzyl alcohol	>99%	Alfa Aesa
1-Butanol	>99.5%	Penta
Butyl acetate	>99%	Alfa Aesa
Chloroform	>99%	Alfa Aesa, Fisher Scientific
Cyclohexanol	>99%	Alfa Aesa
1,1-Dichloroethane	>98%	Реахим
Dichloromethane	99.7%	Alfa Aesa
Dimethylsulfoxide	>99%, USP	Penta
1,4-Dioxane	>99.9%	Sigma-Aldrich
Ethanol	99.97%	LABSCAN
Ethyl acetate	>99.5%	Penta
Glycerine	>98%, Ph. Eur.	Penta
Isobuthanol	>99%	Alfa Aesa
Isopropyl acetate	>99%	Alfa Aesa
Methanol	>99.8%	Fluka, Fisher Scientific
N,N-Dimethylformamide	>98%	Penta
1-Heptane	>98%	Реахим
1-Hexane	>98%	Реахим
Nitromethane	>98%	Merck
1-Propanol	>99.5%	Penta
2-Propanol	>99.5%	Alfa Aesa
Tetrahydrofuran	>99.5%	Hempur
Toluene	>98%	Реахим
Water	Deionised in the laboratory using Crystal 5, conductivity <0.2 μS	
Acetone-D6	99.9%	Cambridge Isotope Laboratories
Acetonitrile-D3	99.8%	Apollo Scientific
Chloroform-D	99.8%	Euriso-top
Deuterium oxide	99.96%	BDH Chemicals
Dimethyl sulfoxide-D6	99.9%	Cambridge Isotope Laboratories
Formic acid-D2	98%, <5% D_2O	Cambridge Isotope Laboratories
Methanol-D4	99.8%	Cambridge Isotope Laboratories

Appendix 3. Solvent classes

Classifications: A – K-nearest neighbour (KNN) classification;
B – Counter-propagation artificial neural networks (CP-ANN-1) classification;
C – Counter-propagation artificial neural networks (CP-ANN-2) classification (see original publication [287]).

Class: 1 – aprotic polar (AP);
2 – aromatic apolar or lightly polar (AALP);
3 – electron pair donors (EPD);
4 – hydrogen bond donors (HBD);
5 – aliphatic aprotic apolar (AAA).

Table A.3. Solvent classification using the k-nearest neighbour classification method [287].

ID	Solvent	A	B	C	ID	Solvent	A	B	C	ID	Solvent	A	B	C
1	acetic acid	4	4	4	52	diethylene glycol	4	4	4	103	nitrobenzene	1	1	1
2	acetic anhydride	1	1	1	53	dietyl ether	3	3/5	3	104	nitroethane	1	1	1
3	acetone	1	1	1	54	di-isopropyl ether	5	5	3	105	nitromethane	1	1	1
4	acetonitrile	1	1	1	55	1,2-dimethoxyethane	3	1/3	3	106	n-octane	5	5	5
5	acetophenone	2	2	2	56	N,N-dimethylacetamide	1	1	1	107	1-octanol	4	4	4
6	acetylacetone	2	1	1	57	N,N-dimethylaniline	1	1	1	108	n-pentane	5	5	5
7	2-aminoethanol	4	4	4	58	3,3-dimethyl-2-butanone	1	1	1	109	1-pentanol	4	4	4
8	aniline	1	1	1	59	N,N-dimethylformamide	1	1	1	110	2-pentanol	4	4	4
9	anisole	2	2	2	60	2,4-dimethylpyridine	1	1	1	111	3-pentanol	4	4	4
10	benzaldehyde	2	2	2	61	2,6-dimethylpyridine	1	1	1	112	2-pentanone	1	1	1
11	benzene	2	2	2	62	dimethylsulfoxide	1	1	1	113	3-pentanone	1	1	1
12	benzonitrile	1	1	1	63	2,6-dimethyl-4-heptanone	1	1	1	114	pentyl acetate	1	1	1
13	benzyl alcohol	2	2	2	64	2,4-dimethyl-3-pentanone	1	1	1	115	phenetole	2	2	2

Table continues in next page

Table A.3. continuation

ID	Solvent	A	B	C	ID	Solvent	A	B	C	ID	Solvent	A	B	C
14	bromobenzene	2	2	2	65	1,4-dioxane	1	1	3	116	Phenol	2	2	2
15	1-bromobutane	3	3	3	66	diphenyl ether	2	2	2	117	3-picoline	1	1	1
16	bromoethane	3	1/3	3	67	di-n-propyl ether	5	5	3	118	4-picoline	1	1	1
17	1-butanol	4	4	4	68	DMEU	1	1	1	119	piperidine	4	4	4
18	2-butanol	4	4	4	69	DMPU	1	1	1	120	1-propanol	4	4	4
19	2-butanone	1	1	1	70	ethanol	4	4	4	121	2-propanol	4	4	4
20	n-butyl acetate	1	1	1	71	ethyl acetate	1	1	1	122	n-propylamine	4	4	4
21	n-butylamine	4	4	4	72	ethyl benzoate	2	2	2	123	propyl formate	1	1	1
22	butyronitrile	1	1	1	73	ethyl formate	1	1	1	124	propylene carbonate	1	1	1
23	carbon disulfide	2	2/5	5	74	ethyl propionate	1	1	1	125	propionitrile	1	1	1
24	carbon tetrachloride	5	4	4	75	ethylenediamine	4	4	4	126	Pyridine	1	1	1
25	chlorobenzene	2	2	2	76	ethylene glycol	4	4	4	127	pyrrolidine	4	4	4
26	1-chlorobutane	3	3	3	77	fluorobenzene	2	2	2	128	quinoline	1	1	1
27	chloroform	4	4/1/3	3	78	formamide	4	4	4	129	Styrene	2	2	2
28	1-chloropropane	3	3/1	3	79	furfuryl alcohol	1	2/4	2	130	Sulfolane	1	1	1
29	2-chloropropane	3	3/1	3	80	glycerol	4	4	4	131	tert.-butyl alcohol	4	4	4
30	m-cresol	2	2	2	81	n-heptane	5	5	5	132	tert.-butyl methyl ether	3	5/3	3
31	cyclohexane	5	5	5	82	HMPTA	1	1	1	133	TEGDME	1	1/3	3
32	cyclohexanol	4	4	4	83	n-hexane	5	5	5	134	1,1,2,2-tetrachloroethane	1	3	1
33	cyclohexanone	1	1	1	84	1-hexanol	4	4	4	135	tetrachloroethylene	5	4/2	5
34	cyclohexene	2	5/2	5	85	iodobenzene	2	2	2	136	tetraethylene glycol	4	4	4
35	cyclopentane	5	5	5	86	iodoethane	3	1/3	3	137	tetrahydrofuran	3	3	3
36	cyclopentanone	1	1	1	87	isobutyl alcohol	4	4	4	138	1,1,3,3-tetramethyl urea	1	1	1
37	cis-decaline	5	5	5	88	iso-octane	5	5	5	139	Toluene	2	2	2
38	n-decane	5	5	5	89	mesitylene	2	2	2	140	tributylamine	3	3	3
39	DEGDEE	3	3/1	3	90	methanol	4	4	4	141	1,1,1-trichloroethane	1	1	1
40	DEGDME	1	1/3	3	91	methyl acetate	1	1	1	142	trichloroethylene	1	1	1

Table continues in next page

Table A.3. continuation

ID	Solvent	A	B	C	ID	Solvent	A	B	C	ID	Solvent	A	B	C
41	dibenzyl ether	2	2	2	92	methyl benzoate	2	2	2	143	triethylamine	3	3	3
42	di-n-butyl ether	5	5/3	3	93	2-methyl-2-butanol	4	4	4	144	triethylene glycol	4	4	4
43	m-dichlorobenzene	2	2	2	94	3-methyl-1-butanol	4	4	4	145	trifluoroacetic acid	4	4	4
44	o-dichlorobenzene	2	2	2	95	3-methyl-2-butanone	1	1	1	146	2,2,2-trifluoroethanol	4	4	4
45	1,2-dichloroethane	1	1	1	96	methyl formate	1	1	1	147	trimethylene glycol	4	4	4
46	1,1-dichloroethane	1	1	1	97	4-methyl-2-pentanone	1	1	1	148	2,4,6-trimethylpyridine	1	1	1
47	1,1-dichloroethylene	1	1	1	98	2-methoxyethanol	4	4	4	149	m-xylene	2	2	2
48	Z-1,2-dichloroethylene	1	1	1	99	N-methylacetamide	1	1	1	150	o-xylene	2	2	2
49	dichloromethane	1	1	1	100	N-methylformamide	1	1	1	151	p-xylene	2	2	2
50	diethylamine	4	4	4	101	N-methyl-pyrrolidin-2-one	1	1	1	152	Water	4	4	4
51	diethyl carbonate	1	1	1	102	morpholine	1	4/1	4					

Table A.4. Solvent groups based on cluster analysis of following solvent property parameters, hydrogen bond acceptor propensity, hydrogen bond donor propensity, polarity/dipolarity, dipole moment, and dielectric constant [288]**.**

Group	Solvents
Group 1	n-Dodecane (0.0), n-decane (0.1), Cyclohexane (0.1), n-octane (0.1), n-hexane (0.2), n-heptane (0.2), cis-decalin (0.2), n-pentane (0.2), carbon tetrachloride (0.3), tetrachloroethene (0.3)
Group 2	Ethyl acetate (0.2), diethyl sulfide (0.4), propyl ethanoate (0.6), methyl benzoate (0.8), methyl ethanoate (0.8), butyl ethanoate (1.1), tetrahydrofuran (1.4), methyl tertiary-butyl ether (1.6), diethyl ether (1.9), ethyl formate (2.3), diisopropyl ether (2.8), methyl methanoate (2.8), dibutylether (3.1), dimethyl disulfide (3.5)
Group 3	2-methyl-1-propanol (0.3), 2-butanol (0.5), 1-butanol (0.9), 2-methoxyethanol (1.1), 1-pentanol (1.3), 2-propanol (2.8), 2-methyl-2-propanol (4.0), 1-propanol (4.1), 1-octanol (6.6), ethanol (8.4), morpholine (9.0), butylamine (11.9), methanol (16.2)
Group 4	m-Xylene (0.1), p-xylene (0.1), benzene (0.1), mesitylene (0.2), carbon disulfide (0.3), toluene (0.3)
Group 5	2-hexanone (0.0), cyclopentanone (0.8), 2-pentanone (1.1), pyridine (1.2), 4-methyl-2-pentanone (1.2), cyclohexanone (1.5), 4-methylpyridine (2.2), 2-heptanone (2.5), 3-pentanone (2.7), acetophenone (3.4), butanone (4.1), 2,4-dimethylpyridine (4.7), acetone (6.4), 2,6-dimethylpyridine (7.0)
Group 6	N,N-dimethylacetamide (0.8), N,N-dimethylformamide (1.3), N-methyl-2-pyrrolidone (6.3), dimethylsulfoxide (8.3)
Group 7	1-iodobutane (0.4), chlorobenzene (0.6), fluorobenzene (0.8), 1,1,1-trichloroethane (0.9), dibromomethane (1.0), diiodomethane (1.0), 1,2-dibromoethane (1.4), chloroform (1.6), iodobenzene (1.7), anisole (2.0), bromoform (2.1), ethyl phenyl ether (2.1), dichloromethane (2.7), trichloroethene (2.9), 1,1-dichloroethane (3.8), o-dichlorobenzene (3.9), 1,2-dichloroethane (3.9)
Group 8	Acetic acid (0.1), propanoic acid (2.8), pentanoic acid (3.5), m-cresol (6.2)
Group 9	Propanenitrile (1.0), benzonitrile (4.7), acetonitrile (5.4), butanenitrile (6.0), nitromethane (6.3)
Group 10	Benzyl alcohol (2.8), aniline (2.8)
Group 11	Triethylamine (0.4), 1,4-dioxane (0.4)
Group 12	Formic acid (4.9), ethylene glycol (4.9)
Group 13	Diethylamine
Group 14	Glycerol
Group 15	Water

The Euclidean distance of each solvent to the centre of the corresponding group is provided in the parentheses.

Appendix 4. EpiCalc calculations for potential lattice match

Table A.5. EpiCalc calculation for potential lattice matching between {100}, {110} and {010} face of β tegafur and {001}, {011} and {010} face of α tegafur. V/V_0 is the dimensionless potential energy parameter used to measure the goodness-of-fit.

α face (hkl)	β face (hkl)	V/V_0
010	100	0.9941
010	110	0.9675
010	010	0.9836
001	100	0.9908
001	110	0.9925
001	010	0.9902
011	100	0.9985
011	110	0.9923
011	010	0.9908

The value of V/V_0 indicates the goodness-of-fit between the substrate lattice and the overlayer lattice, where $V/V_0=1$ indicates that there is no match between lattice points, $V/V_0=0.5$ – a partial match (for non-hexagonal substrate), and $V/V_0=0$ – complete matching of the lattice points or crystal faces.

The default setting for overlayer dimensions (25 x 25) and the orientation angle (60° with a step size of 0.25°) was used to test α and β tegafur lattice match.

Appendix 5. Scientific articles

JPP Journal of Pharmacy and Pharmacology
ROYAL PHARMACEUTICAL SOCIETY

JPP Journal of Pharmacy and Pharmacology

JPP 2011, 63: 1136–1140

Received November 17, 2010
Accepted May 23, 2011
DOI
10.1111/j.2042-7158.2011.01319.x
ISSN 0022-3573

Research Paper

Determination of trace amounts of β tegafur in commercial α tegafur by powder X-ray diffractometric analysis

Sanita Petkune, Raitis Bobrovs and Andris Actiņš

The Faculty of Chemistry, University of Latvia, Riga, Latvia

Abstract

Objectives The main objective of this work was to develop a suitable analytical technique for determining trace amounts of the thermodynamically stable solid form in bulk samples of metastable form, to a sensitivity of 0.005%–1.0%. Tegafur (5-fluoro-1-(tetrahydro-2-furyl)-uracil) α and β crystalline forms were used as a model for this problem.

Methods The trace content of the thermodynamically stable β polymorphic form in tegafur samples was increased by promoting phase transition from the bulk of thermodynamically metastable α form to β form, and achieving sufficient β form content for a quantitative powder X-ray diffractometry (PXRD) analysis. The phase transition was stimulated by adding water to the samples and then grinding in controlled conditions (temperature, time, grinding speed). A calibration line was constructed using the least squares method.

Key findings By using a solvent that does not form hydrates with the analysed polymorphs, it was possible to promote the phase transformation from metastable form to the thermodynamically stable form. After sample preparation, the thermodynamically stable solid form content in the analysed mixture had increased proportionally to the initial weight fraction (0.005%–1.0%) of the stable form seed crystals in the samples, and the coefficient of proportionality was 43.0 ± 0.9, with a standard deviation $S_n = 1.5\%$.

Conclusions A simple, sensitive, semi-quantitative analytical method was developed for the low-level determination of the thermodynamically stable polymorphic form in mixtures of thermodynamically stable and metastable polymorphs.

Keywords drug polymorphism; powder X-ray diffraction; semi-quantitative analysis of trace amounts; tegafur

Introduction

The impact of crystal polymorphic transformations on drug product performance is well recognized in the pharmaceutical industry. Various crystal structures of a given substance often exhibit different physical properties.[1]

To ensure product stability, the polymorph most stable in ambient conditions is normally chosen for development into the final dosage product. Recently, however, metastable forms have been utilized due to enhanced dissolution or bioavailability profiles.[2] Sometimes metastable polymorphic forms may be inadvertently generated due to the stress produced by temperature, mechanical treatment and moisture during processing or storage of the drug product.[3] Contamination by polymorphic impurities can influence both the stability and performance of the final product and during the last decade the requirements for identification, specification and control of active pharmaceutical ingredient polymorphs have become a part of the quality assurance process.[4] Therefore it is necessary to develop quantification methods for measuring low level contamination with undesired crystalline phases.[1] A multitude of analytical techniques is available to quantify crystal forms in mixtures but those methods have not been routinely applied to quantify low amounts of one polymorph in the presence of another.[5] FT-infrared spectroscopy has been used to determine polymorph content down to 1–5%.[6,7] Powder X-ray diffraction (PXRD) has been employed to determine low-level polymorph impurities with the minimum quantifiable level of 1–2.5%.[6,8,9] Solid-state NMR spectroscopy has also been applied to the detection of polymorph traces,[8] though solid-state NMR methods involve significant sample preparation or analysis time.

Correspondence: Sanita Petkune, The Faculty of Chemistry, University of Latvia, Kr. Valdemara iela 48, Riga, LV-1013, Latvia.
E-mail: sanitapetkune@yahoo.com

Due to the growing quality requirements directed at active pharmaceutical substances there is a demand for a rapid and simple quantification of unwanted solid forms at low levels (<1%).[10]

Advantages like the non-destructive nature, simplicity and ambient temperature measurements of either drug substances or final dosage forms make PXRD the most preferred and extensively used technique for quantification of polymorphic mixtures.[4] In addition, PXRD is one of the most sensitive methods for detection of low-level solid forms, therefore PXRD was chosen as the most appropriate method for phase quantification in this study.

The purpose of this study was to investigate the quantification of low-level polymorphic impurities and to establish an analytical method with a detection limit below 1% for the determination of the thermodynamically stable polymorphic form in mixtures with a metastable polymorphic form. The α and β forms of tegafur (5-fluoro-1-(tetrahydro-2-furyl)-uracil), a cancer chemotherapy drug,[11] were selected as the model system for this study. Our low-level determination technique was based on a new approach to the sample preparation process, which included a solvent-promoted stimulation of phase transition from a thermodynamically metastable form to the stable form. The conditions were selected to increase the stable form content to a level high enough to enable the quantification of mixture with PXRD. Consequently, a new, sensitive semi-quantitative PXRD analytical method was developed for detection of trace amounts (0.005–1.0% weight fraction) of thermodynamically stable polymorphic impurity in a metastable commercial product. Since the ever-growing quality requirements for active pharmaceutical ingredients tend to increase the expense of quality assurance, our contribution of a simple, rapid and low-cost analytical technique will be useful to the pharmaceutical industry as a part of quality control for active pharmaceutical ingredients.

Materials and Methods

Materials

The α and β forms of pharmaceutical-grade tegafur were obtained from JSC Grindeks (Riga, Latvia).

Optimization of sample preparation

A mixture of tegafur α and β forms containing 1.5% weight fraction of the β form was prepared and separated into six samples of 0.50 g. An analytical balance (BOECO, Hamburg, Germany) of $\pm$0.0001 g accuracy was used. Weighted samples were ground at 20°C with a Retsch MM300 shaker (Retsch GmbH, Haan, Germany) at a shaking frequency of 15 Hz for 3, 5 and 7 min with the addition of one or two drops (~0.07 ml or ~0.15 ml, respectively) of water before each grinding operation. Water was added to the samples before grinding to ensure faster phase transition.

Sample preparation

Pure α and β polymorphs of tegafur were ground in a mortar separately for 2 min, to ensure sample homogeneity. The ground β form was weighed and mixed in various ratios (1.0, 0.50. 0.25, 0.10, 0.050, 0.010 and 0.0050% w/w) with the ground α form. The total mass of each mixture was 0.75 g. The prepared samples were homogenized at 20°C by shaking in a Retsch MM300 shaker for 5 min at a shaking frequency of 15 Hz.

In each case 0.50 g of homogenized sample was weighted for wet grinding, but the rest of the mixture was used for the next sample preparation. A drop of water (~0.07 ml) was added to each sample before grinding. The prepared samples were ground for 5 min at 20°C with a Retsch MM300 shaker with shaking frequency 15 Hz.

Two parallel samples were prepared and analysed for each mixing ratio of α and β tegafur.

Powder X-ray diffractometric analysis

Samples were analysed with a powder X-ray diffractometer Bruker D8 Advance (Bruker AXS, Karlsruhe, Germany). The divergence and scattering slits were set at 1.0 mm, and the receiving slit was set at 0.6 mm. Diffraction patterns within the 2θ range of 9° to 13° were recorded at room temperature using CuK_α radiation at 1.54180 Å, with the following measurement conditions: tube voltage 40 kV, tube current 40 mA, step-scan mode with the step size $2\theta = 0.02°$, and the counting time 10 s/step.

Powder samples were packed into glass holders with ~150 mg weight capacity and pressed by a clean glass slide to ensure coplanarity of the powder surface with the surface of the holder. Obtained diffractograms were analysed with DIFFRAC^{plus} EVA (version 9.0) software.

Quantitative analysis of tegafur α and β form mixtures

A full profile analysis was used for quantitative analysis, in which all points of X-ray patterns were used for quantification of tegafur α and β forms. Experimental points were saved as **.raw* file format and then converted to **.uxd* file format, which can be used for quantification. In *MS Excel* worksheet columns were created for 2θ angles (step size 0.02°), intensities of pure tegafur α and β forms (counts/s), intensities of the analysed tegafur α and β form mixture (counts/s), theoretically calculated intensities of the mixture (counts/s) and least square values of differences between theoretically calculated and experimental intensities. Reflex intensities for pure α and β forms and intensities of analysed mixtures were copied from previously prepared **.uxd* files. Theoretical intensities were calculated using Equation 1.

$$I = Q \cdot \left(I_\beta \cdot \omega_\beta + I_\alpha \cdot \left(1 - \omega_\beta\right)\right) \quad (1)$$

where I is the theoretical intensity in the analysed sample (counts/s); I_α, I_β are the intensities of pure tegafur α and β forms, prepared using the same method as the sample (counts/s); ω_β is the weight fraction of tegafur β form in the sample; Q is a normalization coefficient. This coefficient must be close to 1, and it was established to prevent errors related to the sample preparation.

The weight fraction of tegafur β form ω_β was calculated using *MS Excel* add-in *Solver*. The minimum values of least square sums were found by optimizing the normalization coefficient Q and weight fraction ω_β, by using Equation 2.

$$S^2 = \sum_{i=1}^{n} \left[(I_{teor})_i - (I_{\exp})_i \right]^2 \quad (2)$$

Results and Discussion

It has been reported that tegafur β form is stable at temperatures under 34–39°C, while tegafur α form is stable at higher temperatures.[12] The X-ray patterns of tegafur α and β forms in 2θ interval from 9° to 13° are shown in Figure 1.

It is evident that the β form diffraction reflex at $2\theta = 12.2°$ overlapped with the strongest α form reflex, which was twice as intensive as the rest of α form reflexes, but full profile analysis allowed us to use this area for quantification. The homogenous composition of the analysed mixture and the normalization coefficient close to 1 ensured that the reflex intensities of each phase were linearly dependent on phase weight fractions in the sample. Therefore it was possible to use a calibration line.

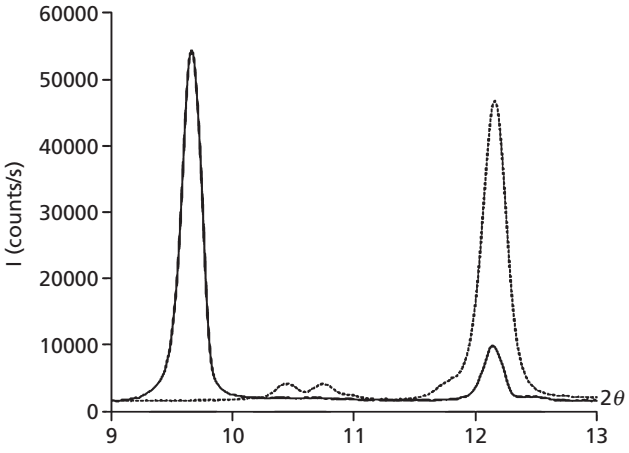

Figure 1 Powder X-ray diffraction patterns of tegafur α (- - -) and β (—) form.

Six experiments were carried out to establish the optimal grinding conditions for reproducible multiplication of the thermodynamically stable phase content in the samples. The samples containing 1.5% weight fraction of β tegafur were treated with a drop (~0.07 ml) or two drops (~0.15 ml) of water and subsequently ground for 3, 5 and 7 min. The aim of these experiments was to investigate sample preparation conditions in which α modification after grinding does not completely transform to the β form, but the sample still contains a reasonably high content of α tegafur. The samples that were ground for 5 and 7 min had practically the same composition, but the samples that were ground for 3 min had a noticeably lower fraction of the β form (Figure 2a). To promote the phase transformation of β tegafur to the α form, one drop (~0.07 ml) or two drops (~0.15 ml) of water was added to the sample before grinding. In all experiments the content of β tegafur in the samples was significantly higher if a single drop of water was added to the sample before grinding (Figure 2b).

Any solvent that does not form solvates or hydrates with analysed polymorphic forms could be used to promote the phase transformation. We chose water (one drop for each 0.50 g sample), followed by grinding for 5 min.

Powder X-ray diffraction patterns of calibration samples after this optimized treatment are shown in Figure 3.

Our developed method was found to be linear in the range of 0.005–1.0% weight fraction of β form in the initial mixture. The relationship between tegafur β form initial and final weight fraction after grinding is shown in Figure 4.

The calibration factor was equivalent to the slope of the linear regression equation. The regression line was described by the function $y = ax$, taking into account the intersection with the origin. If the calibration factor would be calculated from the equation $y = ax + b$, then the approximated line would intersect the y-axis at a non-zero value, meaning positive phase content at zero peak intensity ($I_{peak} \neq 0$, when $\omega = 0$), which is physically impossible. The optimal linear slope was calculated using *MS Excel* function *Linest*. The

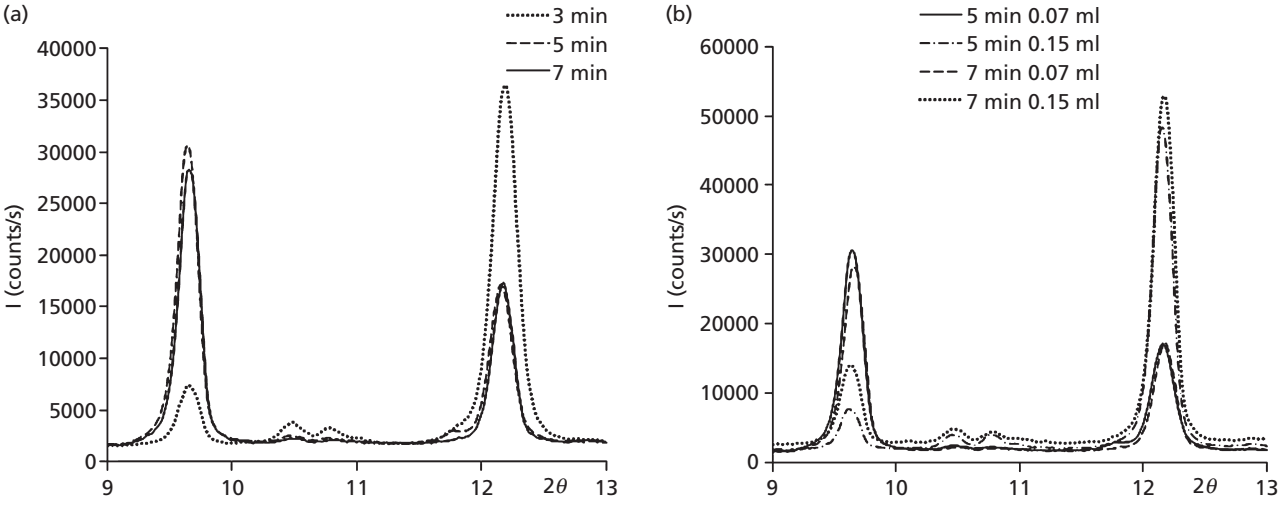

Figure 2 (a) Powder X-ray diffraction patterns of the tegafur α and β form mixture containing 1.5% weight fraction of β tegafur after grinding for 3, 5 and 7 min. (b) Powder X-ray diffraction patterns of the tegafur α and β form mixture containing 1.5% weight fraction of β tegafur after grinding for 5 and 7 min if the phase transition was induced adding a drop (~0.07 ml) or two drops (~0.15 ml) of water.

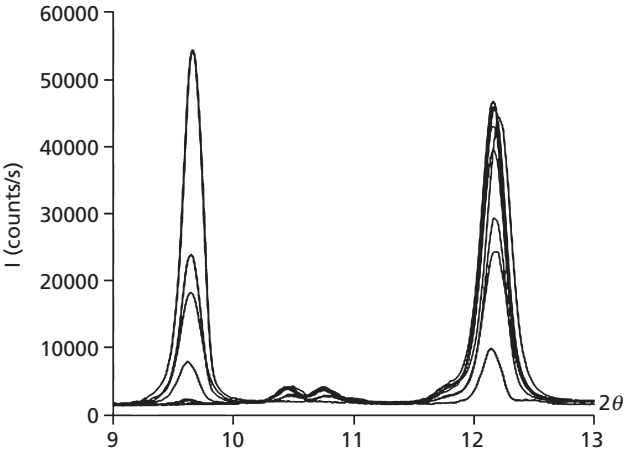

Figure 3 Powder X-ray diffraction patterns of calibration samples after inducing the phase transformation with adding a drop of water to the sample and grinding for 5 min.

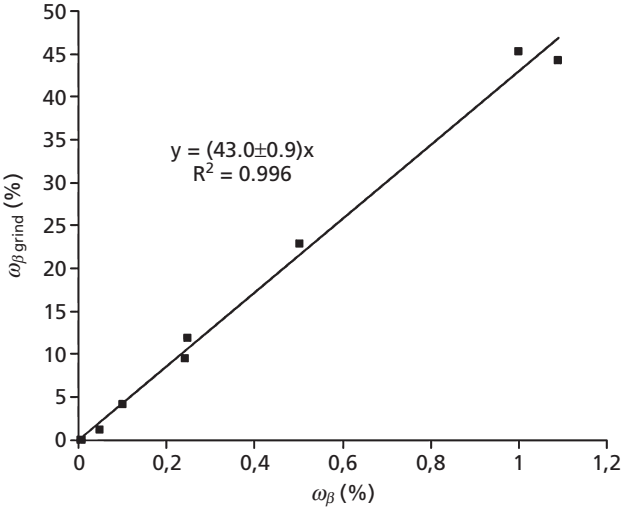

Figure 4 The dependence of tegafur β form weight fraction after grinding upon the initial β form content in the sample.

equation for the calibration curve was $y = (43.0 \pm 0.9)x$, the correlation coefficient $R^2 = 0.996$, and the regression residual mean square error or the standard deviation S_n, which characterized the dispersion between the measured (y_i) and theoretically calculated value (Y_i), was 1.5%.

The detection and quantitation limits were calculated from standard deviation through Equation 3 and Equation 4, respectively, as recommended by the ICH guideline:[13]

$$\text{Limit of detection (LOD)} = 3.3\, S_n/S \quad (3)$$

$$\text{Limit of quantitation (LOQ)} = 10\, S_n/S \quad (4)$$

where S_n is the standard deviation of the response and S is the slope of the calibration curve.

The calculated LOD was 0.12%, and the calculated LOQ was 0.35%. However, taking into account that these LOD and LOQ values were calculated from standard deviation, and the standard deviation was determined as deviation from the linear calibration slope, we could not expect low LOD and LOQ values. The developed quantitation method was based on crystal seeding and solvent-promoted phase transition that led to relatively high statistical deviation. During the development process we determined that the PXRD method allowed detection of the analytical signal if β tegafur weight fraction was as low as 0.005% (i.e. 24 times smaller than the LOD). Despite the large dispersion of experimental data points, the developed sample preparation method allowed rapid and simple determination of trace amounts as low as 0.005%, that so far have been difficult to achieve with any known method of polymorphic form analysis. The essence of this method is in the sample processing phase, while the subsequent quantitative analysis of prepared mixtures could be done not only with PXRD, but any other quantitative technique that allows the construction of a calibration curve.

Through this method it becomes possible to quantify trace amounts of thermodynamically stable polymorphic impurities in bulk drug samples. In addition to active pharmaceutical ingredients, this method is generally able to detect trace amounts of polymorphic impurities in final dosage forms, but as the dosage forms contain excipients affecting the grinding efficiency, it is necessary to construct new calibration plots for each analysed object.

Conclusions

This study demonstrates that very low levels (0.005–1.0%) of unwanted polymorphs in pharmaceuticals can be determined by using a sensitive semi-quantitative method. This trace polymorph analysis is based on a new approach to sample preparation, including solvent-promoted stimulation of phase transition from a thermodynamically metastable form to the stable form. The method was developed for model mixtures of α and β tegafur. The optimal grinding time for tegafur α and β phase analysis at 20°C was 5 min, if the shaking frequency was 15 Hz. The phase transition was facilitated by the addition of a single drop of water to each 0.50 g sample. The content of tegafur β form after the sample preparation was linearly proportional to the initial β form weight fraction in the sample, and the coefficient of proportionality was 43.0 ± 0.9, while the standard deviation S_n was 1.5%. Through this method it becomes possible to quantify trace amounts of stable polymorph impurities in thermodynamically metastable bulk drug samples.

Declarations

Conflict of interest

The Author(s) declare(s) that they have no conflicts of interest to disclose.

Funding

This work was financially supported by the European Social Foundation (agreement number 2009/0138/1DP/1.1.2.1.2/09/IPIA/VIAA/004).

Acknowledgements

The authors are grateful to JSC Grindeks for supplying α and β polymorphic forms of tegafur.

References

1. Vippagunta SR *et al*. Crystalline solids. *Adv Drug Deliv Rev* 2001; 48: 3–26.
2. Bugay DE. Characterization of the solid-state: spectroscopic techniques. *Adv Drug Deliv Rev* 2001; 48: 43–65.
3. Zang GGZ *et al*. Phase transformation considerations during process development and manufacture of solid oral dosage forms. *Adv Drug Deliv Rev* 2004; 56: 371–390.
4. Stephenson GA *et al*. Characterization of the solid state: quantitative issues. *Adv Drug Deliv Rev* 2001; 48: 67–90.
5. Patel AD *et al*. Low-level determination of polymorph composition in physical mixtures by near-infrared reflectance spectroscopy. *J Pharm Sci* 2001; 90: 360–370.
6. Bugay DE *et al*. Quantitation of cefepime 2HCl dihydrate in cefepime 2HCl monohydrate by diffuse reflectance IR and powder X-ray diffraction techniques. *J Pharm Biomed Anal* 1996; 15: 49–61.
7. Rocco WL *et al*. Solid-state characterization of zanoterone. *Int J Pharm* 1995; 122: 17–25.
8. Kustrin SA *et al*. Powder diffractometric assay of two polymorphic forms of ranitidine hydrochloride. *Int J Pharm* 1999; 184: 107–114.
9. Tanninen VP, Yliruusi J. X-ray powder diffraction profile fitting in quantitative determination of two polymorphs from their powder mixture. *Int J Pharm* 1992; 81: 169–177.
10. Német Z *et al*. Quantitative determination of famotidine polymorphs: X-ray powder diffractometric and Raman spectrometric study. *J Pharm Biomed Anal* 2009; 49: 338–346.
11. Uchida T *et al*. Polymorphism of tegafur: physico-chemical properties of four polymorphs. *Chem Pharm Bull* 1993; 41: 1632–1635.
12. Bobrovs R *et al*. Phase Equilibrium of polymorphic forms of tegafur, air humidity and particle size effects on the α- and β-phase transition kinetics. *Latv J Chem* 2010; 1: 3–16.
13. ICH harmonized guideline. Q2B: Validation of analytical procedures: Methodology. 1996.

RESEARCH ARTICLE

Optimization of Sample Preparation Conditions for Detecting Trace Amounts of β-Tegafur in α- and β-Tegafur Mixture

RAITIS BOBROVS, ANDRIS ACTIŅŠ

University of Latvia, The Faculty of Chemistry, Riga LV-1013, Latvia

Received 13 March 2012; revised 21 August 2012; accepted 31 August 2012

Published online in Wiley Online Library (wileyonlinelibrary.com). DOI 10.1002/jps.23323

ABSTRACT: We report a semiquantitative method for determining trace amounts (<1%) of thermodynamically stable forms in polymorphic mixtures, focusing on sample preparation effects on solid phase transitions. Tegafur [5-fluoro-1-(oxolan-2-yl)-1,2,3,4-tetrahydropyrimidine-2,4-dione] was used as a model material in this study. The amounts of the thermodynamically stable β tegafur were increased to levels detectable by powder X-ray diffractometry by grinding the samples in a ball mill in the presence of water. The limit of detection for this method was as low as 0.0005% of β tegafur in α and β tegafur mixtures. The amount of β tegafur after sample preparation was found to be proportional to the initial weight fraction of β tegafur. The sum of Langmuir and Cauchy–Lorentz equations was used to describe the change in conversion degree due to the added water volume, where Langmuir equation described water sorption during the sample preparation and Cauchy–Lorentz equation described the grinding efficiency. © 2012 Wiley Periodicals, Inc. and the American Pharmacists Association J Pharm Sci

Keywords: polymorphism; polymorph contamination; trace amount detection; semiquantitative analysis; tegafur; X-ray powder diffractometry; milling; solid state; thermodynamics

INTRODUCTION

About two-thirds of organic compounds and about 80% of active pharmaceutical ingredients under certain conditions can exist in more than one polymorphic form. Polymorphism is defined as the ability of a drug compound to crystallize into more than one different crystalline form that differs with molecule packing arrangements and/or conformations within the crystal lattice.[1–4] The often encountered differences in stability, solubility, and bioavailability of active pharmaceutical ingredient polymorphs require a control over solid phase composition of these products. It is a common requirement in Pharmacopeia monographs that active pharmaceutical ingredients in drugs must exist in one fixed crystalline form.

The most thermodynamically stable form is usually chosen for pharmaceutical use, but sometimes a metastable form has better solubility or bioavailability, and is selected for manufacturing.[5] In this case, it becomes very important that the final manufactured product is free from the thermodynamically stable form because even trace amounts can facilitate a phase transition to the unwanted thermodynamically stable form. Therefore, methods for detecting the stable form in trace amounts (<1%) are necessary to ensure kinetic stability of metastable solid pharmaceutical ingredients.

As shown in a previous publication,[6] it is possible to determine trace amounts (<0.01%) of the thermodynamically stable form in mixtures of thermodynamically stable and metastable forms. Our aim for this work was to determine sample processing impact on phase quantification. The amount of the thermodynamically stable form was increased by grinding the sample with water additive in a way similar to literature precedents.[7–11] The increased amount of the stable form could then be determined with X-ray diffractometry, which was selected as the most appropriate method for phase quantification. Also infrared, Fourier transform Raman, solid-state nuclear magnetic resonance spectroscopy, and thermal analysis methods can be used for phase analysis.[1,2]

Accurate measurement of intensity, height, and plotted area of diffraction peaks is most important for obtaining reliable and reproducible results and

Correspondence to: Raitis Bobrovs (Telephone: +371-26465235; Fax: +371-67378736; E-mail: raitis.bobrovs@gmail.com)

Journal of Pharmaceutical Sciences

calibration curves.[12] Nature of the samples, instrument and sample preparation parameters, type of sample holders, sample rotation, particle size, powder packing, and dominant orientation are also crucial factors that affect diffraction peak intensities and areas, thus influencing quantification results.[12–14]

Tegafur [5-fluoro-1-(oxolan-2-yl)-1,2,3,4-tetrahydropyrimidine-2,4-dione] was chosen as a model material in this study because it does not form hydrates and solvates that could gradually loose associated solvent during sample preparation, and thus affect phase quantification. Tegafur is an antitumor agent, widely used in the treatment of various malignancies, particularly gastrointestinal and breast cancers.[15] Over years, α, β, γ, δ, and ε forms of tegafur have been reported in pharmaceutical literature,[15–17] but only α and β modifications are used for therapeutic purposes.

MATERIALS AND METHODS

Materials

Commercial samples of α and β tegafur were supplied by JSC *Grindeks* (Riga, Latvia).

Sample Preparation

The entire batches of α- and β-tegafur used in experiments were ground separately for 3 min to ensure required sample homogeneity and avoid preferred crystal orientation effects.

Determination of Optimum Grinding Frequency

Mixtures of 2.0%, 1.0%, 0.50%, 0.10%, 0.050%, 0.010%, 0.0050%, 0.0010%, 0.00050%, and 0.00010% β tegafur in α tegafur (3.0 g each) were prepared from a 2.0% stock mixture that was diluted to the required concentrations. Samples during preparation were homogenized in a Retsch MM300 ball mill (Retsch GmbH, Haan, Germany) for 5 min at 20°C, with 15 Hz shaking frequency. The analytical balance (BOECO, Hamburg, Germany) had an accuracy of ±0.0001 g. The samples of homogenized mixtures (0.50 g) were each treated with 0.07 mL water and ground in the ball mill at 7, 10, and 15 Hz shaking frequencies for 5 min.

Determination of the Optimum Added Water Volume

A mixture of tegafur α and β forms containing 1.0% weight fraction of β form was weighed and homogenized in the ball mill for 5 min at 20°C, with 15 Hz shaking frequency. The 0.50 g samples of homogenized mixture were ground in the ball mill with variable water additive amounts for 5 min at 20°C, with 10 Hz shaking frequency. The added water volume was from 0.02 to 0.20 mL, with 0.01 mL step size. When the amount of water additive exceeded 0.06 mL, a thick paste formed, and it became necessary to dry the samples for 30 min after grinding.

Sample Preparation for Recrystallization Studies

A sample (0.50 g) of tegafur α and β form mixture, containing 1.0% weight fraction of β form, was ground in the ball mill for 5 min at 20°C with 15 Hz shaking frequency, with 0.20 mL water added just before grinding. The obtained thick paste was pressed into glass sample holder right after grinding, and powder X-ray diffraction (PXRD) pattern was recorded. Consecutive PXRD patterns were recorded every 5 min, until no further phase transition was observed (∼1 h).

Determination of Surface Area

Three samples of tegafur α and β form mixture (0.50 g each), containing 1.0% weight fraction of β form, were ground in the ball mill for 5 min at 20°C, with 10 Hz shaking frequency. The first sample had no added water, the second had 0.06 mL of water, and the third had 0.12 mL of water. Water was added just before grinding. The samples were removed from grinding vessels immediately, and were dried at ambient temperature for 3 h. Surface area determination requires a 1–2 g sample; therefore, three parallel samples for each volume of added water were ground in the ball mill and then combined to obtain the required sample mass.

Surface area was determined by a modified chromatograph "Hrom 3," detecting the amount of argon involved in a monolayer adsorption–desorption process.

PXRD Analysis

Samples were analyzed with a Bruker D8 Advance powder X-ray diffractometer (Bruker AXS, Karlsruhe, Germany), equipped with a PSD LYNXEYE detector. Measurements were performed with CuK radiation (1.54180 Å) at room temperature. The following conditions were used: step-scan mode with a step size of 0.01°; scan speed: 0.2°/min; 2θ range: 9.0°–12.7°; voltage: 40 kV; current: 40 mA; divergence slit: 0.6 mm; scattering slit: 8 mm.

Powder samples were packed into glass holders with a weight capacity of approximately 150 mg and pressed by a clean glass slide to ensure coplanarity of the powder surface with the surface of the holder. The obtained diffractograms were analyzed with DIFFRAC^{plus} EVA (ver. 9.0) software (Bruker AXS, Karlsruhe, Germany).

Quantitative Analysis of α and β Polymorph Mixture

Individual diffraction peaks area method was used in tegafur α and β form quantification. The areas of the plotted diffraction peaks were calculated by using the computer program TOPAS 3 (Bruker AXS, Karlsruhe, Germany), and weight fractions of β form were

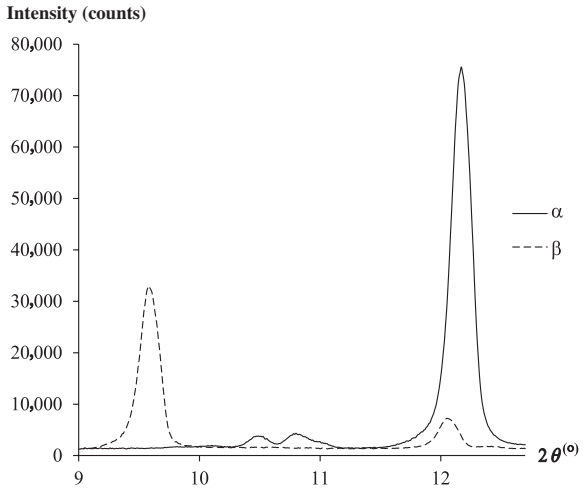

Figure 1. Powder X-ray diffraction patterns of tegafur α and β forms.

calculated by using the Eqs. 1–3:

$$\omega_{\beta;\%} = \frac{S_{\text{mixture; 9.6}}}{S_{\beta;\,9.6}} \times 100\% \quad (1)$$

$$\omega_{\alpha;\%} = \left[\frac{S_{\text{mixture; 12.1}} - \left(S_{\text{mixture; 9.6}} \times \frac{S_{\beta;\,12.1}}{S_{\beta;\,9.6}} \right)}{S_{\alpha;\,12.1}} \right] \times 100\% \quad (2)$$

$$\omega_{\beta\,\text{norm};\%} = \frac{\omega_{\beta;\%}}{\omega_{\beta;\%} + \omega_{\alpha;\%}} \times 100\% \quad (3)$$

where $\omega_{\beta;\%}$, $\omega_{\alpha;\%}$ are weight fractions of α and β forms; $S_{\beta;9.6}$, $S_{\beta;\,12.1}$ are diffraction peaks plot areas for pure β form at 9.6° and 12.1°; $S_{\text{mixture; 9.6}}$, $S_{\text{mixture; 12.1}}$ are the diffraction peaks plot areas at 9.6° and 12.1° for the analyzed mixture; $S_{\alpha;\,12.1}$ is the diffraction peaks plot area of pure α form at 12.1°; and $\omega_{\beta\,\text{norm};\%}$ is a normalized weight fraction of the β form. Weight fraction calculations for α and β forms differ because the most intensive α form diffraction peak at 12.1° is overlapping with a β form diffraction peak (see Fig. 1).

RESULTS AND DISCUSSION

Chemical composition uniformity of tegafur polymorphs ensures that each phase's diffraction peaks intensity is linearly dependent on phase weight fraction in mixture; therefore, it is possible to use calibration line method for quantitative tegafur α and β phase analysis.[12,18] To determine trace amounts of the thermodynamically stable polymorphic form in mixtures of thermodynamically stable and metastable forms, the amount of thermodynamically stable form need to be reproducibly multiplied to a degree that allows its quantification with PXRD. Our first experiments in this direction indicated that phase transition did not occur when pure α- and β-tegafur were ground separately without a solvent; therefore, the initial sample preparation by grinding of pure α- and β-tegafur did not promote phase transition and could not affect the results of quantitative analysis.

Optimum Grinding Frequency Determination

Tegafur α and β form mixtures with β form weight fraction from 2.0% to 0.0001% were ground at three different grinding frequencies: 7, 10, and 15 Hz to establish an acceptable grinding frequency. The low intensity α-tegafur diffraction peak at 2θ 10.1° may mask the β form peak at 2θ 9.6° (see Fig. 2); hence, the quantification of very small amounts of β-tegafur may be distorted. To minimize the influence of this α form diffraction peak, the β form diffraction peak area at 2θ 9.6° was calculated in the 2θ region from 9.0° to 10.0°.

The recorded X-ray patterns and calibration curves for all three grinding frequencies are shown in the Figure 3. In the higher range of initial β-tegafur weight fraction (up to ~20%), all of the calibration curves had an exponential nature, but in the lower range of β form mass fraction (<2.0%), the calibration curves of samples ground at 7 and 10 Hz frequencies could be considered as linear. At the same time, the conversion degree curve for samples ground at a 15 Hz frequency maintained an exponential nature also in the lower range. Conversion degree dependence on the initial β-tegafur weight fraction most likely exhibits an exponential nature because the degree of phase transition is more affected by the surface area of β-tegafur, thus also the phase boundary area, and less by the initial weight fraction of β-tegafur. The weight fraction of β-tegafur in the sample is not linearly proportional to phase boundary area, and therefore, the weight fraction after grinding does not depend linearly on the initial weight fraction of β-tegafur.

The calibration factor for samples ground at 7 and 10 Hz frequencies was equivalent to the linear slope of the linear regression equation. The regression line was described by the relationship $y = ax$, taking into account the intersection with the origin. If the calibration factor would be calculated from the equation $y = ax + b$, in this case, the approximated line would intersect y axis at nonzero value and that would mean positive phase content at zero peak intensity ($I_{\text{peak}} \neq 0$, when $\omega = 0$), which is physically impossible. The optimal linear slope with minimized slope error and standard deviation S_n was calculated using MS Excel function Linest.

Calibration equation for those samples ground with 7 Hz frequency was $y = (8.3 \pm 0.4)x$ with correlation coefficient $R^2 = 0.97$ and standard deviation $S_n = 1.1\%$, but for samples ground with 10 Hz frequency,

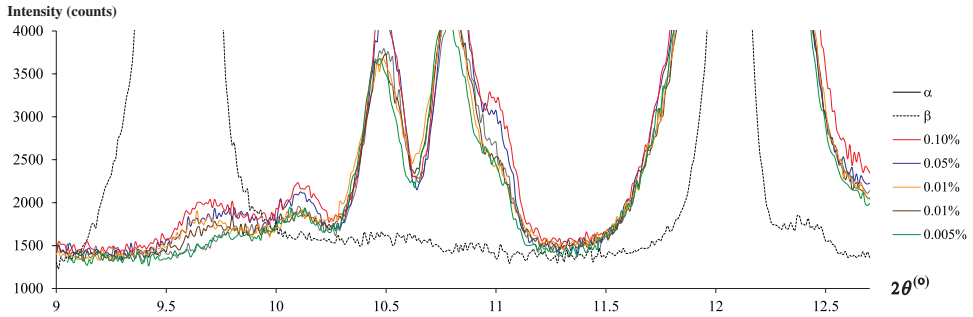

Figure 2. Powder X-ray diffraction patterns of pure α- and β-tegafur and calibration samples with initial β form weight fraction from 0.10% to 0.005% after grinding with 7 Hz frequency for 5 min in 20°C.

the calibration equation was $y = (35.1 \pm 1.1)x$ with the correlation coefficient $R^2 = 0.997$ and standard deviation $S_n = 1.4\%$.

Experimental points for samples ground with 15 Hz frequency could be described with the exponential equation

$$\omega_{\beta,\text{theor}} = \omega_{\beta;\infty}(\omega_{\beta;\infty} - \omega_{\beta;0})e^{-k\omega_{\beta;\text{initial}}} \quad (4)$$

where $\omega_{\beta,\text{ theor}}$ was the theoretically calculated weight fraction of β-tegafur after grinding, $\omega_{\beta;\infty}$ was the final weight fraction of β-tegafur when the phase transition had ceased, $\omega_{\beta;0}$ was the weight fraction of β-tegafur after grinding when $\omega_{\beta;\text{initial}} = 0$, k was the phase transition rate constant, and $\omega_{\beta;\text{initial}}$ was the weight fraction of β-tegafur before grinding. The MS Excel Solver optimization software, based on the least squares method, was used to optimize Eq. 4 constants. The following equation was thus obtained.

$$\omega_{\beta} = 96.6(1 - e^{-12.4\omega_{\beta;\text{initial}}}) \quad (5)$$

Experimental point dependence on the initial weight fraction of β-tegafur ($\omega_{\beta;\text{initial}}$) was empirical in this case, and the exponential nature of experimental curve may be considered as coincidence. The polymorphic phase transition rate depends on the mass transition rate from one phase to another[19]; therefore, it may be considered that the main factor influencing overall phase transition rate is related to the surface properties of both phases.

If the weight fraction of β-tegafur in the sample ground at 15 Hz frequency does not exceed 0.10%, then it is possible to use a linear regression equation $y = (770.0 \pm 0.1)x$ with the correlation coefficient $R^2 = 0.995$ and standard deviation $S_n = 2.2\%$.

In the initial β-tegafur weight fraction region from 2.0% to approximately 0.05%, the best correlation was achieved, when the samples were ground with 10 Hz frequency, but if lower thermodynamically stable form contamination in metastable form must be determined, then the grinding frequency of 15 Hz is preferred.

Optimum Water Additive Amount Determination

Tegafur α and β form mixture with the β form weight fraction of 1.0% was ground with various amounts of added water. The conversion degree was

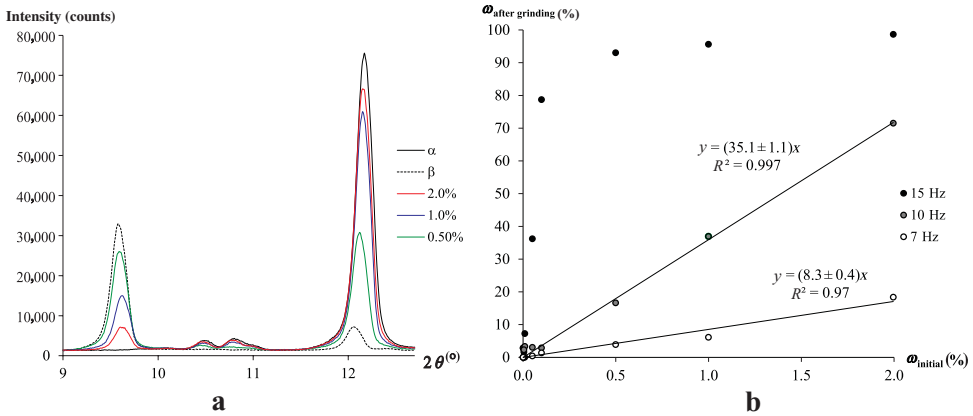

Figure 3. (a) Powder X-ray diffraction patterns of pure α and β tegafur and calibration samples after grinding with 7 Hz frequency for 5 min in 20°C and (b) conversion degree depending from initial β form weight fraction and grinding frequency.

 DOI 10.1002/jps

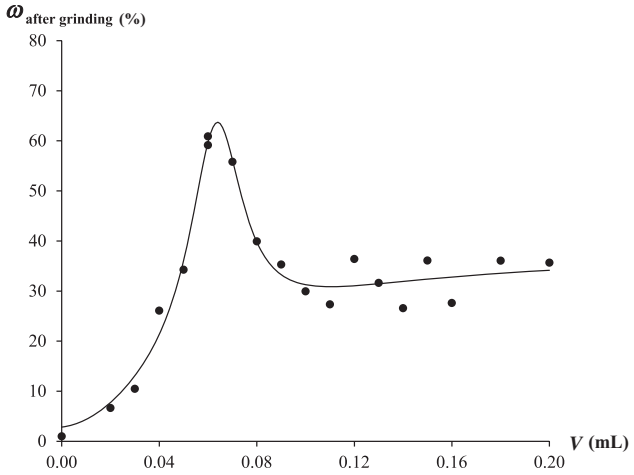

Figure 4. Conversion degree of ground (10 Hz, 5 min at 20°C) 1.0% β-tegafur sample, depending on the added water volume.

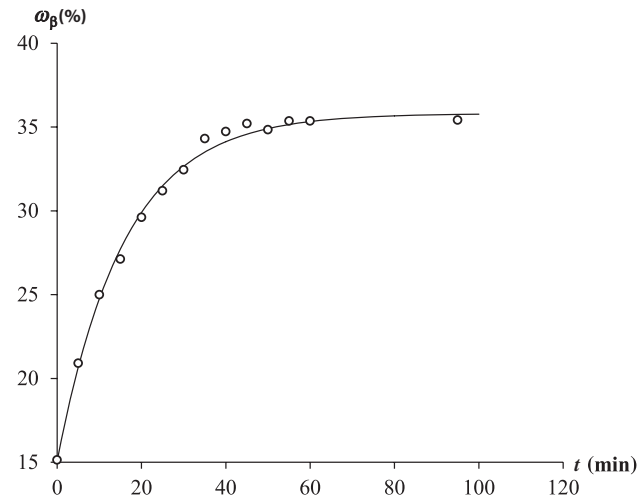

Figure 5. β-Tegafur weight fraction changes during recrystallization process of 1.0% β-tegafur sample after grinding with 10 Hz frequency for 5 min at 20°C with 0.20 mL water additive.

determined, depending on the volume of added water, and is shown in the Figure 4. The sum of two empirical equations (Langmuir and Cauchy–Lorentz equations; Eq. 6) was chosen to describe the experimental data because there are no equations in literature that would fit these experimental data:

$$\omega = \frac{dkV}{1+kV} + f \times \frac{1}{\pi}\left[\frac{b}{(V-a)^2+b^2}\right] \qquad (6)$$

where ω is the weight fraction of β-tegafur in the samples after grinding, V is the volume of added water (mL), f is the contribution factor, a is the volume of added water at which the highest conversion degree was observed, b is the distribution width ratio, and d and k are empirical constants.

Cauchy–Lorentz equation term or another statistical "bell shaped" function was introduced into the Eq. 6 to describe the grinding efficiency depending on the volume of added water. A "bell shaped" statistical distribution term was selected because surface area determination experiments demonstrated (see section *Surface Area Determination*) that the grinding efficiency, and thus also the surface, is dependent on the added water volume, matching a statistical "bell shaped" distribution. Thus, if no water sorption on the surface of tegafur occurs, the conversion degree depends only on the grinding efficiency, which depends on the amount of water added. Langmuir equation term was introduced into the Eq. 6 to describe a phase transition occurring in the adsorbed water layer on the surface of tegafur, and it is not related to the phase transition promoted by grinding.

It was observed that samples with additive volume of less than 0.06mL were free flowing powders after grinding, but when the water additive volume was greater than 0.06 mL, the samples formed thick paste and stuck to the grinding vessel walls. Water can be considered as a lubricant in this process, and increasing the volume of water additive above 0.06 mL decreased the conversion degree, whereas at water volumes below 0.06 mL, the conversion degree of β-tegafur to α-tegafur increased.

Phase Transition During Sample Drying

The metastable phase α transforms to the thermodynamically stable phase β during a process involving tegafur dissolution in water, followed by crystallization (this process proceeds until the eventual evaporation of the added water). The kinetic curve of this process is shown in the Figure 5. The highest conversion degree was observed for samples prepared with 0.06 mL of water (section *Optimum Water Additive Amount Determination*), yet this experiment was performed with 0.20 mL of water to extend the water evaporation time and to enable acquisition of more experimental data. Experiments with smaller amounts of water exhibited the same trend, but results were less obvious. The kinetic curve can be described with a kinetic equation $\omega_\beta = 35.8 - 20.7 \times e^{-0.063t}$ (equation constants were optimized with MS Excel Solver). Not only an increase of β-tegafur signal was observed during this process, but there was also a minimal increase of α form diffraction peaks indicating increasing crystallinity of α form, or an increasing preferred orientation due to the fracture of crystals along certain cleavage planes. As can be seen in Figure 5, the conversion degree of β-tegafur was highly dependent on sample drying time; thus, for a precise trace amount quantification, all samples should be dried for the same duration (at least 1 h).

Table 1. Surface Areas of Unground, Dry Ground, and with 0.06 and 0.12 mL Water Additive Ground (5 min, 10 Hz, 20°C) Samples

Sample	Surface Area (m^2/g)
Unground	13.4
Ground without additive	16.9
Ground with 0.06 mL water additive	18.3
Ground with 0.12 mL water additive	13.9

Surface Area Determination

Surface areas of unground samples, as well as samples ground without water, and with 0.06 and 0.12 mL of water were determined for estimating the impact of water on grinding efficiency. The determined surface areas are shown in the Table 1. The surface area of unground 1.0% β-tegafur in mixture with α-tegafur was 13.4 m^2/g, but the surface area of sample ground with 0.12 mL water was 13.9 m^2/g, which indicated that water volume above 0.06 mL did not improve grinding efficiency, as discussed in section *Optimum Water Additive Amount Determination*. The surface area of the sample ground without water was significantly higher than for the sample ground with a 0.12 mL water additive. These differences can be related to different sample dispersion in the grinding vessels; dry sample after grinding was homogenously distributed in the grinding vessel, whereas the wet sample after grinding was located on the mill walls. The maximum surface area, hence the maximum grinding efficiency, was achieved when phase transition during grinding was stimulated with a 0.06 mL water additive.

CONCLUSIONS

We found that it is possible to determine down to 0.0005% of the thermodynamically stable form mixed within a metastable form by using tegafur model material. The amount of the thermodynamically stable form after sample processing was proportional to its initial weight fraction.

In β-tegafur weight fraction range from 2.0% to approximately 0.05%, the best correlation was achieved when samples were ground for 5 min at 20°C with 10 Hz frequency. At lower weight fraction of β-tegafur, the grinding frequency of 15 Hz was preferred. The optimum results were achieved when 0.06 mL of water was added to 0.50 g of tegafur. A sum of Langmuir and Cauchy–Lorentz equations could be used to describe the change in conversion degree depending on the added water volume. The indirectly determined surface areas and the dependence of conversion degree on water additive volume demonstrated that increasing the added water volume above 0.06 mL did not improve grinding effectiveness. Conversion degree of β-tegafur was highly dependent on sample drying time, and the recrystallization process could be described with a kinetic equation $\omega_\beta = 35.8 - 20.7 \times e^{-0.063t}$.

This method is generally applicable when the sample has phases with similar particle properties, and the peak intensity is not particularly dependent on preferred orientation and perhaps line broadening effects.

ACKNOWLEDGMENTS

The authors are grateful to the European Social Foundation for financial support and to JSC *Grindeks* for supplying α and β polymorphic forms of tegafur.

REFERENCES

1. Brittain H; Ed. 1999. Polymorphism in pharmaceutical solids. London, UK: Informa Healthcare.
2. Hilfiker R. 2006. Polymorphism in the pharmaceutical industry. Weinheim, Germany: Wiley-VchVerlagGmbH & Co. KGaA.
3. Vippagunta S, Brittain H, Grant D. 2001. Crystalline solids. Adv Drug Deliv Rev 48(1):3–26.
4. Allesø M, van den Berg F, Cornett C, Jørgensen FS, Halling Sørensen B, de Diego HL, Hovgaard L, Aaltonen J, Rantanen J. 2008. Solvent diversity in polymorph screening. J Pharm Sci 97(6):2145–2159.
5. Bugay DE. 2001. Characterization of the solid-state: Spectroscopic techniques. Adv Drug Deliv Rev 48(1):43–65.
6. Petkune S, Bobrovs R, Actiņš A. 2011. Determination of micro amounts of β tegafur in the α and β polymorph mixture by powder X ray diffractometric analysis. J Pharm Pharm 63(9):1136–1140.
7. Trask A, Shan N, Motherwell W, Jones W, Feng S, Tan R, Carpenter K. 2005. Selective polymorph transformation via solvent-drop grinding. Chem Commun 2005(7):880–882.
8. Trask A, Motherwell W, Jones W. 2004. Solvent-drop grinding: Green polymorph control of cocrystallisation. Chem Commun 2004(7):890–891.
9. Toda F, Tanaka K, Sekikawa A. 1987. Host–guest complex formation by a solid–solid reaction. J Chem Soc Chem Commun (4):279–280.
10. Shan N, Toda F, Jones W. 2002. Mechanochemistry and co-crystal formation: Effect of solvent on reaction kinetics. Chem Commun (20):2372–2373.
11. Kwan CC, Chen YQ, Ding YL, Papadopoulos DG, Bentham AC, Ghadiri M. 2004. Development of a novel approach towards predicting the milling behaviour of pharmaceutical powders. Eur J Pharm Sci 23(4–5):327–336.
12. Campbell Roberts SN, Williams AC, Grimsey IM, Booth SW. 2002. Quantitative analysis of mannitol polymorphs. X-ray powder diffractometry—Exploring preferred orientation effects. J Pharm Biomed Anal 28(6):1149–1159.
13. Hurst VJ, Schroeder PA, Styron RW. 1997. Accurate quantification of quartz and other phases by powder X-ray diffractometry. Anal Chim Acta 337(3):233–252.
14. Takehira R, Momose Y, Yamamura S. 2010. Quantitative analysis of crystalline pharmaceuticals in tablets by pattern-fitting procedure using X-ray diffraction pattern. Int J Pharm 398(1–2):33–38.
15. Uchida T, Yonemochi E, Oguchi T, Terada K, Yamamoto K, Nakai Y. 1993. Polymorphism of tegafur:

Physico-chemical properties of four polymorphs. Chem Pharm Bull 41(9):1632–1635.
16. Actiņš A, Beļakovs S, Orola L, Veidis MV. 2006. Molecular and crystal structure of novel form of tagefur. Latvijas Ķīmijas Žurnāls 2:120–124.
17. Needham F, Faber J, Fawcett T, Olson D. 2006. X-ray powder diffraction analysis of tegafur. Powder Diffraction 21:245.
18. Sheikhzadeh M, Rohani S, Jutan A, Manifar T. 2007. Quantitative and molecular analysis of buspirone hydrochloride polymorphs. J Pharm Sci 96(3):569–583.
19. Actiņš A, Petkune S. 2009. Tegafūra β- un α- modifikāciju maisījuma rentgendifraktometriskā analīze un sastāva maiņa ilgstošas glabāšanas apstākļos. Latvijas Ķīmijas Žurnāls 1:43–52

International Journal of Pharmaceutics 443 (2013) 193–198

Contents lists available at SciVerse ScienceDirect

International Journal of Pharmaceutics

journal homepage: www.elsevier.com/locate/ijpharm

Organic solvent vapor effects on phase transition of α and β tegafur upon grinding with solvent additives

Raitis Bobrovs*, Olga Saveļjeva, Agnese Kapace, Zane Plauka, Andris Actiņš

University of Latvia, Faculty of Chemistry, Kr. Valdemara iela 48, Riga LV-1013, Latvia

ARTICLE INFO

Article history:
Received 22 August 2012
Accepted 4 January 2013
Available online xxx

Keywords:
Grinding
Phase transition
Polymorphism
Tegafur
Sorption
Desorption
Solubility
X-ray powder diffractometry

ABSTRACT

Solvent effects on α tegafur (5-fluoro-1-(tetrahydro-2-furyl)uracil) phase transition to β tegafur during grinding with solvent additive, as well as phase transition in samples exposed to 95% relative solvent vapor pressure has been studied in this research. Samples containing 0.5% and 0.1% of β tegafur in α and β tegafur mixture, as well as samples of pure α tegafur were ground with different solvent additives, and conversion degrees depending on the solvent were determined using PXRD method. Samples with α and β tegafur weight fraction of 1:1 were exposed to 95% relative solvent vapor pressure, and phase transition rates were determined. Solubility of α tegafur, solvent sorption and desorption behavior on α and β tegafur have been examined.

It was found that the conversion degree of α tegafur to β tegafur mainly depends on solubility of α tegafur in the relevant solvent, and the conversion degree to β tegafur is higher in such solvents, where solubility of α tegafur is higher. The samples ground in a ball mill with solvent additive had a trend of phase transition dynamics from α tegafur to β tegafur similar to the samples exposed to 95% relative solvent vapor pressure.

1. Introduction

Polymorphism is a well-known phenomenon, which is defined as ability of a compound to crystallize into more than one crystalline form that differs with molecule packing arrangements and/or conformations within the crystal lattice (Brittain, 2009; Hilfiker, 2006; Vippagunta et al., 2001). Most of active pharmaceutical ingredients exhibit polymorphism, therefore it is a common Pharmacopoeia requirement that active pharmaceutical ingredients in drugs must exist in one, fixed crystalline form. The thermodynamically stable form is usually chosen for pharmaceutical use, but recently, metastable forms are manufactured more often due to enhanced dissolution or bioavailability profiles and patent concerns (Brittain, 2009).

It is known that grinding can promote phase transition (Boldyrev, 2006; Chieng et al., 2006; Lin et al., 2006; Otsuka and Kaneniwa, 1986) of polymorphs, and solvent additive accelerates the process even more (Shan et al., 2002; Trask et al., 2004, 2005). In our previous experiments (Petkune et al., 2011) we developed a semi-quantitative analytical method for determining trace amounts of the thermodynamically stable polymorphic form in the mixture of thermodynamically stable and metastable polymorphic modifications, where the amount of the thermodynamically stable form was increased by grinding samples with a solvent additive. However, there is a lack of research on how solvents affect phase transition of polymorphs during the grinding.

The purpose of this study was to investigate the effect of solvent additive on phase transition of α and β tegafur and to take a look at possible causes that could affect phase transition during the grinding.

Tegafur (5-fluoro-1-(tetrahydro-2-furyl)-uracil) (see Fig. 1) α and β modifications were selected as a model material in this study.

Tegafur is an antitumor agent widely used in the treatment of various malignancies, particularly gastrointestinal and breast cancers (Uchida et al., 1993). Over years α, β, γ, δ and ε forms of tegafur have been reported in pharmaceutical literature (Actiņš et al., 2006; Needham et al., 2006; Uchida et al., 1993), but only α and β modifications are used for therapeutic purposes.

2. Materials and methods

2.1. Materials

Commercial samples of α and β tegafur were supplied by JSC Grindeks.

Used solvents – methanol, ethanol, *n*-propanol, 2-propanol, *n*-butanol, *n*-pentanol, *n*-heptanol, benzyl alcohol, ethyl acetate, *n*-propyl acetate, *n*-butyl acetate, 1,2-dichloroethane, chloroform,

* Corresponding author. Tel.: +371 26465235.
E-mail address: raitis.bobrovs@gmail.com (R. Bobrovs).

0378-5173/$ – see front matter © 2013 Elsevier B.V. All rights reserved.
http://dx.doi.org/10.1016/j.ijpharm.2013.01.009

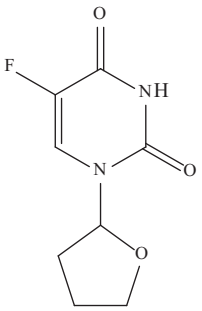

Fig. 1. Tegafur (5-fluoro-1-(tetrahydro-2-furyl)-uracil).

acetone, tetrahydrofuran, acetonitrile and toluene were supplied by Merck and used without any further purification. All of the used reagents had a reported purity >98%.

2.2. Methods

2.2.1. Sample preparation

The entire batches of α and β tegafur used in experiments were ground separately for 3 min to ensure the required sample homogeneity and to avoid preferred crystal orientation effects.

2.2.2. Determination of solvent effect on phase conversion degree during grinding

A sample (10 g) of tegafur α and β form mixture, containing 0.5% weight fraction of β form, was prepared from a 5.0% stock mixture that was diluted to the required concentration. Samples during preparation were homogenized in a Retsch MM300 ball mill (Retsch GmbH, Germany) for 5 min at 20 °C with 15 Hz shaking frequency. The analytical balance (BOECO, Germany) had an accuracy of ±0.0001 g.

The 0.20 g samples of prepared 0.5% mixture were each treated with 0.025 mL of solvent and ground in the ball mill at 10 Hz shaking frequency for 5 min. The solvents used in this experiment were methanol, ethanol, *n*-propanol, *n*-butanol, *n*-pentanol, *n*-heptanol, isopropanol, benzyl alcohol, ethyl acetate, *n*-propyl acetate, *n*-butyl acetate, 1,1-dichloroethane, chloroform, acetone, tetrahydrofuran, acetonitrile and toluene. Prepared samples were dried in opened grinding vessel for 30 min at 20 °C after the grinding. Dried samples were packed into glass holders with a weight capacity of ~150 mg and PXRD patterns were record.

2.2.3. Determination of α tegafur solubility in the solvents used

Approximately 0.2 g of α tegafur was added to ~12 mL of solvent in weighing bottle, and the prepared mixture was held at 30 °C for 48 h in a sealed weighing bottle and stirred occasionally to obtain a saturated tegafur solution. The clear, saturated mixture (4.0 mL, without any precipitate) was transferred to a clean, tared weighing bottle with a pipet that was also held at 30 °C. The weighing bottle with the saturated solution was left to evaporate at 30 °C, and then the weighing bottle with the dry residue was weighed on analytical balance (BOECO, Germany, $d = \pm 0.0001$ g). PXRD pattern was recorded for the dry residue. Solubility of α tegafur was determined in all the previously mentioned solvents.

2.2.4. Determination of solvent vapor effect on phase transition

Two samples (4 g each) of α and β tegafur mixture with weight ratio 1:1 were prepared. Samples were homogenized during the preparation in a ball mill for 5 min at 20 °C with 15 Hz shaking frequency. The prepared homogeneous samples were packed into glass holders and PXRD patterns for initial mixtures and pure α and β forms of tegafur were recorded. The samples were placed in desiccators with 95% relative solvent vapor pressure at 30 ± 0.5 °C, and depending on the transition rate, PXRD data were recorded at fixed moments.

Obtaining 95% relative solvent vapor pressure. To obtain a relative solvent vapor pressure of 95%, methanol, ethanol, *n*-propanol, 2-propanol, *n*-butanol, *n*-pentanol, *n*-heptanol and benzyl alcohol solution in glycerol were prepared, and acetone, acetonitrile, ethyl acetate, *n*-propyl acetate, *n*-butyl acetate, chloroform, tetrahydrofuran, 1,2-dichloroethane and toluene solution in dimethyl sulfoxide were prepared according to the Raoult's law (Eq. (1))

$$X = \frac{p_o - p}{p_o} = \frac{n}{n_o + n} \quad (1)$$

where X is the solvent's mole fraction in solution; p_o is the vapor pressure of pure solvent; p is the solvent's partial vapor pressure over a solution; n represents the investigated solvent molar amount in the solution; n_o is the moles of glycerol or dimethyl sulfoxide in the solution.

Temperature control. Desiccators with the prepared solvent solutions were placed in an air thermostat (Memmert, Universal Oven UFB-500) at 30 ± 0.5 °C 24 h prior to sample insertion.

2.2.5. Solvent sorption studies

Solvent sorption experiments were performed in weighing dishes at 30 °C by using pure α and β tegafur. The 0.20 g samples of pure α and β tegafur were weighed in separate weighing dishes with accuracy ±0.0001 g and placed in desiccators with 95% partial pressure of the relevant solvents (see Section 2.2.4). Depending on the sorption rate, samples were weighed at fixed moments.

2.2.6. Solvent desorption studies

Desorption experiments were performed using completely solvent-saturated samples from the sorption experiment (described in Section 2.2.5). The 30 ± 2 mg of solvent-saturated samples were quickly placed (in less than 20 s) in aluminum sample pan, and desorption experiments were performed using a *TG/DTA6300 EXSTAR6000* instrument with open aluminum sample pans having internal diameter of 5 mm and height of 2.5 mm, under dry nitrogen atmosphere with flow rate of 250 mL/min in isothermal conditions at 30 °C. Desorption rate was highly dependent on mass of the sample; therefore samples with equal mass were used. The highest possible mass (30 ± 2 mg) was placed into each sample pan to minimize the error of sample weighing and to reduce the time of weighing (the sample holder was simply filled up to the edge). Mass changes were recorded every 0.5 s.

2.2.7. Karl Fischer titration

The water amount in solvents was quantified by a volumetric Karl Fischer titrator Metrohm 836 Titrando with one-component system using HYDRANAL – Composite 5 (Fluka, Germany) as titrating solution. The mixture was calibrated against pure water.

The volume of solvents used in Karl Fischer titration was 5.0 and 1.0 mL depending on the expected water content in solvents.

The water content (ω_{H_2O}) of sample was calculated using the following equation:

$$\omega_{H_2O} = \frac{V_{KF} \cdot W_{eq} \cdot 100}{W_{sample}} \quad (2)$$

where V_{KF} is the consumption of titrant (mL), W_{eq} is the titer of titrant (mg H_2O/mL) and W_{sample} is the weight of sample (mg).

2.2.8. PXRD analysis

Samples were analyzed with a Bruker D8 Advance powder X-ray diffractometer (Bruker AXS, Karlsruhe, Germany), equipped with a PSD *LYNXEYE* detector. Measurements were performed with CuK radiation (1.54180 Å) at room temperature. The following conditions were used: step-scan mode with a step size of 0.02°; scan

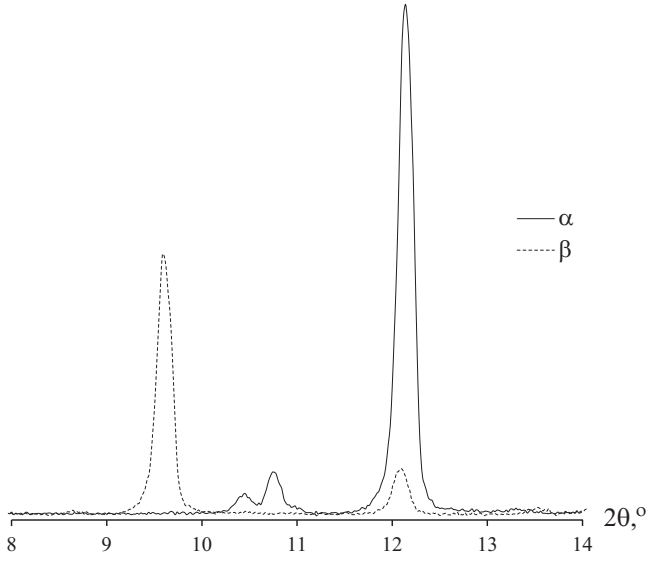

Fig. 2. Powder X-ray diffraction patterns of α and β tegafur.

speed: 0.2°/min; 2θ range: 8.0–13°; voltage: 40 kV; current: 40 mA; divergence slit: 0.6 mm; anti-scattering slit: 8 mm.

Powder samples were packed into glass holders with a weight capacity of ~150 mg and pressed by a clean glass slide to ensure coplanarity of the powder surface with the surface of the holder. The obtained diffractograms were analyzed with DIFFRAC.EVA (ver. 2.0) software.

2.2.9. Quantitative analysis of α and β polymorph mixtures

Majority of peaks in PXRD patterns of α and β tegafur is overlapping, therefore only the most intensive, non-overlapping peaks are used for quantification (see Fig. 2).

The peaks at 2θ = 12.1° for α tegafur and at 9.6° for β tegafur were used for quantification with the individual peak area method. The α tegafur peak at 2θ = 12.1° was used for quantification even though it is overlapping with a peak of β tegafur, because it is twice as intensive as the rest of the peaks for α tegafur and, thus, introduces the smallest error in quantitative analysis, even if the area of β tegafur peak at 2θ = 12.1° is subtracted from the total of mixture peak areas.

The areas of the plotted peaks were calculated by using the computer program *TOPAS 3*, and weight fractions of β form were calculated by using the Eqs. (3–5):

$$\omega_{\beta;\%} = \frac{S_{\text{mixture};9,6}}{S_{\beta;9,6}} \times 100\% \quad (3)$$

$$\omega_{\alpha;\%} = \left(\frac{S_{\text{mixture};12,1} - \left(S_{\text{mixture};9,6} \times S_{\beta;12,1}/S_{\beta;9,6} \right)}{S_{\alpha;12,1}} \right) \times 100\% \quad (4)$$

$$\omega_{\beta\,\text{norm};\%} = \frac{\omega_{\beta;\%}}{\omega_{\beta;\%} + \omega_{\alpha;\%}} \times 100\% \quad (5)$$

where $\omega_{\beta;\%}$, $\omega_{\alpha;\%}$ are weight fractions of α and β forms; $S_{\beta;9.6}$, $S_{\beta;12.1}$ are peak plot areas for pure β form at 9.6° and 12.1°; $S_{\text{mixture};9.6}$, $S_{\text{mixture};12.1}$ are the peak plot areas at 9.6° and 12.1° for the analyzed mixture; $S_{\alpha;12,1}$ is the peak plot area of pure α form at 12.1°, and $\omega_{\beta\,\text{norm};\%}$ is a normalized weight fraction of the β form.

Table 1
Conversion degrees of 0.5% and 0.1% β tegafur mixture in α tegafur and pure α tegafur during the grinding (5 min at 20 °C with 15 Hz shaking frequency), depending on the used solvent additive.

Solvent	$\omega_{\beta\ \text{after grinding}}$ (%)		
$\omega_{\beta\ \text{initial}}$ (%)	0.5% β	0.1% β	α
Methanol [HBD]	100	82	<3
1,2-Dichloroethane [AP]	100	72	92
n-Propyl acetate [AP]	100	37	–
Tetrahydrofuran [EPD]	100	15	–
Ethyl acetate [AP]	100	13	13
Acetonitrile [AP]	100	6	8
n-Butanol [HBD]	100	3	<3
Acetone [AP]	100	<3	–
Benzyl alcohol [AA]	95	52	25
n-Butyl acetate [AP]	92		–
Ethanol [HBD]	86		–
Toluene [AA]	83		6
n-Pentanol [HBD]	57		–
n-Propanol [HBD]	57		–
Chloroform	44		42
2-Propanol [HBD]	31		–
n-Heptanol [HBD]	30		–

AP, aprotic polar; AA, aromatic apolar; EPD, electron pair donor; HBD, hydrogen bond donors.

3. Results and discussion

3.1. Solvent effect on the degree of phase conversion during grinding

Initially conversion degrees for samples containing 0.5% of β tegafur in α and β tegafur mixture were determined, and a complete conversion to β tegafur occurred when *n*-propyl acetate, acetonitrile, ethyl acetate, 1,2-dichloroethane, acetone, tetrahydrofuran, *n*-butanol and methanol were used as additives (see Table 1). To find out, which of these solvents promotes the α conversion to β tegafur the most, samples containing 0.1% of β tegafur in α and β tegafur mixture were examined. None of the solvents promoted complete conversion to β tegafur in the case of samples containing 0.1% of β tegafur in α and β tegafur mixture with current grinding conditions. Experiments with pure α tegafur were also performed, to find out if there might be any solvents that promote phase transition without any β tegafur seeds in the sample.

Our quantitative composition calculation method was not suitable for quantifying phases with weight fraction below 3% after the grinding, so the results for samples, where β tegafur peak was detected, but was not large enough to quantify, are given as "<3%".

The most complete phase transition to β tegafur, for samples containing 0.1% of β tegafur, occurred when methanol or 1,2-dichloroethane additive was used – the weight fraction for β tegafur increased during grinding from 0.1% to 82% and 72%, respectively. The most marked decrease in conversion degree between samples with the initial β tegafur content of 0.5% and 0.1% occurred in those cases, when acetone or *n*-butanol additive was used – complete conversion was detected when samples with the initial β tegafur content of 0.5% were ground, but when 0.1% mixture was ground, only a slight increase of β tegafur content was detected (less than 5%).

As we can see, a 1,2-dichloroethane additive promotes almost complete phase transition in all cases, even when pure α tegafur is used. Similar situation can be observed when chloroform additive is added, only then the conversion proceeds by ~40%. This could be related to a solvent structure that promotes only one polymorphic form regardless of whether the seed crystals are added to a sample or not. Conversion of pure α tegafur to β tegafur occurs due to solvent structure factors, similar to those in crystallization (Allesø et al., 2008). Hydrogen bond donor solvents do not promote phase

Table 2
Solubility of α tegafur, solvent vapor sorption on the α and β tegafur, and phase transition rates depending on the used solvent.

Solvents	Solubility (g/100 mL)	Sorption ($\times 10^{-3}$ mol/g)		k (days^{-1})
		α	β	
Tetrahydrofuran [EPD]	7.46	32.9	41.8	1.878
Acetonitrile [AP]	6.07	14.2	9.5	0.194
Acetone [AP]	5.11	18.4	69.5	2.167
Methanol [HBD]	4.86	2.5	2.3	0.073
Ethyl acetate [AP]	2.98	7.6	5.8	0.042
Ethanol [HBD]	2.78	0.75	3.3	0.019
1,2-Dichloroethane [AP]	2.43	8.4	4.6	0.049
n-Propyl acetate [AP]	1.62	0.90	0.62	–
n-Butanol [HBD]	1.16	1.5	1.9	0.015
n-Pentanol [HBD]	1.15	0.75	1.5	0.007
n-Butyl acetate [AP]	1.09	1.0	0.75	0.004
n-Propanol [HBD]	0.83	0.58	1.3	0.058
2-Propanol [HBD]	0.69	2.5	1.5	0.007
n-Heptanol [HBD]	0.59	2.5	1.1	0.007
Toluene [AA]	0.42	0.71	1.3	0.017
Chloroform [AP0,0 EPD0,0 HBD]	0.20	2.7	2.5	0.007
Benzyl alcohol [AA]	–	1.2	1.2	0.033

AP, aprotic polar; AA, aromatic apolar; EPD, electron pair donor; HBD, hydrogen bond donors.

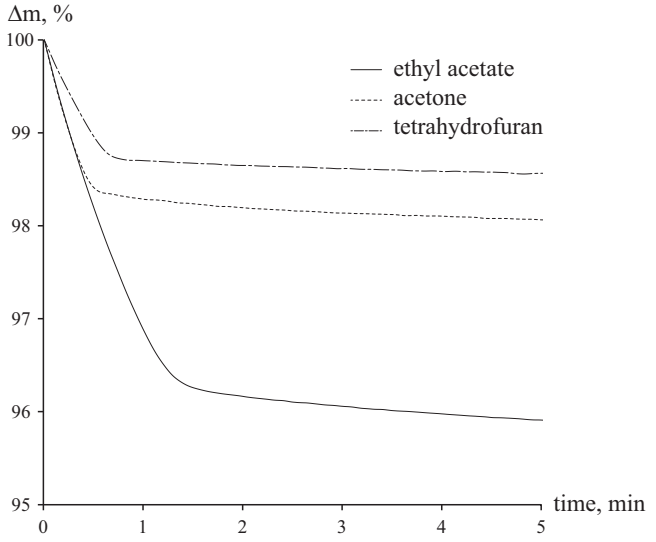

Fig. 3. Ethyl acetate, acetone and tetrahydrofuran desorption curves from α tegafur.

transition of pure α tegafur, but both investigated aromatic aprotic solvents promote phase transition of pure α tegafur, even though they do not ensure a complete phase transition for samples with 0.5% β tegafur additive.

Changes in conversion degrees are not proportional from one solvent to another when the initial weight fraction of β tegafur changes from 0.5% to 0.1%. For example, when acetone additive is added to a sample, conversion degree changes form 100% to less than 3%, but when methanol additive is added, conversion degree changes form 100% to 82%. There is no clear understanding about the causes of these differences, but it could be related to solubility or dissolution rates of tegafur in the investigated solvents, or simply due to structural peculiarities of each solvent.

To ensure that phase transition is not stimulated by the water impurity in solvents, Karl Fischer titration was performed for all used solvents, and it was determined that water amount in the solvents did not correlate with the conversion degree to β tegafur.

The rest of the experiments were performed to find out is there any relationship between conversion degree of α tegafur to β tegafur, solubility of α tegafur, solvent sorption and desorption behavior on α and β tegafur.

3.2. Determination of α tegafur solubility in several solvents

Solubility of α tegafur in a series of solvents (see Table 2) was determined to clarify, whether the conversion degree of tegafur depends on α tegafur solubility in a particular solvent. Solubility was determined only for α tegafur was, because in the investigated samples α tegafur was present in large excess, and also the solubility of α and β tegafur differ minimally at 30 °C, because it is close to the polymorphic transition temperature (~36 °C) (Uchida et al., 1993). Solubility of α tegafur in benzyl alcohol could not be determined, because this solvent did not evaporate completely and formed a thick paste of tegafur and some decomposition products.

It is evident that α tegafur dissolves better in polar solvents, and its solubility in nonpolar solvents is very low because of the lack of possibilities to form hydrogen bonds between solvent and tegafur molecules. From solubility data we can see that there is no relation between the type of solvents used (aprotic polar, electron pair donors or hydrogen bond donors) and solubility of α tegafur, except that solubilities in aromatic apolar solvents were very low.

Experimental data strongly suggests that the conversion degree of α tegafur to β tegafur mainly depends on solubility of α tegafur in the particular solvent – upon increase of solubility, the conversion degree also increases. Most likely this is due to the fact that phase transition occurs in solution, which is formed on particle surface. The outer layer of tegafur particles dissolves in the solvent, and seed crystals of β tegafur encourage crystallization of the thermodynamically stable polymorph.

3.3. Solvent sorption studies

From experimental data it can be seen (see Table 2) that the solvent sorption on α and β tegafur did not differ significantly, and the highest sorption was observed for solvents, in which α tegafur solubility was the highest. The greatest sorption was observed for tetrahydrofuran, acetone and acetonitrile, but the lowest sorption was with alcohols and toluene. The general trend is that aprotic polar solvents with small molecules were better absorbed on tegafur surface, and that could be related to the fact that small molecules with electron donor groups are suitable for hydrogen bond formation with the NH moiety of tegafur, thus promoting an interaction between solvent and tegafur. In all cases except acetone, sorption of aprotic polar solvents on α tegafur was greater than sorption on β tegafur, and in most cases hydrogen bond donors absorbed better on β tegafur. Aromatic non-polar solvents exhibited low sorption potential, and the differences between sorption on α and β tegafur were minor.

3.4. Solvent desorption studies

As can be seen from ethyl acetate, acetone and tetrahydrofuran desorption curves (see Fig. 3), desorption occurs in two steps – at the beginning part of the solvent is desorbed from the surface of tegafur, and afterwards desorption progresses throughout the volume of tegafur particles.

Solvent desorption from the surface can be associated with the linear part of desorption curve. The next stage, after the initial rapid loss of solvent, appears exponential and involves solvent desorption from the entire volume. Solvent surface desorption rate was compared by using the average desorption rate equation

$$\alpha = \frac{dm}{dt} \quad (6)$$

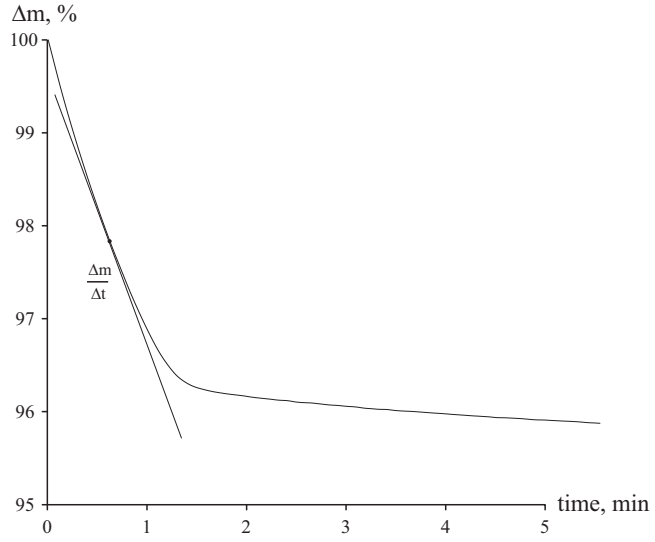

Fig. 4. Example of desorption rate calculation.

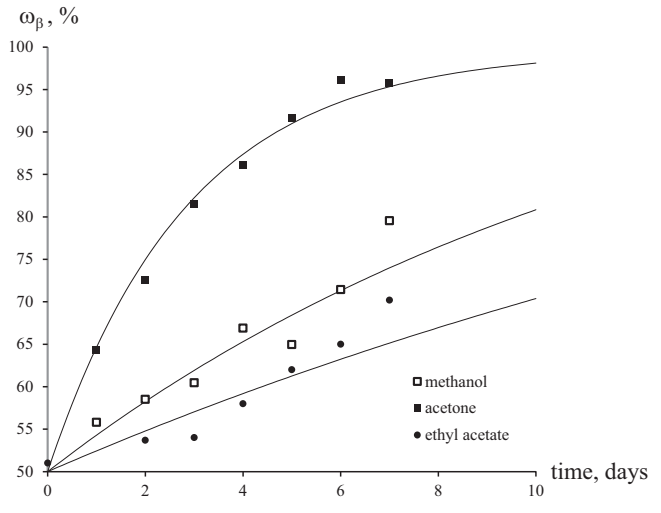

Fig. 5. β Tegafur weight fraction changes during sample exposure to 95% relative vapor pressure of methanol, acetone and ethyl acetate.

where α is desorption rate, m is sample mass, and t is time. An obstacle to the determination of desorption rate was the posed by the observation that the beginning of desorption curve cannot be used due to a possible desorption delay. The best way for avoiding this problem could be to calculate desorption rate in the middle of a desorption process, using a middle point calculated from the sample mass before and after desorption, thereby preventing errors stemming from desorption delay and from imprecise end point determination (see Fig. 4). Desorption rates for both tegafur polymorphs are shown in Table 3. Most rapid desorption from α tegafur was observed in the case of tetrahydrofuran, acetone, ethyl acetate and acetonitrile – the same solvents that sorbed the most on α tegafur. The desorption rates of these four solvents from β tegafur were surprising, especially because sorption of tetrahydrofuran and acetone on β tegafur is even greater than on α tegafur. One of the possible interpretations on this phenomenon could be that α and β tegafur surfaces interact differently with the investigated solvents. A similar situation was observed with *n*-butyl acetate, but in that case the desorption rate was greater for β tegafur. Desorption rates of toluene, *n*-propanol, *n*-butanol and chloroform did not differ significantly from α to β tegafur.

3.5. Solvent vapor effect on phase transition

It is known that solvent vapors accelerate phase transition (Petkune et al., 2012; Trask et al., 2004), however it is not known if the effect on solid phase transition is the same for solvent vapors and liquid solvent additives. For this purpose an atmosphere of solvent vapor with 95% relative pressure was created by using the same solvents as in the previous experiments. Phase transition kinetic curves were recorded by using PXRD, and transition rates were calculated as described in Petkune et al. (2012) (see Fig. 5).

Saturated solvent vapor atmosphere was not used to prevent condensation and sample wetting with a condensed solvent. Mixture with a weight ratio of 1:1 was used because no phase transition was observed for samples with only 0.5% of β tegafur.

Phase transition rates for samples exposed to solvent vapor atmosphere with a 95% relative pressure are given in Table 2. The general tendency matches the observations from solubility and sorption studies – aprotic polar solvents with the smallest molecules are the best promoters of this phase transition. Sorption data indicates that phase transition is faster when solvent sorption on the thermodynamically stable β tegafur is greater than that on α tegafur.

In the case of ethyl acetate and *n*-propyl acetate there was a very high conversion degree, despite the low sorption and phase transition rates in samples exposed to these solvents at 95% relative pressure, indicating that the phase transition during the grinding procedure is affected not just by solvents in gaseous state, but also in their liquid state.

Table 3
Solvent desorption rate from α and β tegafur.

Solvent	dm/dt (μg/min)	
	α	β
Tetrahydrofuran [EPD0,0 AP]	958	36
Acetone [AP]	885	8
Ethyl acetate [AP]	612	23
Acetonitrile [AP]	437	27
Toluene [AA]	239	261
n-Propanol [HBD]	118	135
Chloroform [AP]	38	76
n-Butyl acetate [AP]	9	129
n-Butanol [HBD]	4	7

AP, aprotic polar; AA, aromatic apolar; EPD, electron pair donor; HBD, hydrogen bond donors.

4. Conclusions

The results of this study demonstrate that the conversion degree of metastable α tegafur to the thermodynamically stable β tegafur upon a grinding with solvent additive is highly dependent on the solvent used. The most complete phase transition to β tegafur occurs when methanol or 1,2-dichloroethane additive is used. The conversion degree of α tegafur to β tegafur mainly depends on the solubility of α tegafur in the relevant solvent, and the conversion degree to β tegafur is higher in those solvents, in which the solubility of α tegafur is higher. The conversion degree of α tegafur to β tegafur does not correlate with the presence of trace water in the investigated solvents.

Phase transition dynamics of α tegafur to β tegafur is in a good agreement for samples ground in ball mill with solvent additive and samples,that were exposed to 95% solvent relative vapor pressure. The highest solvent vapor sorption is observed for solvents, in which the solubility of α tegafur is the highest. Solvent sorption on both of the tegafur polymorphs does not differ significantly. The highest desorption rate from α tegafur is observed for solvents

that were best sorbed – tetrahydrofuran, acetone, ethyl acetate and acetonitrile, but desorption of these solvents from β tegafur is between 15 and 100 times slower.

Acknowledgements

The authors are grateful to the European Social Foundation for financial support and to JSC *Grindeks* for supplying α and β polymorphic forms of tegafur.

References

Actiņš, A., Beļakovs, S., Orola, L., Veidis, M.V., 2006. Molecular and crystal structure of novel form of tegafur. Latvijas Ķīmijas Žurnāls 2, 120–124.
Allesø, M., van den Berg, F., Cornett, C., Jørgensen, F.S., Halling Sørensen, B., de Diego, H.L., Hovgaard, L., Aaltonen, J., Rantanen, J., 2008. Solvent diversity in polymorph screening. J. Pharm. Sci. 97, 2145–2159.
Boldyrev, V.V., 2006. Mechanochemistry and mechanical activation of solids. Russ. Chem. Rev. 75, 177–189.
Brittain, H.G., 2009. Polymorp. Pharm. Solids, 427.
Chieng, N., Zujovic, Z., Bowmaker, G., Rades, T., Saville, D., 2006. Effect of milling conditions on the solid-state conversion of ranitidine hydrochloride form 1. Int. J. Pharm. 327, 36–44.
Hilfiker, R., 2006. Polymorphism in the pharmaceutical industry, 433.
Lin, S.-Y., Cheng, W.-T., Wang, S.-L., 2006. Thermodynamic and kinetic characterization of polymorphic transformation of famotidine during grinding. Int. J. Pharm. 318, 86–91.
Needham, F., Faber, J., Fawcett, T.G., Olson, D.H., 2006. X-ray powder diffraction analysis of tegafur. Powder Diffr. 21, 245.
Otsuka, M., Kaneniwa, N., 1986. Effect of seed crystals on solid-state transformation of polymorphs of chloramphenicol palmitate during grinding. J. Pharm. Sci. 75, 506–511.
Petkune, S., Bobrovs, R., Actiņš, A., 2011. Determination of micro amounts of β tegafur in the α and β polymorph mixture by powder X ray diffractometric analysis. J. Pharm. Pharmacol. 63, 1136–1140.
Petkune, S., Bobrovs, R., Actiņš, A., 2012. Organic solvents vapor pressure and relative humidity effects on the phase transition rate of α and β forms of tegafur. Pharm. Dev. Technol. 17, 625–631.
Shan, N., Toda, F., Jones, W., 2002. Mechanochemistry and co-crystal formation: effect of solvent on reaction kinetics. Chem. Commun. 2002, 2372–2373.
Trask, A.V., Motherwell, W.D.S., Jones, W., 2004. Solvent-drop grinding: green polymorph control of cocrystallisation. Chem. Commun. (Cambridge, England), 890–891.
Trask, A.V., Shan, N., Motherwell, W.D.S., Jones, W., Feng, S., Tan, R.B.H., Carpenter, K.J., 2005. Selective polymorph transformation via solvent-drop grinding. Chem. Commun. 2005, 880–882.
Uchida, T., Yonemochi, E., Oguchi, T., Terada, K., Yamamoto, K., Nakai, Y., 1993. Polymorphism of tegafur: physico-chemical properties of four polymorphs. Chem. Pharm. Bull. 41, 1632–1635.
Vippagunta, S.R., Brittain, H.G., Grant, D.J.W., 2001. Crystalline solids. Adv. Drug Deliv. Rev. 48, 3–26.

International Journal of Pharmaceutics 457 (2013) 110–117

Contents lists available at ScienceDirect

International Journal of Pharmaceutics

journal homepage: www.elsevier.com/locate/ijpharm

Organic solvent desorption from two tegafur polymorphs

Raitis Bobrovs*, Andris Actiņš

University of Latvia, The Faculty of Chemistry, Kr. Valdemara iela 48, Riga LV-1013, Latvia

ARTICLE INFO

Article history:
Received 25 June 2013
Received in revised form 9 September 2013
Accepted 15 September 2013
Available online xxx

Keywords:
Tegafur
Polymorphs
Solvent desorption kinetics
Solvent–surface interaction
Solvent vapor
Solvent monolayer

ABSTRACT

Desorption behavior of 8 different solvents from α and β tegafur (5-fluoro-1-(tetrahydro-2-furyl)uracil) has been studied in this work. Solvent desorption from samples stored at 95% and 50% relative solvent vapor pressure was studied in isothermal conditions at 30 °C. The results of this study demonstrated that: solvent desorption rate did not differ significantly for both phases; solvent desorption in all cases occurred faster from samples with the largest particle size; and solvent desorption in most cases occurred in two steps. Structure differences and their surface properties were not of great importance on the solvent desorption rates because the main factor affecting desorption rate was sample particle size and sample morphology. Inspection of the structure packing showed that solvent desorption rate and amount of solvent adsorbed were mainly affected by surface molecule arrangement and ability to form short contacts between solvent molecule electron donor groups and freely accessible tegafur tetrahydrofuran group hydrogens, as well as between solvents molecule proton donor groups and fluorouracil ring carbonyl and fluoro groups. Solvent desorption rates of acetone, acetonitrile, ethyl acetate and tetrahydrofuran multilayers from α and β tegafur were approximately 30 times higher than those of solvent monolayers. Scanning electron micrographs showed that sample storage in solvent vapor atmosphere promotes small tegafur particles recrystallization to larger particles.

1. Introduction

Pharmaceutical compounds are mostly produced in defined crystalline forms that are commonly crystallized from solutions. Most of the crystalline pharmaceutical ingredients possess the ability to form more than one crystalline form, and this property of substances is called polymorphism. Polymorphs usually have different, precisely known dissolution rates and bioavailability, but crystal size and shape can affect these properties. Therefore, the crystal shape is monitored during drug manufacturing process and a lot of work in the area of crystal engineering has been devoted to controlling the crystal habit and determination of crystal properties (Brittain, 2009; Hilfiker, 2006; Vippagunta et al., 2001).

The solvent used for the crystallization of an organic compound can have a large effect on the resulting crystal shape and morphology (Lahav and Leiserowitz, 2001; Schöll et al., 2006; Stoica et al., 2004; Weissbuch et al., 2005); therefore solvent effects on crystal surface have been comprehensively studied, and two theories about solvent and surface interaction effects on crystal growth have been developed. One of them suggests that favorable interactions between solvent and specific crystal faces leads to reduced interfacial tension, causing phase transitions and crystal growth at specific directions (Bennema and Gilmer, 1973; Bourne and Davey, 1976). The second theory postulates that solvent adsorption on specific faces inhibits their growth as removal of adsorbed solvent creates an additional energy barrier for continued growth (Weissbuch et al., 1991). Most of the research regarding solvent effects on surfaces has been performed with solutions, but an identical situation should occur in solvent vapor atmosphere as well.

In our previous works we explored the solvent vapor effects on phase transition (Petkune et al., 2012) and solvent effects on phase transition during grinding (Bobrovs and Actiņš, 2012; Petkune et al., 2011), but no information about the exact phase transition mechanism was gained. In this research we discuss the nature of solvent and surface interaction using data from solvent desorption studies.

Tegafur (5-fluoro-1-(tetrahydro-2-furyl)-uracil) (see Fig. 1) α and β modifications were selected as a model material in this study. Tegafur is an antitumor agent widely used in the treatment of various malignancies, particularly gastrointestinal and breast cancers (Uchida et al., 1993). Over years, the α, β, γ, δ and ε forms of tegafur have been reported (Actiņš et al., 2006; Needham et al., 2006; Uchida et al., 1993), but only the α and β modifications are used for therapeutic purposes.

2. Materials and methods

2.1. Materials

Commercial samples of α and β tegafur were supplied by JSC Grindeks (Latvia).

* Corresponding author. Tel.: +371 67372576.
E-mail addresses: raitis.bobrovs@lu.lv, raitis.bobrovs@gmail.com (R. Bobrovs).

0378-5173/$ – see front matter © 2013 Elsevier B.V. All rights reserved.
http://dx.doi.org/10.1016/j.ijpharm.2013.09.008

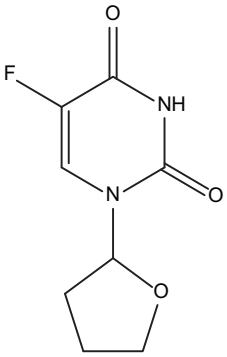

Fig. 1. Molecular structure of tegafur (5-fluoro-1-(tetrahydro-2-furyl)-uracil).

The solvents (methanol, ethanol, ethyl acetate, *n*-butyl acetate, acetone, tetrahydrofuran, acetonitrile and toluene) were supplied by Merck (Germany) and used without further purification. All of the reagents used were certified >98% pure.

2.2. Methods

2.2.1. Sample preparation and fractionation

A sample (~6 g) of α tegafur was ground in a mortar for 3 min and then gradually sieved through sieves with mesh sizes of 150, 75 and 40 μm. Three fractions of α tegafur (~2 g each) were obtained with the following particle sizes: 150–75 μm; 75–40 μm; and less than 40 μm. The same procedure was repeated for β tegafur.

2.2.2. Obtaining 95% and 50% relative solvent vapor pressure

To obtain the relative solvent vapor pressure of 95% and 50%, methanol and ethanol solutions in glycerol were prepared, and acetone, acetonitrile, ethyl acetate, *n*-butyl acetate, tetrahydrofuran, and toluene solutions in dimethyl sulphoxide were prepared according to the Raoult's law (Eq. (1))

$$X = \frac{p}{p_0} = \frac{n}{n_0 + n} \quad (1)$$

where X is the solvent mole fraction in solution; p_0 is the vapor pressure of pure solvent; p is the partial solvent vapor pressure over the solution; n represents the amount of used solvent in the solution; n_0 is the moles of glycerol or dimethyl sulphoxide in the solution. Desiccators with the prepared solutions were placed in an air thermostat (Memmert, Universal Oven UFB-500) at 30.0 ± 0.5 °C 48 h prior to the sample insertion.

2.2.3. Solvent desorption studies

Samples (~50 mg) of each fraction were placed into separate 2 mL vials and positioned in the prethermostated desiccators with the prepared solvent mixtures for at least 72 h to obtain completely solvent-saturated samples.

The solvent-saturated samples were quickly placed (in less than 20 s) in aluminum sample pan, and solvent desorption was recorded using a *SII TG/DTA6300 EXSTAR6000* (Japan) instrument with open aluminum sample pans having internal diameter of 5 mm and height of 2.5 mm, under dry nitrogen atmosphere with flow rate of 250 mL/min in isothermal conditions at 30 °C. It was observed that desorption rate was highly dependent on mass of the sample; therefore samples with equal mass were used. For fast weighting of the equal amount of sample the sample holder each time was filled up to the edge. The following technique allowed to prepare the samples with mass 30 ± 2 mg and to reduce the time of weighing. If sample weight after this procedure were out of the range, procedure was repeated with fresh solvent-saturated sample. During the experiment mass of the sample was recorded every 0.5 s.

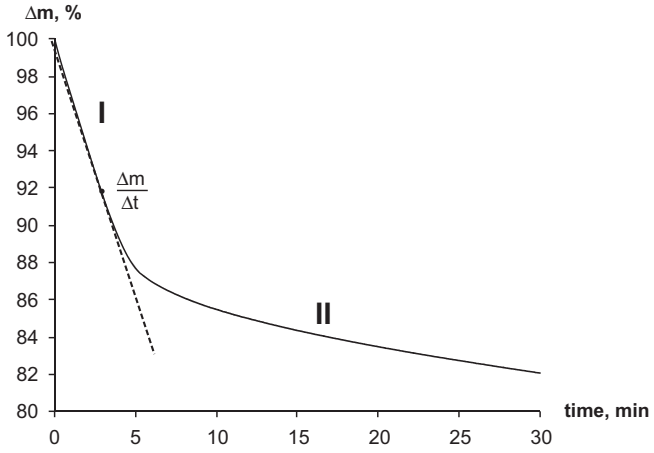

Fig. 2. Acetonitrile desorption curve from β tegafur with particle size 40–75 μm.

2.2.4. Determination of surface area

Surface area was determined by a modified chromatograph "Hrom 3", detecting the amount of argon involved in a monolayer adsorption–desorption process.

2.2.5. Calculations of crystal morphology

Predictions of crystal morphology from structure data were done based on Bravais, Friedel, Donnay and Harker (BFDH) theory using Mercury 3.0 (Macrae et al., 2008). Crystal structures of both polymorphs were retrieved from the Cambridge Structural Database (refcodes are BIPDEJ for α tegafur and BIPDEJ02 for β tegafur).

2.2.6. Sample morphology studies

Particle morphology of β tegafur fraction with particle size of less than 40 μm before and after storage in 95% relative solvent (acetone) vapor pressure for 72 h was analyzed on a scanning electron microscope *Hitachi S4800 SEM* (Japan) at an accelerating voltage of 2.0 kV.

3. Results and discussion

Desorption process of several solvents from both polymorphic forms of tegafur was examined to compare solvent–tegafur surface interaction behavior. The solvent desorption experiment indicated that in most cases desorption occurred in two steps (see Fig. 2). There is no clear understanding on this phenomenon, but it could be a case of classical monolayer and multilayer (with possible capillary condensation) desorption. Solvent molecule desorption from the top solvent multilayers can be associated with the beginning of desorption curve (part I in Fig. 2), where rapid sample mass decrease was detected. The next stage, after the initial rapid loss of solvent, in most cases appeared exponential and involved solvent monolayer desorption (part II in Fig. 2). Following experiments were performed to get some understanding about these processes.

3.1. Surface area and relative sample surface coverage

Amount of each solvent necessary to form solvent monolayer was calculated using determined surface area data (see Table 1), adsorbed solvent mass and solvent molecule dimensions. Using mass of solvent, adsorbed during sample storage in 95% relative solvent vapor pressure, and theoretical mass of solvent in monolayer,

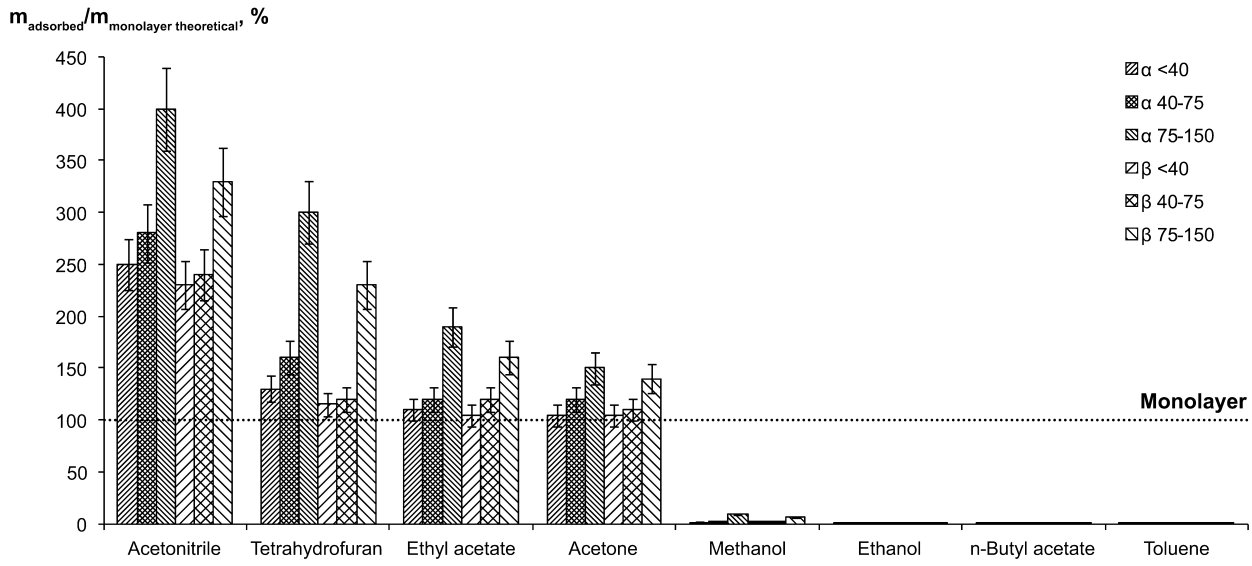

Fig. 3. Relative sample surface coverage with used solvents in 30 °C, for samples stored in 95% relative solvent vapor pressure ($m_{adsorbed}/m_{theoretical}$).

sample surface coverage for each sample was calculated. These results are given in Fig. 3.

If we take a look at sample surface areas (Table 1), it can be seen that the surface areas of samples with particle size 40–75 μm and less than 40 μm were almost the same for both polymorphs. SEM examinations shows distinct differences in particle size distribution for both fractions, therefore similar surface areas for both fractions most likely are due to differences in bulk density – fraction with smaller particles forms more dense sample, but fraction with larger particles forms less dense sample. These changes in the sample density affects the effective/accessible surface area of the sample and the greater bulk density for fraction with particle size less than 40 μm causes the apparent reduction of the surface area in the experimental measurement.

From relative sample surface coverage data we see that the amount of acetonitrile, tetrahydrofuran, ethyl acetate and acetone adsorbed on the tegafur surface is enough to form at least solvent monolayer and that the decrease of sample surface area increases the relative sample surface coverage. These calculations shows that amount of acetonitrile adsorbed on the surface is enough to form up to 4 solvent molecular layers in the case of 75–150 μm α tegafur sample, but adsorbed methanol amount is sufficient to cover up to 10% of the sample surface (for samples with particle size 75–150 μm), while adsorbed toluene, ethanol and *n*-butyl acetate covers less than 3% of the sample surface.

The decrease of particle size from 75–150 μm to 40–75 μm increases the relative sample surface coverage by about 20–40%, but particle size decrease from 40–75 μm to less than 40 μm increases the relative sample surface coverage by about 5–15%. We believe that the observation that less solvent multilayers formed on the smaller particles if compared to the larger particles, is related to previously mentioned differences in the bulk densities.

Table 1
Surface areas of α and β tegafur samples depending on particle size.

Polymorph	Particle size (μm)	Surface area (m^2/g)
α	<40	12.4
	40–75	12.2
	75–150	5.9
β	<40	14.8
	40–75	12.8
	75–150	9.2

Sample with the smallest particles (less than 40 μm) has higher bulk density then the rest fractions and therefore effective/accessible surface area of this sample is lower than it would be if all the samples had the same density. It is also possible that such results could be due to the effective surface area decrease during the solvent adsorption process because of sample recrystallization and/or solvent sorption on the previous solvent layers; especially for sample with particle size less than 40 μm.

3.2. Solvent desorption rate

From solvent desorption curves desorption rate of used solvents can be calculated using equation:

$$\alpha = \frac{dm}{dt} \quad (2)$$

where α is desorption rate, m is sample mass, and t is time. Solvent desorption rates for all solvents monolayers were calculated from data points obtained 15 min after experiment beginning, but solvent desorption rate of the first step (solvent multilayer) for solvents which formed solvent multilayers – acetone, acetonitrile, ethyl acetate and tetrahydrofuran – was calculated by using a middle point from the sample mass before and after the desorption (shown in Fig. 2), thereby preventing errors stemming from desorption delay and from imprecise end point determination. Solvent desorption rates depending on tegafur polymorphic form, particle size and the selected solvent for samples stored at 95% relative solvent vapor pressure are summarized in Fig. 4 (monolayer desorption in Fig. 4A and multilayer desorption in Fig. 4B). No acetonitrile and tetrahydrofuran monolayer desorption from α and β tegafur were observed.

The general trend was that desorption rates increased with increasing particle size and there was no distinct difference between desorption rates from both polymorphs. Faster desorption from the samples with the larger particles was due to easier solvent removal from the sample surface, which is favored by large volume between particles where solvent can diffuse more easily if compared to sample with smaller particles. A lack of major changes between both polymorphs indicated that differences in crystal structure and surface properties had no great importance on the solvent desorption rates, therefore the main factor affecting desorption rate is sample particle size and morphology. Difference in multilayer solvents desorption rates from samples with particle

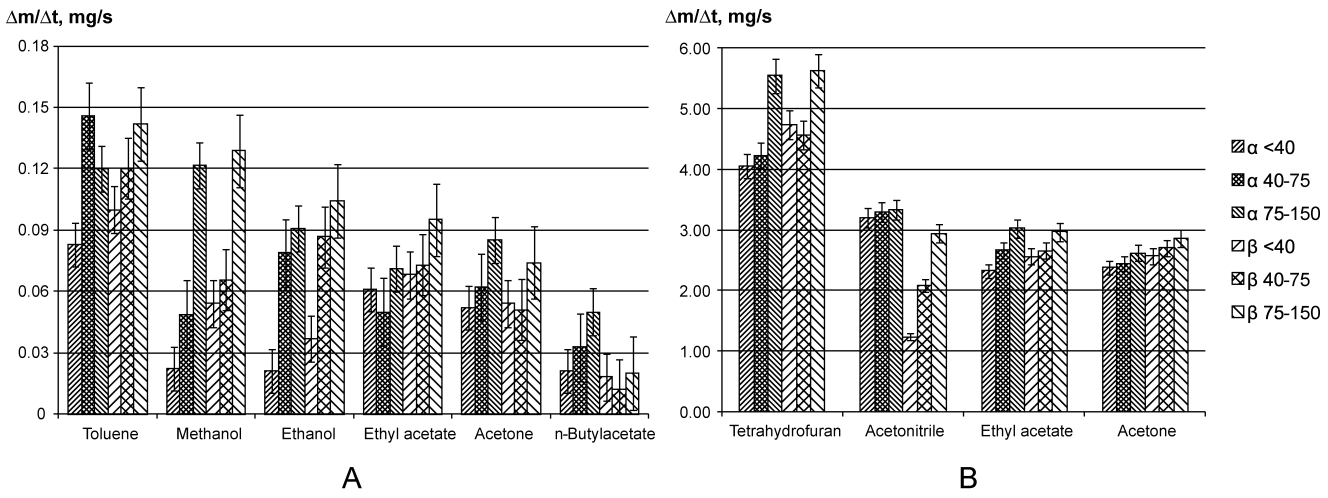

Fig. 4. Desorption rates of (A) acetone, ethyl acetate, *n*-butyl acetate, ethanol, methanol and toluene monolayers; (B) acetone, acetonitrile, ethyl acetate and tetrahydrofuran multilayers; depending on tegafur polymorphic form and particle size.

size 40–75 μm and less than 40 μm in most cases was considerably lower than those for multilayer solvent desorption rates from samples with particle size 75 to 150 μm and 40 to 75 μm just like the surface areas of the analyzed samples.

Solvent desorption rates from α and β tegafur samples showed that desorption rates of acetone, acetonitrile, ethyl acetate and tetrahydrofuran from solvent multilayers were approximately 30 times higher than those from solvent monolayers. Further experiments with samples stored in 50% relative solvent vapor pressure confirmed that the higher desorption rates for tetrahydrofuran, acetonitrile, acetone and ethyl acetate most likely were due to multilayer sorption. Thus, at 95% relative solvent vapor pressure the sample surface was covered with tetrahydrofuran, acetonitrile, acetone and ethyl acetate as molecular multilayer, and the desorption rates for molecules situated at the higher layers were much higher than for molecules in direct contact with the surface. However, if samples were stored in the same solvents at 50% relative solvent vapor pressure, then monolayer solvent sorption dominated and only partial surface saturation above the monolayer occurred. This information was also confirmed by sorption results, as the amount of adsorbed solvent at 95% and 50% relative solvent vapor pressure differed 1.5–3 times for tetrahydrofuran, acetonitrile, acetone and ethyl acetate. This suggests that at 95% relative solvent vapor pressure of acetone, acetonitrile, ethyl acetate and tetrahydrofuran, the solvent sorption noticeably exceeded monolayer coverage, but for *n*-butyl acetate, ethanol, methanol and toluene the sorption on the tegafur surface was significantly below monolayer coverage.

Schematically solvent desorption process from the surface and its effect on the desorption kinetics are illustrated in Fig. 5A shows the solvent desorption process, the solvent molecules in monolayer having a different interaction energy than the rest of the solvent molecules (multilayer molecules), and two separate solvent desorption phases were observed (solvent molecules with higher interaction energy than the rest of the molecules are schematically represented by filled circles). From the solvents used, acetone and ethyl acetate exhibited such a desorption behavior. Desorption of acetonitrile and tetrahydrofuran differed from the rest of the solvents by the absence of the monolayer desorption part (see Fig. 5B). This means that all of the adsorbed solvent molecules were energetically equal and the ground layer solvent molecule interaction with sample surface was not significantly stronger than interaction between the solvent molecules themselves. Our assumption was that this phenomenon could be related to solvent ability to form hydrogen bonds and other effective intermolecular interactions between solvent and surface, as well as between two solvent molecules. Ethanol, *n*-butyl acetate, methanol, and toluene desorption behavior is schematically illustrated in Fig. 5C. These solvents were desorbed in one step like in the previously described case; with the difference that in this case it was a monolayer desorption.

The effect of the particle size and solvent vapor relative pressure on desorption curve are summarized in Fig. 6, by illustrating that solvent relative vapor pressure affects only the amount of solvent adsorbed on the surface (Fig. 6A), but particle size affects the solvent desorption rate, if the same amount of solvent was adsorbed (Fig. 6B).

3.3. Solvent–surface interaction

Crystal morphology for both polymorphs was predicted in order to understand on which of the crystal faces most of the solvent

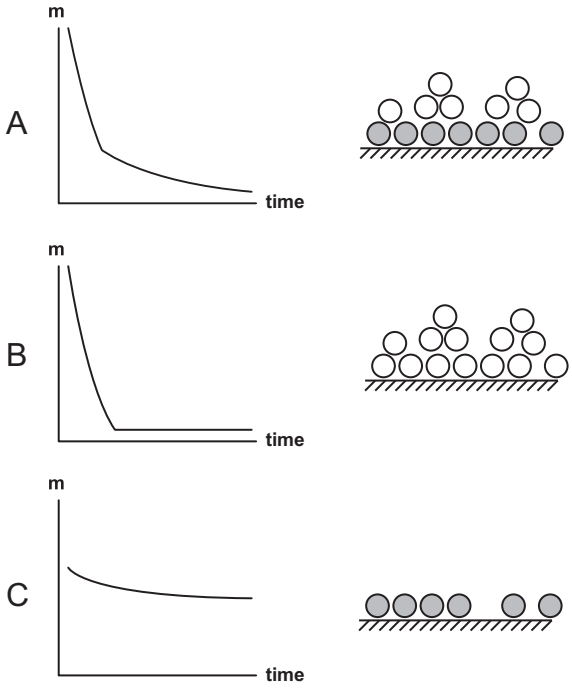

Fig. 5. Schematic depiction of solvent desorption behavior and solvent molecule position on the surface.

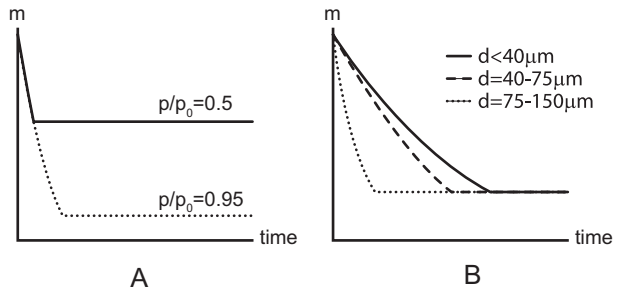

Fig. 6. Schematic representation of (A) solvent relative vapor pressure and (B) particle size effect on solvent desorption curve.

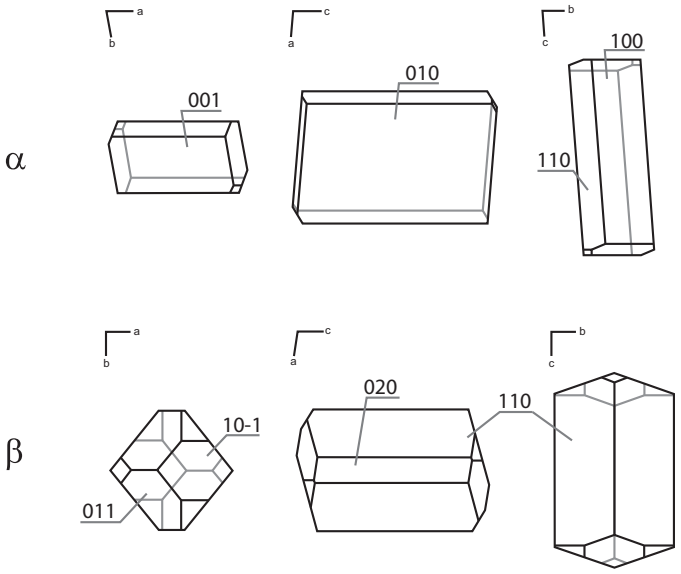

Fig. 7. Predicted crystal morphology of α and β tegafur.

sorption will occur. Predicted crystal morphologies can be seen in Fig. 7. Predicted α tegafur crystal has columnar morphology with large {0 1 0} faces, whereas the β tegafur crystal has prismatic morphology with large {1 1 0} faces.

Predicted crystal morphologies were fitted to sample crystals observed in scanning electron micrographs (see Fig. 8). This comparison showed that the same crystal faces dominated in the calculated morphologies and in experimental samples; although there were some differences in crystal shape at the crystal tips (especially for α tegafur). This was due to fact that small elongated crystalline particles with irregular crystal tips were obtained by breaking long needled α tegafur crystals during the grinding. Thus it was possible to ascertain this coincidence of few dominant crystal faces only for the fractions with the largest particles, as the crystal shape irregularity increases by decreasing the particle size. There were some more important differences between experimentally observed and calculated crystal shape for β tegafur. Crystal face family {0 2 0} was noticeably larger in experimental crystals, if compared with calculated ones; and smallest calculated crystal faces, those with relative surface areas below 3%, cannot be distinguished in experimental samples at all. For the fractions with smallest particles it was almost impossible to discern any crystal faces at all (see Fig. 11 in Section 3.4).

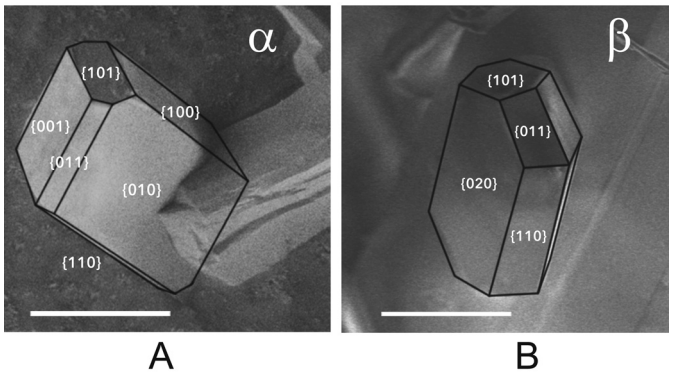

Fig. 8. Comparison of sample crystal shape and predicted crystal morphology of (A) α tegafur and (B) β tegafur samples with particle size 40–75 μm. White scale bar is 50 μm.

To get some understanding on the possible solvent–surface interactions, packing diagrams of α and β tegafur at the crystal faces with largest relative areas were modeled from crystal structure data using Mercury 3.0 (see Fig. 9). Theoretically largest crystal faces of the α tegafur is of the families {0 1 0}, {1 0 0}, {0 0 1} and {1 1 0} with relative areas 49.8%, 19.8%, 14.2% and 9.8% respectively, but for β tegafur faces of the families {1 1 0}, {0 1 1}, {0 2 0} and {1 0 1} with relative areas 64.4%, 12.8%, 10.4% and 8.2% respectively.

Inspection of the packing diagrams of α tegafur crystal structure revealed that {0 1 0} face family comprise regular pockets on a molecular level and can be regarded as corrugated in two dimensions (see Fig. 9A), but the rest of the face families were comparatively smooth (see Fig. 9B–D).

We may therefore explain the solvent–surface interaction qualitatively as follows. The surface at the {0 1 0} faces exposes primarily tetrahydrofuran rings, but electrophilic fluorouracil group atoms are situated at the bottom of these pockets (see Fig. 9A). Fluorouracil group electrophilic atoms are acting as proton acceptors for the proton donor groups of the solvent molecules and at the same time electrophilic atoms of solvents are able to form short contacts with freely accessible tetrahydrofuran group hydrogen atoms.

Common property for solvents, which formed relatively high sample surface coverage – acetone, acetonitrile, ethyl acetate and tetrahydrofuran, is that all of these molecules are relatively small and they are able to fit in these pockets on {0 1 0} faces and they also have electron donor groups which can form weak intermolecular interactions. Acetone carbonyl group, ethyl acetate and *n*-butyl acetate carboxylate groups, and tetrahydrofuran ether group interacts with freely accessible tegafur tetrahydrofuran group hydrogens and forms weak CH···O interactions, but acetonitrile cyano group forms weak C≡N···H interactions. At the same time alkyl parts of these solvents forms weak CH···O and CH···F interactions with fluorouracil ring carbonyl groups and fluoro group. Sorption of tetrahydrofuran on the face family {0 1 0} is also enhanced by the fact that tetrahydrofuran can "continue the crystal structure" of the tegafur in this direction (see Fig. 10).

If we take a look at systems, where relatively low sample surface coverage was observed – *n*-butyl acetate, ethanol, methanol and toluene, we see that the main difference between these two solvent groups are that these solvents have weaker electron donor groups than previously mentioned solvents and most likely this is the main reason for mayor differences in solvent sorption–desorption behavior. Another reason why toluene and *n*-butyl acetate falls in to this solvent group must be the size of the solvent molecule. As previously mentioned, *n*-butyl acetate carboxylate group can interact with proton donors of tegafur molecule, however the size of *n*-butyl acetate alkyl part makes it difficult to position the molecule completely in the pockets on {0 1 0} faces and therefore only part of the molecules enters the pockets and therefore blocks the surface for the rest of the solvent molecules.

Similar surface–solvent interactions are observed on other crystal faces as well, with main difference that on crystal face families {1 0 0}, {0 0 1} and {1 1 0} there are no such deep pockets where

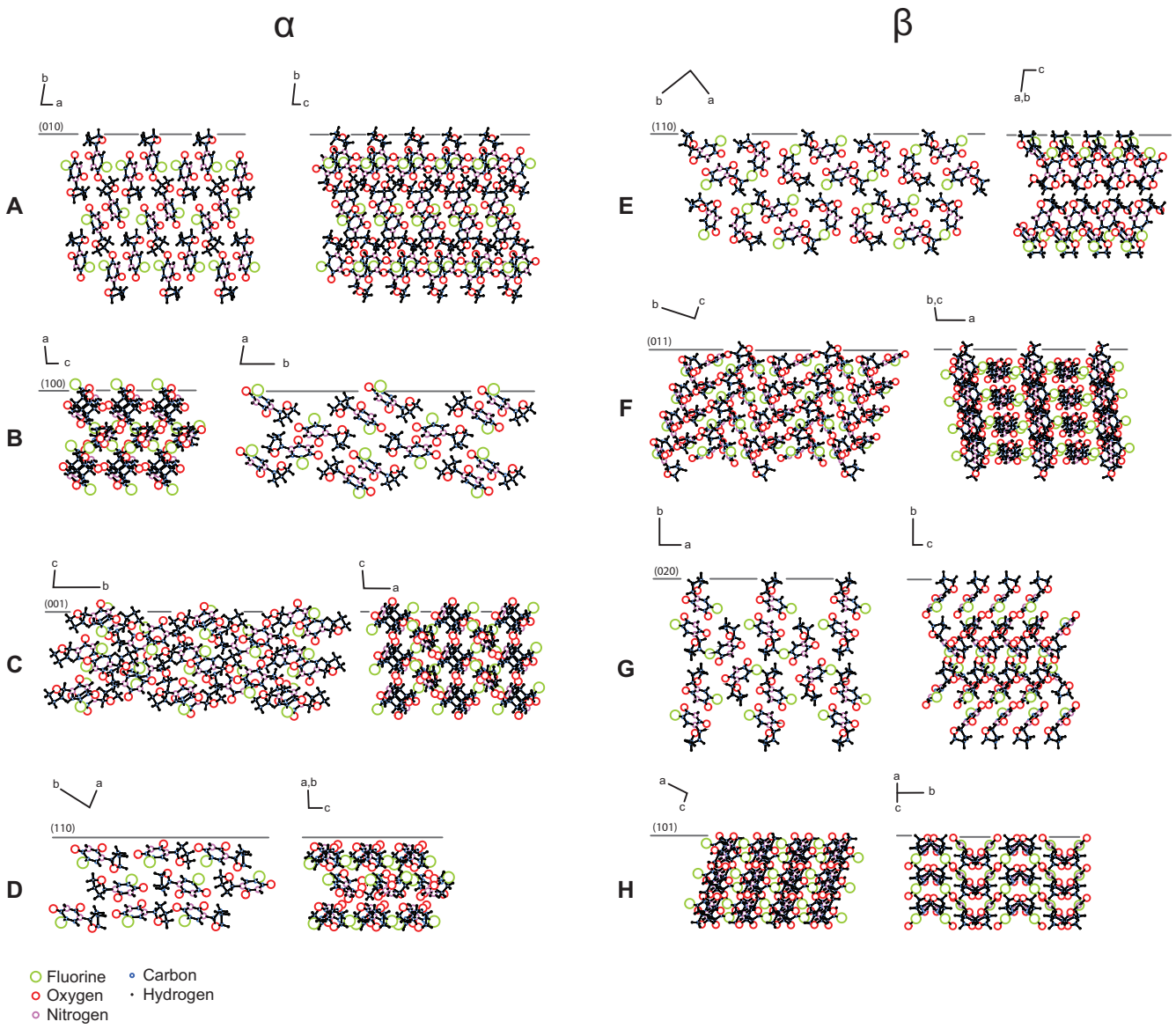

Fig. 9. Packing diagrams of α and β tegafur.

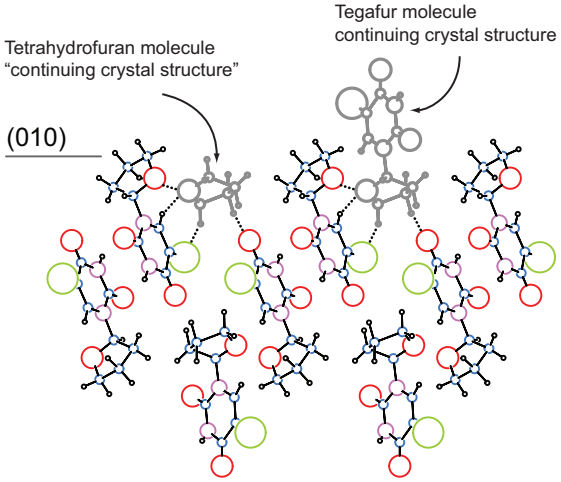

Fig. 10. Schematic comparison of adsorbed tetrahydrofuran and tegafur molecule position and location on the (0 1 0) face of α tegafur. Dashed lines represents CH···O and CH···F interactions.

solvent molecules could be stabilized and therefore solvent desorption from these faces occur more rapidly than form face family {0 1 0}.

The largest (theoretically) β tegafur face families {1 1 0} and {0 1 1} are comparatively smooth (see Fig. 9E and F), but face family {0 2 0}, which seems to be the largest in experimental crystals, have somehow similar packing arrangement as {0 1 0} face family of α tegafur (see Fig. 9G) – with regular pockets on a molecular level, tetrahydrofuran rings exposed on the surface and electrophilic fluorouracil groups situated deeper in the pockets.

This relatively high degree of similarity of packing at the largest crystal faces for α and β tegafur might explain why there were almost no differences in the solvent sorption behavior for both polymorphs.

3.4. Sample morphology changes during sample storage

Tegafur sample morphology studies with scanning electron microscope were performed for the β tegafur fraction with particle size of 40 μm and less. Scanning electron micrographs for sample before and after the experiment (storage at 95% relative

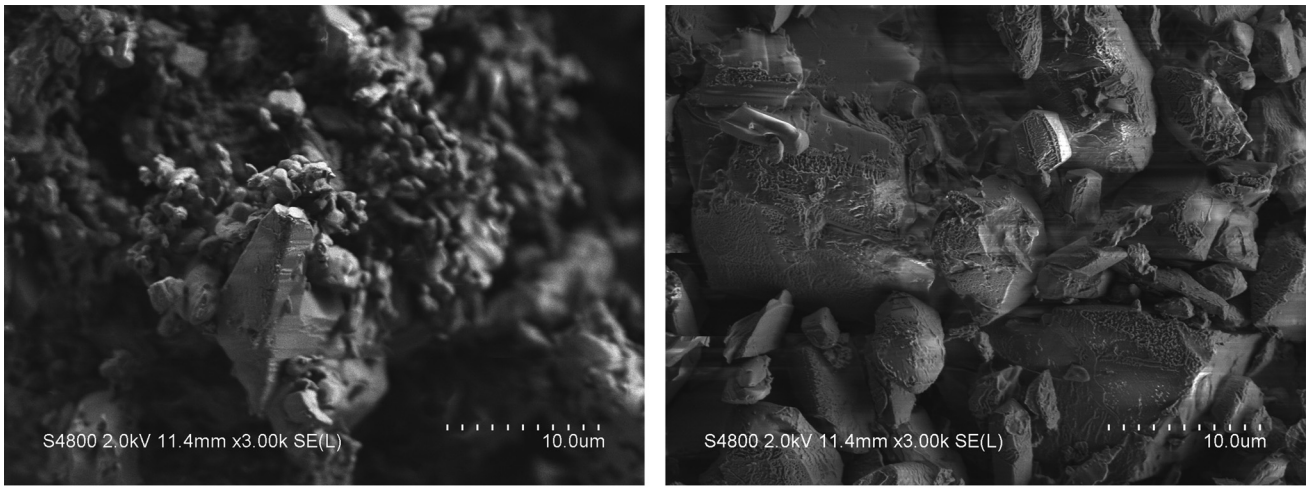

Fig. 11. Scanning electron micrographs of β tegafur samples with particle size 40 μm and less; (A) before and (B) after sample storage at 95% relative acetone vapor pressure for 72 h.

acetone vapor pressure for 72 h) are shown in Fig. 11. An accelerating voltage of 2.0 kV was chosen because of the high sample charging.

Scanning electron micrographs show that the sample before storage in solvent atmosphere consisted of small particle (<2 μm) agglomerates, but after storage there were almost no such particles. This was due to Ostwald's ripening – small particles with large surface, thus high surface energy, tend to reduce their free energy by reducing the ratio of surface to mass, and this occurs by recrystallization to larger particles. Another difference between samples before and after storage in solvent atmosphere can be seen if we take a look at the edges and faces of the large particles. The edges of β tegafur particles were quite sharp and well defined before storage, but after storage became rounded and hardly visible. Differences could be seen also on the surface of large particles – after the sample storage at 95% relative acetone vapor pressure the surface of the particles became rough and there are signs that tegafur crystallized from the solution (see Fig. 11B). This experiment shows that minor changes in sample morphology occur during sample storage, and actually sample with slightly different particle size and morphology are analyzed during the experiment.

4. Conclusions

The results of this study demonstrated that solvent desorption from α and β tegafur did not differ significantly between these two phases, and solvent desorption in all cases occurred faster from samples with the largest particle size. Structure differences and their surface properties are not of great importance on the solvent desorption rates and the main factor affecting desorption rate is sample particle size and sample morphology.

Two different solvent desorption behaviors can be distinguished depending on the solvent and surface interaction energy. If the solvent and surface interaction was stronger than interaction between solvent molecules, than multilayer and monolayer desorption was observed, but, if the adsorbed solvent molecules were of equal energy, then only one desorption phase was observed.

Solvent desorption rates of acetone, acetonitrile, ethyl acetate and tetrahydrofuran multilayers from α and β tegafur were approximately 30 times higher than those from solvent monolayers.

The largest crystal face families for α and β tegafur are {0 1 0} and {0 2 0}, respectively. Both of them comprise regular pockets on a molecular level and can be regarded as corrugated in two dimensions. Solvent desorption rate and amount of adsorbed solvent were mainly affected by the ability to form short contacts between solvent molecule electron donor groups and freely accessible tegafur tetrahydrofuran group hydrogens, as well as solvents molecule proton donor groups and fluorouracil ring carbonyl groups and fluorine atoms.

Small tegafur particles recrystallized to larger particles during sample exposure to solvent vapor atmosphere, and there were morphological signs of tegafur recrystallization from solution on the surface of the particles.

Acknowledgments

This work has been supported by the European Social Fund within the project "Support for Doctoral Studies at University of Latvia". Authors acknowledge JSC Grindeks for supplying α and β polymorphic forms of tegafur. We also acknowledge Institute of Chemical Physics, University of Latvia for possibility to carry out SEM imaging.

References

Actiņš, A., Beļakovs, S., Orola, L., Veidis, M.V., 2006. Molecular and crystal structure of novel form of tagefur. Latv. J. Chem. 2, 120–124.
Bennema, P., Gilmer, G.H., 1973. Crystal growth: an introduction. In: Hartman, P. (Ed.), Kinetics of Crystal Growth. Amsterdam, North-Holland.
Bobrovs, R., Actiņš, A., 2012. Optimization of sample preparation conditions for detecting trace amounts of β tegafur in α and β tegafur mixture. J. Pharm. Sci. 101, 4608–4614.
Bourne, J.R., Davey, R.J., 1976. The role of solvent–solute interactions in determining crystal growth mechanisms from solution: II. The growth kinetics of hexamethylene tetramine. J. Cryst. Growth 36, 287–296.
Brittain, H.G., 2009. Polymorphism in Pharmaceutical Solids, 2nd ed. Informa Healthcare.
Hilfiker, R., 2006. Polymorphism in the Pharmaceutical Industry. Wiley-VCH, Weinheim.
Lahav, M., Leiserowitz, L., 2001. The effect of solvent on crystal growth and morphology. Chem. Eng. Sci. 56, 2245–2253.
Macrae, C.F., Bruno, I.J., Chisholm, J.A., Edgington, P.R., McCabe, P., Pidcock, E., Rodriguez-Monge, L., Taylor, R., Streek, J., van de, Wood, P.A., 2008. Mercury CSD 2.0 - new features for the visualization and investigation of crystal structures. J. Appl. Cryst. 41, 466–470.
Needham, F., Faber, J., Fawcett, T.G., Olson, D.H., 2006. X-ray powder diffraction analysis of tegafur. Powder Diffr. 21, 245.
Petkune, S., Bobrovs, R., Actiņš, A., 2011. Determination of trace amounts of β tegafur in commercial α tegafur by powder X ray diffractometric analysis. J. Pharm. Pharmacol. 63, 1136–1140.
Petkune, S., Bobrovs, R., Actiņš, A., 2012. Organic solvents vapor pressure and relative humidity effects on the phase transition rate of α and β forms of tegafur. Pharm. Dev. Technol. 17, 625–631.

Schöll, J., Bonalumi, D., Vicum, L., Mazzotti, M., Müller, M., 2006. In situ monitoring and modeling of the solvent-mediated polymorphic transformation of L-glutamic acid. Cryst. Growth Des. 6, 881–891.

Stoica, C., Verwer, P., Meekes, H., Van Hoof, P., Kaspersen, F.M., Vlieg, E., 2004. Understanding the effect of a solvent on the crystal habit. Cryst. Growth Des. 4, 765–768.

Uchida, T., Yonemochi, E., Oguchi, T., Terada, K., Yamamoto, K., Nakai, Y., 1993. Polymorphism of tegafur: physico-chemical properties of four polymorphs. Chem. Pharm. Bull. 41, 1632–1635.

Vippagunta, S.R., Brittain, H.G., Grant, D.J.W., 2001. Crystalline solids. Adv. Drug Delivery Rev. 48, 3–26.

Weissbuch, I., Addadi, L., Lahav, M., Leiserowitz, L., 1991. Molecular recognition at crystal interfaces. ChemInform 22, 637–645.

Weissbuch, I., Torbeev, V.Y., Leiserowitz, L., Lahav, M., 2005. Solvent effect on crystal polymorphism: why addition of methanol or ethanol to aqueous solutions induces the precipitation of the least stable β form of glycine. Angew. Chem. Int. Ed. 44, 3226–3229.

CrystEngComm

PAPER

Cite this: *CrystEngComm*, 2014, **16**, 10581

Solvent-mediated phase transformation between two tegafur polymorphs in several solvents†

Raitis Bobrovs,*[ab] Linda Seton[b] and Andris Actiņš[a]

Received 13th June 2014,
Accepted 9th September 2014

DOI: 10.1039/c4ce01215a

www.rsc.org/crystengcomm

This paper describes a study of the solvent-mediated polymorphic transformation (SMPT) of the metastable α tegafur to the thermodynamically stable β tegafur in several solvents. Phase transformation in acetone, ethanol, i-propanol, toluene, and water at 22 °C was described using the solid-state kinetic model P2; the rate constants for this process were in the range from 0.028 min^{-1} to 0.0056 min^{-1}. In all of the employed solvents, an induction time was observed. Kinetic, solubility and scanning electron microscopy data indicated that nucleation kinetics corresponded to a second-order power function and according to the kinetic model, the nuclei growth rate was constant in the examined SMPT. Surface nucleation was observed, and the possible nucleation mechanism was given. The phase transition rate depended linearly on the difference between the equilibrium solubilities of α and β tegafur in the respective solvent, *i.e.* supersaturation.

Introduction

Different crystalline forms of the same molecular entity are known as polymorphs. Polymorphism is a very common phenomenon in chemical manufacturing, for example, in pigments, food, and most of all in the pharmaceutical industry,[1] where at least two-thirds of active pharmaceutical compounds have more than one solid form.[2–5] One of the tasks of the pharmaceutical industry is to find and select the solid forms with the optimal characteristics for the intended use, because the solubility, dissolution rate, and bioavailability of drug substances are influenced by polymorphism. Therefore, it is a common requirement in the pharmaceutical industry that a manufactured compound must be in one, strictly defined crystalline phase.[3,5] To ensure product stability, the thermodynamically stable polymorph under ambient conditions is normally chosen for manufacturing. However, due to enhanced dissolution or bioavailability profiles, a metastable form might be chosen for manufacturing. To ensure that polymorphs do not transform over time, the polymorphic stability must be evaluated with respect to ambient, storage, and packaging conditions. The stability of polymorphs under certain temperature and pressure conditions is defined by their free energy, with the most stable polymorph having the lowest free energy under the given conditions.[3–5]

Crystallization is the most common method of chemical compound isolation from solution on the manufacturing scale, and it is governed by a combination of thermodynamic and kinetic factors.[3–6] Crystallization of polymorphs often follows Ostwald's rule of stages,[7] which postulates that crystallization in a polymorphic system progresses from the supersaturated state to the equilibrium state in stages. Thus, according to Ostwald's rule of stages, the metastable form should crystallize first and then the system should move through each possible polymorphic structure before the thermodynamically stable polymorph crystallizes. In the majority of cases, the thermodynamically stable polymorph under the given conditions can be isolated; however, the solvent used for crystallization can affect the crystallization outcome and it might promote the crystallization of a specific metastable polymorph. The metastable polymorph will attempt to transform to the stable form if possible, therefore it is important to study polymorphic transformation 'reactions' to determine the factors influencing the outcome of polymorphic crystallization. One type of polymorphic transformation 'reaction' that has been drawing attention is solvent-mediated polymorphic transformation (SMPT).[4,8–10] This is a process where the metastable polymorph interacts with a bulk solvent phase and gradually transforms to the more stable polymorph by dissolution and crystallization. SMPT is interpreted as a three-step process – dissolution of the metastable phase, nucleation of the stable phase, and growth of the stable phase.[11,12] The driving force in this process is the difference between the solubilities and the dissolution rates of both

[a] *Faculty of Chemistry, University of Latvia, Kr. Valdemara iela 48, Riga, LV-1013, Latvia. E-mail: raitis.bobrovs@lu.lv; Tel: +371 67372576*
[b] *Formulation and Drug Delivery Research Group, School of Pharmacy and Biomolecular Sciences, Liverpool John Moores University, Liverpool, L3 3AF, UK*
† Electronic supplementary information (ESI) available. See DOI: 10.1039/c4ce01215a

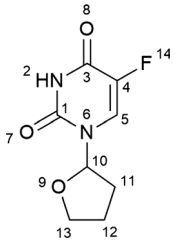

Fig. 1 Molecular structure of tegafur (5-fluoro-1-(tetrahydrofuran-2-yl)pyrimidine-2,4(1*H*,3*H*)-dione).

polymorphs, which consequently determines the supersaturation level during the crystallization of the thermodynamically stable form. SMPTs have been extensively studied over the years;[8,9,13–30] however, there are no comprehensive studies on the choice of solvent in the SMPTs. Such studies might be useful for the pharmaceutical industry in order to use SMPTs in pharmaceutically active compound manufacturing. SMPTs can be used to produce the thermodynamically stable polymorph if crystallization from a solvent gives a metastable polymorph. On the other hand, if a metastable polymorph is desired, knowledge of possible SMPTs of the respective system is important, because there might be situations when the metastable polymorph crystallizes and through unwanted SMPT subsequently transforms to the thermodynamically stable polymorph.

Here we study SMPT of the metastable α tegafur to the thermodynamically stable β tegafur in several popular solvents from different solvent classes: aprotic polar, aliphatic aprotic apolar, hydrogen bond donor and aromatic apolar. Both polymorphs of tegafur are produced commercially; therefore, knowledge of the SMPT of these polymorphic systems might be relevant for the pharmaceutical industry. The pharmaceutically active compound used in this research, tegafur (5-fluoro-1-(tetrahydrofuran-2-yl)pyrimidine-2,4(1*H*,3*H*)-dione) (Fig. 1), is an antitumor agent, which is widely used in the treatment of various malignancies, particularly gastrointestinal and breast cancers.[31] Over many years, the α, β, δ, γ and ε forms of tegafur have been reported in the pharmaceutical literature,[31–33] but only the α and β modifications are used for therapeutic purposes.

1. Materials and methods

1.1. Materials

Commercial samples of α and β tegafur were supplied by JSC Grindeks (Latvia). Acetone, cyclohexane, ethanol, i-propanol, and toluene of analytical grade were purchased from commercial sources, and deionized water (electrical conductivity <0.1 μS) was prepared using an Adrona Crystal 5 system (Latvia). Solvents were used without further purification. All of the reagents used were certified >99% pure.

1.2. Methods

1.2.1. Solvent-mediated polymorphic transformations. The SMPT was investigated in acetone, cyclohexane, ethanol, i-propanol, toluene, and water. Slurrying was performed in Erlenmeyer flasks, where 0.5 g of the α and β tegafur mixture at a weight ratio of 1 : 1 was added to 5 mL of solvent and suspended for 5 min, 30 min, 3 h, and 72 h at room temperature (22 ± 1 °C). The mixture of α and β tegafur was weighed using an analytical balance (BOECO, Germany, d = ±0.0001 g) and homogenized by shaking for 5 min using a Retsch MM300 shaker (Retsch GmbH, Germany) at a shaking frequency of 10 Hz. Slurrying was performed using a Biosan OS-10 orbital shaker (Latvia) at a stirring rate of 200 rpm.

The transformation of α tegafur to stable β tegafur was monitored and quantified *via ex situ* powder X-ray diffraction (PXRD) analysis. Quantification of the polymorphic composition of the dry residue was carried out as described in section 1.2.3.

In order to assess the impact of sample suspension and sample drying on the phase transition, comparison experiments were performed, where α and β tegafur mixtures were placed in glass PXRD sample holders (~0.2 g) and moistened with appropriate solvents (100 μL) using a micropipette (±0.3 μL). Sample compositions were quantified using PXRD.

Analogous experiments were performed with pure metastable α tegafur to ensure that such treatment does not promote phase transition even for samples without β tegafur impurities.

1.2.2. The kinetics of solvent-mediated polymorphic transformations. Acetone, ethanol, i-propanol, toluene, and water solutions (~100 mL) saturated with respect to α tegafur were prepared by stirring excess α tegafur for ~3 h at 22 ± 1 °C. The excess tegafur was filtered off and the clear solution was used for SMPT. In order to ensure that the solution was saturated with respect to α tegafur, PXRD patterns of filtrates were recorded. Solution concentration was determined as described in section 1.2.5.

SMPT kinetic experiments were performed at 22 °C in a thermostated (an accuracy ±0.1 °C, Grant TC120, England) glass flow-through cell (250 mL) with a magnetic stirrer. 1.0 g of α tegafur (used as received) was added to the saturated solution and the solid phase was monitored every 10 min for a period of 2 h throughout the transformation. The stirring of the slurry was stopped for 20 seconds to allow the suspended solid particles to settle. Solid phase samples (~10 mg) for polymorphic composition determination were collected with a metal spoon from the suspension. The collected solid phase was quickly filtered through 2–3 μm filter paper using a glass filter funnel with a Büchner flask under reduced pressure. The quantity of α tegafur in the sample was monitored and quantified *via ex situ* powder X-ray diffraction (PXRD) analysis. The PXRD patterns of dry samples were recorded and analyzed as described in section 1.2.3.

The tegafur concentration in solution was measured every 20 to 40 min throughout SMPT. Samples for solution concentration measurements were gathered at the same time as solid phase samples for polymorphic composition determination were collected. Approximately 2 mL of the saturated

solution was filtered through a 0.20 μm syringe filter and then 1.00 mL of the clear solution was transferred to a pre-weighed vial with a micropipette (±10 μL). The solution was left to evaporate at room temperature, weighed and tegafur solubility was calculated. Two parallel experiments were performed.

1.2.3. The PXRD analysis. The samples were analyzed using Bruker D8 Advance and Bruker D8 Discover powder X-ray diffractometers (Bruker AXS, Karlsruhe, Germany) equipped with a LynxEye PSD. Measurements were performed with Cu K_α radiation (1.54180 Å) at room temperature. The following conditions were used: step-scan mode with a step size of 0.02°; scan speed: 0.2° min^{-1}; 2θ range: 8.0°–20.0°; voltage: 40 kV; current: 40 mA; divergence slit: 0.6 mm; anti-scattering slit: 8 mm.

PXRD calibration was performed using mixtures of 5.0%, 10.0%, 20.0%, 50.0%, 80.0%, 90.0% and 95.0% β tegafur in α tegafur (~0.3 g total sample weight). The mixtures were weighed using an analytical balance and samples were homogenized by shaking for 5 min using a Retsch MM300 shaker at a shaking frequency of 10 Hz. The powder samples were packed into glass holders and pressed by a glass slide to ensure coplanarity of the powder surface with the surface of the holder.

Quantitative phase analyses were performed using fundamental parameter-based Rietveld software BGMN.[34] Structure data necessary for quantitative analysis were acquired from the Cambridge Structural Database (CSD) with the reference codes BIPDEJ for α tegafur and BIPDEJ02 for β tegafur.

PXRD patterns of calibration samples and samples collected from experiments were recorded and analyzed identically.

1.2.4. Scanning electron microscopy (SEM). SEM imaging was performed using a Quanta 200 SEM (FEI, Holland) system. Samples were initially gold-coated using a K550X sputter coater (EMITECH, UK) and subsequently scanned using an acceleration voltage of 5.0 kV at a working distance of approximately 10 mm. SEM analyses were performed for the same samples that were used for PXRD analysis.

1.2.5. Tegafur solubility measurements. An excess amount of thermodynamically stable β tegafur was added to 15 mL of acetone, cyclohexane, ethanol, i-propanol, toluene, and water, and was left to stir overnight at 22 ± 1 °C. The saturated solution was filtered through a 0.20 μm syringe filter and then 10.0 mL of the clear solution was transferred to a pre-weighed vial. The solution was left to evaporate at room temperature, weighed and tegafur solubility was calculated. The solubility of metastable α tegafur was determined identically, except solutions were stirred for ~3 h at 22 ± 1 °C in order to prevent phase transformation to thermodynamically stable β tegafur. PXRD patterns of the filtrate were recorded to ensure that the solubility of the desired polymorph was determined. Two parallel experiments were performed.

1.2.6. Crystallographic face indexing. Crystallographic face indexing was done by single-crystal X-ray diffraction using a Nonius Kappa CCD diffractometer (Bruker AXS, Karlsruhe, Germany) with Mo K_α radiation (0.71073 Å) at 60 kV and 30 mA. Data were collected at room temperature. Face indexing was performed using Collect software.[35]

2. Results and discussion

2.1. The characterization of starting materials

The α and β forms of tegafur were analyzed using PXRD and were confirmed to have equivalent peak positions to those simulated from crystal structure data (CSD, reference codes BIPDEJ and BIPDEJ02) (Fig. 2). No impurities of other polymorphs or any contamination were detected in the starting materials. A preferred crystal orientation was observed for α tegafur because of its needle-like crystal morphology. Typical crystal shapes of both polymorphs are given in Fig. 3.

Crystallographic information of α and β tegafur is given in Table 1. The base motif of α and β tegafur crystal structures is a tegafur molecule dimer with a $R_2^2(8)$ motif, where tegafur molecules are connected *via* two N2–H···O7 hydrogen bonds (Fig. 4). The dimers are not identical in both polymorphs, because the crystal structure of α tegafur consists of two

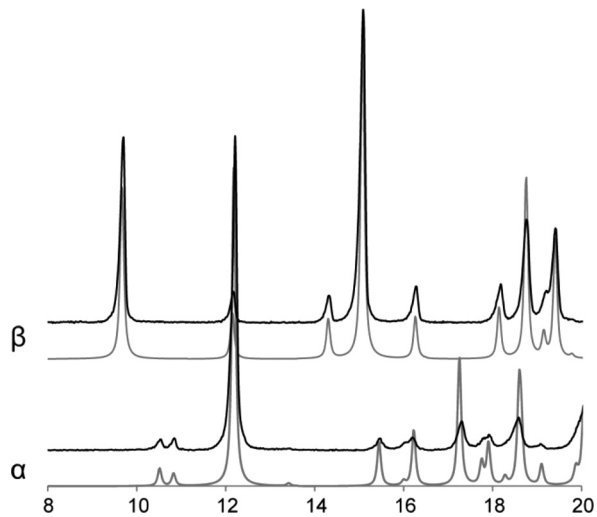

Fig. 2 Experimentally measured (black line) and calculated (grey line) PXRD patterns of α and β tegafur polymorphs.

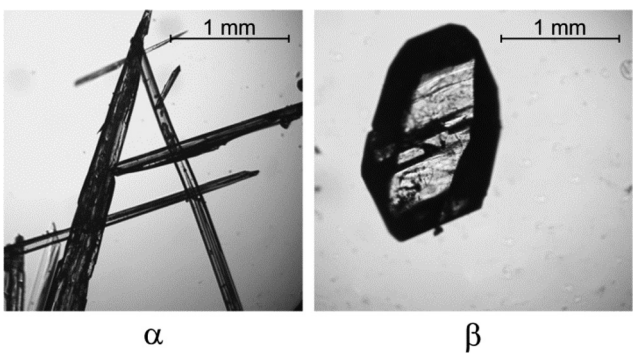

Fig. 3 Photomicrographs of α and β tegafur crystals.

Table 1 Crystallographic information of α and β tegafur[36]

	α tegafur	β tegafur
System	Triclinic	Monoclinic
Space group	$P\bar{1}$	$P2_1/n$
a, Å	8.994(8)	11.891(5)
b, Å	16.612(9)	14.556(2)
c, Å	5.981(5)	5.062(1)
α, °	86.40(6)	90
β, °	94.06(15)	99.05(2)
γ, °	80.29(8)	90
Z	4	4

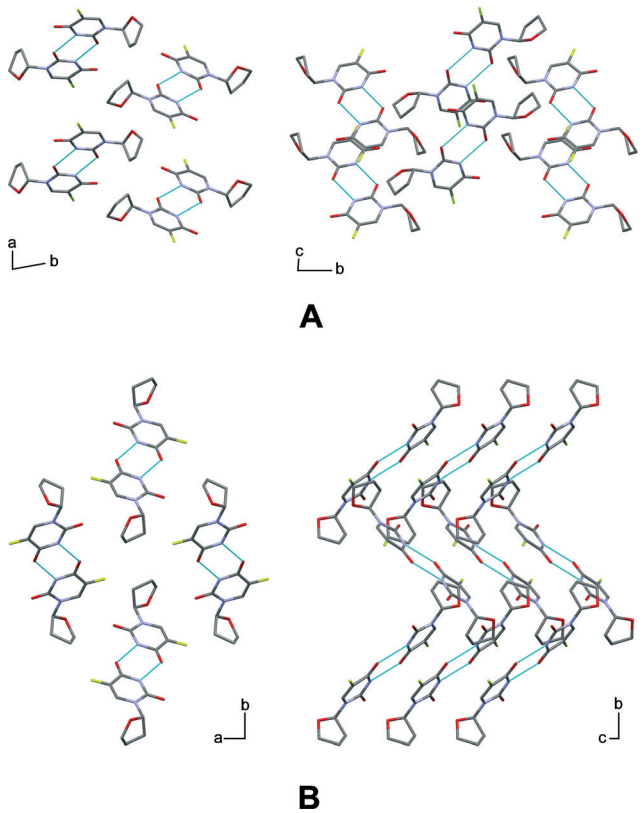

Fig. 4 Crystal packing of (A) α tegafur and (B) β tegafur. Hydrogen atoms are omitted for clarity.

conformationally different molecules (A and B), whereas β tegafur has one molecule in its asymmetric unit and the conformation of this molecule matches the conformation of molecule B in α tegafur.[37] Dimers in α tegafur are formed between conformationally identical molecules; that is, one α tegafur dimer is formed by two A molecules and the second by two B molecules. Tegafur dimers in the α polymorph are cross-linked by weak C5–H···O9 and C11–H···O8 hydrogen bonds, whereas in β tegafur dimers are stabilized by weak C5–H···O7 and C12–H···F14 hydrogen bonds. It is worth noting that α tegafur dimers form between the same enantiomers (there are two enantiomerically and conformationally different dimers), whereas β tegafur dimers form between two enantiomerically different molecules.[37] Crystallographic face indexing of α tegafur crystals (see section 2.4) indicated that crystal growth along the *a* axis is promoted. This is because of the relatively easy tegafur dimer access to the growing surface and the possibility of forming multiple weak hydrogen bonds between F14, O8, O9 and C5–H, C11–H. Hydrogen bonds in β tegafur are distributed more evenly and they are stronger than those in α tegafur. The same groups are involved in hydrogen bonding for β tegafur, with the difference that instead of C11–H hydrogen, C12–H forms a hydrogen bond with the fluorine atom. Hydrogen bonding in β tegafur enables cross-linked *zigzag chains* in the *b* direction; however, no preferred crystal growth orientation is observed for β tegafur.

2.2. Quantitative phase analysis

The calibration curve of the α and β tegafur mixture is given in Fig. 5. The homogenous composition of the analysed mixtures and the equivalent extinction effects for both polymorphs could ensure that the diffraction peak intensity of each phase depends linearly on the phase weight fractions in the sample.[38] It is evident that the correlation was not completely linear and the calculated content of β tegafur in the samples was up to 2% higher than was actually weighed. We believe that this was because of the preferred orientation of α tegafur, different degrees of crystallinity for both polymorphs and possible microabsorption. Nevertheless, experimental data can be described by the linear equation $y = (1.02 \pm 0.01)x$ with an R^2 value of 0.9990. The method used was found to be linear in the range of 0–100% with the limit of detection (LOD) and limit of quantification (LOQ) calculated[39] to be 3.0 and 9.2%, respectively. The method was found to be precise with a relative standard deviation (RSD)

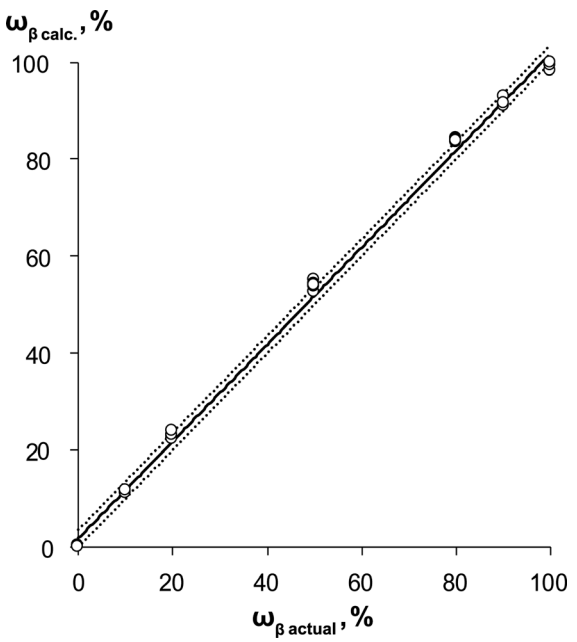

Fig. 5 Dependence of the calculated β tegafur weight fraction ($\omega_{\beta\ calc.}$) upon the actual β tegafur content in the sample ($\omega_{\beta\ actual}$). Statistical probability $p < 0.05$.

of 2.0%. Statistical probability (p) used was $p < 0.05$. The relatively high LOD, LOQ and RSD values obtained are because of the fast scan speed (0.2° min^{-1}) used in the experiments. In order to maintain consistency, the scan speed used for calibration was the same as that used for SMPT quantitative analysis. The scan speed of 0.2° min^{-1} was chosen because of the ability to provide fast PXRD measurements necessary for kinetic SMPT studies.

2.3. Solvent-mediated polymorphic transformations

Initially, SMPT experiments for the α and β tegafur mixture with a weight ratio of 1 : 1 were performed to estimate the approximate phase transition rate. The results of the slurry bridging experiments showed that in all of the employed solvents the metastable form converted into the thermodynamically stable form. The weight fraction of β tegafur in the starting material was 50 ± 2%. The weight fractions of β tegafur in the samples after slurry bridging experiments with various solvents are given in Fig. 6.

It is known[3,5,40–42] that substantial phase transition from one phase to another in a polymorph mixture can be promoted even by solvent addition (without any external influence). This is because both polymorphs of the substance dissolve in the solvent added and then the stable polymorph under the given conditions will crystallize. In order to evaluate the impact of residual solvent on SMPT during drying, experiments where samples were only moistened and dried were performed. The weight fractions of β tegafur after these experiments are given in Fig. 6 and are indicated as "moistened/dried starting material".

Experiments showed that phase transformation took place over a period of time, which varied across the solvents studied. Almost complete phase transition to the thermodynamically stable β polymorph was observed in acetone, ethanol, and water after only 5 min of slurrying. The phase transition was slower in i-propanol and toluene, and complete phase transition to the β polymorph was observed only after more than 3 h of slurrying. Minor changes (<10%) in the weight fraction of β tegafur were observed for samples slurried in cyclohexane for 3 days. We believe that no or only minor phase transition occurred in cyclohexane because of its aprotic apolar nature and the negligible solubility of tegafur in this solvent. It is also possible that the observed negligible weight fraction changes in cyclohexane could be related to sample homogeneity and accuracy of the PXRD method (RSD = 2.0%).

As previously mentioned, the experiments where no slurrying was performed, but instead the sample was only moistened and dried were performed for comparison purposes. This procedure gave a major increase in the weight fraction of β tegafur for samples that were moistened with water and toluene, but for samples that were moistened with acetone, cyclohexane, ethanol, and i-propanol a minor increase in the weight fraction of β tegafur was found. One of the explanations for such results could be as follows. As previously mentioned, SMPTs are considered as three-step processes consisting of dissolution of the metastable phase, nucleation of the stable phase, and growth of the stable phase. All of these stages and hence the phase transition extent are affected by the solvent and solid phase interaction time; therefore, it is possible that phase transition extent was affected by the solvent evaporation time. Acetone, ethanol, and i-propanol are relatively volatile compared to water and toluene, thus phase transitions in acetone, ethanol, and i-propanol have less time to occur. In order to understand solvent effect on studied SMPT and to find out factors affecting this phase transformation, more detailed phase transformation kinetic experiments were performed.

2.4. The kinetics of solvent-mediated polymorphic transformations

During our first SMPT kinetic experiments, we noticed that the sample drying time has an impact on the extent of phase

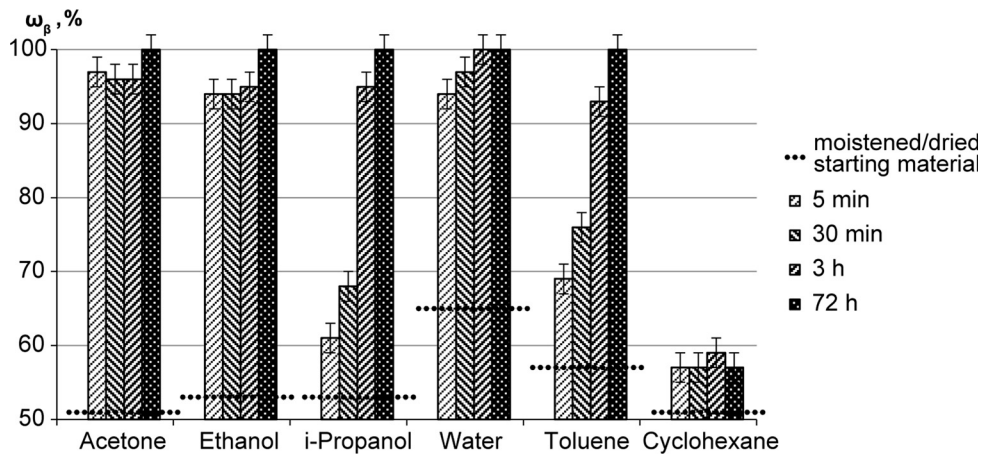

Fig. 6 Weight fraction of β tegafur in the samples after slurrying a 1 : 1 mixture of α and β tegafur for 5 min, 30 min, 3 h and 72 h in acetone, ethanol, i-propanol, water, toluene, and cyclohexane. The dashed line (···) represents the weight fraction of β tegafur in the sample after the experiment, where no slurrying was performed and the sample was only moistened and dried at ambient temperature (indicated as "moistened/dried starting material").

transition – samples dried at ambient temperature have increased β tegafur content. This was because the thermodynamically stable β tegafur crystallized from the saturated tegafur solution that was sampled together with the solid phase, *i.e.*, phase transition to β tegafur not only occurred during slurrying but also partially occurred during sample drying. In order to avoid this effect, samples for SMPT kinetic experiments were quickly filtered using a glass filter funnel with a Bunsen flask under reduced pressure.

Kinetic experiments with cyclohexane were not performed, since only negligible changes in the β tegafur weight fraction during slurrying in cyclohexane were observed in the previous experiments.

For further data analysis, it is worth mentioning that in the previously discussed experiments, samples were treated with pure solvents, but in kinetic experiments tegafur-saturated solvents were used to analyze tegafur dissolution effects.

The results of the kinetic experiments performed at room temperature (22 ± 1 °C) represent a series of plots documenting the composition of the solid phase during SMPT, as detected by the PXRD method. Fig. 7 shows the composition of the solid phase during the SMPT in acetone, ethanol, i-propanol, toluene, and water. These data were used to generate an additional data plot where phase transition kinetic curves were normalized to a state where a complete transition to β tegafur was observed (Fig. 8). This means that the phase transformation time throughout SMPT was expressed in percents, where the beginning of SMPT in each solvent was regarded as 0% and time necessary for complete phase transformation was regarded as 100%. Using this approach, we could compare the reaction rate and reaction path in all of the solvents used. This figure clearly demonstrates that the phase transition models were the same in all of the solvents, and the only factor that changed was the phase transition rate. An induction time was observed at the beginning of phase transitions in all solvents. We cannot clearly assure whether the observed delay of phase transition is an induction time or it is the time necessary for β tegafur crystals to grow; however, we believe that this was the limiting step in investigated SMPTs. We see that the induction times in all of the solvents were proportionally

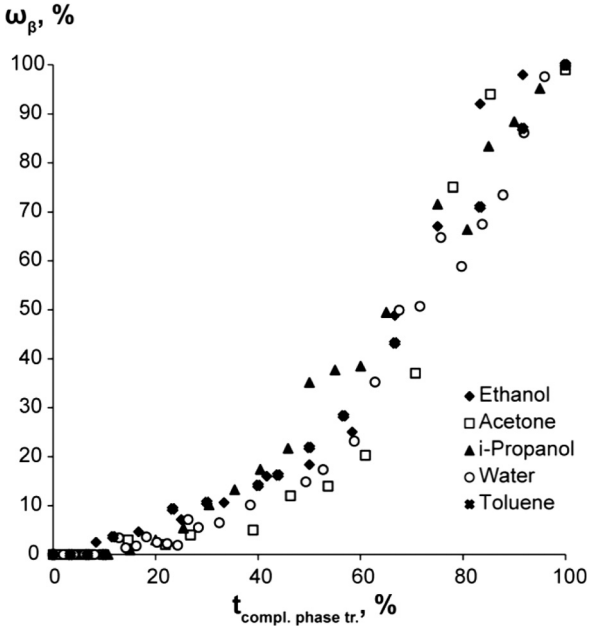

Fig. 8 Weight fraction of β tegafur during the SMPT in acetone, ethanol, i-propanol, toluene, and water at 22 °C, normalized to a state where the transition to β tegafur is complete.

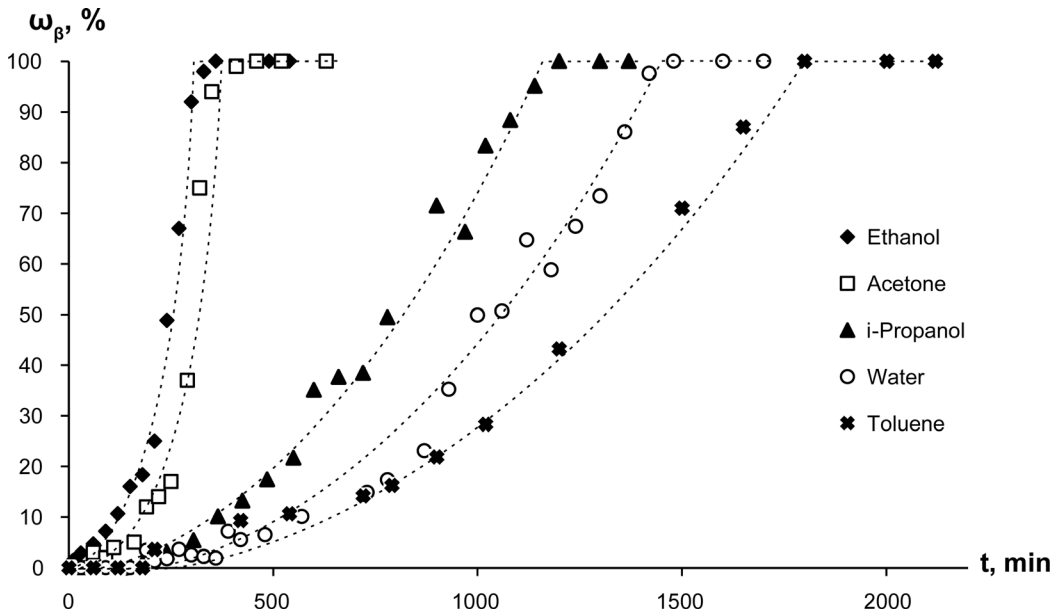

Fig. 7 Weight fraction of β tegafur during the SMPT from α tegafur to β tegafur in acetone, ethanol, i-propanol, toluene, and water at 22 °C. Line added as a guide.

the same – about 10% of the phase transition time. It is worth noting that the LOD of our quantitative analysis method was 3.0%, therefore the observed induction time might be the time necessary to overcome this 3.0% range.

Solution concentration throughout SPMT remained at the level of α tegafur solubility and started to decay only when all α tegafur transformed to stable β tegafur (Fig. 9). This means that the overall rate of consumption of supersaturation by β tegafur crystal growth was lower than the overall rate of α tegafur dissolution. This case is denoted as "nucleation–growth controlled polymorphic transformation".[16]

The induction time was followed by a gradual increase of the thermodynamically stable β tegafur fraction. SEM analysis of the sample, where β tegafur was first detected by the PXRD method, revealed that the blocky β tegafur crystal was in contact with the surface of α tegafur needle-like crystal side faces (Fig. 10). Although it is possible that α and β tegafur crystals simply agglomerated together during sample filtration and drying, the fact that it was not possible to separate these crystals without damaging them indicated that β tegafur most likely nucleated epitaxially on the surface of α tegafur. These observed epitaxially driven polymorphic transformations are common in SMPTs.[8,9,14,21,23,25,43] The surface of α tegafur here acted as a nucleation substrate for β tegafur by either decreasing the solution–nucleus interfacial energy by topographical contribution or by a crystal lattice match.[9] Surface nucleation might have also been a consequence of a local lattice disorder or an amorphous region that has a similarity to crystallizing β tegafur.[8]

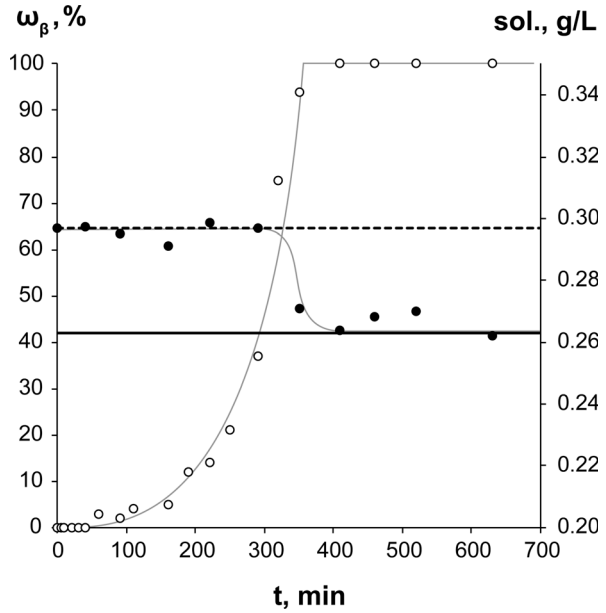

Fig. 9 Solution concentration (●) and weight fraction (○) of β tegafur in the solid phase during the SMPT from α tegafur to β tegafur in acetone at 22 °C. The dashed line (- - -) represents the solubility of α tegafur; continuous line (—) represents the solubility of β tegafur. Grey line added as a guide.

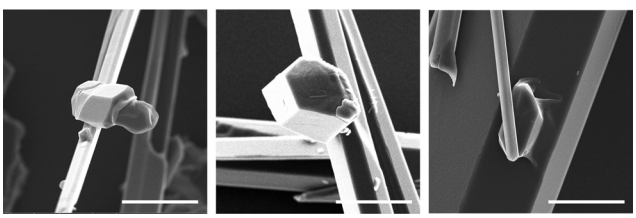

Fig. 10 SEM images of the solid phase of SMPT in acetone taken at 60 min. Scale bar: 40 μm.

In order to estimate the nucleation mechanism and understand which α and β tegafur crystal faces were in contact, crystal face indexing was performed for both polymorphs. Crystals, where β tegafur was in contact with α tegafur (like those in Fig. 10), were not suitable for β tegafur crystal face indexing, therefore individual β tegafur crystals were indexed. Crystals for β tegafur face indexing were collected at a period of 300 min, when individual β tegafur crystals suitable for crystal face indexing were in the sample. Appropriate β tegafur crystals were picked out from the phase mixture. Face indexing of α tegafur crystals was performed for samples collected at a period of 60 min.

SEM images showed that β tegafur nucleated on one of the needle-like crystal side faces, while crystallographic face indexing of the α tegafur crystal (Fig. 11A) indicated that these faces were {001}, {011} and {010}. A visual comparison of epitaxially nucleated β tegafur crystal morphology and indexed crystal morphology (Fig. 11B) indicated that the crystal face family {100}, {110} or {010} must be in contact with the α tegafur surface. Intermolecular distance and molecule alignment analysis along these faces revealed that there was a good agreement at a molecular level between the {110} face of β tegafur and the {010} face of α tegafur (Fig. 12), while no match was observed along other crystal faces. A possible lattice match between {100}, {110} and {010} faces of β tegafur and {001}, {011} and {010} faces of α tegafur was examined using EpiCalc Version 5.0 software.[44] Lattice matching calculations indicated that there was no lattice matching between any of the studied faces (EpiCalc data can be found in the ESI†).

However, it should be taken into account that crystal surface molecules are not static – they change their position,

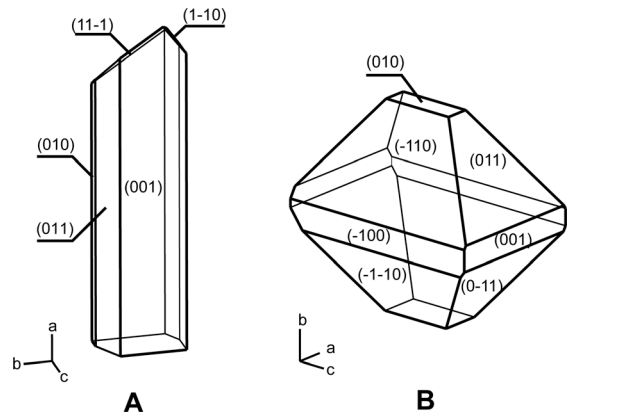

Fig. 11 Single crystal face indexing of (A) α tegafur and (B) β tegafur.

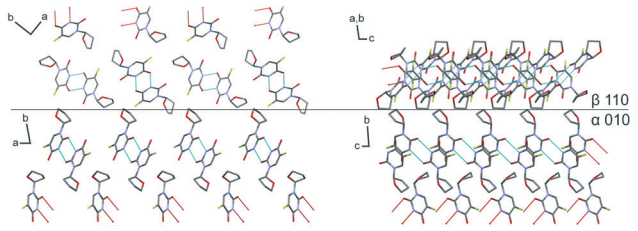

Fig. 12 Schematic model of β tegafur growing on the α tegafur (010) surface. Hydrogen atoms are omitted for clarity.

arrangement and conformation,[45,46] and therefore they could arrange into a state which promotes the growth of β tegafur. This means that the nucleation of β tegafur might be favoured by surface molecule rearrangement. The {110} surface of β tegafur and the {010} surface of α tegafur have similar tegafur molecular arrangement at the surface and distances between tegafur dimers are the same for both polymorphs in relevant directions. Because of this, nucleation of β tegafur on the {010} face of α tegafur might be initiated by minor surface tegafur dimer displacement, conformation change, and rotation. The strongest hydrogen bond donor and acceptor groups are involved in dimer formation and interactions between dimers are relatively weak. These weak interactions at the growing surface are less efficient at directing the orientation of an incoming dimer synthon and therefore tegafur dimers at the surface are relatively mobile. Fig. 13 shows that the tegafur dimer arrangement similar to that in β tegafur could be achieved by minor α tegafur surface molecule rotation. Such local lattice disorder would spread and eventually thermodynamically stable β tegafur would nucleate and continue to grow.

In order to quantitatively compare SMPT rates in different solvents, experimental data were described with an appropriate kinetic model. Solid-state kinetic models are theoretical, mathematical descriptions of experimental data and are usually expressed as rate equations.[47] Many solid-state kinetic models have been developed based on certain mechanistic assumptions, while other models are more empirical and may have little mechanistic meaning. Models currently used in solid-state kinetic studies are classified according to their mechanistic features, such as nucleation, geometrical contraction, diffusion, and reaction order.[47] SEM imaging of the studied SMPT revealed that the phase transition took place on the solid phase surface (the phase transition was heterogeneous); therefore attempts were made to describe experimental data points with the most common solid-state kinetic models.[47] Evaluation of the observed phase transformation nature and crystal growth morphology indicated that experimental data were in agreement with those for power solid-sate kinetic models. The best correlation was observed when the experimental data points were fitted to the power model P2:

$$\alpha = (kt)^2 \quad (1)$$

where k is the phase transition rate constant, α is the weight fraction of β tegafur in the sample, and t is time. The correlation of the experimental data with the theoretical model and the phase transition rate constants in each solvent are given in Table 2. Rate constants were calculated using MS Excel Solver optimization software based on the least squares method.[48,49]

The power law model P2 used here assumes that the nucleation rate follows the power law, while nuclei growth is assumed to be constant.[47,50,51] Nuclei and crystal growth was constant, because it took place through crystallization from a saturated α tegafur solution. The limiting step in nuclei growth was the transport of the tegafur molecule to the crystallization zone. Diffusion of tegafur molecules was expected to occur at a constant rate throughout the phase transition, because the studied phase transition occurred in solution, which was saturated with respect to α tegafur (supersaturation was constant during phase transformation). Taking this into account, the nuclei growth rate can be assumed to be constant. This means that the rate-controlling step in the examined SMPT was nucleation. There are two scenarios for nucleation.[51] The first option is the simultaneous formation of all nuclei; the second option is that nucleation occurs stepwise, with nuclei forming over a period of time. SEM imaging (Fig. 10) shows that β tegafur crystals, observed in the sample where β tegafur was first detected, had deviations in the crystal size. This indicates that nucleation in the examined SMPT

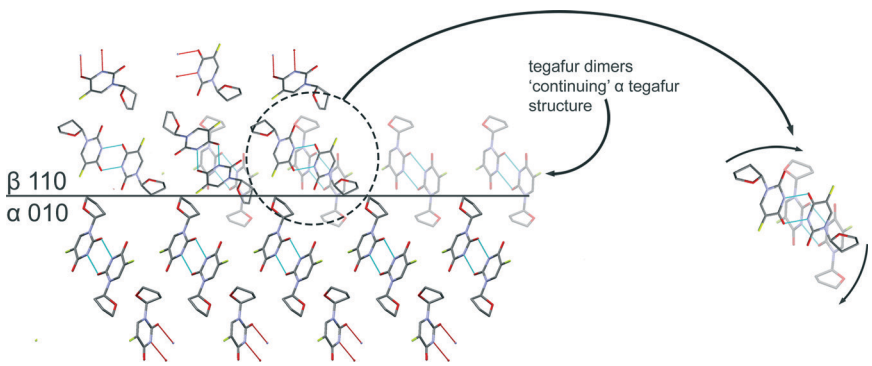

Fig. 13 Schematic representation of the tegafur dimer rearrangement on the α tegafur surface to initiate the growth of β tegafur. Hydrogen atoms are omitted for clarity.

Table 2 The P2 model rate constants for SMPT and correlation coefficients depending on the solvent used; the experiment was performed at 22 °C

Solvent	Rate constant, min^{-1}	Correlation with the P2 model, R^2
Acetone	0.028	0.92
Ethanol	0.023	0.96
i-Propanol	0.0090	0.92
Water	0.0065	0.98
Toluene	0.0056	0.98

occurred over a period of time. Besides, it is very unlikely that all of the nucleation sites would have approximately the same minimum reaction (phase transition) activation energy, which would be necessary for simultaneous nucleation. Clearly, nuclei formed first at the nucleation sites with the lowest activation energy, and then nucleation gradually spread to the other nucleation sites in an increasing activation energy order. Since nuclei and crystal growth was constant, this nucleation behavior can be described with a second-order power function.

The fact that the best experimental and theoretical data correlation was observed for the 2-dimensional model indicates that the phase transition rate most likely was proportional to the surface area of the β tegafur crystals formed.[51] With that said, we can conclude that in the examined SMPT, nucleation of β tegafur crystals corresponds to a second-order power function, their growth rate was constant, and the phase transition rate was proportional to the β tegafur crystal surface area.

Despite the fact that solubility and phase transformation kinetic data suggested that this phase transformation was limited by nucleation, the correlation between the SMPT rate constant and the difference between α and β tegafur solubilities in the respective solvent was observed: a faster phase transition was observed for the samples slurried in solvents where the difference in polymorph solubilities was high (Fig. 14). This trend in the SMPT from α tegafur to β tegafur was described by the equation:

$$k = (0.72 \pm 0.07)\Delta\text{sol.} + (0.005 \pm 0.001) \quad (2)$$

where Δsol. is the difference between α and β tegafur equilibrium solubilities in the respective solvent, and k is the rate constant for the SMPT in the same solvent. The correlation coefficient was $R^2 = 0.97$. This correlation means that the driving force in the studied SMPT was excess concentration above the equilibrium concentration of β tegafur, *i.e.* supersaturation with respect to β tegafur. Supersaturation provided the necessary driving force to overcome the energy barrier to promote β tegafur nuclei and crystal growth.[3] In this case, supersaturation coincided with the difference between α and β tegafur equilibrium solubilities in the respective solvent, because the solution concentration throughout the phase transformation was fixed at the equilibrium concentration of α tegafur. Such a solution concentration profile also means

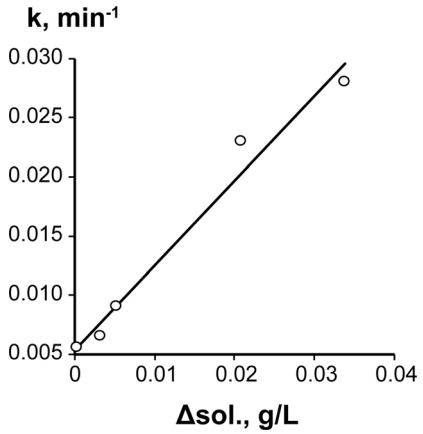

Fig. 14 Correlation between the SMPT rate constant in acetone, ethanol, i-propanol, toluene, and water and the difference between α and β tegafur solubilities (Δsol.) in the respective solvent. Correlation equation $y = (0.72 \pm 0.07)x + (0.005 \pm 0.001)$; $R^2 = 0.97$.

that the driving force was constant throughout the SMPT. Higher tegafur supersaturation in the solution promoted faster phase transformation to the thermodynamically stable β tegafur because of the increased degree of local organization in the solution necessary for crystallization[46] and the faster tegafur molecule transfer to the crystallization zone (molecules were relatively close). Absolute tegafur solubility and the difference between polymorph solubilities depend on the chosen solvent, however, the free energy (ΔG) difference between polymorphs does not depend on the solvent.[28] This means that the overall driving force of phase transformation was not dependent on the chosen solvent, and the SMPT rate depended only on the difference between polymorph solubilities (supersaturation). The only SMPT step that might be affected by solvent choice was β tegafur nucleation.[52–55] Tegafur molecules were solvated in the solution, similar to the surface of molecular aggregates and crystals. In order to nucleate and continue crystallization, tegafur molecules have to be desolvated, and solvent molecules on the nuclei or crystal surface have to be replaced by incoming tegafur molecules. This process, most likely, was affected by the nature of the solvent and its electron donor/acceptor properties, because strong solute–solvent interaction would inhibit desolvation and therefore nuclei growth, while weak solute–solvent interaction would not have a significant impact on nuclei growth.

3. Conclusions

The SMPT from α tegafur to β tegafur in acetone, cyclohexane, ethanol, i-propanol, toluene, and water at 22 °C is nucleation–growth controlled and can be described by the P2 power model. The rate constants for this process were in the range from 0.028 min^{-1} to 0.0056 min^{-1}. In all of the employed solvents, an induction time (about 10% of the time required for complete phase transition) was observed, indicating that nucleation and/or initial crystal growth was the

limiting factor for SMPTs performed in saturated solutions. In the examined SMPT, the nucleation of β tegafur crystals corresponded to a second-order power function, the nuclei and crystal growth rate was constant, and the phase transition rate was proportional to the β tegafur crystal surface area. Surface nucleation was observed in the studied SMPT. Crystal habit investigation indicated that β tegafur nucleated on the {010} face of α tegafur, and the {110} face of β tegafur was in contact with the α tegafur crystal. The SMPT rate depended linearly on the supersaturation level, *i.e.* the difference between α and β tegafur equilibrium solubilities in the respective solvent.

Acknowledgements

This work has been supported by the European Social Fund within the project "Support for Doctoral Studies at the University of Latvia". Authors acknowledge JSC Grindeks for supplying the α and β polymorphic forms of tegafur. We also acknowledge Liverpool John Moores University for allowing us to perform SEM imaging and Olga Paškova for conducting some of the experiments.

References

1 J. Bernstein, Polymorphism in Molecular Crystals, *IUCr Monographs on Crystallography*, Oxford University Press, 2007, p. 430.
2 J. Haleblian and W. McCrone, *J. Pharm. Sci.*, 1969, **58**, 911–929.
3 R. Hilfiker, *Polymorphism in the Pharmaceutical Industry*, ed. R. Hilfiker, Wiley-VCH, Weinheim, 2006, p. 433.
4 S. R. Vippagunta, H. G. Brittain and D. J. W. Grant, *Adv. Drug Delivery Rev.*, 2001, **48**, 3–26.
5 H. G. Brittain, *Polymorphism in Pharmaceutical Solids*, ed. H. G. Brittain, Informa Healthcare USA, Inc., New York, NY, 2nd edn, 2009, vol. 192, p. 640.
6 M. R. Caira, in *Design of Organic Solids*, ed. E. Weber, 1998, vol. 198, pp. 163–208.
7 W. Ostwald, *Z. Phys. Chem., Stoechiom. Verwandtschaftsl.*, 1897, **22**, 289.
8 D. Murphy, F. Rodríguez-Cintrón, B. Langevin, R. C. Kelly and N. Rodríguez-Hornedo, *Int. J. Pharm.*, 2002, **246**, 121–134.
9 N. Rodríguez-Hornedo and D. Lechuga-Ballesteros, *Int. J. Pharm.*, 1992, **85**, 149–162.
10 N. Rodríguez-Hornedo and D. Murphy, *J. Pharm. Sci.*, 1999, **88**, 651–660.
11 P. T. Cardew and R. J. Davey, *Proc. R. Soc. London, Ser. A*, 1985, **398**, 415–428.
12 R. J. Davey, P. T. Cardew, D. McEwan and D. E. Sadler, *J. Cryst. Growth*, 1986, **79**, 648–653.
13 D. M. Croker, R. J. Davey, Å. C. Rasmuson and C. C. Seaton, *CrystEngComm*, 2013, **15**, 2044.
14 M. A. O'Mahony, C. C. Seaton, D. M. Croker, S. Veesler, Å. C. Rasmuson and B. K. Hodnett, *Cryst. Growth Des.*, 2013, **13**, 1861–1871.
15 A. Maher, D. M. Croker, Å. C. Rasmuson, B. K. Hodnett and M. A. O'Mahony, *Cryst. Growth Des.*, 2012, **12**, 1925–1932.
16 A. Maher, D. M. Croker, Å. C. Rasmuson and B. K. Hodnett, *Cryst. Growth Des.*, 2012, **12**, 6151–6157.
17 A. Maher, C. C. Seaton, S. Hudson, D. M. Croker, Å. C. Rasmuson and B. K. Hodnett, *Cryst. Growth Des.*, 2012, **12**, 6223–6233.
18 P. Lehto, J. Aaltonen, M. Tenho, J. Rantanen, J. Hirvonen, V. P. Tanninen and L. Peltonen, *J. Pharm. Sci.*, 2009, **98**, 985–996.
19 J. H. T. Horst and P. W. Cains, *Cryst. Growth Des.*, 2008, **8**, 2537–2542.
20 H. Qu, M. Louhi-Kultanen, J. Rantanen and J. Kallas, *Cryst. Growth Des.*, 2006, **6**, 2053–2060.
21 J. Schöll, D. Bonalumi, L. Vicum, M. Mazzotti and M. Müller, *Cryst. Growth Des.*, 2006, **6**, 881–891.
22 J. Aaltonen, P. Heinänen, L. Peltonen, H. Kortejärvi, V. P. Tanninen, L. Christiansen, J. Hirvonen, J. Yliruusi and J. Rantanen, *J. Pharm. Sci.*, 2006, **95**, 2730–2737.
23 E. S. Ferrari and R. J. Davey, *Cryst. Growth Des.*, 2004, **4**, 1061–1068.
24 S. Maruyama and H. Ooshima, *Chem. Eng. J.*, 2001, **81**, 1–7.
25 C. Cashell, D. Corcoran and B. K. Hodnett, *Cryst. Growth Des.*, 2005, **5**, 593–597.
26 G. T. Beckham, B. Peters, C. Starbuck, N. Variankaval and B. L. Trout, *J. Am. Chem. Soc.*, 2007, **129**, 4714–4723.
27 E. S. Ferrari, R. J. Davey, W. I. Cross, A. L. Gillon and C. S. Towler, *Cryst. Growth Des.*, 2003, **3**, 53–60.
28 R. J. Davey, N. Blagden, S. Righini, H. Alison and E. S. Ferrari, *J. Phys. Chem. B*, 2002, **106**, 1954–1959.
29 G. J. Tanoury, R. Hett, D. W. Kessler, S. A. Wald and C. H. Senanayake, *Org. Process Res. Dev.*, 2002, **6**, 855–862.
30 K. Saranteas, R. Bakale, Y. Hong, H. Luong, R. Foroughi and S. Wald, *Org. Process Res. Dev.*, 2005, **9**, 911–922.
31 T. Uchida, E. Yonemochi, T. Oguchi, K. Terada, K. Yamamoto and Y. Nakai, *Chem. Pharm. Bull.*, 1993, **41**, 1632–1635.
32 A. Actiņš, S. Beļakovs, L. Orola and M. V. Veidis, *Latv. Kim. Z.*, 2006, **2**, 120–124.
33 F. Needham, J. Faber, T. G. Fawcett and D. H. Olson, *Powder Diffr.*, 2006, **21**, 245–247.
34 J. Bergmann, P. Friedel and R. Kleeberg, *CPD Newsl.*, 1998, vol. 20, pp. 5–8.
35 B. V. Nonius, *Nonius KappaCCD Collect*, 1998.
36 Y. Nakai, K. Yamamoto, K. Terada and T. Uchida, in *Proceedings of the 5th symposium on development and evaluation of pharmaceutical preparations*, Naoya, 1983, vol. 7, p. s–22.
37 Y. Nakai, K. Yamamoto, K. Terada, T. Uchida, K. Yamaguchi and N. Shimizu, *Chem. Pharm. Bull.*, 1986, **34**, 1242–1248.
38 R. Jenkins and R. L. Snyder, *Introduction to X-ray Powder Diffractometry*, John Wiley & Sons, Inc., Hoboken, NJ, USA, 1996, p. 432.
39 S. N. Campbell Roberts, A. C. Williams, I. M. Grimsey and S. W. Booth, *J. Pharm. Biomed. Anal.*, 2002, **28**, 1149–1159.
40 R. Bobrovs, S. Petkune and A. Actiņš, *Latv. Kim. Z.*, 2010, **1**, 3–16.

41 S. Petkune, R. Bobrovs and A. Actiņš, *Pharm. Dev. Technol.*, 2012, **17**, 625–631.
42 S. Khoshkhoo and J. Anwar, *J. Phys. D: Appl. Phys.*, 1993, **26**, B90–B93.
43 D. Croker and B. K. Hodnett, *Cryst. Growth Des.*, 2010, **10**, 2806–2816.
44 A. Hillier and M. Ward, *Phys. Rev. B: Condens. Matter Mater. Phys.*, 1996, **54**, 14037–14051.
45 H.-H. Tung, E. L. Paul, M. Midler and J. A. McCauley, *Crystallization of Organic Compounds: An Industrial Perspective*, John Wiley & Sons, Inc., Hoboken, NJ, USA, 2009, p. 304.
46 J. W. Mullin, *Crystallization*, Butterworth-Heinemann, Oxford, 4th edn, 2001, p. 600.
47 A. Khawam and D. R. Flanagan, *J. Phys. Chem. B*, 2006, **110**, 17315–17328.
48 A. Bērziņš and A. Actiņš, *J. Pharm. Sci.*, 2014, **103**, 1747–1755.
49 M. Berman, E. Shahn and M. F. Weiss, *Biophys. J.*, 1962, **2**, 275–287.
50 A. R. Allnatt and P. W. M. Jacobs, *Can. J. Chem.*, 1968, **46**, 111–116.
51 L. G. Harrison, in *The Theory of Kinetics*, ed. R. G. Compton, C. H. Bamford and C. F. H. Tipper, Elsevier Scientific Publishing Company, 1969, vol. 2, pp. 377–462.
52 D. Musumeci, C. A. Hunter and J. F. McCabe, *Cryst. Growth Des.*, 2010, **10**, 1661–1664.
53 R. J. Davey, G. Dent, R. K. Mughal and S. Parveen, *Cryst. Growth Des.*, 2006, **6**, 1788–1796.
54 S. A. Kulkarni, E. S. McGarrity, H. Meekes and J. H. ter Horst, *Chem. Commun.*, 2012, **48**, 4983–4985.
55 R. Davey and J. Garside, *From Molecules to Crystallizers*, Oxford University Press, 2000, p. 96.

CrystEngComm

PAPER

View Article Online
View Journal

Cite this: DOI: 10.1039/c4ce02484b

The reluctant polymorph: investigation into the effect of self-association on the solvent mediated phase transformation and nucleation of theophylline†

Raitis Bobrovs,*[ab] Linda Seton*[a] and Nicola Dempster[a]

Received 17th December 2014,
Accepted 15th February 2015

DOI: 10.1039/c4ce02484b

www.rsc.org/crystengcomm

Little is known concerning the pathway of the crystallization of the thermodynamically stable polymorph of theophylline, form IV. Here we study the reasons why the thermodynamically stable theophylline form IV can be obtained only by slow, solvent mediated phase transformation (SMPT) in specific solvents, and whether the presence of prenucleation aggregates affect the polymorphic outcome. Solution concentration, polymorphic composition and morphology were monitored over time during the transformation from form II to form IV in several solvents. NMR and FTIR spectroscopy were used to detect prenucleation molecular aggregates present in the solutions. It was determined that theophylline self-associates in solvents which are good H-bond donors and the presence of these aggregates hinder the nucleation and phase transformation. SMPT from form II to form IV is a nucleation-growth controlled polymorphic transformation, nucleation is most likely homogenous, and form IV crystals grow along the (001) plane, forming plate-like crystals.

1. Introduction

Polymorphism is a well-known phenomenon whereby a chemical compound may exist in more than one crystalline form, and each of these forms displays different physical characteristics such as density, melting point and solubility. Polymorphism is of great importance in the pharmaceutical industry, because these differences in physical properties among the polymorphs can sometimes lead to apparent differences in drug processing, formulation, and bioavailability. Therefore, it is a common requirement in Pharmacopeia for active pharmaceutical ingredients to be produced in one fixed crystalline form, and for this reason the thermodynamically stable form is generally preferred for pharmaceutical production. However, a metastable polymorph may be preferred if the solubility and/or bioavailability of the thermodynamically stable polymorph does not meet required criteria.[1–3] In such cases knowledge of the possible phase transformation in a given polymorphic system is essential.

Theophylline – a methyl xanthine derivative (3,7 dihydro-1,3-dimethyl-1*H*-purine-2,6-dione) is an example of a pharmaceutically active compound that has been manufactured and used in a metastable crystalline phase (clearly, because of the lack of comprehensive knowledge of the polymorphic landscape of this compound) (Scheme 1). Theophylline is known to exist in four polymorphic forms (I, II, III and IV), as a monohydrate and a dimethyl sulfoxide solvate.[4] Theophylline form II is a metastable polymorph crystallized from most non-aqueous solution at room temperature. It is kinetically stable and was historically considered as the thermodynamically stable polymorph, until form IV was presented[5] and proved to be more stable. The fact that the thermodynamically stable theophylline polymorph was discovered only recently, is because it does not crystallize directly from solution, and is obtained only by slow, solvent mediated transformation (SMPT) from form II in contact with solvent *e.g.* methanol, 2-propanol or chloroform.[5] Theophylline form I has been reported as the stable polymorph at higher temperatures, whereas form III is highly metastable and has been obtained only during the dehydration of monohydrate.[6,7] Theophylline monohydrate (referred to as form M) is a monoclinic channel

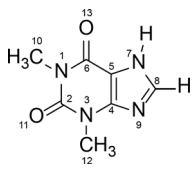

Scheme 1 Molecular structure of theophylline (3,7 dihydro-1,3-dimethyl-1*H*-purine-2,6-dione).

[a] *Drug Delivery and Materials Science Research Group, School of Pharmacy and Biomolecular Sciences, Liverpool John Moores University, Liverpool, L3 3AF, UK. E-mail: raitis.bobrovs@gmail.com, L.Seton@ljmu.ac.uk*
[b] *Faculty of Chemistry, University of Latvia, Kr. Valdemāra iela 48, Rīga, LV-1013, Latvia*

† Electronic supplementary information (ESI) available. See DOI: 10.1039/c4ce02484b

type hydrate which has been shown to lose water, either in low humidity or at temperatures above 353 K, to produce form II.[8,9] Theophylline has been screened for cocrystallization and shown to produce co-crystals with a range of coformers; many complexes formed between theophylline and acids (*e.g.* oxalic acid, malonic acid, salicylic acid, sulfathiazole, acetaminophen, *etc.*) as well as bases (*e.g.* urea, benzylamine, phenobarbital, *etc.*) have been summarized by Childs *et al.*[10]

The aim of this work is to understand why the thermodynamically stable theophylline form IV can be obtained only by solvent mediated transformation in specific solvents, and to investigate the presence of prenucleation aggregates which direct the polymorphic outcome of crystallization.

Hunter *et al.*[11–13] and Davey *et al.*[14,15] have shown that there is a correlation between supramolecular aggregates in solution and the solid state structure which subsequently crystallizes. Early experiments[16–19] on theophylline self-association provide evidence that theophylline does self-associate in aqueous solution and the proposed aggregate is the theophylline dimer. The theophylline dimer discussed in these studies is present in the thermodynamically stable form IV, and theophylline monohydrate, form M, which crystallizes from aqueous solutions. Theophylline form II, the polymorph commonly crystallized from most non-aqueous solutions, does not contain this dimer motif (crystal structures of theophylline polymorphs are discussed in detail in section 2.1). Such behaviour raises two questions: why does metastable form II crystallize from non-aqueous solvents; what prenucleation aggregates are present in non-aqueous solvents? In order to answer these questions, we need to determine (a) does theophylline self-associate in other solvents besides water, and, if it does, what is the nature of the association, and (b) since the nucleation of form IV is kinetically slow, does solution aggregation change over time?

2. Background

2.1. Polymorphism of theophylline

Crystal structures of theophylline crystalline forms relevant for this research are shown in Fig. 1. In the form II structure the best hydrogen bond donor (N7–H) bonds to the best hydrogen bond acceptor (N9),[20,21] consistent with Etter's rules,[22] forming an $R_2^2(8)$ motif. The structure has two weak, bifurcated C8–H···O13 hydrogen bonds. Theophylline molecules are linked in chains and stacked along (010). This catemer arrangement promotes crystal growth along the molecular chains leading to an elongated crystal morphology. Form IV has two molecules in its asymmetric unit,[23] forming a dimer with the $R_2^2(10)$ motif and connected *via* (N7–H···O13) hydrogen bonds. The dimer is discrete and only links to other dimers by weak interactions: C8–H···N9, C8–H···O11, and by π–π stacking, forming a two-dimensional network parallel to the (001). The dimer is similar to the motif observed in the monohydrate and in a number of theophylline cocrystals.[10,21] The presence of this dimer motif in the thermodynamically stable form IV and theophylline monohydrate, considered to be the most stable structure in an aqueous environment, may account for the thermodynamic stability of this structural motif compared to the chain motif of form II. In form M, two centrosymmetrically related theophylline molecules form a dimer through two hydrogen bonds (N7–H···O13).[24] Theophylline dimers are connected by water molecules through hydrogen bonds, forming parallel, crosslinked chains, leading to two-dimensional hydrogen bonded layers, parallel to (10–1) plane. Water molecules are situated in channels along the *a* axis, where they form hydrogen bonds to the theophylline N9 atom. In theophylline dimethyl sulfoxide solvate theophylline is hydrogen bonded to the dimethyl sulfoxide molecule through an N7–H···O=S hydrogen bond.[4] The packing consists of molecular chains lying parallel to the (010), stacked by π–π interaction between pyrimidine and imidazole rings, and weak hydrogen bonds between dimethyl sulfoxide methyl groups and theophylline carbonyl group (C_{DMSO}–H···O13).

2.2. Solvent mediated phase transformations

Solvent mediated phase transformations (SMPTs) are common in polymorphic materials which often follow Ostwald's rule of stages.[25] The transformation proceeds by three stages:

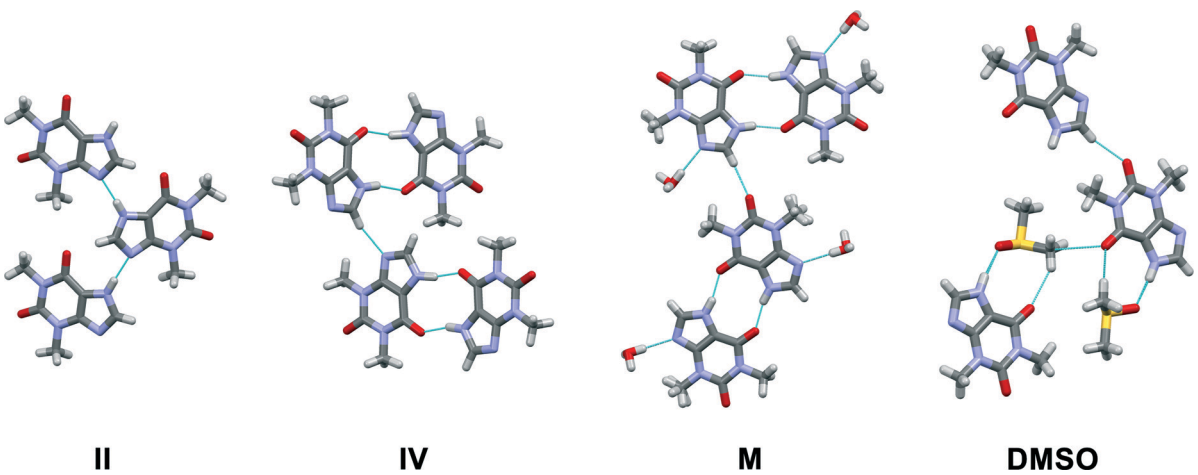

Fig. 1 Crystal packing motifs in theophylline form II, form IV, theophylline monohydrate and DMSO solvate.

firstly, the metastable polymorph in contact with solution dissolves into the bulk. Secondly, the stable form nucleates, and thirdly undergoes crystal growth. When complete, only the stable form remains in solution. The thermodynamic driving force is the Gibbs free energy difference between the two solid structures, whereas the kinetic driving force is the difference in the solubilities of the two polymorphs and thus the level of supersaturation with respect to the stable form.[26–30]

SMPTs are characterized by the phase transformation time, induction time, and active phase transformation time. The term "phase transformation" refers to the whole process from the beginning of the experiment until the phase transformation is complete; the initial period during which no phase transformation product is observed is called "induction"; and the time from the point when thermodynamically stable phase appears until the sample has been fully converted is called the "active transformation phase".[31] All of these parameters can be influenced by choice of solvent and solution composition.

2.3. Spectroscopic self-association studies

NMR spectroscopy is mainly used as a method for organic compound identification and characterization; however NMR methods have been demonstrated to be useful for the study of molecular aggregation and self-association in solution. It is possible to use solution NMR measurements to study molecular association because ^{1}H chemical shifts are sensitive to changes in the local environment. Hydrogen bonding between solute molecules and associate formation affects the ^{1}H local environment and a result of this interaction is a chemical shift displacement in the NMR spectrum.[32–34]

It is generally recognized that dimer and other associate formation and their concentration are affected by solution concentration – the more concentrated the solution, the more dimers and other associates are present, therefore dependence of ^{1}H chemical shifts on concentration is analysed. This approach has been used in numerous studies.[35–44] Most of the previous studies show a decrease in the ^{1}H chemical shifts with concentration increase, suggesting that the analysed compounds are involved in self-association processes. Upon self-association, ^{1}H chemical shifts are displaced to lower field due to proton deshielding – the bond of the proton involved in self-association weakens, bond length increases, stretching frequency decreases.[45–49] The limitations for ^{1}H NMR self-association studies are that ^{1}H NMR shifts for nonexchangeable hydrogens only can be measured, and the NMR method has a limited sensitivity at the low concentrations often necessary for initial self-association studies.

In recent years, ^{1}H NMR chemical shift displacement measurements have been used to provide information on the structure of prenucleation aggregates in the solution.[50] Hunter *et al.*[13,51] showed that the predictions from concentration-dependent changes in ^{1}H NMR chemical shifts agreed with the structures of dimers found in the corresponding X-ray crystal structures.

Other magnetically active nuclei (^{13}C, ^{15}N and others) involved in hydrogen bonding or aromatic stacking also show displacement in chemical shifts upon concentration changes.[35,52–55]

Theophylline self-association in aqueous solution has been previously studied using NMR spectroscopy,[17,18] partitioning between water and chloroform–isooctane mixture,[19] analytical ultracentrifuge;[16] and in chloroform-D solution using IR spectroscopy.[56] These studies suggest that theophylline does self-associate in aqueous solutions and chloroform-D solution; however there is no consensus between these studies on the degree of self-association and nature of aggregates present in the solution.

3. Results and discussion

3.1. Characterisation of solvent mediated phase transformation

The SMPT of unprocessed commercial anhydrous theophylline form II in methanol was investigated. Three parallel experiments were performed, but for the sake of clarity only one case is taken as an example of the whole set of experiments to describe and discuss in detail the results obtained.

During the solvent mediated phase transformation qualitative and quantitative analysis of the solid phase were performed using powder X-ray diffractometry (PXRD), Fourier transform infrared spectroscopy (FTIR) and scanning electron microscopy (SEM) methods; while the solution concentration throughout the transformation was monitored using ultraviolet-visible (UV/Vis) spectroscopy. The composition of solid phase determined by PXRD method and solution concentration throughout SMPT is presented in Fig. 2. Results of all three parallel experiments showed that the phase transformation from theophylline form II to form IV took ~6 to 8 days. Phase transformation had a considerable induction time with a relatively high dispersion (4 to 6 days), while the active phase transition (actual form IV increase in the sample) consistently took ~2 days. Such behaviour, that induction time for parallel experiments had a great variation, while the active phase transition time in all cases was approximately the same, suggests that the limiting step for this SMPT is the nucleation of form IV. The main factors that might affect the nucleation and hence the induction time are discussed further.

The equilibrium saturation of the metastable form II was reached ~3 h after the theophylline addition to methanol. The concentration of the solution remained the same until phase transformation was completed. Solution concentration dropped to the equilibrium saturation of the thermodynamically stable form IV within a few hours of the phase transformation being completed, indicating that, once all of the form II in the sample had dissolved, form IV continued to grow until the solution reached the form IV equilibrium concentration. This shows that the dissolution rate of theophylline

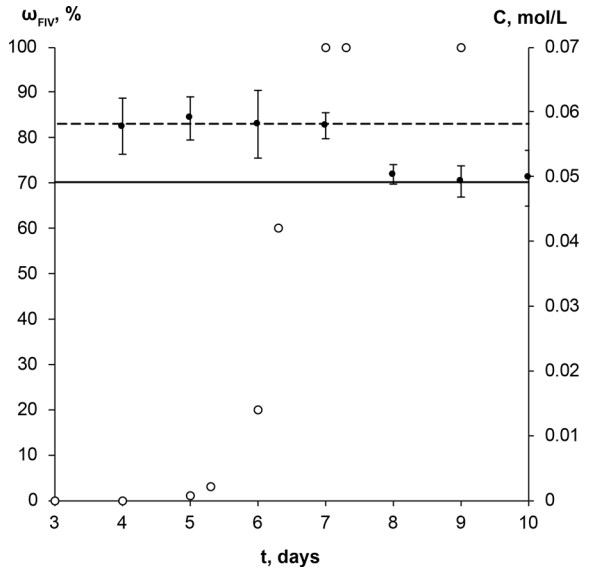

Fig. 2 Solution concentration (●), and weight fraction of the theophylline form IV in the solid phase (○) during the solution mediated transformation from theophylline form II to form IV in methanol at 23 °C. The dashed line (—) represents the solubility of theophylline form II, continuous line (—) – solubility of theophylline form IV.

form II was faster than the growth of form IV and dissolution was not the limiting step in the phase transformation. Such a solution concentration profile and pronounced induction period indicates that the SMPT was a 'nucleation-growth controlled polymorphic transformation'.[57] The fact that phase transformation is also growth limited was confirmed by the time scale of the studied SMPT – most of the SMPTs described in the literature take place within a few hours,[29,57–65] but here phase transformation took ~2 days from the moment when form IV nucleated. This might be due to low supersaturation, which provided the necessary driving force to overcome the energy barrier and promoted form IV crystallization.[3] In this case, supersaturation is the difference between the solubilities of form II and form IV.

The increase of the form IV content in the sample exhibited an *exponential* nature – the amount of form IV increased slowly in the initial stage and then accelerated. Such behaviour suggests that the growth of form IV might be limited by the surface area of form IV in the sample; hence, the rate of SMPT increased as the crystal size (surface area) in the sample increased. This assumption was consistent with SEM imaging data, shown in Fig. 3.

It is known[5] that theophylline form II exhibits a needle-like morphology, while form IV crystallizes in hexagonal plate-like crystals. These distinct differences in the crystal shape allowed phase transition monitoring using microscopy methods. SEM imaging of the solid phase throughout SMPT (Fig. 3) revealed that during the first days, while no phase transformation was observed, the only apparent change in the solid phase was the agitation and Ostwald's ripening of the theophylline form II crystals – small theophylline form II crystals dissolved as growth occurred on the larger form II crystal side planes (see Fig. 3, day 1 and day 3). Thus, larger theophylline form II crystals grew at the expense of the small particles. The reason for this process was the difference in dissolution rate between small and large particles.[66] Theophylline form IV crystals were first observed after 5 days, and all observed hexagonal form IV crystals were approximately the same size: ~40 μm in diameter and 1–2 μm thick. A similar size for all observed form IV crystals suggests that they nucleated simultaneously or in a very short time interval. Recent studies[60,65,67,68] show that surface nucleation dominates in most of SMPTs, however in our case there was no clear evidence of such behaviour. We believe that theophylline form IV nucleated by homogeneous primary nucleation from saturated solution because none of the observed form IV crystals were clearly merged together with metastable form II.

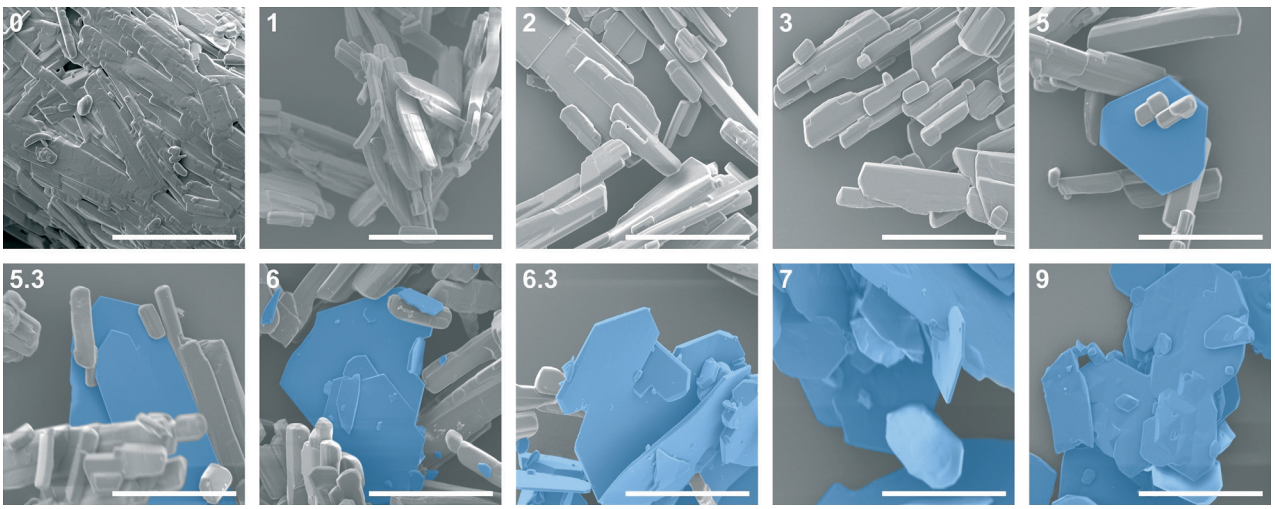

Fig. 3 SEM images throughout SMPT from theophylline form II to form IV in methanol at 23 °C. Inset: time of sample gathering (days); 40 μm scale bar, crystals of theophylline form IV indicated with blue colour.

Moreover, taking in to account that theophylline form IV nucleated only after several days, homogeneous nucleation is more likely as heterogeneous nucleation usually takes place in shorter time scale due to lower energy barrier. Over time form IV crystals grew significantly in 2 dimensions, forming large, plate-like crystals. This growth pattern indicates that the growth of the form IV was governed by the surface of the crystal edges. Eventually, breakage of form IV crystals was observed (day 6), which would lead to increased surface area of the edge faces, where crystal growth was fastest, thereby accelerating the crystallization rate of form IV.

Preferred form IV crystal growth directions were determined by the PXRD method. It is observed that the PXRD pattern of form IV crystals after the SMPT have two very intensive peaks at 12 and 23° 2θ (Fig. 4), suggesting that the sample exhibits preferred orientation. Comparison of the pattern with that simulated from the crystal structure revealed that these intensive diffraction peaks arise from crystal planes (002) and (004) – the multiple planes of the {001} face family. Since plate-like crystals tend to lay down with the dominant faces parallel to the PXRD sample holder, the most intense diffraction should occur from this plane. It can therefore be concluded that the dominant face in the form IV crystals obtained during SMPT is (001) and crystal growth occurred almost exclusively along this plane. The reason for such crystal growth behaviour is that there are no significant intermolecular interactions in the *c*-direction of theophylline form IV, whereas crystal growth along (001) plane is favoured by hydrogen bonding and π–π stacking (Fig. 5).

Based on morphological observation, form IV crystal growth perpendicular to (001) was observed only when phase transformation was finished – during the SMPT the surfaces of form IV crystal plane (001) were flat (Fig. 3, day 8.3), whereas 2 days after the SMPT elevations on the surface of the form IV were observed because of crystal agitation (Fig. 3, day 10). The crystal growth rate along (001) was considerably higher than growth rate perpendicular to (001) during phase transformation, likely to be because energy released on solution molecule attachment to growing crystal edge surface was higher.[69] When phase transformation was complete, Ostwald's ripening[66] took place and crystals tended to achieve minimum total surface energy by reducing the crystal surface area. Here, this means that crystals grew perpendicular to the large (001) plane at the expense of the crystal edges, which dissolved more easily.[66]

Surface nucleation dominates in the majority of SMPTs, therefore experiments with ground and lyophilized theophylline as a starting material were performed to evaluate the effect of the form II surface on the nucleation and crystallization of form IV. There were no significant differences in the phase transformation behaviour when ground and unground theophylline was used. PXRD and SEM data showed that when the ground form II was agitated, Ostwald's ripening took place, and crystallization of form IV followed only after 6 days. If theophylline form IV nucleated on the surface of the form II, the increase of the form II surface area in the ground sample should reduce the induction time. However, this was not observed, suggesting that form IV did not nucleate on the surface of form II. When lyophilized theophylline, confirmed as a mixture of amorphous theophylline and microcrystalline form II, was used, no phase transition to form IV was observed within the studied time (90 days). The crystallinity of lyophilized material increased due to transformation of amorphous material to form II (Fig. 6), but no phase transformation to form IV was detected. It is not clear why crystallinity of the form II starting material should influence the nucleation of form IV since this is not a surface nucleation process. Later experiments on water content (see below) indicate that the ability of amorphous material to absorb water might be more important than crystallinity.

In order to ascertain whether theophylline aggregates present in the methanol solution affect the phase transformation, an experiment using methanol solution saturated with respect to form IV as a solution medium was performed. The SMPT held approximately the same induction and active phase transformation time (5 and 2 days, respectively) as experiments in methanol.

Similar experiments with theophylline form II and form IV mixture (w_{II}/w_{IV}; 90/10) as a starting material were performed to exclude induction time and observe only phase

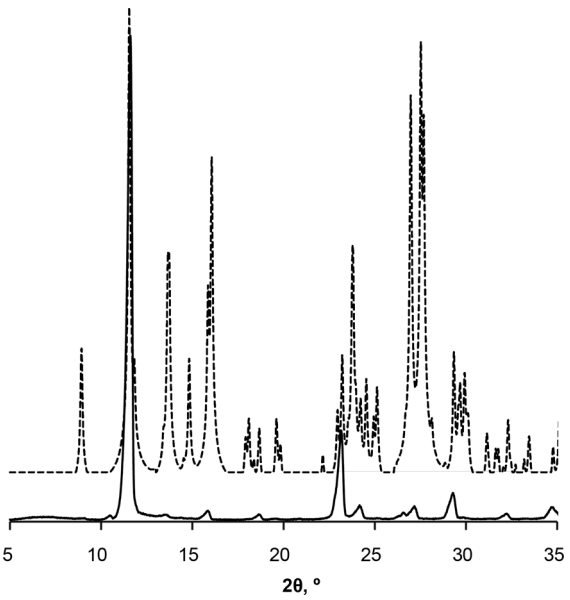

Fig. 4 PXRD patterns of form IV obtained by SMPT in methanol (solid line); and simulated from crystal structure (dashed line).

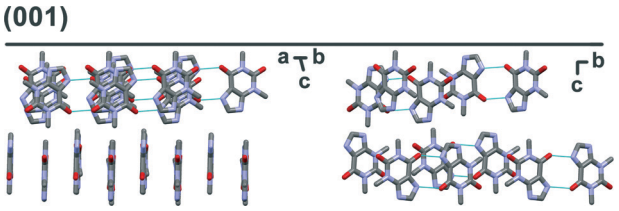

Fig. 5 Crystal packing in theophylline form IV along (001) plane. Hydrogens are omitted for clarity.

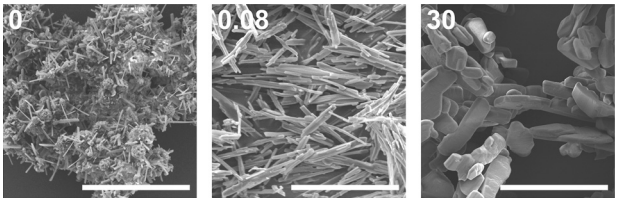

Fig. 6 SEM images throughout lyophilized theophylline slurrying in methanol at 23 °C. Inset: time of sample gathering (days) and 20 μm scale bar.

transformation. No induction times were observed in either case, and phase transformation rates were the same regardless of solution composition (Fig. 7). This means the molecular aggregates, if there were any at all, in both saturated solutions were the same and/or they did not play a significant role in the phase transformation. If we compare theophylline form IV weight fraction change over the time in these experiments and those performed with commercial form II as a starting material, we see that active phase transformation with theophylline form II and IV mixture as a starting material occurs three times faster. It is possible that this phase transformation rate mismatch is due to differences in the form IV crystal *active* edge surface areas for the samples. SEM imaging confirmed that form IV edge surface area in prepared polymorphic mixtures were larger, than in the sample where the same amount of form IV was generated by SMPT. Since this is the region in which growth of form IV dominates, larger surface area leads to faster rate of growth,

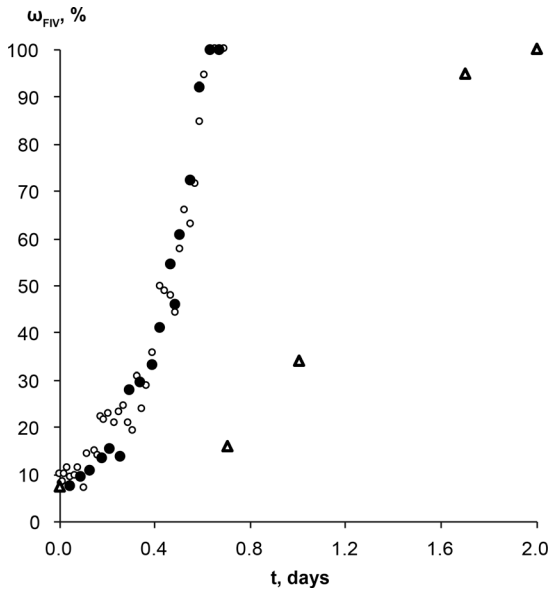

Fig. 7 Weight fraction of the theophylline form IV in the SMPT from theophylline form II/form IV mixture (w_{II}/w_{IV}; 90/10) to form IV, in saturated (○) form IV and (●) form II methanol solutions at 23 °C. Δ represents the weight fraction of the theophylline form IV in the solid phase during the SMPT from theophylline form II in methanol at 23 °C. All kinetic curves are aligned to the point when solid phase of respective SMPT contained 10% of form IV.

therefore a faster transformation. It is also possible that in the studied SMPT the initial nucleation is homogeneous, but, once form IV is present, then secondary nucleation may subsequently occur, leading to increasing transformation rate as observed. By seeding with form IV in this experiment, the initial phase was skipped and form IV nucleated by secondary nucleation. Secondary nucleation promoted faster phase transformation by detachment of weak outgrowths of form IV seed crystals or fragmentation of a weak polycrystalline form IV mass.[66]

Seton *et al.*[5] reported that theophylline equilibrium solid phase depends on the water activity in the solution, and that form IV is preferred when water activity in the solution is below 0.69 (V_{MeOH}/V_{H_2O}, 55/45). To investigate the possibility that water activity also influences the phase transformation rate to form IV, SMPT was observed in methanol samples with different water contents. SMPT from theophylline form II to form IV, performed in dried methanol and methanol/water mixtures with volume ratios (V_{MeOH}/V_{H_2O}) 99 : 1, 95 : 5 and 80 : 20, clearly showed that increased water in the solution increased the induction time (Fig. 8A). Given the stochastic nature of nucleation, it can be difficult to draw conclusions from a few experiments, however, the three parallel SMPT showed relatively good reproducibility and a clear trend. Active phase transformation time also increased but with a lesser effect – from 1.5 days in dried methanol to 5 days in methanol/water mixture (V_{MeOH}/V_{H_2O}; 95/5).

These results might explain why fluctuation of induction time were observed in the earlier SMPTs. Methanol used in initial experiments was used as received and was taken from different batches, therefore the water content (adsorbed from the air) was not the same in all samples. Karl Fisher titration showed that batch methanol contained ~0.2% of water, whereas methanol dried with anhydrous $NaSO_4$ contained less than 0.1% water. These minor water impurities affected the induction time of the SMPT. This might be the reason why phase transformation with lyophilized theophylline as starting material was hindered. Theophylline lyophilisation resulted in partially amorphous theophylline, which tends to absorb more water from the air than crystalline phases,[70] and it is possible that the phase transition in this case was slowed down by adsorbed water.

The induction times and transformation times in a range of solvents were measured and compared (Fig. 8B). We see that phase transition times correlated to induction times – the longer the induction time, the slower the phase transformation. This might indicate that nucleation and form IV growth were limited by the same factors. The solvents were used as received and were from newly opened bottles. Water doping experiments were not performed in the other solvents, so further investigation would show whether induction and transformation times were similarly affected in all solvents.

It has been shown previously[30] that in the nucleation-growth controlled SMPT between α and β tegafur, the phase transformation rate and induction time linearly depends on

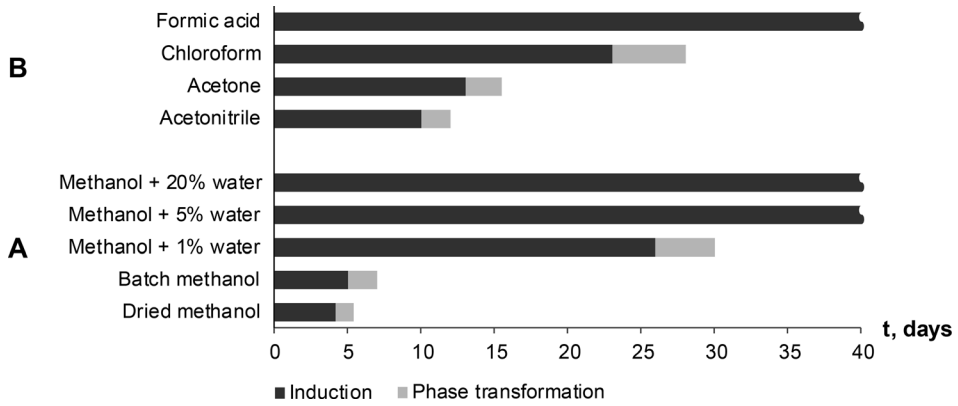

Fig. 8 Induction and phase transformation times of SMPT from theophylline form II to form IV at 23 °C depending on used solvent environment. No phase transformation to form IV was observed in formic acid and methanol/water mixtures with 5% and 20% of water within the studied period (40 days).

supersaturation level, *i.e.* difference between solubilities of the polymorphs. The difference in solubility of the two forms in methanol is low, so supersaturation with respect to form IV is always low. In formic acid, the solubility of form II is high, (30 times that in methanol, see ESI†) which might favour the metastable form according to Ostwald's rule.

Crystallization always gave form II, including crystallization from solutions with form IV equilibrium concentration. Even seeding with form IV, gave form II and form IV mixture.

Induction and phase transition times were longer in solvents (solvent mixtures) which had good proton donor groups. Fastest phase transformation and shortest induction time were observed in dried methanol, followed by stock methanol, acetonitrile and acetone. Longest induction times were observed in proton donor solvents – chloroform and formic acid, and previously discussed methanol/water mixtures. In fact, no form IV has been detected in formic acid and methanol/water mixtures 95/5 and 80/20 within the studied period of 90 days. An influencing factor might be behaviour of solvated/aggregated theophylline molecules in solution. Theophylline molecules are solvated in the solution, but in order to nucleate form IV and continue its growth, theophylline molecules have to be desolvated, and solvent molecules on the nuclei or crystal surface be replaced by incoming theophylline molecules. Taking in to account that induction time was several days and phase transformation was very slow, we can assume that solute–solvent interaction in studied SMPT was strong compared to solute–solute interaction and thus the desolvation process inhibited form IV nucleation and growth.

In order to further understand how the solvent environment affects SMPT rate and induction time, NMR spectroscopy was used to investigate for prenucleation aggregates in the solution.

3.2. Theophylline self-association studies

To understand solution chemistry and ascertain possible aggregation of theophylline molecules in solution, the influence of theophylline solution concentration on ^{1}H NMR chemical shift displacement was analysed. ^{1}H NMR experiments were carried out in seven solvents (methanol-D4, chloroform-D, acetone-D6, dimethyl sulfoxide-D6, deuterium oxide, acetonitrile-D3 and formic acid-D2). These solvents were chosen because: (a) it is known that in dimethyl sulfoxide and water theophylline crystallizes as solvates and the crystal structures of these solvates are not similar; (b) they have different H-bond donor/acceptor properties: acetone, acetonitrile and dimethyl sulfoxide are H-bond acceptor; chloroform is H-bond donor; water, methanol and formic acid are both – H-bond donor and acceptor; and (c) from formic acid theophylline crystallizes into form II with no subsequent transformation observed.

The concentration range covered in this experiment was the same for all solvents – from saturated to 1 μM theophylline form II solution. The number of scans for NMR spectra acquisition was adjusted depending on solution concentration. Theophylline solutions with lower concentrations were not studied because the NMR spectra acquisition time, necessary to obtain spectra with acceptable signal/noise ratio, would be unreasonably long.

The theophylline used in the experiment had natural ^{1}H/^{2}H abundances and therefore the most acidic imidazolium group proton (N7–H) took part in proton exchange with the deuterated solvent deuterium atoms. As a result, the imidazolium group proton was visible in the NMR spectra in solvents where only partial proton exchange took place – chloroform-D, dimethyl sulfoxide-D6 and acetonitrile-D3. Methyl group protons and alkene group proton (C8–H) did not showed any effect on proton exchange.

If there are multiple structures that have different thermodynamic stabilities and perturb the ^{1}H NMR chemical shifts in different ways, the shapes of the dilution curves differ for different signals. While this does not rule out the possibility of multiple structures, the data can be treated as a simple two state equilibrium, and the complexation-induced changes in chemical shift are assumed to relate to a single specific aggregate structure.[51] Since the solubility of the theophylline

in all selected solvents except formic acid is low (>0.06 M) multiple aggregate structures are not expected.

No chemical shift displacement upon concentration changes were observed in methanol-D4, acetone-D6, dimethyl sulfoxide-D6 and acetonitrile-D3. This means that no self-association takes place in these solvents, or theophylline undergoes dimerization or other self-association at concentrations lower than those covered in the experiment, *i.e.* below 1 μM, and other agglomerates do not form in the concentration region studied. It is unlikely that self-association occurs at such low concentrations, and it is probable that solvated theophylline monomers were the main species in the solution.

^{1}H NMR dilution studies in chloroform-D, deuterium oxide and formic acid-D2 showed large concentration-dependent changes in chemical shifts. In the chloroform-D all chemical shifts were displaced to lower fields as concentration increased (Fig. 9A). In deuterium oxide methyl groups ^{1}H chemical shifts were displaced to higher field while the alkene group proton (C8–H) chemical shift was displaced to the lower field (Fig. 9B). Imidazolium group proton (N7–H) chemical shift was not observed in the deuterium oxide due to proton exchange. In formic acid-D2 alkene group proton (C8–H) chemical shift was displaced to higher field, whereas imidazolium group proton (N7–H) chemical shift was displaced to lower field (Fig. 9C). Minor methyl groups ^{1}H chemical shift displacement to higher and field were observed as concentration increased. The pattern and magnitude of chemical shift changes are completely different in all solvents, indicating that aggregates present in these solutions are different. It is likely the associate existing in the deuterium oxide is the theophylline dimer which is also present in the crystal structure of theophylline monohydrate (Fig. 10A). The associates in chloroform-D solution might be the asymmetric dimer corresponding to Etter's rule (Fig. 10B), π–π stacked dimer or some associate involving solvent molecules. It is also possible, that chemical shift displacement is reflecting the average structure of multiple aggregates. Since theophylline solubility in formic acid is noticeably higher than in other solvents (more than 30 times), it is possible

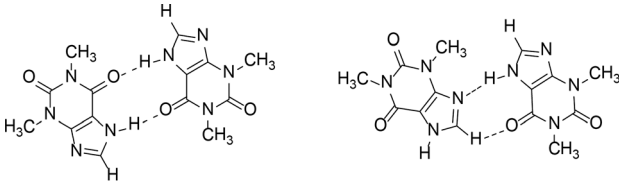

Fig. 10 Theophylline dimer present in crystal structures of monohydrate, form IV and most cocrystals (A); and the preferred theophylline dimer according to Etter's rules (B).

that associates present in formic acid-D2 were oligomers and not dimers. Data shows that theophylline concentration at which associates were formed were different in each solvent. In deuterium oxide theophylline formed self-associates at 10^{-4} M solution, in chloroform at 10^{-3} M solution, and in formic acid-D2 at 10^{-2} M solution.

No change in chemical shift displacement was observed with time (>20 days) in any studied solvents. Small scale SMPT performed in methanol-D4 showed the same – solution composition did not change over time; hence, no aggregates are formed or disarranged during slurrying indicating that this is not the reason for long induction times.

Theophylline aggregates formed in solvents which are good proton donors.[71] These were the solvents where SMPT exhibited longest induction times and phase transition rates (we should mention that SMPT in water does not occur, because theophylline monohydrate is the most stable crystalline form in aqueous environments). Such correlation implies that the presence of theophylline dimers or aggregates in the solution hinders the nucleation and growth of form IV. It is likely that the reason why good proton donors inhibit phase transformation and extend induction time is the formation of solvent molecule stabilized theophylline aggregates. Trask *et al.*[21] have suggested that the theophylline dimer motif is favoured by the presence of a competing strong hydrogen bond donor in the system (in this case formic acid, chloroform or water in methanol/water mixture). The strongest hydrogen bond donor in theophylline solution forms a

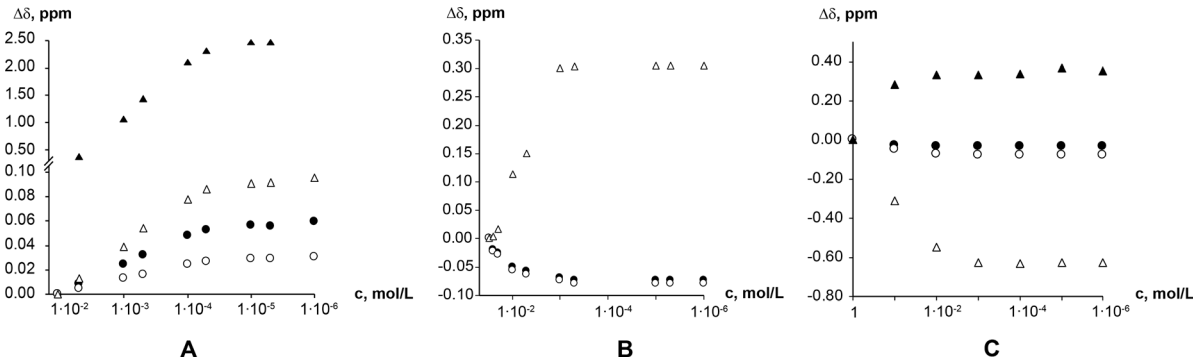

Fig. 9 Theophylline chemical shift displacement depending on chloroform-D (A); deuterium oxide (B); and formic acid-D2 (C) concentration. Chemical shifts are indicated as: methyl group C10 protons (●); methyl group C12 protons (○); alkene group proton (C8–H) (Δ); and imidazolium group proton (N7–H) (▲).

hydrogen bond with the system's most basic group – theophylline imidazole group nitrogen (N9). This bond fulfils the 'best-donor–best-acceptor' rule and consequently permits theophylline dimer formation by secondary hydrogen bonding (N7–H···O13). Such solvated theophylline dimer should be the most stable aggregate in the solution, since it uses the system's best donors and acceptors. This explains why increasing water in the methanol sample increased induction time and extended phase transformation time. The increase of water in methanol/water mixture increased the level of hydrated aggregates in the solution, and the more solution theophylline molecules were bound in these dimers, the more formation of form IV was hindered.

Solvated theophylline aggregates inhibit nucleation and growth of form IV, either because they are not the correct structure to nucleate form IV or because these associates need to be desolvated or disarranged in order to crystallize. If the solute solvent bonds are stronger than the weak inter dimer interactions in the solid structure, then the desolvation process is unfavourable and therefore phase transition is slow. Recent work by Sullivan *et al.*[72] shows that desolvation is a significant factor in the nucleation process and can dominate nucleation kinetics.

3.3. FTIR studies of theophylline crystallization from saturated solutions

It is known[2,3,73–75] that FTIR spectra of polymorphs and their solutions are different. Parveen *et al.*[76] have shown that FTIR spectroscopy can be used to show a direct relationship between molecular self-associates in solution and motifs in the subsequently crystallized solid phases. Here we use FTIR spectroscopy to monitor theophylline crystallization from acetone, acetonitrile, chloroform, methanol and water. FTIR spectra of saturated theophylline solution were continuously recorded during solvent evaporation and subsequent theophylline crystallization. FTIR spectra of both theophylline polymorphs studied in this work are clearly different and therefore suitable for such an experiment (Fig. 11). However, due to low theophylline solubility in the selected solvents, only the strongest carbonyl group stretching bands were visible in the initial spectra.

It is known[77] that hydrogen bonding lengthens and weakens the C═O bond, therefore the carbonyl group stretching band is observed at a lower frequency; thus the stronger the hydrogen bonding, the lower the stretching frequency. FTIR can be used to show hydrogen bonding of the carbonyl group.[78] This rule can be clearly seen in the case of theophylline. Carbonyl group C2═O11, which is not involved in the hydrogen bonding in either polymorph (there are only weak interactions with theophylline methyl group hydrogens), has an identical band position in the FTIR spectra (1706 cm^{-1}) and the stretching frequency is higher than that of C6═O13 carbonyl group. In form IV, the carbonyl group C6═O13 is involved in strong hydrogen bonding with the best hydrogen bond donor (N7–H) and this results in a stretching

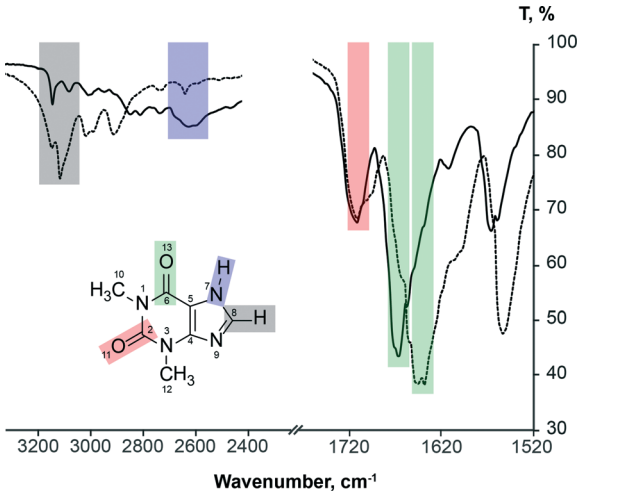

Fig. 11 FTIR spectra of theophylline form II (solid line) and form IV (dashed line), showing carbonyl group, alkene group hydrogen bond and imidazolium group hydrogen bond stretching band assignment.

frequency of 1640 cm^{-1}; while in form II, the C6═O13 group is involved in two weak bifurcated C8–H···O13 hydrogen bonds, stretching band is observed at 1664 cm^{-1}.

Fig. 12 illustrates the carbonyl group stretching band position and intensity changes during theophylline crystallization from saturated form II solutions during solvent evaporation.

The stretching bands of other groups/bonds expected to take part in self-association – alkene group hydrogen bond and imidazolium group hydrogen bond – were not visible in solution FTIR spectra due to low theophylline solubility in the chosen solvents, and they were observed only when all the solvent had evaporated. During the solvent evaporation the intensities of all theophylline bands increased because of increasing theophylline concentration in the solution. An exception to this was the final part of crystallization from saturated methanol solution, where theophylline carbonyl group intensities decreased. For clarity these spectra are shifted by *y* axis. Crystallization from acetone, acetonitrile, chloroform, methanol and formic acid gave theophylline form II, and water produced theophylline monohydrate. Intensive water OH bending band was overlapping with both theophylline carbonyl group stretching bands, therefore the crystallization experiment from saturated water solution was not suitable for studies.

The strongest carbonyl group stretching bands in theophylline solution spectra were observed in concentrated solution, whereas weaker spectral bands appeared only when theophylline crystals emerged. In all solvents the most distinct changes in theophylline band positions and intensities were observed at the moment when solid theophylline emerged. This was due to fact that, before the crystallization FTIR spectra represented mostly solvated theophylline and theophylline associates, whereas during the crystallization, spectra were reflecting the average spectra of solvated theophylline, multiple theophylline associates and crystalline theophylline. The ratio of these species changed during the evaporation/

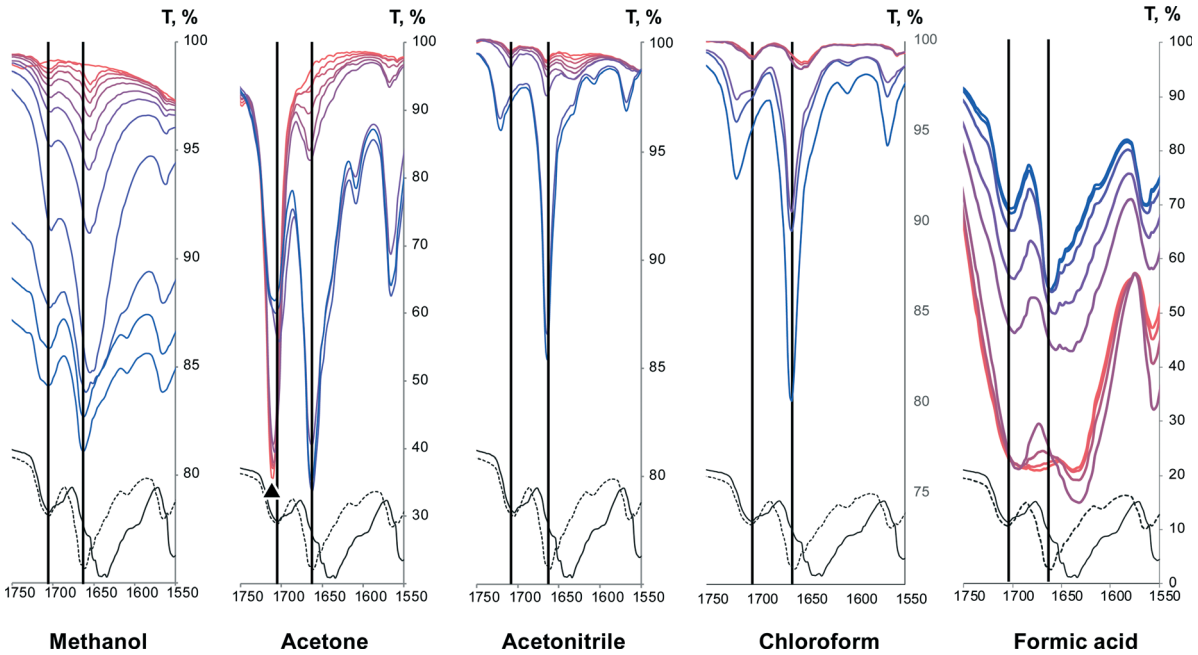

Fig. 12 FTIR spectra of carbonyl group stretching band region during theophylline crystallization from saturated solutions upon solvent evaporation at room temperature. Colour gradient shows FTIR spectra changes throughout crystallization (red – saturated solution, blue – crystallization product). FTIR spectra of solid theophylline form II (dashed line) and IV (continuous line) are added for comparison purpose. Acetone carbonyl group stretching band is marked with ▲.

crystallization and therefore, the band position of functional groups involved in these processes also changed. Finally, when all solvent have evaporated, FTIR spectra of crystalline theophylline was observed.

The position of C2═O11 carbonyl group stretching band in methanol, acetonitrile and chloroform solutions were the same (1706 cm^{-1}) and it coincided with the position of this group in both polymorphs, therefore we can conclude that this group was not involved in strong hydrogen bonding in the solution (similar to crystalline theophylline) and the nearby environment of this group was similar to that in both polymorphs. The position of this stretching band in acetone solution cannot be determined, as acetone carbonyl group stretching bands overlaps with this carbonyl group stretching band. The position of C2═O11 carbonyl group stretching band does not change during the crystallization from methanol solution, whereas during the crystallization from acetonitrile and chloroform solutions the band shifted to 1720 cm^{-1} indicating a change in bonding. The final position of this group stretching band does not match that in the solid form II. FTIR spectra did not change within 5 h. Such band shift to higher frequency indicates that hydrogen bonding was weaker in the crystallized material than in solution. Crystallizations from both solvents were repeated in larger scale. PXRD showed that crystallization products were form II, and FTIR spectra of obtained material coincided with form II spectra. The reason why C2═O11 carbonyl group stretching band position in FTIR *in situ* experiment does not match the position of this band in form II spectra might be related to theophylline crystallization manner from acetonitrile and chloroform. No distinct theophylline crystals were observed on the FTIR spectrometer liquids plate after solvent evaporation, meaning that theophylline crystallized as a thin film. Such crystallization behaviour might promote *monolayer* product along (100) plane, where this carbonyl group is on the surface and it is not involved in any hydrogen bonding. Consequently, C2═O11 carbonyl group stretching band would be shifted to higher frequency for such crystallization product.

In saturated formic acid solution position of C2═O11 carbonyl group stretching band was 1696 cm^{-1} and during the crystallization it gradually shifted to the position of this carbonyl group in crystalline theophylline. This happened because in the solution this carbonyl group was involved in hydrogen bonding with formic acid proton, whereas during the crystallization this hydrogen bond was disarranged.

Unlike C2═O11 carbonyl group, the position of the C6═O13 carbonyl group stretching bands were not the same in the methanol solution and crystallized material (Fig. 12A). In the methanol solution the carbonyl group C6═O13 stretching band was observed at 1656 cm^{-1}, *i.e.* in between the stretching bands of this carbonyl group in solid form II and form IV. This suggest that the associates (dimers, aggregates, solvated entities) in the solution were not the same as in the solid phases and that the hydrogen bonding in the solution was stronger than that in the form II and weaker than that in form IV. From ^{1}H NMR experiment we know that there was no theophylline self-association in methanol, therefore we can conclude that the association causing band shift must be hydrogen bonding between the carbonyl group and

methanol –OH group proton. The changes of the C6═O13 stretching band position were observed at the final part of the crystallization and the band position shifted from 1656 to 1664 cm^{-1}, which is the position of this band in theophylline form II.

In chloroform, analogous C6═O13 carbonyl group stretching band shift were observed (Fig. 12D), with the only difference that initially this band had two maxima – at 1656 cm^{-1} and 1648 cm^{-1}. The band at 1656 cm^{-1} corresponds to solvated theophylline species, analogous to those in methanol, whereas the band at 1648 cm^{-1} most likely corresponds to the dimer detected by NMR measurements. A similar situation was observed when theophylline crystallized from formic acid; with the difference that in saturated formic acid solution a wide band in this region was observed. The wider carbonyl group stretching band must be a result of multiple associates. The concentration of saturated formic acid solution was ~100 times higher than the concentration of saturated chloroform solution, therefore it was expected that associates formed were more complex than dimers and with some diversity. Upon crystallization these agglomerates were disarranged and desolvated, and the final position of C6═O13 carbonyl group stretching band matched the position of form II.

Minor changes in the position of the C6═O13 carbonyl group stretching band were observed when theophylline crystallized from acetone solution. This suggests that theophylline hydrogen bonding did not change significantly upon crystallization from acetone, at least as regards to this carbonyl group. The position of C6═O13 carbonyl group stretching band remained the same during the crystallization from acetonitrile. Such behaviour points out, that this theophylline carbonyl group does not form hydrogen bonds in acetone and acetonitrile solutions, neither to solvent molecules, nor to other theophylline molecules. It is understandable – acetone and acetonitrile are not proton donor solvents. However it was expected that these solvents would compete with the basic theophylline imidazole group nitrogen (N9) to form a hydrogen bond with the most acidic theophylline proton (N7–H). NMR experiments showed that theophylline molecules in the acetone and acetonitrile solution are monomeric and self-association does not occur in these solvents, meaning that species with solvated (N7–H) group dominated in acetone and acetonitrile.

The same FTIR *in situ* crystallization experiment was repeated with saturated form IV solution in methanol and identical results were obtained, suggesting that there are the same associates in the solution regardless of to which polymorph the solution is saturated.

4. Conclusions

The SMPT from theophylline form II to form IV is a very slow nucleation-growth controlled polymorphic transformation. Form IV nucleation is most likely homogenous and is slow. Nucleation of and therefore induction of the phase transformation is hindered by solution aggregates. Form IV crystals grow along the (001) direction, forming plate-like crystals. SMPT induction times correlate to phase transition times in studied solvents, indicating that nucleation and form IV growth is limited by the same factors. Theophylline forms associates in solvents which are good H-bond donors *i.e.* chloroform, water and formic acid. There are the same molecular aggregates in the solutions saturated with respect to form II and form IV. The theophylline aggregates present in solution do not change over time and therefore the long induction time of form IV is not dependent on aggregation kinetics. NMR and FTIR data suggest that the nature of solution aggregates is solvent dependent, most likely linked to hydrogen bonding character of the solvent.

5. Experimental section

5.1. Materials

Anhydrous theophylline was obtained from Sigma-Aldrich and was certified >99% pure. Anhydrous theophylline was confirmed to be form II and was used as received. Methanol (HPLC grade), acetonitrile (HPLC grade), acetone (ARC grade) and chloroform (HPLC grade) were obtained from Fischer Scientific, formic acid (>98%) from Sigma-Aldrich. Solvents were used without further purification. Distilled water was used. Methanol-D4 (CD_3OD, 99.8%), acetone-D6 ($(CD_3)_2O$, 99.9%), dimethyl sulfoxide-D6 ($(CD_3)_2SO$, 99.9%) and formic acid-D2 (98%; <5% D_2O) were obtained from Cambridge Isotope Laboratories, deuterium oxide (D_2O, 99.96%) from BDH Chemicals, chloroform-D (CCl_3D, 99.8%) from Euriso-top, and acetonitrile-D3 (CD_3CN, 99.8%) from Apollo Scientific.

5.2. Preparation of theophylline crystalline forms

Theophylline form IV. Theophylline form IV was prepared as described previously.[5] An excess amount of anhydrous theophylline (1.0 g) was added to 25 mL of methanol and stirred at 600 rpm for 14 days at 23 ± 1 °C (temperature was controlled because temperature deviations was found to hinder form IV nucleation). The resulting solid phase was filtered through a Buchner funnel under reduced pressure. The polymorphic form of the dry residue was confirmed using PXRD.

Theophylline form I. Anhydrous theophylline form II (~1.0 g), was ground in a mortar with pestle for 3 min, transferred to a petri dish, covered by a glass slide and heated at 268 ± 1 °C for 2 h. The sample was cooled to room temperature and the polymorphic form was confirmed using PXRD.

Lyophilized (microcrystalline) theophylline. The excess amount of anhydrous theophylline (~5.0 g) was added to 250 mL of water and was left to stir overnight. The solid phase was removed by filtration and the remaining clear solution was spray dried using a Buchi mini spray dryer B-290. A top spray method was used with the inlet temperature set at 120 °C, the outlet at 70 °C and the pressure at 6 bar. The crystallinity of the material obtained was examined using PXRD.

Theophylline monohydrate. The excess amount (~3.0 g) of anhydrous theophylline was dissolved in ~100 mL of warm water (~70 °C) and was left to stir overnight. The precipitated solid phase was filtered, air dried and the crystalline phase obtained was confirmed using PXRD.

5.3. Examination of solution mediated phase transformation

An excess amount (2.5 g) of anhydrous theophylline form II (used as received) was added to 100 mL of methanol. The suspension was stirred at 600 rpm for 14 days at room temperature (23 ± 1 °C) and the following measurements were performed every 7 to 24 h.

(a) Solution concentration monitoring. Theophylline concentration in the solution was measured every 1 h to 1 day. The solution (~1 mL) was filtered through a syringe filter of 0.20 μm size, and solution concentration was determined as described in section 5.7. Three parallel solution concentration determination experiments were performed.

(b) Crystallization product from solution. 2 mL of the solution was filtered through 0.20 μm syringe filter, transferred to a Petri dish and was left to evaporate at room temperature. Crystallized dry residue of three parallel experiments was combined and phase composition was examined using PXRD.

(c) FTIR spectra of the solution. ~0.3 mL of the filtered solution was gathered as described above, and the FTIR spectra of solution were recorded immediately after sample gathering.

(d) Phase composition of the solid phase. The stirring of the slurry was stopped 30 seconds prior to sample gathering, to allow the suspended solid particles to settle. Solid phase sample (10–20 mg) was collected with a metal spoon from the suspension and was quickly filtered through Buhner funnel filter under reduced pressure. The solid phase was examined using PXRD, FTIR and SEM.

SMPT was repeated in triplicate.

SMPT was additionally performed with different starting materials and solvents (given in Table 1). Single runs were performed for these experiments. The phase composition of the solid phase was monitored every 1 to 7 days, except experiments where form II and form IV mixture was used; the phase composition in these experiments was monitored every 10 min to 1 h. The solvent and theophylline ratio in all SMPT experiments were the same (2.5 g of theophylline and 100 mL of solvent), except SMPT in formic acid, where 15.0 g of theophylline were added to 25 ml of formic acid due to high theophylline solubility in formic acid.

SMPT in methanol-D4 was performed for H^1 NMR studies. An excess amount (0.5 g) of commercial theophylline form II was added to 4.0 mL of methanol-D. The suspension was stirred at 600 rpm for 10 days at room temperature (23 ± 1 °C). PXRD patterns of solid phase and solution H^1 NMR spectra (see section 5.9) were recorded each day. Stirring was stopped 1 min prior to sample collection, and: (a) clear solution (~1 mL) was transferred to NMR tube; (b) solid phase (10–20 mg) was collected with a metal spoon and quickly filtered through a Buchner funnel filter under reduced pressure. PXRD and H^1 NMR measurements were performed immediately after sample collection. Solution from NMR experiment was returned back to the reaction vial immediately after recording the NMR spectrum.

5.4. Determination of theophylline solubility

Theophylline form II solubility in acetone, acetonitrile, methanol, chloroform and formic acid and form IV solubility in methanol were determined as follows. An excess amount of theophylline was added to 15 mL of solvent and was left to stir overnight at 23 ± 1 °C. The saturated solution was filtered through a 0.20 μm syringe filter and then 10.0 mL of clear solution was transferred to a preweighed vial. Solution was left to evaporate at room temperature, weighed and theophylline solubility was calculated. The PXRD pattern of the filtrate was recorded to ensure that the solubility of the desired polymorph was determined. Two parallel experiments were performed.

Table 1 Starting materials and solvents used in SMPT

Starting material	Solvent
Commercial form II	Methanol
Form II, ground in mortar with pestle for 3 min	Methanol
Lyophilized form II[a]	Methanol
Commercial form II	Methanol saturated to theophylline form IV
Commercial form II/form IV[a] mixture (w_{II}/w_{IV}; 90/10)	Methanol saturated to theophylline form II
Commercial form II/form IV[a] mixture (w_{II}/w_{IV}; 90/10)	Methanol saturated to theophylline form IV
Commercial form II	Methanol/water mixture (V_{MeOH}/V_{H_2O}; 99/1)
Commercial form II	Methanol/water mixture (V_{MeOH}/V_{H_2O}; 95/5)
Commercial form II	Methanol/water mixture (V_{MeOH}/V_{H_2O}; 80/20)
Commercial form II	Acetone
Commercial form II	Acetonitrile
Commercial form II	Chloroform
Commercial form II	Formic acid
Commercial form II	Methanol-D4[b]

[a] Prepared as described in section 5.2. [b] Small scale experiment, V_{total} = 4.0 Ml.

5.5. Powder X-ray diffraction (PXRD)

Samples were analysed with a Rigaku Miniflex powder X-ray diffractometer. Diffraction patterns within the 2θ range of 5° to 40° were recorded at room temperature using Cu Kα radiation at 1.54180 Å, with the following measurement conditions: tube voltage 30 kV, tube current 15 mA, step-scan mode with the step size 2θ = 0.02°, and the counting time 2 s per step. Diffractometer slits were set as follows: divergence slit – variable; scattering slit – 4.2°, receiving slit – 0.3 mm. Powder samples were packed into aluminium sample holders and pressed by a glass slide to ensure co-planarity of the powder surface with the surface of the holder.

Qualitative phase analysis. Reference powder patterns were calculated with Mercury 3.3 (ref. 79) software from Cambridge Structural Database (CSD) crystal structure data with the reference codes BAPLOT for theophylline form II and BAPLOT03 for theophylline form IV.

Quantitative phase analysis. The quantitative Rietveld phase analysis were performed using BGMN software (version 1.8.6b)[80] with Profex (version 3.1.1) interface. Crystal structure data previously mentioned were used for Rietveld analysis.

5.6. FTIR spectroscopy

FTIR spectra were recorded using a Perkin-Elmer Spectrum BX spectrometer fitted with a PIKE Technologies MIRacle sampling accessory. MIRacle liquids plate was used when spectra of solutions were recorded. The samples were scanned at a resolution of 4 cm^{-1} between 4000 cm^{-1} and 600 cm^{-1}. Each spectrum consisted of 16 co-added scans if not otherwise stated.

5.7. UV/Vis spectroscopic solution concentration monitoring

Solution concentration throughout SPMTs in methanol was monitored by measurements of the UV/Vis absorption at 272 nm using a Perkin-Elmer Lambda 25 UV/Vis spectrophotometer. Calibration was performed in the concentration region between 0.2 mM and 0.01 mM (R^2 = 0.99990). For solution concentration determination 20 μL aliquot of filtered reaction medium was diluted with 40 mL of methanol.

5.8. Scanning electron microscopy (SEM)

SEM imaging was performed using Inspect S SEM (FEI, Holland) system. Samples were initially gold coated using a K550X sputter coater (EMITECH, UK) and subsequently scanned using an acceleration voltage of 5.0 kV at a working distance of approximately 10 mm.

5.9. NMR spectroscopic self-association studies

^{1}H NMR spectra were recorded as a function of theophylline concentration in the solution. Experiments were performed in methanol-D4, chloroform-D, acetone-D6, dimethyl sulfoxide-D6, deuterium oxide, acetonitrile-D3 and formic acid-D2 concentration region from nearly saturated solutions (1.0 M in formic acid-D2, 0.050 M in methanol-D4, 0.015 M in acetone-D6, 0.10 M in dimethyl sulfoxide-D6, deuterium oxide, chloroform-D and acetonitrile-D3) to 1 μM solutions was covered. Ground anhydrous theophylline form II was used to prepare the most concentrated solution in each solvent and the rest of the solutions were prepared by subsequent dilution. Additional samples, where an excess amount of ground theophylline was added to deuterated solvents, were prepared to simulate suspensions similar to that examined in SMPT. The mass of theophylline added was 120% of the mass necessary to prepare saturated solution in the respective solvent. An analytical balance (±0.1 mg) and micropipettes (±1 μL) were used for solution preparation. NMR spectra of prepared solutions were recorded right after solution preparation, and repeated after 1 and 2 weeks. NMR tubes of prepared solutions were closed with lids and sealed with parafilm. Samples were stored at 20.0 ± 0.5 °C between measurements.

^{1}H NMR spectra were recorded on a Bruker Avance DRX 300 MHz spectrometer using residual solvent as an internal standard. NMR spectra were recorded at 26.8 ± 0.5 °C (300.0 ± 0.5 K).

Theophylline ^{1}H chemical shifts were allocated by ^{1}H-^{13}C HSQC according to literature assignments.[81] ^{1}H-^{13}C HSQC experiments were carried out using the standard Bruker program hsqcetgpsi2.[82,83]

5.10. *In situ* monitoring of crystallization process

Two drops (~0.07 mL) of saturated theophylline methanol, acetone, acetonitrile, chloroform, water and formic acid solutions from solubility determination experiments (section 5.4) were placed on a FTIR spectrometer liquids plate and spectra of the solution were continuously recorded during solvent evaporation/theophylline crystallization. Each FTIR spectra showed the average of 16 co-added scans, recorded in 75 s. For acetone solution 4 co-added scans (recorded in 17 s) were averaged. Spectra were recorded until three continuous spectra were identical and no peaks of solvents were visible. The experiment with each solvent was repeated in triplicate.

Acknowledgements

This work has been supported by the European Social Fund within the project "Support for Doctoral Studies at University of Latvia". The authors gratefully acknowledge the support of Erasmus Student Mobility programme. We thank Dace Rasiņa and Alessandro Pozzoli for fruitful discussions.

Notes and references

1 S. R. Vippagunta, H. G. Brittain and D. J. W. Grant, *Adv. Drug Delivery Rev.*, 2001, **48**, 3–26.
2 H. G. Brittain, *Polymorphism in Pharmaceutical Solids*, Informa Healthcare USA, Inc., New York, NY, 2nd edn, 2009, vol. 192.
3 R. Hilfiker, *Polymorphism: in the Pharmaceutical Industry*, Wiley-VCH, Weinheim, 2006.

4 C. Cardin, Y. Gan and T. Lewis, *Acta Crystallogr., Sect. E: Struct. Rep. Online*, 2007, **63**, o3175.
5 L. Seton, D. Khamar, I. J. Bradshaw and G. A. Hutcheon, *Cryst. Growth Des.*, 2010, **10**, 3879–3886.
6 K. Matsuo and M. Matsuoka, *Cryst. Growth Des.*, 2007, **7**, 411–415.
7 C. Nunes, A. Mahendrasingam and R. Suryanarayanan, *Pharm. Res.*, 2006, **23**, 2393–2404.
8 H. Zhu, *Int. J. Pharm.*, 1996, **135**, 151–160.
9 M. D. Ticehurst, R. A. Storey and C. Watt, *Int. J. Pharm.*, 2002, **247**, 1–10.
10 S. L. Childs, G. P. Stahly and A. Park, *Mol. Pharmaceutics*, 2007, **4**, 323–338.
11 M. Cioffi, C. A. Hunter, M. J. Packer, M. J. Pandya and M. P. Williamson, *J. Biomol. NMR*, 2009, **43**, 11–19.
12 D. Musumeci, C. A. Hunter and J. F. McCabe, *Cryst. Growth Des.*, 2010, **10**, 1661–1664.
13 C. A. Hunter, J. F. McCabe and A. Spitaleri, *CrystEngComm*, 2012, **14**, 7115–7117.
14 K. Chadwick, R. J. Davey, G. Dent, R. G. Pritchard, C. A. Hunter and D. Musumeci, *Cryst. Growth Des.*, 2009, **9**, 1990–1999.
15 R. J. Davey, G. Dent, R. K. Mughal and S. Parveen, *Cryst. Growth Des.*, 2006, **6**, 1788–1796.
16 J. Kirschbaum, *J. Pharm. Sci.*, 1973, **62**, 168–169.
17 D. Guttman and T. Higuchi, *J. Pharm. Sci.*, 1971, **60**, 1269–1270.
18 A. L. Thakkar, L. G. Tensmeyer and W. L. Wilham, *J. Pharm. Sci.*, 1971, **60**, 1267–1269.
19 D. Guttman and T. Higuchi, *J. Am. Pharm. Assoc.*, 1957, **46**, 4–10.
20 Y. Ebisuzaki, P. D. Boyle and J. A. Smith, *Acta Crystallogr., Sect. C: Cryst. Struct. Commun.*, 1997, **53**, 777–779.
21 A. V. Trask, W. D. S. Motherwell and W. Jones, *Int. J. Pharm.*, 2006, **320**, 114–123.
22 M. C. Etter, *Acc. Chem. Res.*, 1990, **23**, 120–126.
23 D. Khamar, R. G. Pritchard, I. J. Bradshaw, G. A. Hutcheon and L. Seton, *Acta Crystallogr., Sect. C: Cryst. Struct. Commun.*, 2011, **67**, o496–o499.
24 C. Sun, D. Zhou, D. J. W. Grant and V. G. Young, *Acta Crystallogr., Sect. E: Struct. Rep. Online*, 2002, **58**, o368–o370.
25 W. Ostwald, *Z. Phys. Chem.*, 1897, **22**, 289.
26 P. T. Cardew and R. J. Davey, *Proc. R. Soc. London, Ser. A*, 1985, **398**, 415–428.
27 R. J. Davey, P. T. Cardew, D. McEwan and D. E. Sadler, *J. Cryst. Growth*, 1986, **79**, 648–653.
28 R. J. Davey, N. Blagden, S. Righini, H. Alison and E. S. Ferrari, *J. Phys. Chem. B*, 2002, **106**, 1954–1959.
29 R. J. Davey, N. Blagden, S. Righini, H. Alison and E. S. Ferrari, *J. Phys. Chem. B*, 2002, **106**, 1954–1959.
30 R. Bobrovs, L. Seton and A. Actiņš, *CrystEngComm*, 2014, **16**, 10581–10591.
31 J. E. House, *Principles of chemical kinetics*, Academic Press, 2007.
32 E. D. Becker, *J. Chem. Phys.*, 1959, **31**, 269.
33 C. M. Huggins, G. C. Pimentel and J. N. Shoolery, *J. Phys. Chem.*, 1956, **60**, 1311–1315.
34 E. D. Becker, U. Liddel and J. N. Shoolery, *J. Mol. Spectrosc.*, 1958, **2**, 1–8.
35 Y. Lam and G. Kotowycz, *Can. J. Chem.*, 1977, **55**, 3620–3630.
36 I. Horman and B. Dreux, *Helv. Chim. Acta*, 1984, **67**, 754–764.
37 I. J. McLennan, R. E. Lenkinski and Y. Yanuka, *Can. J. Chem.*, 1985, **63**, 1233–1238.
38 N. Marchettini, G. Valensin and E. Gaggelli, *Biophys. Chem.*, 1990, **36**, 65–70.
39 A. N. Veselkov, L. N. Dymant, S. F. Baranovskii, P. A. Bolotin, O. S. Zav'yalova, D. A. Veselkov, H. Parkes and D. Davies, *J. Struct. Chem.*, 1995, **36**, 69–75.
40 D. B. Davies, L. N. Djimant and A. N. Veselkov, *J. Chem. Soc., Faraday Trans.*, 1996, **92**, 383.
41 M. Bastian and H. Sigel, *Biophys. Chem.*, 1997, **67**, 27–34.
42 M. P. Evstigneev, V. P. Evstigneev and D. B. Davies, *J. Mol. Struct.*, 2006, **784**, 162–168.
43 M. Bogdan, C. G. Floare and A. Pîrnău, *J. Phys.: Conf. Ser.*, 2009, **182**, 012002.
44 J. S. Chen and R. B. Shirts, *J. Phys. Chem.*, 1985, **89**, 1643–1646.
45 E. D. Becker, *Spectrochim. Acta*, 1961, **17**, 436–447.
46 L. P. Kuhn and R. E. Bowman, *Spectrochim. Acta*, 1961, **17**, 650–660.
47 U. Liddel and E. D. Becker, *Spectrochim. Acta*, 1957, **10**, 70–84.
48 R. J. Abraham and M. Mobli, *Magn. Reson. Chem.*, 2007, **45**, 865–877.
49 F. Hibbert and J. Emsley, *Adv. Phys. Org. Chem.*, 1990, **26**, 255–379.
50 C. A. Hunter and M. J. Packer, *Chem. – Eur. J.*, 1999, **5**, 1891–1897.
51 A. Spitaleri, C. A. Hunter, J. F. McCabe, M. J. Packer and S. L. Cockroft, *CrystEngComm*, 2004, **6**, 489–493.
52 W. H. Gmeiner and C. D. Poulter, *J. Am. Chem. Soc.*, 1988, **110**, 7640–7647.
53 D. V. Waterhous and D. D. Muccio, *Magn. Reson. Chem.*, 1990, **28**, 223–226.
54 S. L. Cockroft, J. Perkins, C. Zonta, H. Adams, S. E. Spey, C. M. R. Low, J. G. Vinter, K. R. Lawson, C. J. Urch and C. A. Hunter, *Org. Biomol. Chem.*, 2007, **5**, 1062–1080.
55 C. E. Hughes, S. Hamad, K. D. M. Harris, C. R. A. Catlow and P. C. Griffiths, *Faraday Discuss.*, 2007, **136**, 71.
56 S. Ng, *Mol. Pharmacol.*, 1971, **7**, 177–182.
57 A. Maher, D. M. Croker, Å. C. Rasmuson and B. K. Hodnett, *Cryst. Growth Des.*, 2012, **12**, 6151–6157.
58 P. Lehto, J. Aaltonen, M. Tenho, J. Rantanen, J. Hirvonen, V. P. Tanninen and L. Peltonen, *J. Pharm. Sci.*, 2009, **98**, 985–996.
59 N. Rodríguez-Hornedo and D. Lechuga-Ballesteros, *Int. J. Pharm.*, 1992, **85**, 149–162.
60 J. Schöll, D. Bonalumi, L. Vicum, M. Mazzotti and M. Müller, *Cryst. Growth Des.*, 2006, **6**, 881–891.
61 S. Dharmayat, J. Calderon De Anda, R. B. Hammond, X. Lai, K. J. Roberts and X. Z. Wang, *J. Cryst. Growth*, 2006, **294**, 35–40.

62 F. Tian, T. Rades and N. Sandler, *AAPS PharmSciTech*, 2008, **9**, 390–394.
63 S. Dharmayat, R. B. Hammond, X. Lai, C. Ma, E. Purba, K. J. Roberts, Z. Chen, E. Martin, J. Morris and R. Bytheway, *Cryst. Growth Des.*, 2008, **8**, 2205–2216.
64 A. Maher, D. M. Croker, Å. C. Rasmuson, B. K. Hodnett and M. A. O'Mahony, *Cryst. Growth Des.*, 2012, **12**, 1925–1932.
65 M. A. O'Mahony, C. C. Seaton, D. M. Croker, S. Veesler, Å. C. Rasmuson and B. K. Hodnett, *Cryst. Growth Des.*, 2013, **13**, 1861–1871.
66 J. W. Mullin, *Crystallization*, Butterworth-Heinemann, Oxford, 4th edn, 2001.
67 D. Croker and B. K. Hodnett, *Cryst. Growth Des.*, 2010, **10**, 2806–2816.
68 E. S. Ferrari and R. J. Davey, *Cryst. Growth Des.*, 2004, **4**, 1061–1068.
69 R. Docherty, G. Clydesdale, K. J. Roberts and P. Bennema, *J. Phys. D: Appl. Phys.*, 1991, **24**, 89–99.
70 B. C. Hancock and G. Zografi, *J. Pharm. Sci.*, 1997, **86**, 1–12.
71 L. R. Snyder, *J. Chromatogr.*, 1974, **92**, 223–230.
72 R. A. Sullivan, R. J. Davey, G. Sadiq, G. Dent, K. R. Back, J. H. Ter Horst, D. Toroz and R. B. Hammond, *Cryst. Growth Des.*, 2014, **14**, 2689–2696.
73 H. G. Brittain, *J. Pharm. Sci.*, 1997, **86**, 405–412.
74 G. A. Stephenson, R. A. Forbes and S. M. Reutzel-Edens, *Adv. Drug Delivery Rev.*, 2001, **48**, 67–90.
75 D. E. Bugay, *Adv. Drug Delivery Rev.*, 2001, **48**, 43–65.
76 S. Parveen, R. J. Davey, G. Dent and R. G. Pritchard, *Chem. Commun.*, 2005, 1531–1533.
77 P. B. Coleman, *Practical sampling techniques for infrared analysis*, CRC Press, London, 1993.
78 S. M. Kashid and S. Bagchi, *J. Phys. Chem. Lett.*, 2014, **5**, 3211–3215.
79 C. F. Macrae, I. J. Bruno, J. A. Chisholm, P. R. Edgington, P. McCabe, E. Pidcock, L. Rodriguez-Monge, R. Taylor, J. van de Streek and P. A. Wood, *J. Appl. Crystallogr.*, 2008, **41**, 466–470.
80 J. Bergmann, P. Friedel and R. Kleeberg, *CPD Newsl.*, 1998, vol. 20, pp. 5–8.
81 E. D. L. Smith, R. B. Hammond, M. J. Jones, K. J. Roberts, J. B. O. Mitchell, S. L. Price, R. K. Harris, D. C. Apperley, J. C. Cherryman and R. Docherty, *J. Phys. Chem. B*, 2001, **105**, 5818–5826.
82 L. Kay, P. Keifer and T. Saarinen, *J. Am. Chem. Soc.*, 1992, **114**, 10663–10665.
83 A. G. Palmer, J. Cavanagh, P. E. Wright and M. Rance, *J. Magn. Reson.*, 1991, **93**, 151–170.

I hereby declare and confirm with my signature that the doctoral dissertation "**Solvent mediated phase transformations of active pharmaceutical compounds tegafur and theophylline**" is exclusively the result of my own autonomous work based on my research and literature published, which is seen in the notes and bibliography used. I also declare that no part of the paper submitted has been made in an inappropriate way, whether by plagiarizing or infringing on any third person's copyright. Finally, I declare that no part of the paper submitted has been used for any other paper in another higher education institution, research institution or educational institution.

Author: Raitis Bobrovs

Signature _____

Supervisor: Prof., Dr. Chem., Andris Actiņš

Signature _____

Thesis submitted in the Promotion Council in chemistry of University of Latvia for the commencement of the degree of Doctor of Chemistry at _____.

Secretary of the Promotion Council: Vita Rudoviča _____

Thesis defended at the session of Promotion Council in chemistry of University of Latvia for the commencement of the degree of Doctor of Chemistry
at 26th of June, 2015, protocol No. _____

Secretary of the Promotion Council: Vita Rudoviča _____